Synthesis, Modification and Characterization of Biocompatible Polymers and Nanoparticles

Dissertation zur Erlangung des Grades Doktor der Naturwissenschaften im Promotionsfach Chemie
am Fachbereich Chemie, Pharmazie, Geographie und Geowissenschaften der Johannes Gutenberg-Universität Mainz

Filiz Karagöz
geboren in Ankara

Mainz, 2022

Dekan: Prof. Dr. Tanja Schirmeister

1. Gutachter: Prof. Dr. Klaus Müllen
2. Gutachter: Prof. Dr. Rudolf Zentel

Tag der mündlichen Prüfung: 17.05.2022

Die vorliegende Arbeit wurde in der Zeit von Februar 2014 bis Juni 2018 am Max-Planck-Institut für Polymerforschung in Mainz unter Betreuung von Prof. Dr. Klaus Müllen durchgeführt.

Canim Aileme

Table of Contents

Index of Abbreviations

ACF	Auto correlation function
AMM	Activated monomer mechanism
ATRP	Atom transfer radical polymerization
BODIPY	Styryl boron-dipyrromethene
BOP	(Benzotriazol-1-yloxy)tris(dimethylamino)phosphonium hexafluorophosphate
BPA	Bisphenol A
Bpy	2,2-bipyridine
β-BL	β-butyrolactone
Cbz-Lysine NCA	N-ε-carbobenzyloxy-L-lysine N-carboxyanhydride
CD	Circular dichroism spectroscopy
CLSM	Confocal laser scanning microscopy
COD	1,5-cyclooctadiene
CMC	Critical micelle concentration
CPP	Cell-penetrating peptide
CRP	Controlled radical polymerization
DCC	*N, N'*-dicyclohexylcarbodiimide
DCM	Dichloromethane
DD	Direct dissolution method
DIPEA	N,N-diisopropylethylamine
DLS	Dynamic light scattering
DMAP	4-(dimethylamino)pyridine
DMF	*N, N'*-dimethylformamide
DMSO	Dimethyl sulfoxide
DOSY	Diffusion ordered spectroscopy
DP	Degree of polymerization
DSC	Differential scanning calorimetry
DXO	1,5-dioxepan-2-one
Đ	Polydispersity index
EDC	1-ethyl-(3-dimethylaminopropyl)carbodiimide
EDTA	Ethylenediaminetetraacetic acid

EPR	Enhanced permeability and retention
FCS	Fluorescence correlation spectroscopy
FDA	Food and drug administration
Fmoc-Lysine NCA	N-ε-fluorenylmethoxycarbonyl-L-lysine N-carboxyanhydride
FS	Fluorescence spectroscopy
FT-IR	Fourier transform infrared spectroscopy
Glu(Bz)-NCA	γ-benzyl-L-glutamic acid N-carboxyanhydride
GFP	Green fluorescent peptide
GPC	Gel permeation chromatography
HBSS	Hank's balanced salt solution
HBTU	2-(1H-benzotriazol-1-yl)-1,1,3,3-tetramethyluronium hexafluoro phosphate
HMDS	Hexamethyldisilazane
HOBt	1-hydroxybenzotriazole
HPLC	High performance liquid chromatography
IMes	1,3-bis(2,4,6-trimethylphenyl)imidazole-2-ylidene
Leucine NCA	L-leucine N-carboxyanhydride
MALDI-TOF-MS	Matrix assisted laser desorption/Ionization-time of flight mass spectroscopy
MMP-2	Matrix metalloproteinases-2
NAM	Normal amine mechanism
NCA	N-carboxyanhydride
NHC	N-heterocyclic carbene
NMP	Nitroxide-mediated polymerization
NMR	Nuclear magnetic resonance spectroscopy
NTSL	N-trityl-L-serine lactone
O/W	Oil-in-water
OEG	Oligo(ethylene glycol)
PCL	Poly(ε-caprolactone)
PDI	Perylene diimide
PDI-NH_2	N-(2,6-diisopropylphenyl)-N'-(4-aminoethyl)-1,6,7,12-tetraphenoxy perylene-3,4:9,10-tetracarboxydiimide
PEG	Poly(ethylene glycol)

PEG-NH_2	α-methoxy-ω-amino-poly(ethylene glycole)
PEG-*b*-PGlu(Bz)	Poly(ethylene glycol)-*b*-poly(γ-benzyl-L-glutamic acid)
PEG-*b*-PGlu(Pyr)	Poly(ethylene glycol)-*b*-poly((1-pyrenyl methyl) glutamate)
PGA	Poly(glycolic acid) or Poly(glycolide)
PGlu	Poly(glutamic acid)
PGlu(Pyr)	Poly(1-pyrenyl methyl glutamate)
Pyrene-Glu NCA	γ-(1-pyrenylmethyl)-L-glutamate N-carboxyanhydride
Phenylalanine NCA	L-Phenylalanine N-carboxyanhydride
PHB	Poly(3-hydroxybutyrate)
PLA	Polylactic acid or Polylactide
PLGA	Poly(lactide-*co*-glycolide)
PLLA	Poly(L-lactide)
PLLA-*b*-PLSL	Poly(L-lactide)-*b*-poly(L-serine lactone)
PLSL	Poly(L-serine lactone)
PI	Poly(isoprene)
PI-*b*-PMMA	Poly(isoprene)-*b*-poly(methyl methacrylate)
PMMA	Poly(methyl methacrylate)
PMI	9-bromo-N-(2,5,8,11,15,18,21,24-octaoxapentacosan-13yl) perylene-3,4-dicarboxy monoimide
PS	Polystyrene
PSE	Poly(serine ester)
PS-*b*-PI	Poly(styrene)-*b*-poly(isoprene)
PU	Polyurethane
RAFT	Reversible addition-fragmentation chain transfer
RGD	Arginylglycylaspartic acid
ROP	Ring opening polymerization
RT	Room temperature
SDS	Sodium dodecyl sulfate
SEM	Scanning electron microscopy
SIMes	1,3-bis(2,4,6-trimethylphenyl)-4,5-dihydroimidazol-2-ylidene
SO_3H-PDI-COOH	N-(2,6-diisopropylphenyl)-N'-(4-aminoethyl)-1,6,7,12-tetra(4-sulfonylphenoxy)-perylene-3,4:9,10-tetracarboxydiimide
SPPS	Solid phase peptide synthesis

TCE	Tetrachloroethane
TFF	Thin film formation
TGA	Thermogravimetric analysis
TEM	Transmission electron microscopy
THF	Tetrahydrofuran
T_g	Glass transition temperature
TMS-Cl	Trimethylsilylchloride
TRIS	Tris(hydroxymethyl)aminomethane
UV-*vis*	Ultraviolet-*visible* spectroscopy
W/O	Water-in-oil
XRD	X-ray diffraction

CHAPTER 1

General Introduction

1. General Introduction

1.1. Polymeric Biomaterials for Pharmaceutical Applications

Biomaterials are in high demand in all emerging pharmaceutical fields such as tissue engineering, drug delivery, gene delivery or nano-biomedicine.[1–4] Over the past fifty years, synthetic biodegradable materials have been greatly explored, leading to the development of a various range of objects with diverse physicochemical properties to match with the specific and unique requirements for individual medical applications.[5–9] In 2020, the global biomaterial market was valued at $35.5 billion and is expected to reach $47.5 billion by 2025.[10]

A biomaterial is a substance intended to be used in biological systems for therapeutic or diagnostic procedures.[11,12] The first and most important property of the material is biocompatibility: when the material gets in contact with a biological system it should not cause an inflammatory or toxic response of the organism, which strongly depends on the chemical, physical and biological properties of the material.[3,13] A second critical requirement for a biomaterial is biodegradability, meaning that no toxic degradation products may be released to the organism during decomposition.[3,13] Additionally, the degradation time of the material should match with the healing or regeneration process.[13,14] Based on the development of materials with aforementioned properties and further advanced, application-specific investigations, following biomaterials can be produced: small implants e.g. sutures;[13,15] large implants such as bone screws and bone plates;[16,17] nano-sized materials as drug delivery vehicles,[18] tumor imaging tools,[19] cell sensor;[20] three dimensional structures for tissue engineering[21,22] etc. In recent years, significant research on designing synthetic biodegradable polymers has been conducted and materials can be custom designed for specific applications. This development gives rise to the utilization of synthetic biodegradable polymers over natural ones. Synthetic polymers can be classified as hydrolytically or enzymatically degradable polymers, as it shown schematically in Figure 1.1.[3]

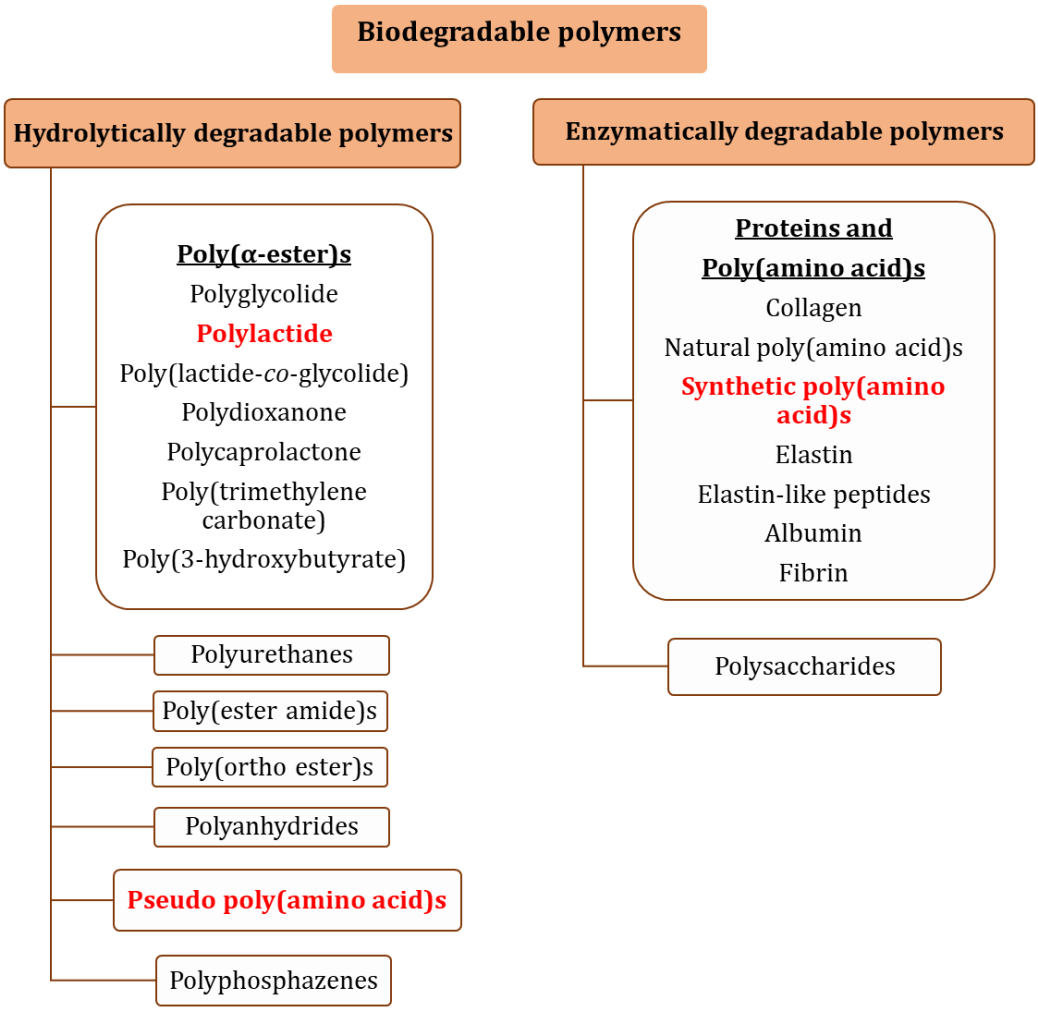

Figure 1.1. Classification of biodegradable polymers

The backbone of hydrolytically degradable polymers consists of e.g., esters, anhydrides, carbonates, ortho esters, urethanes or ester amides.[3] Among them, poly(α-ester)s are the most frequently used materials particularly in drug delivery fields. Well-known members of this class of polymers are poly(lactic acid)-poly(lactide) (PLA),[23] poly(glycolic acid)-poly(glycolide) (PGA),[24] poly(lactide-*co*-glycolide) (PLGA),[25,26] poly(ε-caprolactone) (PCL),[27] poly(3-hydroxybutyrate) (PHB),[28] poly(dioxanone)[29] and poly(trimethylene carbonate)[30] (Figure 1.1). Additionally, pseudo-poly(amino acid)s which are the structural analogues of traditional poly(α-amino acid)s received considerable attention in recent years.[31,32] Pseudo-poly(tyrosine),[33] pyroline[31] and serine (poly(serine ester), (PSE))[34,35] are the most noteworthy pseudo-poly(amino acid)s (see PSE in Figure 1.2).

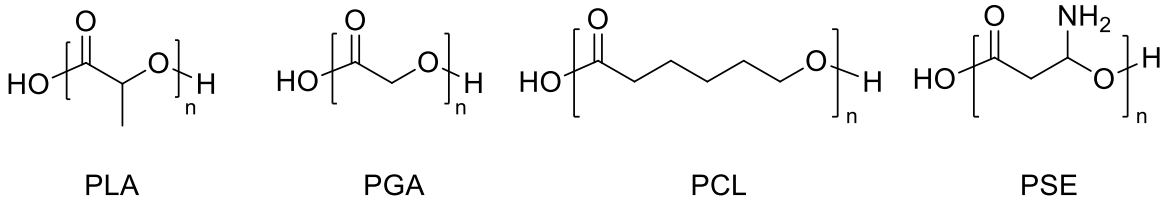

Figure 1.2. Structures of common biodegradable poly(α-ester)s

Enzymatically degradable polymers are another significant class of biodegradable polymers utilized in pharmaceutical industry with its well-known members like proteins, poly(amino acid)s and polysaccharides.[36] Synthetic poly(amino acid)s are receiving great attention in literature due to their easy synthesis, design and modification opportunities.[37] The structure of some of the common poly(α-amino acid)s are shown in Figure 1.3: polylysine,[38] polyglutamic acid,[39] polyaspartic acid,[40] polyserine,[41] polyleucine[42] and, polyphenyl alanine[43] from left to the right, respectively.

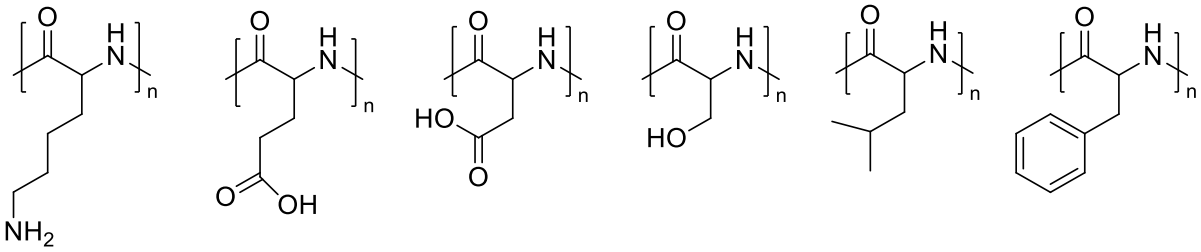

Figure 1.3. Structures of common poly(α-amino acid)s

Materials consisting of polylactide, pseudo-poly(amino acid)s and poly(α-amino acid)s mainly form the basis of this research thesis (Figure 1.4). This chapter provides the general introduction of these materials; synthesis, properties and biomedical applications.

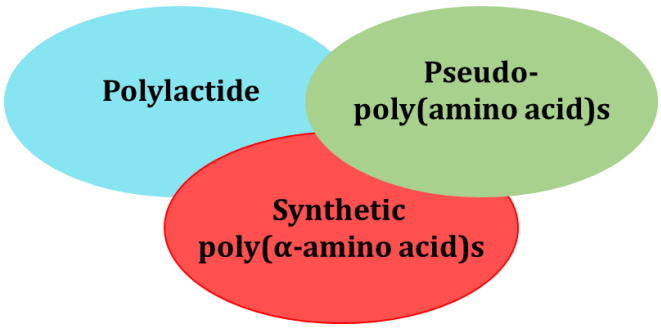

Figure 1.4. The materials that form the basis of the thesis

1.1.1. Polylactide

Polylactic acid or polylactide (PLA) is one of the most highly consumed biodegradable thermoplastic aliphatic polyesters which was derived from renewable resources such as wheat, corn starch and sugarcane.[44–47] PLA was synthesized for the first time by Théophile-Jules Pelouze by polycondensation in 1845[48], followed by the ring opening polymerization of lactide by Wallace Hume Carothers et al. in 1932.[49] Development of the industrial production of high molecular weight PLA started at 1990's by Cargill Inc. as the biodegradable alternative to polystyrene or poly(ethylene terephthalate). The interest was inspired by its easy thermal processability by extrusion, stretch blow molding, injection molding, film casting, and fiber spinning. Additionally, production of PLA requires 5%-55% less energy in comparison to the petroleum-based polymers.[44] These overall properties makes PLA attractive for the use as packaging materials and films, cups, cutlery, bottles etc.[50] PLA is hydrolysable by microorganisms to lactic acid and further to carbon dioxide and water. Due to its these environmentally friendly, biocompatible, and biodegradable nature, PLA has been used in pharmaceutical industry for applications including drug delivery systems[51–53], tissue engineering[54], protein delivery[55] and as a material for sutures and prostheses.[56]

PLA is mainly synthesized by two methods: direct polycondensation of lactic acid and ring-opening polymerization (ROP) of lactide. Additionally, it can also be obtained by an enzymatic process. Physicochemical properties of the polymer can change depending on the molecular weight, stereochemistry, polydispersity and crystallinity which can be adjusted by using different catalytic systems and stereoisomers of the monomer.

Lactic acid can be polymerized by the **condensation method** and mostly leads to the low molecular weight PLA.[57] The equilibrium of hydration/dehydration of the carboxyl and hydroxyl terminal groups makes high molecular PLA unfavorable, due to the difficulty to remove water from the reaction mixture. Ring/chain equilibrium between L-lactide and oligomeric PLA can also affect the polymerization degree (Scheme 1.1).[57] Polycondensation can proceed either in solution or melt/solid state. In both cases obtaining the higher molecular weight polymer requires harsh conditions like high temperature (~200 °C), low pressure (~5 mmHg) and long reaction times which can cause racemization.[58] Low molecular weight PLA obtained by this method can further couple

with chain extension reagents e.g., with isocyanates to increase the molecular weight of the polymer.[59]

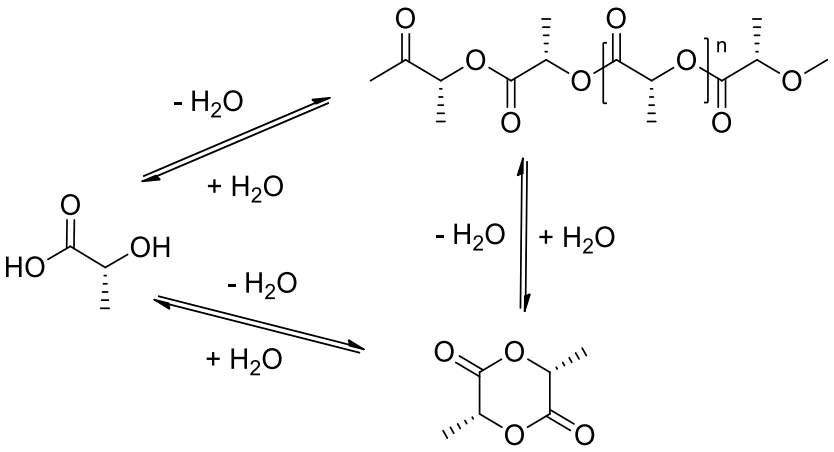

Scheme 1.1. Polycondensation equilibrium of PLA

Ring-opening polymerization (ROP) of lactide is a convenient method to obtain high molecular weight polymer with a narrow molecular weight distribution in relatively mild conditions. Lactide (3,6-dimethyl-1,4-dioxane-2,5-dione) is a chiral molecule with three stereo-isomers D-, L-, and meso-lactide which are produced by depolymerization of oligo(lactic acid) (Figure 1.5).[57,60]

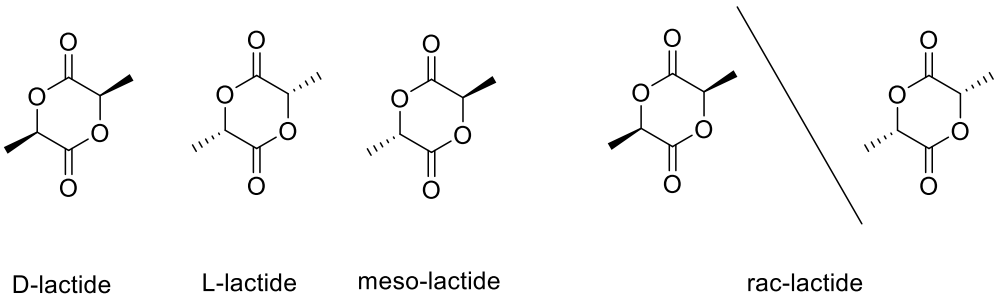

Figure 1.5. Stereo-isomers of lactide

Lactide polymerization was investigated in the literature with various catalytic systems proceeding through anionic, cationic or coordination-insertion mechanisms. General catalysts are metal powders or salts, Lewis acids or bases and organometallic compounds. Alkyl metals, metal halides, oxides, carboxylate and alkoxides are effective catalysts for the synthesis of high molecular weight PLA.[45,61,62]

The anionic mechanism requires nucleophilic attack of the initiator anion on the carbonyl group of the lactide, resulting in the cleavage of the carbonyl carbon and the endocyclic oxygen bond (Scheme 1.2). The negatively charged oxygen can in turn attack another monomer's carbonyl group and hence enable chain propagation.[63,64] Metal alkoxides are well-known anionic initiators for this type of mechanism. In the case of a very basic initiator, the monomer can be deprotonated, resulting in racemization. High temperature can also cause racemization with highly active catalysts. Additionally, inter- or intramolecular back biting reactions possibly stop the propagation of the chain.[45]

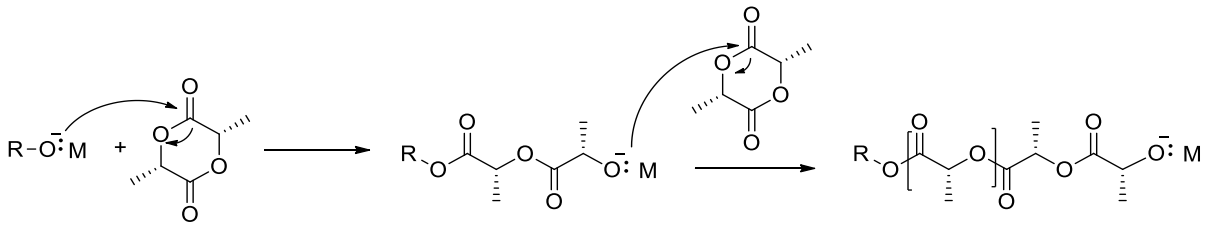

Scheme 1.2. Mechanism of the anionic ROP of L-lactide

Cationic ROP can be catalyzed by strong acids such as triethyloxonium tetrafluoroborate, borontrifluoride, and trifluoroacetic acid.[65] The initiation step of the polymerization starts with the alkylation or protonation of the exocyclic oxygen of one of the lactide carbonyls which results in a positively charged O-CH bond, followed by the nucleophilic attack of the initiating alcohol or the end group of the growing polymer chain (under acyl-oxygen cleavage) (Scheme 1.3). In cationic polymerization high temperature can cause racemization since the second monomer attacks at the chiral center of propagating chain. Racemization can be minimized at temperature <50 ˚C, but in this case, the rate of the reaction is very slow and does not yield high molecular weight polymers.[45,62,65]

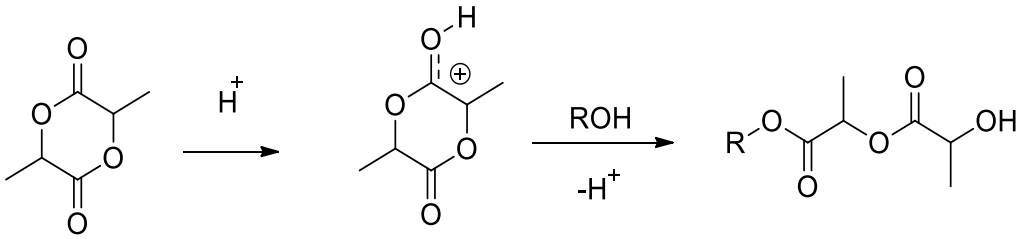

Scheme 1.3. Mechanism of the cationic ROP of lactide

Metal compounds with vacant d-orbitals catalyze the ROP of lactones *via* a coordination insertion mechanism.[57,62] The metal compound coordinates with one of the exocyclic oxygen of lactide resulting in the cleavage of the acyl oxygen bond. Propagation of the chain continues *via* coordination of the monomer to the active species followed by insertion of the monomer into the metal-oxygen bond (Scheme 1.4). Polymerization is catalyzed mostly by Sn, Zn, Mg, Zr or Ti metals complexes.[57,62,66] A well-known FDA approved catalyst for ROP of lactide is "tin (II) octoate" (stannous bis(2-ethylhexanoate) ($Sn(Oct)_2$) together with alcohol initiators for the industrial production of PLA.[67] Even though the polymerization is fast *via* this system, the high temperature requirements may encourage, inter- or intramolecular transesterification reactions. Aluminum isopropoxide ($Al(OiPr)_3$) is also a commonly employed catalyst for the ROP of lactide (Scheme 1.4).[68]

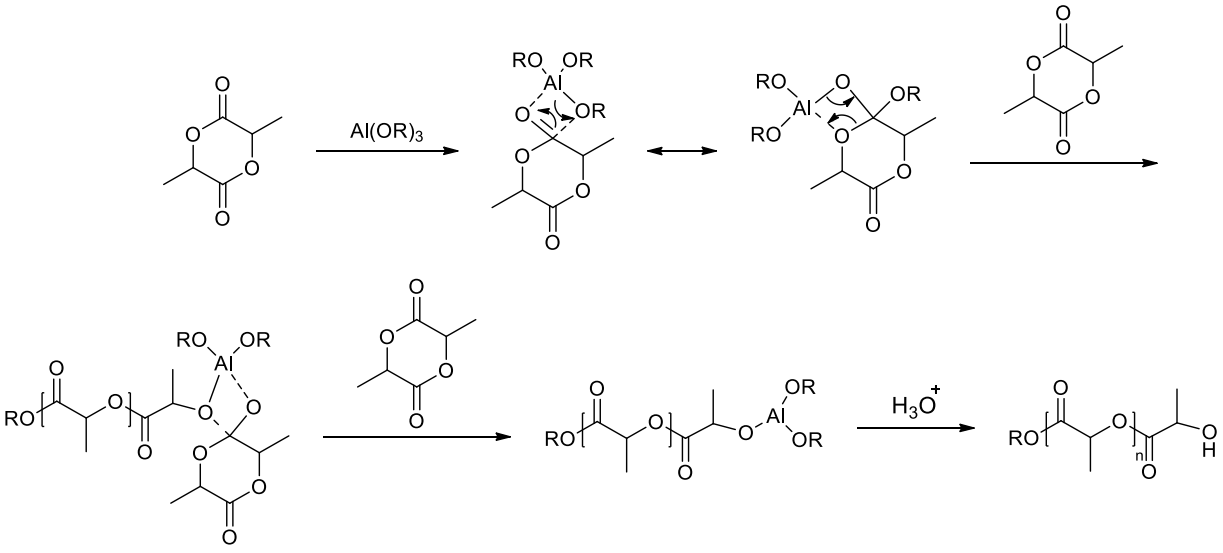

Scheme 1.4. Mechanism of coordination-insertion ROP of lactide by Al(OR) type catalysts

1.1.2. Poly(α-amino acid)s

Since amino acids are the building blocks of proteins, synthetic polymers derived from amino acids have been investigated by many researchers over the years.[69–73] Due to the versatility of the amino acids with different side chains, various polypeptides with different architectures (random, block or graft copolymers) can be designed.[74,75] Moreover, functionalities of the amino acid side chains or chain ends allow bio-conjugation with targeting agents, peptides, drugs, dyes, crosslinking agents etc. for biological applications.[76,77] These opportunities are increasing the demand for this type

of synthetic polymers which can be degraded by enzymes.[78–80] Polypeptides can adopt various secondary (α-helix, β-sheet), tertiary or quaternary structures.[81] Thus, they can assemble hierarchically into the micro- or nano-scale aggregates. Particularly self-assembled polypeptide amphiphilic block copolymers are potential materials for drug delivery applications.[82–85]

Polypeptides are mainly synthesized by two methods; solid phase peptide synthesis[86] (SPPS) and α-amino acid N-carboxyanhydride (NCA) polymerization.[87] SPPS is convenient for producing short peptide chains containing various amino acids, e.g native sequences or modifications of these; a maximum of about 50 amino acid residues can be coupled, limited by resin bound by-products and impurities. The chain length and sequence order is well-controlled but repeated coupling, protection and de-protection steps reduce the yield and increase cost.[86,88]

NCA polymerization is a more practical method for synthesis of large-scale synthetic homopeptides, random or block copolymers with high molecular weights using α-amino acid N-carboxyanhydride monomers.[89,90] ROP of NCA can be proceeded either by conventional methods using nucleophiles and base or by transition metal complexes.[70] The general polymerization route is shown in Scheme 1.5.

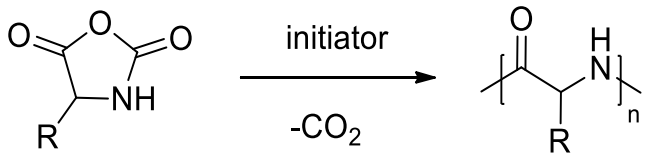

Scheme 1.5. General NCA polymerization

a. Conventional methods

Conventional NCA polymerization was initiated by nucleophiles or bases in solution.[89] Depending on the basic or nucleophilic degree of the initiator, polymerization proceeds by two different mechanisms;

- Normal amine mechanism (NAM)
- Activated monomer mechanism (AMM)

Normal amine mechanism (NAM) is a nucleophilic ROP where polymer chains grow linearly with monomer conversion. In the absence of side reactions, polymerization

proceeds as shown in Scheme 1.6. Common initiators are primary amines or more commonly secondary amines or alcohols. However, obtaining well-defined high molecular weight polypeptides with low polydispersity index is problematic *via* this route because of the difficulties associated with reactivity control over the chain ends.[88,89]

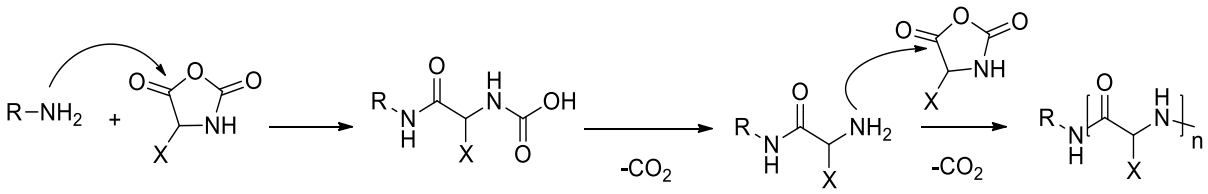

Scheme 1.6. Normal amine mechanism of ROP of NCA

Activated monomer mechanism (AMM) proceeds *via* the deprotonation of NCA monomer by the initiator. The deprotonated species then acts as a nucleophile and initiates chain growth (Scheme 1.7). Initiators more basic than nucleophilic such as metal alkoxides or tertiary amines preferentially proceed *via* AMM. The critical point here is the high polydispersity index of the polymer due to the slow initiation step; however, relatively high molecular weight polypeptides can be produced.[88,89]

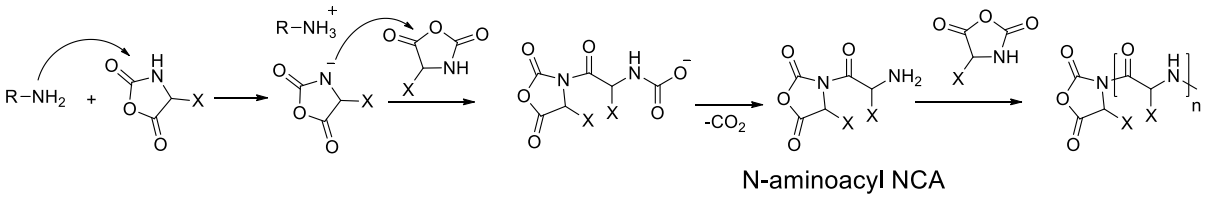

Scheme 1.7. Activated monomer mechanism of ROP of NCA

NAM and AMM are mutually competitive, which means that polymerization can shuttle between the two mechanisms.[88,91] If the polymerization proceeds only *via* the amine mechanism, the C-terminal of the polymer could be functionalized to 100% with the initiating amine's functionality; if the activated monomer mechanism is dominant, C-terminal ends of the polymer cannot be functionalized by the amine initiator, as activated NCA monomer initiates chain growth (Scheme 1.7). Therefore, NCA polymerization commonly suffers from lack of control over the chain end functionality, causing problems for the preparation of hybrid materials.[38] Another issue is the potential heterogeneity

with respect to the growing polymer chain. When the initiator reacts with NCA monomer, it forms the NCA anion and carbamate, while the primary amine remains present in the environment. These three species can form structurally different polymer chains causing heterogeneity and reducing control over the chain end functionality. Additional chlorinated impurities such as traces of acids, acid chlorides or isocyanates, e.g., residuals from monomer preparation, can quench growing polymer chain. Furthermore, water can act as a chain transfer agent or initiator as well. To overcome these side reactions, different catalytic systems were investigated for the polymerization of NCAs.[75,89] There are important studies in the literature concerned with improving the normal amine mechanism by suppressing the activated monomer approach.[38,92,93] NAM is critically important due to the allowance of direct C-terminal modification of the polypeptide chain and results in a polymer with free N-terminus. These free amino groups can be modified with functional moieties or can be used as an initiator for further polymerizations.[91,94–96]

Schlaad et al.,[97] developed polymerization of NCA with primary amine hydrochloride salts to avoid the formation of NCA anion. The ammonium-amine system is an equilibrium-controlled approach to suppress the AMM pathway. The HCl salt of initiating amine, which is less nucleophilic than the parent amine, stops the reaction after single NCA insertion *via* the formation of ammonium chloride (Scheme 1.8). The equilibrium between amine and HCl salt is skewed towards the dominant ammonium species, stopping the chain ends to participate in side reactions. In acidic conditions, NCA anions are protonated, suppressing the AMM partway and thus polypeptides were obtained by that method with low PDI values (<1.03).[97]

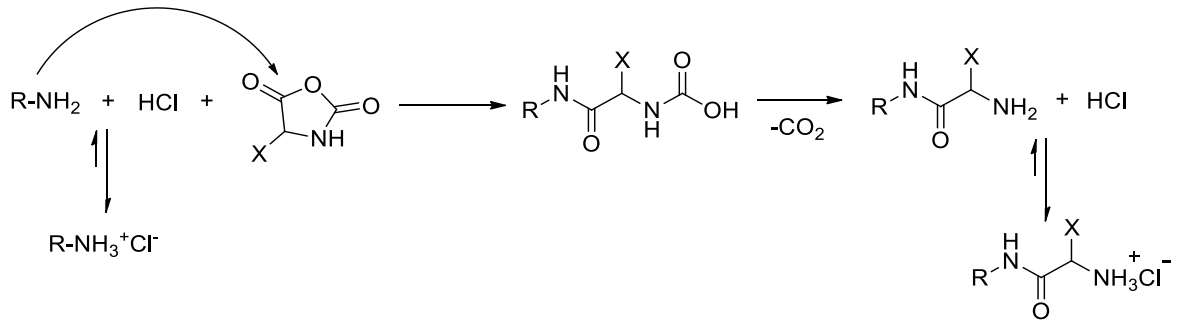

Scheme 1.8. Use of primary amine HCl salts as initiator for NCA polymerization

In 2004, Hadjichristidis et al.[91,92] investigated "High Vacuum Techniques" to improve the degree of control for NCA polymerization. This technique is based on the purification of

solvent and initiator under high vacuum conditions. In their work, γ-benzyl-L-glutamic acid NCA and ε-benzyloxycarbonyl-L-lysine NCA could be polymerized with a living character.[91,92]

Giani et al.[98] studied the polymerization of ε-trifluoroacetyl-L-lysine NCA in DMF as a function of temperature (from RT to 0 ˚C) under atmospheric pressure. The polymer end groups were analyzed by nonaqueous capillary electrophoresis to detect the living (-NH_2) and dead (carboxylate and formyl) chain ends (Scheme 1.9). With polymerizations conducted at 20 ˚C, the proportion of dead chains was around 78%. When the polymerization temperature was reduced to 0 ˚C, 99% of the chain ends were found as living chain ends. It was hence confirmed that low temperature reduces the amount of side reactions significantly and polymerization proceeds with a more "living" character.[98] In recent years, hexamethyldisilazanes (HMDS) were investigated for NCA polymerizations and produced narrowly distributed polypeptides ($M_w/M_n < 1.2$).[99] Cheng et al.[100] reported the polymerization of γ-benzyl-L-glutamic acid NCA by secondary amine HMDS, giving polypeptides with high yields and low heterogeneity index.

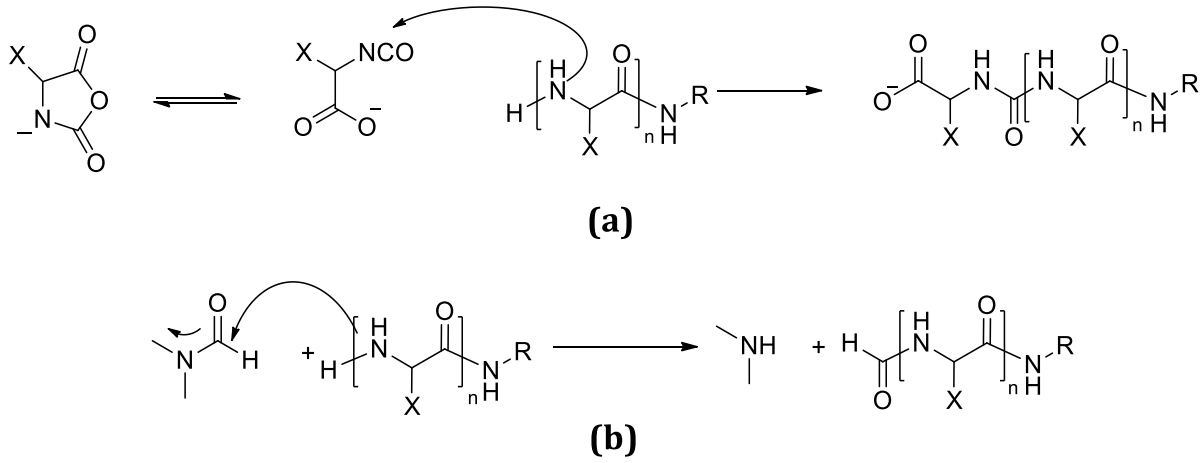

Scheme 1.9. Chain termination by (a) NCA anion (b) solvent DMF

b. Transition metal initiators

Besides the NAM or AMM, NCA of amino acids can be polymerized with the help of transition metal complexes. Zero valent $(PMe_3)_4Co$ and bpyNi(COD) (bpy=2,2'-bipyridil and COD=1,5-cyclooctadiene) complexes were developed for the living polymerization of

NCAs to produce high molecular weight polypeptides by Deming et al.[101–103] The resulting polymers are purified from the metal ions through precipitation or dialysis. With this mechanism, the metal forms metallocyclic complexes with NCA monomers *via* oxidative addition across the anhydride bond of NCAs. Addition of the second NCA monomer forms six-membered amido-alkyl metallaocycles and further interaction with NCA monomer leads to the formation of five-membered amido-amidate metallocycles which forms then the free chain end *via* proton migration (Scheme 1.10). By this method, polymers were obtained with molecular weights in the range of $500 < M_n < 500000$ g/mol with a narrow polydispersity (< 1.2).[101,102] Even though the molecular weight is controllable, this method does not allow C-terminal functionalization of the polypeptide chain because the *in-situ* formation of the propagating species is formed by the NCA monomer itself. To achieve C-terminal modification, the same research group developed a procedure for preparing functional initiators with allyloxycarbonylaminoamides and amido-amidate metallacycles which yield polypeptides with narrow polydispersity and known C-terminal end groups.[104]

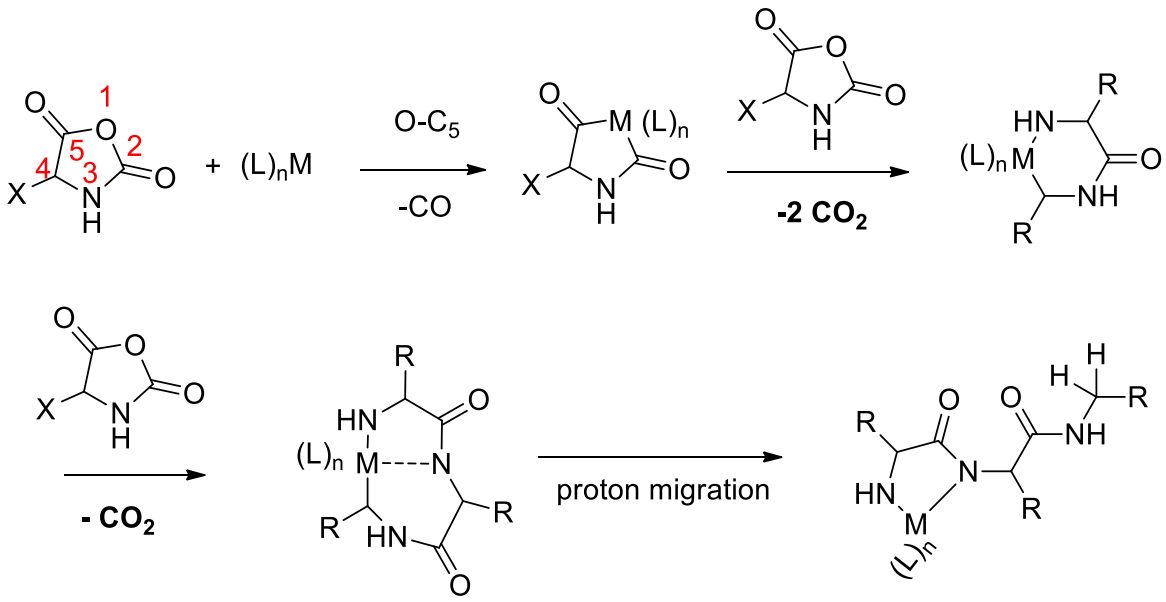

Scheme 1.10. Mechanism of transition metal initiated ROP of NCA

1.1.3. Pseudo-poly(amino acid)s

In contrast to poly(amino acid)s, where amino acids are linked through amide bonds, pseudo-poly(amino acid)s are structural analogues where naturally occurring amino acids are linked together by "non-amide" linkages. Polymeric backbones can include ester, urethane, carbonate or iminocarbonate linkages.[12,105] Kohn et al. first introduced this new family of polymers in 1984 which were a polyester from N-protected trans-4-hydroxy-L-pyroline[31] (Scheme 1.11) and poly(iminocarbonate) from tyrosine dipeptide.[33]

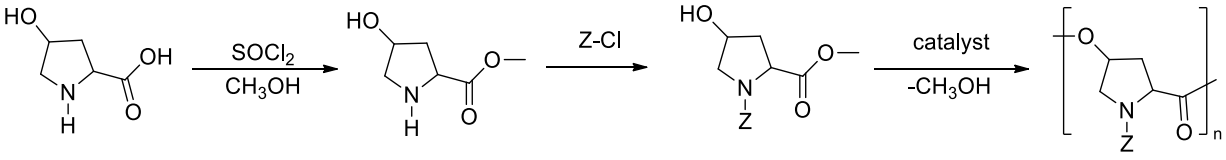

Scheme 1.11. Synthesis of N-protected poly(trans-4-hydroxy-L-pyroline)

This approach can be applied to serine, threonine, cysteine, glutamic acid and lysine as well. Scheme 1.12, demonstrates the synthesis of poly(amide carbonate) polymers.[106] Using dipeptides as monomeric starting materials, additional pseudopoly(amino acid)s can be obtained; hydroxyproline-derived polyesters, tyrosine derived poly(iminocarbonates) and polycarbonates represent specific examples for this type of polymers.

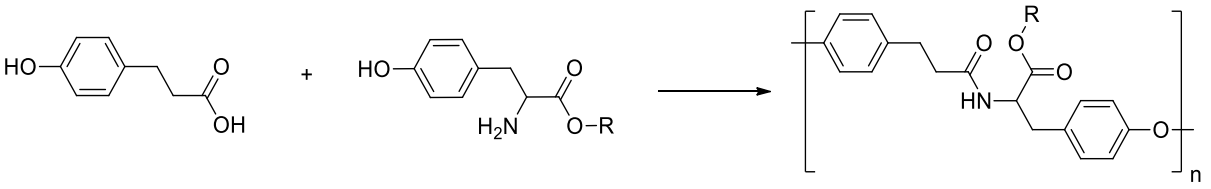

Scheme 1.12. Poly(amide carbonate) derived from desaminotyrosine and tyrosine alkyl esters

The development of pseudo-poly(amino acid)s allows to eliminate some disadvantages stemming from the usage of conventional poly(α-amino acid)s. The strong inter-chain hydrogen bonding, for example, results in secondary structures and often decreases the solubility of the materials and requires higher processing temperatures. A further issue is the antigenicity of polymers containing three or more amino acids which limits their

utilization in biomedical applications.[1,12] In the case of backbone modified pseudo-poly(amino acid)s all or the half of the amide bonds are replaced with other linkages which have a much lower tendency to hydrogen bonding leading to better processability and generally a loss of crystallinity. For example, tyrosine derived polycarbonates are high strength materials that are promising for the formulation of degradable orthopedic implants. In 2012, tyrosine derived pseudo-poly(amino acid), were used in some FDA approved devices.[2,105]

Serine is a prominent motive in the synthesis of pseudo-poly(amino acid)s. The hydroxyl functionality on the side chain leads to the formation of hydrolysable poly(α-ester)s. Two methods have been developed for the synthesis of pseudo-serine polymers over the years; polycondensation of N-protected serine and ROP of N-protected serine lactone (Scheme 1.13).[34,35]

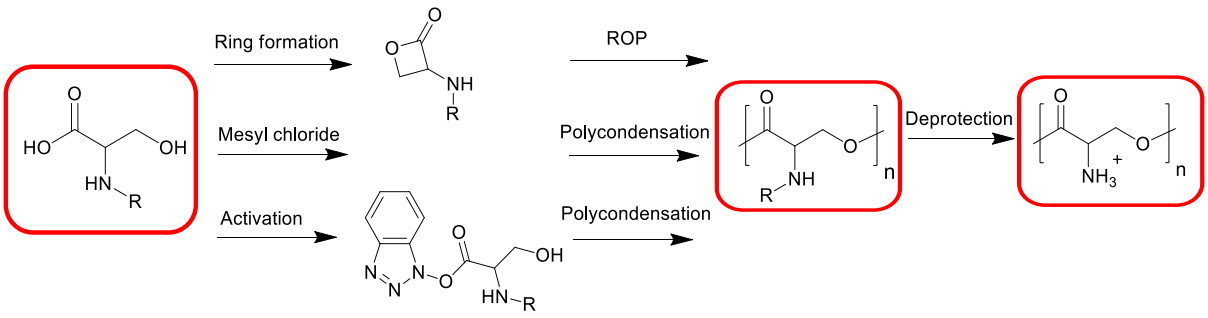

Scheme 1.13. Polymerization routes for amine protected serine monomers

Kohn et al.[107] reported the synthesis of oligomeric poly(N-Z-serine ester) from N-Z-serine by using 1-hydroxybenzotriazole (HOBt) in the presence of N,N'-dicyclohexylcarbodiimide (DCC). The DCC/DMAP catalytic system also produced oligomeric serine copolymers.[108] Furthermore Balme et al.[109] conducted the condensation polymerization of N-Z-serine in the presence of mesylchloride.

ROP of N-protected serine lactone is a convenient method to obtain high molecular weight polymers. Kohn et al.[110] first conducted ROP of N-Z-L-serine-β-lactone with tetraethylammonium benzoate. Spassky et al.[35] synthesized poly(serine ester) for the first time through ROP of N-trityl-serine lactone with tetrabutylammonium acetate as initiator. Likewise, Zhou et al.[34] reported the synthesis of poly(N-Z-serine lactone) and poly(N-boc-serine lactone) using tetraethylammonium benzoate by ROP. These polymerizations are limited by their long reaction times (several days) and termination reactions between the

carboxylate group by the α-hydrogen atoms of the β-lactone prevent the growth of the polymer chain.[111] Later on, in 2013, Wei et al.[112] synthesized poly(serine ester) and PEG-*b*-poly(serine ester) in a very rapid, controlled ROP of NTSL with $ZnEt_2$ as catalyst. Poly(ε-caprolactone-*co*-serine lactone) statistical copolymers were also reported through the same method.[113]

1.2. Amphiphilic Block Copolymers

Amphiphilic block copolymers are a type of block copolymers where a solvophilic block is chemically tethered to a solvophobic block.[84,114] The two immiscible blocks undergo micro-phase separation when placed in solution. In case of a polar/aqueous continuous phase, micro-phase separation leads to the self-assembly of nano-sized aggregates with a hydrophobic core and hydrophilic corona.[115,116] This unique aggregation behavior makes them attractive for drug delivery applications.[16,117–120] Diblock copolymers adopt different morphologies such as planar bilayers, micelles or vesicles (polymersomes).[121] The identity of the nano-structure is dictated by the structural curvature and environmental factors such as solvent, temperature and ionic strength (Figure 1.6).[122] In order to reduce the local frustration of the two immiscible blocks, the supramolecular assembly adopts a specific structural curvature that depends on the identity and volume fraction of each polymeric block.[122] Israelachvili et al.[123] developed the model to predict the shape of the aggregates by correlating the molecular curvature with the dimensionless packing parameter (p) (see Table 1-1). (v is hydrophobic volume, a is interfacial area, l is hydrophobic chain length).

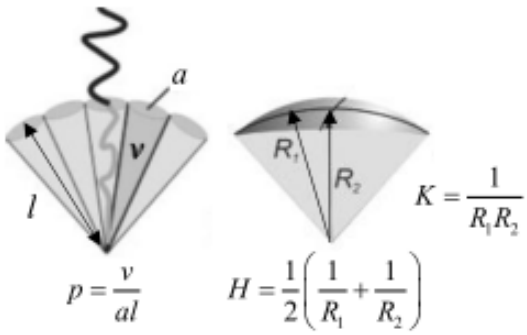

Figure 1.6. Amphiphile shape in terms of molecular packing parameter (p)[122]

Nevertheless, the packing parameter alone does not suffice to accurately predict the supramolecular structure of the material because it is based solely on geometrical aspects. Disher and Eisenberg presented mass or volume fractions of the hydrophilic part of the block copolymer (*f*) as a definition for the prediction of the morphology.[124]

Table 1-1. Type of structure estimated by packing parameter[124,125]

Shape	Packing parameter (p)	Hydrophilic fraction[a] (f)
Spherical micelle	p <1/3	f=0.55-0.70
Cylindrical micelle	1/3<p<1/2	f=0.45-0.55
Vesicle	1/2<p<1	f=0.10-0.40

a Hydrophilic fraction of the block copolymers either mass or volume ratios

Aliphatic polyesters produced by ROP of lactides or lactones are commonly used materials for pharmaceutical applications.[13,60,76] PLA random or block copolymers with various cyclic lactones such as glycolide (GA)[25,26], β-butyrolactone (β-BL)[126], ε-caprolactone (ε-CL)[127], and 1,5-dioxepan-2-one (DXO)[128] are known drug delivery vehicles (Figure 1.7). Dexon and Vicryl are the trade names of polyglycolide and poly[(L-lactide (8%)-*co*-glycolide (92%)] respectively for the application as resorbable sutures.[129] For obtaining the block copolymers, aliphatic polyester pre-polymers are generally used as macro-initiators. For example, poly(ε-caprolactone) (PCL) pre-polymers were prepared by using ethanol initiator with $Sn(Oct)_2$. The resulting polymer was then used as initiator for lactide polymerization, resulting in the block copolymer of PCL-*b*-PLA.[130]

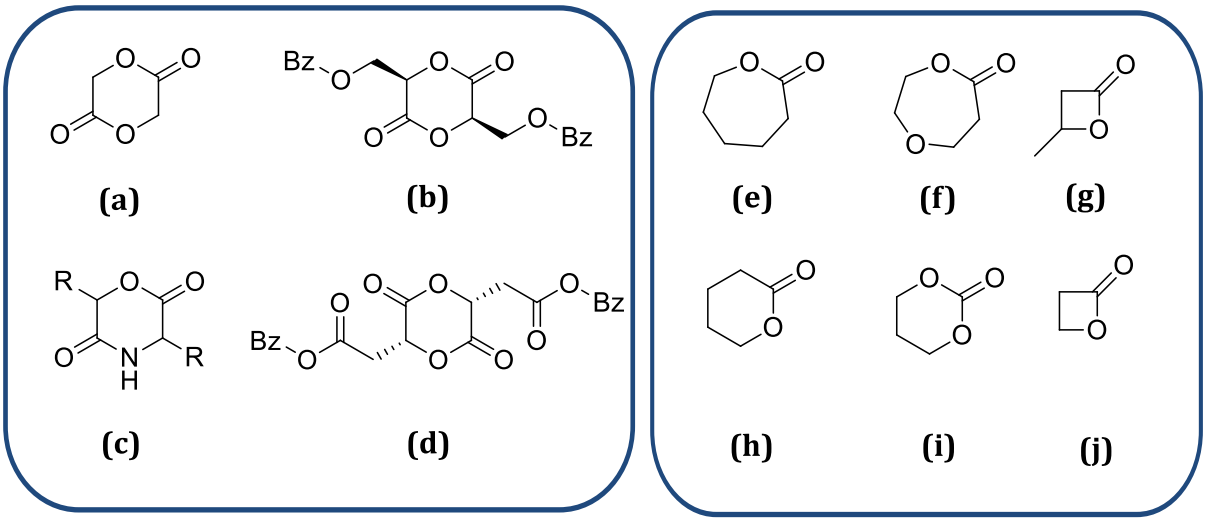

Figure 1.7. Structure of different type of cyclic co-monomers (a) glycolide (b,d) functional glycolides ((1,4)dioxane-2,5-dione skeleton) (c) functional esteramide (morpholine-2,5-dione skeleton) (e) ε-caprolactone (f) 1,5-dioxepan-2-one (g) β-butyrolactone (h) δ-valerolactone (i) 1,3-dioxan-2-one (j) β-propiolactone

Poly(ethylene glycol) (PEG) is an FDA approved, hydrophilic, nonionic polymer which prolongs the blood circulation time of the nanocarrier and diminishes its reticuloendothelial system uptake.[76] Therefore, it is one of the most widely used materials for biological applications.[76] For example, mono hydroxyl end functional PEG can be used to initiate the ROP of lactide to yield PEG-*b*-PLLA amphiphilic block copolymer.[131] Similarly, double –OH functional PEG can be deployed for the synthesis of PLLA-PEG-PLLA triblock copolymers.[132] These amphiphilic copolymers readily form core-shell type micelles in water, with the hydrophobic PLA and hydrophilic PEG segments in the core and shell, respectively. The one major drawback in using PEG is the lack of functionality which offers no opportunity for further bio-conjugation.[132]

Hydrophilic (meth)acrylate monomers can be incorporated with PLA through controlled radical polymerization (CRP) techniques, resulting in functional polymers with narrow molecular weight distribution with various architectures like block, gradient, graft, hyperbranched, and star copolymers.[76] PLA-*b*-poly(2-methacryloyloxyethyl phosphorylcholine), for example, was synthesized with ATRP and self-assembled block copolymer aggregates around 100-160 nm were obtained.[133] The –OH functional RAFT agents, 2-[N-(2-Hydroxyethyl)carbamyl]prop-2-yl dithiobenzoate was synthesized and

utilized for the synthesis of thermo- responsive PLA-*b*-poly(N-isopropylacrylamide-*co*-N,N-dimethylacrylamide) (P(NIPAM-*co*-DMAm)).[134]

Polypeptide-polypeptide block copolymers represent a commonly studied amphiphilic copolymer class in literature.[37,69–71,135,136] Polylysine and polyglutamic acid block copolymers with various hydrophobic amino acid NCA monomers were investigated by sequential NCA polymerizations, yielding amphiphilic block copolymers with various morphologies from micelles to vesicles. Additionally polypeptide copolymers were used as a stabilizer of nanoparticulate systems in emulsions.[69,136] Poly(α-amino acid) block copolymers with PLA have also enjoyed considerable interest by several groups. For example, PLA with -NH_2 end groups was employed for the polymerization of α-amino acids. The subsequent removal of the side protecting groups of the polypeptide resulted in an PLA-*b*-poly(aspartic acid) amphiphilic copolymers (Scheme 1.14) that formed core/shell type biodegradable micelles with a diameter of <50 nm.[137]

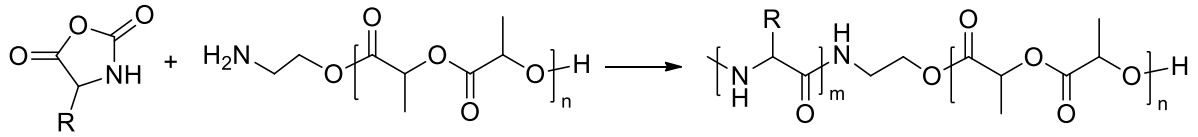

Scheme 1.14. Preparation of PLA-*b*-poly(aspartic acid)

For the synthesis of PEG-*b*-PLA-*b*-poly(L-glutamic acid) (PGlu) triblock copolymers, NH_2-terminated PEG-*b*-PLA, which in turn was prepared by ROP of lactide in the presence of PEG, was utilized.[138] A similar approach has resulted in PLA-*b*-PGlu-*b*-PLA triblock copolymers. The pendant -COOH groups of the triblock copolymer were further modified with RGD peptide for targeted drug delivery applications.[138,139] PEG-*b*-PLA-*b*- poly(L-lysine) and PLA-*b*-poly(L-cysteine) block copolymers were also reported by Jing et al.[6,140] As an alternative the sequential block copolymer formations, PLA block copolymers were obtained *via* end group coupling reactions in literature. An example includes the synthesis of PLGA-*b*-PGlu by the carbodiimide coupling reaction of NH_2-terminated PGlu with COOH-terminated PLGA in the presence of 1-ethyl-(3-dimethylaminopropyl) carbodiimide (EDC) in water. The COOH-terminated PLGA was prepared through the reaction of OH-terminated PLGA with succinic anhydride. These pH responsive

amphiphilic block copolymers exhibited morphologies varying from disordered forms through micelles, and further to vesicles as pH increased from 4 to 10.[141] PLA-*b*-PGlu was prepared by coupling reaction of OH-terminated PLA with NH_2-terminated PGlu in the presence of N,N-carbonyldiimidazole. The resulting amphiphilic block copolymers self-assembled to form micellar NPs.[142]

1.3. Nanocarrier Formation

Polymer-based nanocarriers are colloidal nano-sized particles in the range of 1-1000 nm. These nano-objects exist in various morphologies such as micelles, polymersomes and nanoparticles. They can be prepared mainly via two approaches, i.e. self-assembly of pre-formed polymers in aqueous solutions or by different types of emulsion polymerizations.[143]

1.3.1. Aqueous-based Self-assembly of Amphiphilic Block Copolymers

Polymeric micelles or polymersomes are obtained by the self-assembly of amphiphilic block copolymers in aqueous solutions. In the micellar case, the aggregated hydrophobic block forms a core which is solubilized by the hydrophilic corona. The assembly of such structures is under thermodynamic control and occurs only above a characteristic critical micelle concentration (CMC), below which micelles are disassembled. Polymersomes are a three-dimensional organization of polymeric membranes. A double layer of amphiphilic block copolymers with the hydrophobic block entangled on the inside and the hydrophilic block forming a double brush folds onto itself to form vesicles.[117,144]

Numerous techniques can be used for the preparation of self-assembled amphiphilic block copolymers: direct dissolution, dialysis, solvent evaporation, nanoprecipitation, thin-film formation, electroformation, microfluidic technology. The appropriate method is dictated by the structure of the copolymer. For example, if the polymer is directly soluble in water, direct dissolution method is straightforward, clean and fast under vigorous stirring. Polymersomes from the poly(ε-caprolactone)-*b*-poly(2-aminoethyl-methacrylate), for example can be prepared in water *via* this method.[145]

Dialysis and solvent evaporation methods are solvent switch approaches, applicable if the polymer is not soluble directly in water. In the dialysis method, dissolved polymer in water-miscible organic solvents are dialyzed against water to slowly diffuse and replace the organic solvent.[146] In the solvent evaporation method, the polymer is dissolved in organic solvent, mixed with water under vigorous stirring, after which organic phase is removed by evaporation, dialysis or ultrafiltration.[147] For the nanoprecipitation technique, the polymer is dissolved in organic solvent and mixed with another miscible solvent pair which is non-solvent for the polymer, resulting in a nanoprecipitation. Rapid nanoparticle formation was observed due to the Marangoni effect- interfacial interactions of solvent and non-solvent interface such as flow, diffusion and surface tension variations.[148] Thin-film formation is also based on the dissolution of copolymer in organic solvents and forming a thin film by solvent removal. The formed dry thin film is then hydrated with aqueous-based solutions under vigorous stirring.[149] Electroformation results in large polymersomes by spreading copolymers onto an electrode surface. By applying the electric current, a rehydration process occurs.[150] The microfluidic technology based on two approaches including the formation of a double emulsion template in micro-channels or the hydrodynamic flow- focusing in microfluidics.[151]

1.3.2. Emulsion Polymerizations

Emulsion polymerizations can proceed as suspension, miniemulsion and macroemulsion polymerization. Suspension polymerization is a heterogeneous and emulsifier free system.[152] In contrast, miniemulsion and macroemulsion systems are stabilized by emulsifiers and are hence, more stable.[153,154] Two aggregation phenomena are important to mention in the emulsion process: Coalescence and Ostwald ripening.[155] Coalescence is a fusion of the droplets by time and can be prevented through the use of surfactants for stabilization. Ostwald ripening is a diffusion process where smaller droplets diffuse through the continuous phase into larger ones and cannot be prevented by stabilizers. Only the addition of a hydrophobe to an O/W-emulsion or lipophobe to a W/O-emulsion can slow down of the Ostwald ripening.[155]

Polymerization in macroemulsions for free radical polymerization is given as an example in Figure 1.8.[156] The process starts with the formation of radical initiators in solution that

commence to react with a few non-emulsified monomer in dispersion. These oligomeric radicals diffuse into the monomeric micelles due to their higher surface area in comparison to the monomer droplets. By polymerization, monomer micelles grow larger and require more surfactant for their stabilization. Through such equilibrium, surfactant micelles continuously diffuse to the growing polymeric micelles. 5% of the monomers are polymerized in this stage and the polymerization rate reaches to the maximum. In the second stage, oligomeric radicals attack all the monomer micelles and monomers diffuse from the droplets to micelles continuously. This stage approaches around 50% conversion. In the third stage, there are no more monomer droplets in the continuous phase and polymerization runs via the monomers that still remain in the polymerizing micelles.[156,157] Well-dispersed polystyrene nanoparticles can be synthesized easily through this method.[158]

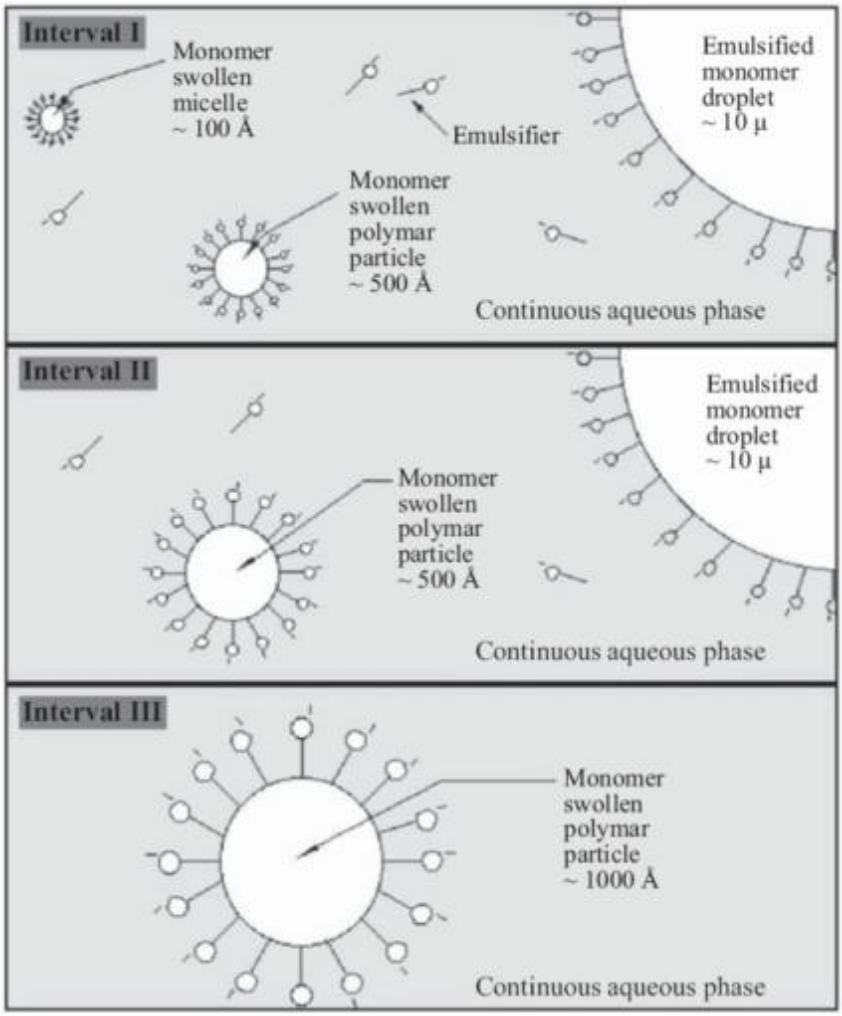

Figure 1.8. Macroemulsion polymerization[156]

Miniemulsion is used in the case of less soluble monomers to overcome the diffusion issue between solvent phases. In this approach radicals are directly dispersed in monomer droplets which are stabilized by emulsifiers and polymerization is carried out in these nanoreactors. Ultrasound or mechanical shearing is necessary for stabilization and co-stabilizer is further necessary to protect the small droplets against Ostwald ripening (Figure 1.9). Generally, highly soluble co-stabilizer in dispersed phase is used in the process in order to keep the monomer droplets more stable.[153,154,156,159]

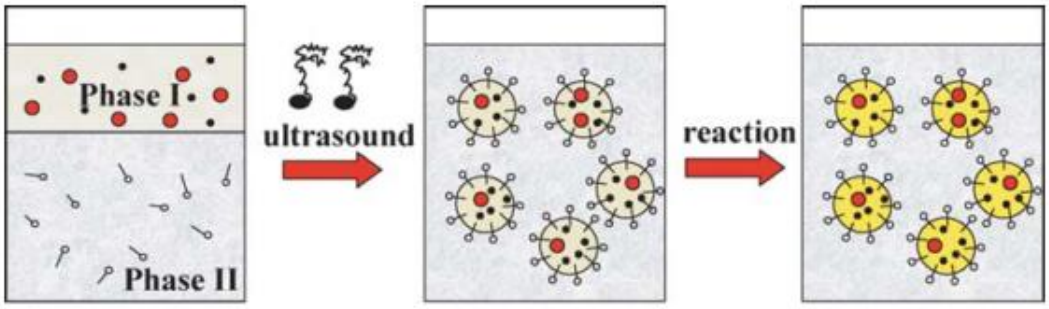

Figure 1.9. Miniemulsion polymerization[159]

In recent years, nonaqueous emulsion was developed for the formation of polymeric dispersions in the presence of water-sensitive components (acid chlorides, catalysts like NHCs) and reactions such as polyaddition and polycondensation (Figure 1.11).[160–164] Nonaqueous emulsion consists of two immiscible organic solvents, where one is dispersed and one is the continuous phase, for instance cyclohexane/acetonitrile or n-hexane/DMF and block copolymer as a stabilizer to reduce the interfacial tension. Nonaqueous emulsion systems consisting of DMF/n-hexane and acetonitrile/cyclohexane were first studied by Riess et al.[165–167] Emulsions of various solvents were investigated by Cameron et al.[168] later on. Antonietti et al.[169] studied the first polymerization in water-free emulsions by using the low molecular weight surfactant sodium dodecyl sulfate, SDS, nevertheless obtained heterogeneous particle distribution. The problem here was the insufficient stabilization efficiency of low molecular weight surfactants in nonaqueous emulsions due to the lower interfacial tension of these two immiscible organic solvents in comparison to the water-oil emulsions. Stabilization of nonaqueous emulsions can be achieved by using high molecular weight block copolymers which immediately forms the aggregates which are kinetically hampered to reach thermodynamic equilibrium.

Therefore, those polymers can sterically shield the droplets and form kinetically frozen aggregates.[170,171]

AB type block copolymers with controlled molecular weights and solubility properties are able to stabilize the nonaqueous emulsions. Poly(styrene)-*b*-poly(propylene oxide), poly(styrene)-*b*-poly(polyethylene oxide), and poly(methyl methacrylate)-*b*-poly(t-butylacrylate) are used for the stabilization of polar continuous phase dispersions. On the contrary, poly(styrene)-*b*-poly(dimethyl methacrylate), poly(styrene)-*b*-poly(methyl methacrylate), poly(styrene)-*b*-poly(ethylene propylene), poly(styrene)-*b*-poly(isoprene) (PS-*b*-PI) and poly(isoprene)-*b*-poly(methyl methacrylate) (PI-*b*-PMMA) are used to prepare dispersions with a non-polar continuous phase, for example, aliphatic hydrocarbons and silicone oil.[164] PI-*b*-PMMA copolymer was developed by Müller et al.[172], in which PI block stabilizes the continuous n-hexane or cyclohexane phase and the PMMA block stabilizes the dispersed DMF or acetonitrile phase. Different polymerizations like free radical, condensation, polyaddition or oxidative polymerizations were performed in this system.[161–163,173–177] Hansen solubility parameters plays important roles for designing these systems (Figure 1.10).[178] If solvent and polymer have the same solubility parameter, the polymer dissolves well. The Hansen solubility parameter (δ) consists of three major types of interactions which are dispersion interaction parameter (δ_D), permanent dipole-permanent dipole interaction parameter (δ_P) and hydrogen bonding interaction parameter (δ_H). The Equation is presented below;

$$\delta^2 = \delta_D^2 + \delta_P^2 + \delta_H^2$$

In Figure 1.10, δ of nonpolar and polar organic solvents and polymers were presented.

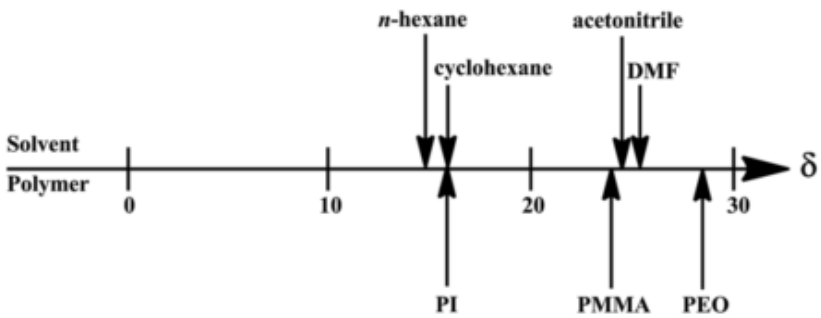

Figure 1.10. Solubility parameters[178]

In order to perform a polymerization in nonaqueous emulsion, at least one of the components; monomer, initiator or catalyst must be selectively soluble in the dispersed phase as the reaction should occur in the droplets.

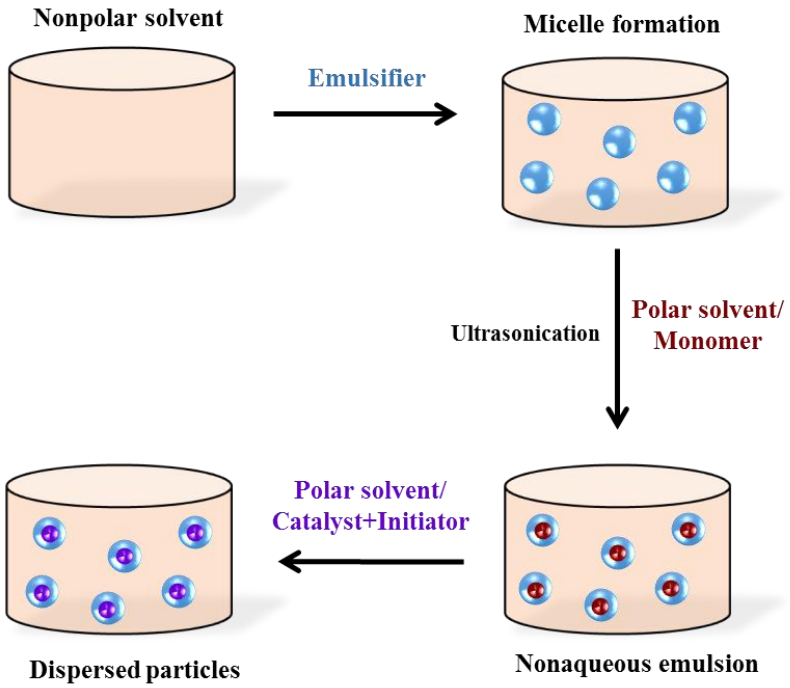

Figure 1.11. Nonaqueous emulsion polymerization

To form nonaqueous emulsion, amphiphilic block copolymer first disperse in continuous apolar phase to form micelles as it shown in Figure 1.11. The monomer is dissolved in the dispersed polar phase and added to the micellar solution followed by the dropwise addition of catalyst/initiator solution of the polar solvent. Polymerization occurs by diffusion of the catalyst/initiator into the droplets and polymer dispersion is obtained. Ultrasonication is a critical step for the homogenization of the droplets.[179]

CHAPTER 2

Motivation and Objectives

2. Motivation and Objectives

Design and development of nanocarriers with various morphologies like micelles, polymersomes, nanoparticles, *etc*. is an emerging topic in the pharmaceutical industry.[143,180] Engineered nanoparticle systems based on biocompatible/biodegradable polymers are one of the most promising candidates due to the great versatility and simplicity of synthesis methods, diverse nature, composition and properties of the materials.[2,3] The goal of this work is the synthesis of biocompatible, enzymatically or hydrolytically degradable nanocarriers and their application for drug delivery especially for cancer therapy and bioimaging. Also, the influence of the nanoparticles in marine environment should be investigated (Figure 2.1).

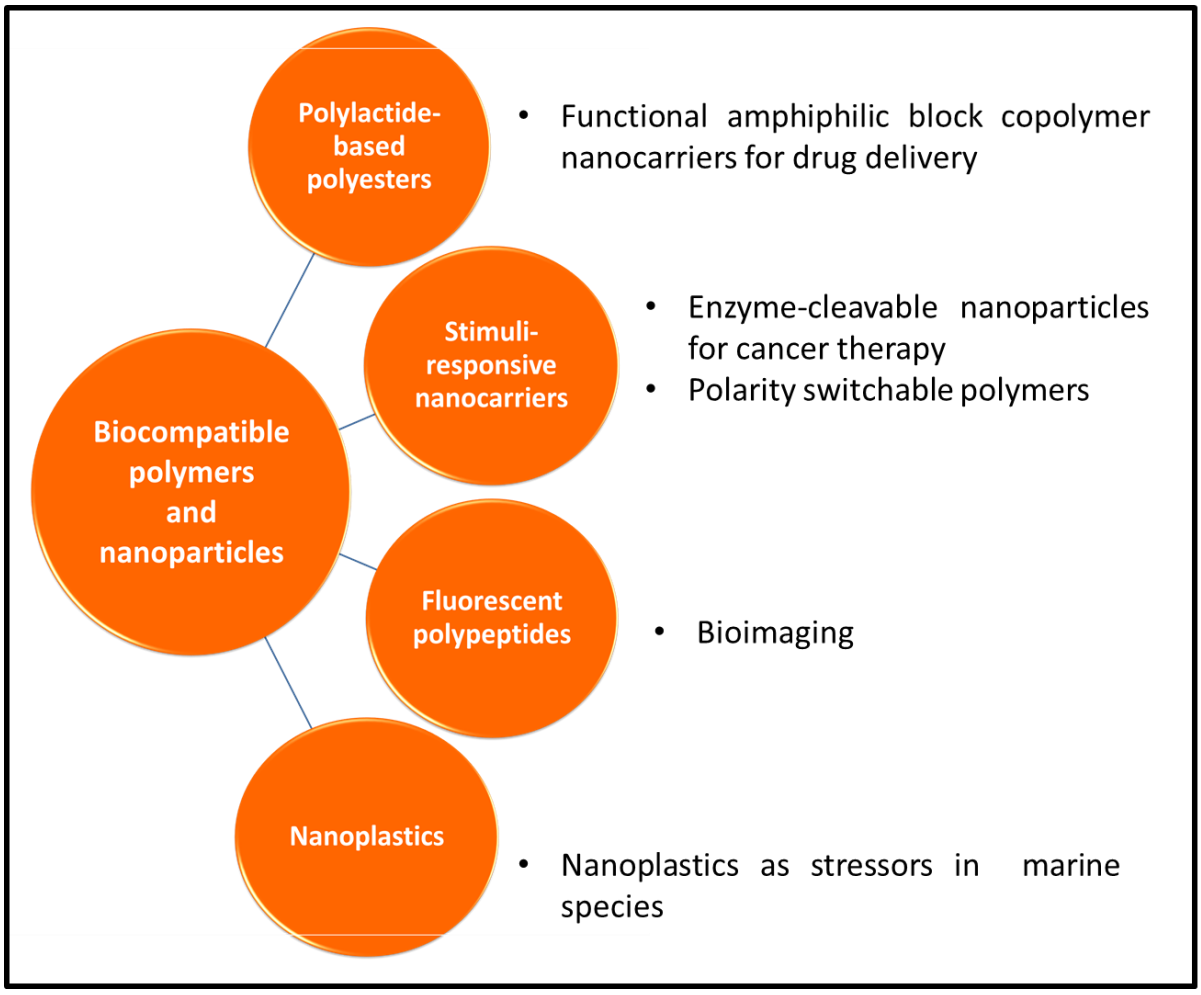

Figure 2.1. General overview of the goals

The main characteristics required for the efficient drug-carrying nanoparticles are:

- Biocompatibility,
- Appropriate carrier size within 50 and 250 nm,
- Stable encapsulation of drug,
- Favorable surface characteristics: hydrophilic corona or anchor groups for the specific recognition or modification with bioactive agents for targeted delivery.

To fulfill the above-mentioned characteristics, various platforms should be used for the fabrication of nanomaterials i.e., self-assembly of pre-synthesized amphiphilic block copolymers and emulsion or nonaqueous emulsion polymerization techniques.[143,156,160] The synthesis of polylactide-based amino-functional biocompatible and hydrolytically degradable polymers and their nanocarrier formation for drug delivery should be studied. Poly(L-Lactide) (PLLA) is a commonly utilized biomaterial, nevertheless, suffers from the lack of functionality and hydrophobicity, which causes the quick digestion of the particles by the mononuclear phagocyte system, resulting in lower drug efficiency *in vivo*.[57] Therefore, incorporation of reactive groups into PLLA is necessary either for better charge-induced interaction with living cells or further bio-conjugation with vitamins, carbohydrates, peptides and proteins, antibodies, aptamers, etc. for targeted delivery. Poly(L-lysine), for example, one of the widely used hydrophilic polymer in such fields because of the amino groups on the side chain offer a great potential for bio-conjugation, grafting or crosslinking. This cationic polymer is used as a nonviral gene delivery vehicle; however, intrinsic toxicity limits further utilization.[181] To circumvent such issues, a non-toxic equivalent copolymer of PLLA with a reactive amine in the side chain should be developed. In this respect, amino-functional poly(serine lactone) shall be considered as a non-toxic alternative to poly(L-lysine). Therefore, it should be investigated whether PLLA/poly(serine lactone) copolymer fulfills the aforementioned requirements of an effective drug delivery system as a cationic drug-nanocarrier. By the self-assembly of these amphiphilic block copolymers, ideal carrier size should be achieved simply through varying the absolute chain lengths and parameters of the particle preparation techniques. Additionally, crosslinking or grafting *via* amino groups would lead to novel materials for tissue engineering.

Furthermore, the focus should be the formation of fully biocompatible and enzyme degradable PLLA-copolymer nanoparticles in a single step by MMP-2 cleavable peptide

sequences using polarity switchable polypeptide emulsifiers for cancer therapy. The appliance of the nonaqueous emulsion as a platform for the synthesis of PLLA-based nanoparticle system for cancer therapy was previously shown in the work of Dorresteijn et al.[179] : MMP-2 cleavable peptide bearing PLLA copolymer nanoparticles were generated *via* nonaqueous emulsion polymerization using non-biocompatible PI-*b*-PEO block copolymer stabilizers. In such systems, formed polymeric particles in organic solvent should be transferred into water by another hydrophilic emulsifier for cell experiments. Nevertheless, this process is challenging and often can cause aggregation. Another technique described for particle transfer to avoid of corresponding challenges is introduction of photo-cleavable block copolymer stabilizers during the particle formation, which leads them phase reverse by polarity change of the surface and get particles through into the water.[182] Based on these studies, PLLA-based enzyme degradable nanoparticle systems stabilized by a biocompatible and polarity-switchable emulsifier are aimed to be developed. This shall be achieved *via* a nonaqueous emulsion platform with pyrene-modified polypeptide stabilizers. Thus, obtained tailor-made particles should be easily transferred into water for triggered drug release studies in cancer tissues. Further research should focus on the development of new synthetic strategies for designing the polypeptide-based photo-sensitive block copolymers. Polypeptides can be designed either by post-polymerization modification or functional monomer approach.[70] Post-polymerization modification is mostly challenging due to the stepwise reactions and purifications, and is not a suitable method in the presence of sensitive moieties e.g., peptides. Alternatively, the functional monomer path is more promising as side reactions from repeated steps can be eliminated. The critical point of this strategy is that the functionality of the NCA side chain should not interfere with the polymerization reaction of NCA. Therefore, the goal is the synthesis of novel pyrene chromophore bearing L-glutamic acid NCA monomer. Using various macro-initiators i.e., PEGs, specific degradable peptides, etc. for polymerizing this monomer should yield new types of biocompatible block copolymers. Using such bio-responsive block copolymers, both, core and shell modified enzymatically and photolytically degradable smart copolymers can be generated.

Apart from the aforementioned characteristics of nanocarriers for drug delivery, fluorescence-modified tools are required for the investigation of dynamic behavior of materials, tracking, monitoring the distribution and localization of the particles in cells or

tissues.[183,184] In general, particles can be labelled with fluorescent probes *via* physical encapsulation, however covalent bonding is preferred as non-leaking systems are obtained.[77] Another issue is to avoid the distribution of the labels on the surface of the nanocarrier. Thereby, the terminal modification of the polymer from the focal point should be considered. In case of the fluorescence dye is at the end of the polymers, nanoparticles for bio-imaging applications would be achievable. This shall be accomplished by NCA polymerization using specifically designed fluorescent initiators. L-lysine is a potential candidate for such polymerization due to the amino functionality and pH-responsive behavior. For tagging the polypeptide by precise number of fluorescent dyes, perylene imide derivatives can be considered as proper candidates due to their chemical and photo-stability, low toxicity, specific reactivity, and easy fine-tunability of optoelectronic properties.[185] It is also known from the literature that perylene imides have high molar extinction coefficients and fluorescence quantum yields.[185] Their absorption and emission maxima could be bathochromically shifted over 600 nm in the near infrared (NIR) region of the visible spectra by chemical modification which is crucial to avoid overlapping with the autofluorescence of biological tissues and materials.[186] Therefore, perylene imides are properly suitable for the labelling of nanocarriers for *in vivo* studies and in particularly specifically designed modified with alkylamino group perylene diimide (PDI-NH_2) selected to conduct the polymerization of amino acid NCAs. The introduction of PDI-NH_2 leads to the fluorescence tagged polypeptide which could precisely be modified with an adjusted number of probes. Such materials would be interesting as a pH sensor for monitoring the pH fluctuations in living systems due to their good water solubility, and long-term bright and stable fluorescence. Further investigations focus on the generation of micelle forming fluorescent amphiphilic block copolymers by sequential NCA polymerizations. The obtained amphiphilic copolymer should also be able to carry various charges to investigate the stability and cell uptake depending on the charge. Thereby, the formation of a fluorescent drug-nanocarriers shall be studied to give insights the potential utilization *in vitro* by Confocal Laser Scanning Microscopy.

Finally, the focus is on the formation of nanoplastics for the investigation of their possible health effects on marine species. Understanding the hazardous effects of the artificial nanoplastics is also a critical issue as environmental pollution poses a great threat for all living beings, particularly for the water ecosystem.[187,188] For such purposes,

polycarbonate and polystyrene nanoparticles as the most disposed of plastic wastes to nature should be selected as model compounds.[189,190] An extensive study of nanoparticle formation of poly(bisphenol A carbonate) and fluorescence-tagged polystyrene are going to be carried out for further biological investigation on marine species in cooperation with Dusan Palic et al. from Ludwig Maximilian University, Munich. Various particle dispersions by different polymerization routes like polycondensation as well as polyaddition reactions, oxidative and ring-opening polymerizations can be formed by nonaqueous emulsion system and shall be utilized also for the preparation of poly(bisphenol A carbonate) nanoparticles for desired applications. The straightforward emulsion polymerization method shall be accomplished for the generation of fluorescence-tagged nanoparticles for investigation of the response of the innate immune system of Fathead Minnow and possible future bioimaging studies *in vivo.*

CHAPTER 3

Polylactide-based Polyesters: Synthesis and Self-assembly Study

3. Polylactide-based Polyesters: Synthesis and Self-assembly Study

3.1. Introduction

Aliphatic polyesters are commonly used materials for biological and medical fields due to their biocompatibility and biodegradability.[143,191,192] Well-known polyesters utilized for drug and gene delivery or tissue engineering applications are polylactide[193] (PLA), polyglycolide[26] (PLGA), poly(ε-caprolactone)[194] (PCL) and their copolymers.[195,196] Among them, FDA approved poly(L-lactide) (PLLA) is low immunogenic, renewable and processable. However, brittleness, hydrophobicity and lack of functionality limits its utilization for biological applications.[61,57] Due to the hydrophobic PLLA, drug loaded nanoparticles are digested easily through the mononuclear phagocyte system, resulting in short circulation time in blood. Thus, drug efficiency is decreased *in vivo*. To increase the circulation time of the hydrophobic PLLA nanoparticles, surface of the PLLA can be functionalized with hydrophilic polymers either by surface modification or copolymerization method.[76] Latter approach, copolymerization is the more versatile route in order to obtain various, well-defined amphiphilic block copolymers by using hydrophilic building blocks such as PEGs, polypeptides, poly(α-amino acid)s, polysaccharides and poly(meth)acrylates.[44,57,61,76] Mostly CRP techniques and ROP are employed for the copolymerization because of the well controllability of these techniques and allowance to produce high molecular weight polymers (Section 1.1.1).

Linear amphiphilic block copolymers can self-assemble in aqueous medium to form core-shell like aggregates in different morphologies such as spherical or cylindrical micelles and vesicles depending on the chain lengths of the blocks.[197] In the case of PLLA-based amphiphilic systems, while the hydrophobic PLLA forms the core which is able to encapsulate the hydrophobic therapeutic agents in solution, hydrophilic corona provides the water dispersability as well as biocompatibility. Another critical purpose of the functionalization of PLLA is making the polymer capable of bio-conjugation for targeted delivery. By employing the comonomers with various reactive groups such as carboxylic acid (–COOH), amino (–NH_2) and hydroxyl (–OH), PLLA-block copolymers can be further modified with biomolecules such as:

- Biologically active small molecules like vitamins (e.g folic acid (B9) and biotin)[198,199], curcumin[200], selegilin[201] or selectin[202],
- Carbohydrates like galactose, lactose and mannose[203,204],
- Peptides or proteins like cell penetrating peptides[205] (CPPs, Tat, polyarginine, penetratin, transportan or nuclear localization sequences) or a special enzyme cleavable sequences like MMP type enzymes which are overexpressed in tumor tissues[206,207],
- Antibodies which are large Y shaped proteins, represent efficient ligands due to their high affinities[208],
- Aptamers: short single stranded DNA or RNA oligonucleotides that can bind specifically to small or large molecule targets.[209]

In this regard, poly(α-amino acid)s are used very often in combination with PLLA to design amphiphilic systems.[210,211] However, the main drawback of these polyamides is the strong hydrogen bonding which results in secondary structures that might limit the processability of the material. Additionally, the highly cationic derivatives of the polypeptides e.g., polylysine cause toxicity, therefore not suitable in biomedical applications. Consequently, the features listed below have to be considered for the selection of the hydrophilic block for designing the amphiphilic PLLA copolymers;

- Biocompatibility,
- Hydrophilicity,
- Hydrolytical degradability,
- Functionality

Pseudo-poly(amino acid)s, which are the backbone-modified structural isomers of the traditional poly(α-amino acid)s, are appropriate candidates to fulfill all these aforementioned requirements (Section 1.1.3).[212,213] In contrast to traditional poly(α-amino acid)s, these materials have lower tendency to hydrogen bonding and have been expected to accomplish the industrial and medical applications because of their great flexibility in designing a wide variety of polymers and compatibility with living systems.[32,76,106] In this context, serine is one of the applicable candidates for the formation of hydrolytically degradable and “amino-functional” pseudo-poly(amino acid)s as seen in

Scheme 3.1. Recently developed ring-opening techniques for lactone type serine monomers allow designing block copolymers by sequential polymerizations.[112,113]

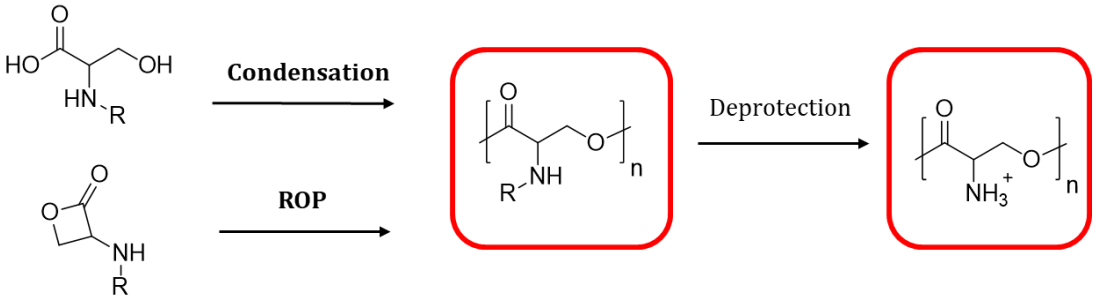

Scheme 3.1. Polymerization of N-protected serine

Herein, PLLA-based amino-functional amphiphilic block polyesters are aimed to be developed. In this respect, side chain amine-bearing poly(serine lactone) is considered as a hydrophilic block to develop non-toxic copolymer of PLLA. As previously discussed, nanocarriers obtained from such copolymers must be biocompatible, must have a carrier size within 50 and 250 nm, and further have a favorable surface characteristic such as hydrophilic corona or anchor groups for the specific recognition or modification. Since PLLA has excellent biocompatibility and mechanical properties,[61] the introduction of other requirements should be demonstrated by the incorporation of pseudo-poly(serine) to the system (Figure 3.1).

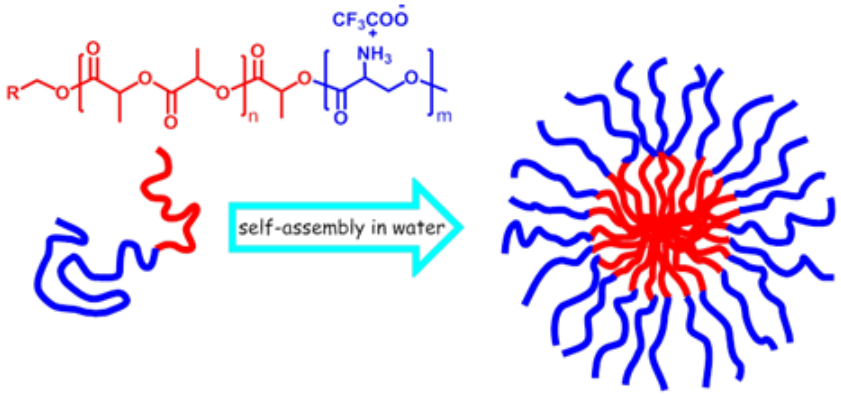

Figure 3.1. Self-assembly of the amphiphilic diblock copolymer

3.2. Results and Discussion

Micelle forming poly(L-lactide)-*block*-poly(L-serine lactone) (PLLA-*b*-PLSL) amphiphilic copolymers are synthesized by sequential ROP of L-lactide and N-trityl L-serine lactone with two different catalytic systems: N-heterocyclic carbene, 1,3-bis(2,4,6-trimethylphenyl)-2-imidazolidinylidene (SIMes) and $ZnEt_2$, respectively. Cleavage of the protecting group leads to the well-defined amino-functional amphiphilic block copolymers (Scheme 3.2).

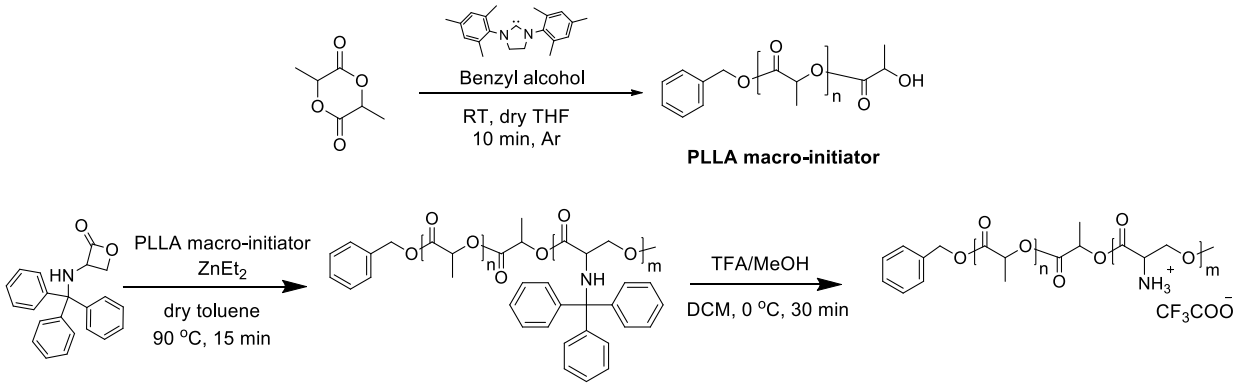

Scheme 3.2. Synthetic route for PLLA-*b*-PLSL block copolymers

3.2.1. Synthesis of N-trityl serine lactone

First of all, preparation of the lactone type serine monomer is performed for the following block copolymer study. N-trityl serine lactone (NTSL) was synthesized in two steps according to the Howell et al.[214] In the first step, the natural amino acid L-serine was used as a starting material. The amine groups were protected with trityl and followed by intra-molecular lactonization by using benzotriazol-1-yloxy-tris(dimethylamino)phosphonium hexafluorophosphate (BOP) as a coupling agent to yield the desired lactone.

To avoid the tritylation of hydroxyl and carboxyl groups of the serine, trimethylsilylchloride (TMS-Cl) was used to protect –OH and –COOH groups, followed by protection of amine with trityl. Cleavage of the TMS led to the formation of amine protected serine monomer N-trityl serine, with an overall of 52% (Scheme 3.3).

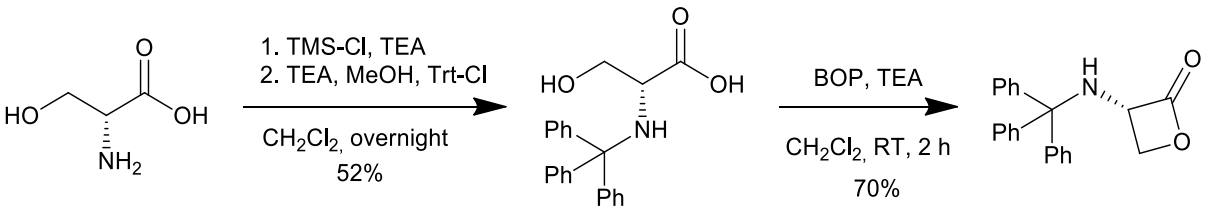

Scheme 3.3. Synthesis of N-trityl serine lactone (NTSL) monomer

In the second step, NTSL was synthesized by intramolecular cyclization of N-trityl serine for two hours at RT by using BOP as a reagent. The resulting monomer was purified (>98) by flash column chromatography with 70% yield and characterized by NMR spectroscopy. The ^{1}H-NMR spectrum and corresponding signal assignments were consistent with the expected structure of NTSL (Figure 3.2). Structure was confirmed by ^{13}C-NMR spectroscopy as well (Appendix D: Supporting Information).

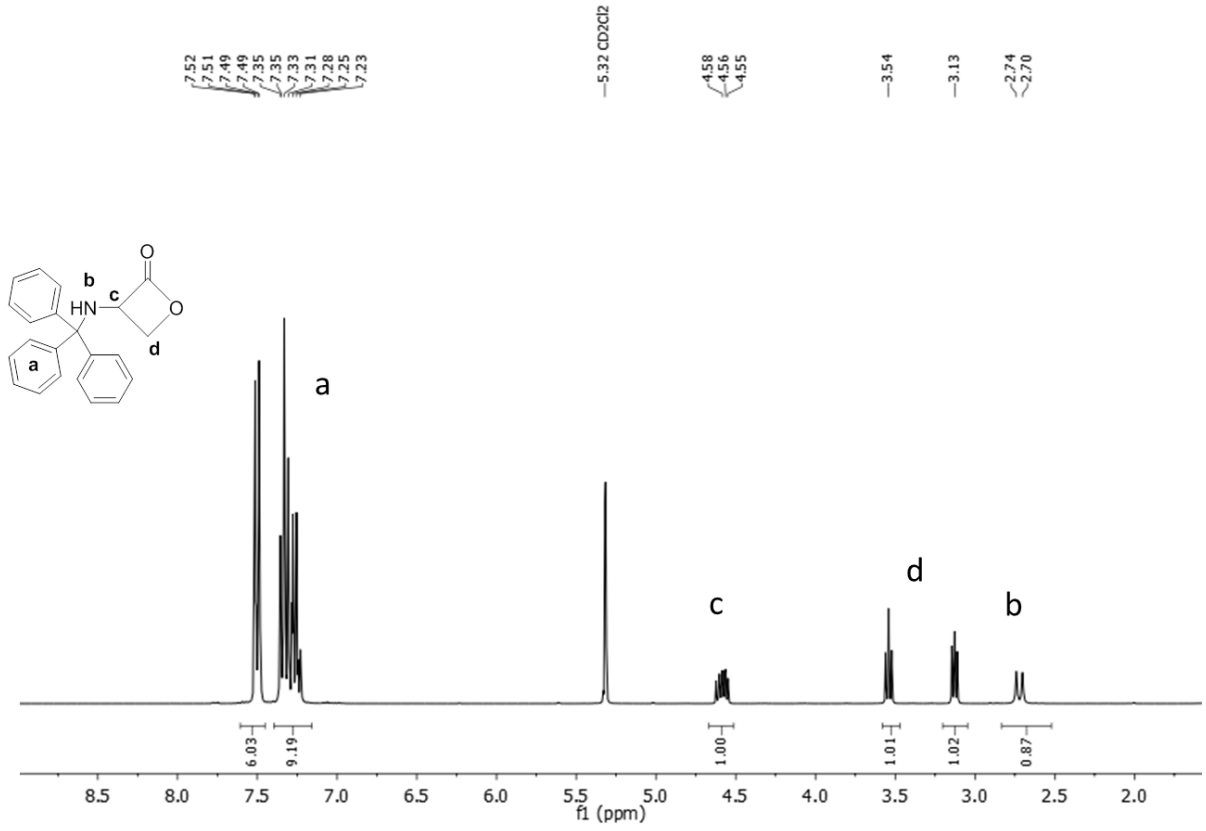

Figure 3.2. ^{1}H-NMR spectrum of NTSL monomer (CD_2Cl_2, 300 MHz, 298 K)

3.2.2. Synthesis of Macro-initiator Poly(L-lactide)

When the material is intended to be used in bio-fields, having a metal residue in the final product is a significant risk that may greatly reduce the fields of application. Therefore, metal-free organic catalysts are much more favorable.[215,216] 4-dimethylaminopyridine (DMAP) and 4-pyrrolidino-pyridines are the first organic base catalysts reported in the literature for the ROP of lactide.[27,217] Also, thiourea/amine combinations, MTBD (7-methyl-(1,5,7-triazabicyclo[4.4.0]dec-5-ene) and DBU (1,8-diazabicyclo[5.4.0]undec-7-ene) are known catalytic systems for ROP of lactones.[218,219] In recent years N-heterocyclic carbenes (NHCs) are developed as effective catalytic systems.[220] Their successful isolation and stabilization was achieved in 1991 by Arduengo et al.[221] and utilization of NHCs for transesterification and ROP of lactones was first reported in 2002.[222] The generation of imidazolium carbenes is generally accomplished via reaction of the respective *N,N'*-substituted ethylenediamines with aldehydes. Subsequent reaction of the corresponding salts/adducts with the appropriate bases or thermolysis releases the carbine. Imidazole-based catalysts are significantly more active towards ROP than the thiazolium-based analogs. Less sterically demanding carbenes were found to be more active towards ROP than their shielded analogues.[220,223] SIMes (1,3-bis(2,4,6-trimethylphenyl)-4,5-dihydroimidazol-2-yliden) and IMes (1,3-bis(2,4,6-trimethylphenyl)-4,5-imidazol-2-yliden) are commonly used rapid and effective catalysts for PLA synthesis in the presence of alcohols as initiators. It should be noted that in the absence of alcohol initiators, IMes forms a zwitterionic active species to generate a cyclic polylactide. [222,224]

Herein, poly(L-lactide) (PLLA) homopolymers with different chain lengths were synthesized by ROP of L-lactide at ambient temperature *via* SIMes catalyst in the presence of benzyl alcohol as an initiator in tetrahydrofuran (THF) under inert atmosphere.[222,224] Synthetic route is shown in Scheme 3.4. SIMes is a very effective NHC catalyst for the ROP of lactide. It yields the polymer with known chain end functionality (-OH) and narrow polydispersity (PDI<1.4) within 10 minutes.[225] Alcohol adducts of SIMes act as a single-component catalyst/initiator and they reversibly liberate the alcohol initiator with the carbene catalyst at room temperature to induce the polymerization (Scheme 3.4). Precipitation of the polymers in methanol resulted in a PLLA with hydroxyl end groups.

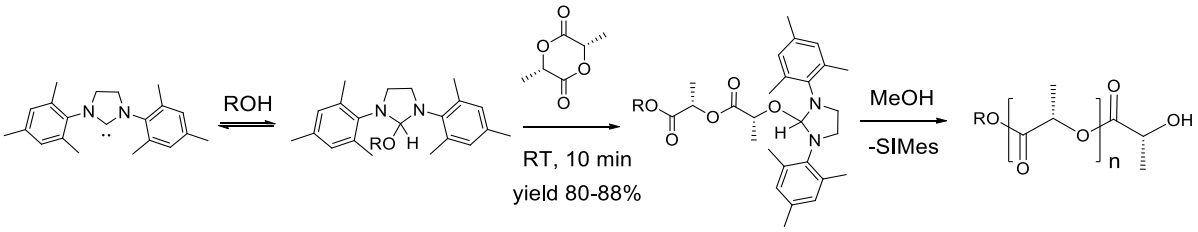

Scheme 3.4. Anionic mechanism of SIMes catalyzed L-lactide polymerization

PLLA homopolymers as macro-initiators **(PLLA 1-5)** exhibit different molar masses according to the different monomer/initiator ratio with low polydispersity (Table 3-1) and yielded within the range of 80-88%. Only the lowest molecular weight PLLA-1 was obtained with a very low yield of around 32%.

Table 3-1. Polymerization data for PLLA

Polymer	M/Cat/I [a]	DP (theo)	DP (exp) [b]	M_n (g/mol) [c]	Đ [c]
PLLA-1	20/1/1	40	30	2800	1.28
PLLA-2	35/1/1	70	70	8500	1.15
PLLA-3	40/1/1	80	95	8800	1.40
PLLA-4	100/1/1	200	120	13800	1.32
PLLA-5	100/1/1	200	190	13500	1.16

(a) Theoretical M/Cat/I molar ratio
(b) Degree of polymerization according to the ^{1}H-NMR end group analysis
(c) GPC against polystyrene standard, eluent THF

The structure of PLLA macro-initiator was verified by ^{1}H-NMR examination and the degree of polymerization was calculated by end group analysis. Benzyl alcohol aromatic peaks at 7.40-7.30 ppm were used to determine the chain length by their integration ratio with CH proton of the polymer at 5.15 ppm. FT-IR analysis also demonstrated the characteristic stretches and vibrations of the PLLA (see Section 3.4.2 and Appendix D: Supporting Information).

The average molecular weight and the molecular weight distribution of the polymers were determined by gel permeation chromatography (GPC) against polystyrene standards (PS) using THF as eluent. The molecular weight distribution (M_w/M_n) of the

polyesters was relatively narrow within the range of 1.15-1.40. Obtained PLLA homopolymers (PLLA 1-5) with hydroxyl end groups were used as macro-initiators for the polymerization of NTSL in the upcoming part.

The thermal stability of the PLLA homopolymers was determined by thermogravimetric analysis (TGA) in the nitrogen atmosphere with a heating rate of 10˚C/min from RT to 600˚C (Figure 3.3.a). All PLLAs demonstrated one step thermal degradation; starting around 220 °C. Glass transition (T_g) and melting (T_m) temperatures of the PLLA were determined by the differential scanning calorimetry (DSC) analysis (Figure 3.3.b). T_g and T_m values of different chain length PLLA are shown in Table 3-2, which are consistent with the values given in the literature.[226]

Table 3-2. Thermal characterization of PLLA homopolymers

Polymer	T_g (˚C)	T_m (˚C)
PLLA-1	66	125
PLLA-2	69	159
PLLA-3	65	149
PLLA-4	58	149

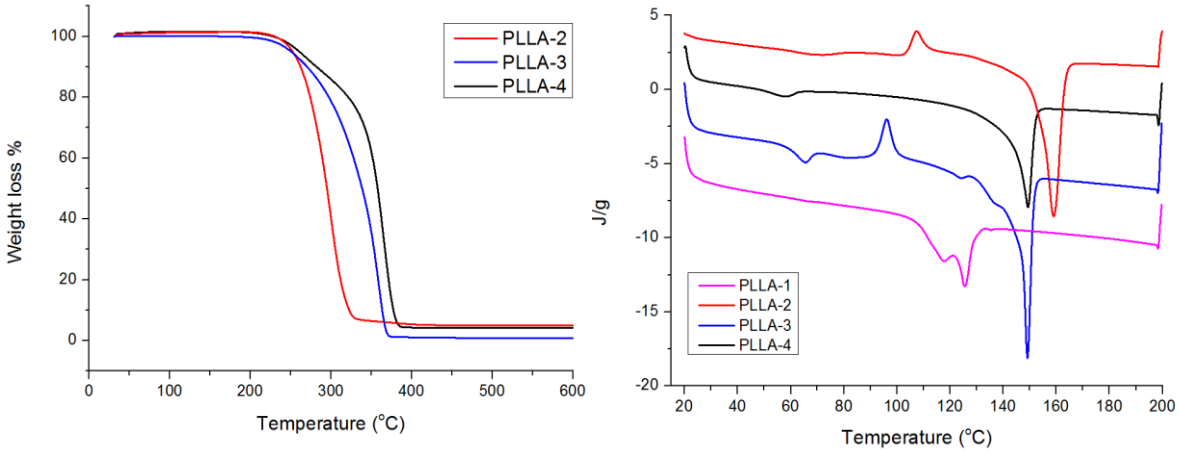

Figure 3.3. (a) TGA and (b) DSC graphs of PLLA homopolymers

3.2.3. Investigation of the Polymerization Behavior of Serine Monomers with Different Catalytic Systems

Polymerization of L-lactide was successfully achieved by SIMes catalytic system as described in the previous section. In order to investigate the polymerization behavior of serine monomer by SIMes, homopolymerizations were performed under the same reaction conditions in different durations (Scheme 3.5).

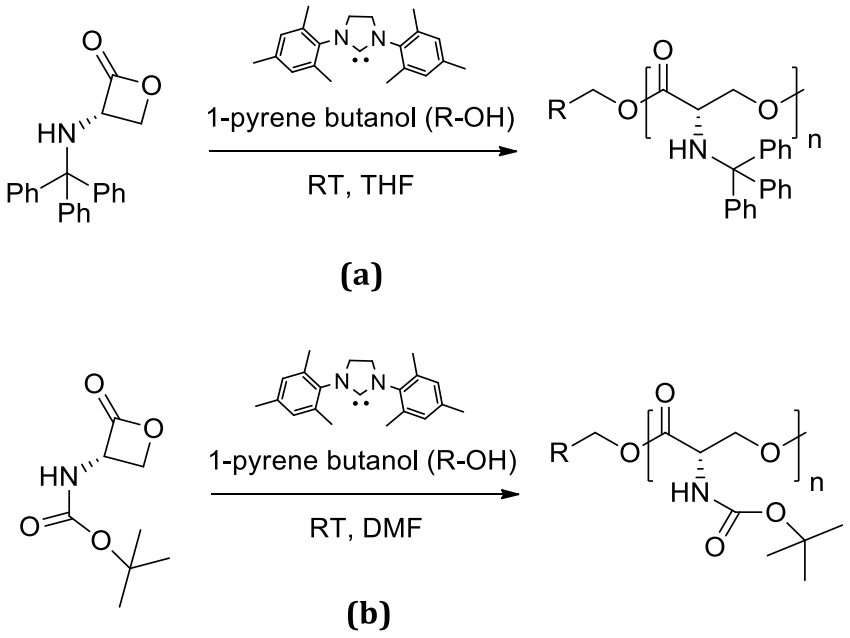

Scheme 3.5. Polymerization of (a) NTSL (b) N-boc-serine-β-lactone by SIMes

PLLA-6 homopolymer was synthesized by SIMes with a typical procedure used for previous synthesis. Obtained polymer possess a molecular weight of around 8000 g/mol with a polydispersity index of 1.39 (Table 3-3). Simultaneously in identical conditions, two polymerizations of NTSL were performed. **PNTSL-1** isolated after 15 minutes, was yielded with a molecular weight of around 1600 g/mol and a molecular weight distribution of 1.18. **PNTSL-2** was isolated after 24 hours and almost no change was observed on molecular weight except of the broadened molecular weight distribution (Scheme 3.5.a). Additionally, copolymerization of L-lactide (50% by mol) and NTSL (50% by mol) by SIMes was attempted in the same reaction conditions. PLLA-*co*-poly(N-trityl serine lactone) (PLLA-*co*-PNTSL) was obtained with a molecular weight of around 10000 g/mol according to GPC measurements. However, ^{1}H-NMR analysis showed that mainly

PLLA was formed rather than PNTSL (only oligomeric PNTSL part was formed with a molecular weight of around 2000 g/mol) (Table 3-3).

Table 3-3. Polymerization data for PNTSL and PLLA-*co*-PNTSL catalyzed by SIMes

Polymer	M/Cat/I [a]	$M_{n\ (theo)}$ (g/mol)	Time	GPC[b]	
				M_n (g/mol)	Đ
PNTSL-1	50/1/1	17000	15 min	1600	1.18
PNTSL-2	50/1/1	17000	24 h	1500	1.79
PLLA-6	50/1/1	7200	15 min	8000	1.39
PLLA-*co*-PNTSL	50/1/1	-	15 min	10000	1.55
PNbocSL-1	50/1/1	9300	3 h	1210	1.16
PNbocSL-2	50/1/1	9300	24 h	1250	1.16

(a) Theoretical M/Cat/I molar ratio
(b) GPC against Polystyrene standards, THF as eluent

Observing only the oligomer formation of PNTSL in described conditions indicated that SIMes was not the appropriate catalyst for this system. However, the steric hindrance of the bulky trityl groups of the NTSL could be the reason for this failure. In order to investigate that issue, polymerization of another serine monomer with less bulky protecting group, N-tert-butoxy carbonyl serine β-lactone (N-boc-serine β-lactone), was studied (Scheme 3.5.b).

Solubility of the N-boc–serine-β-lactone is very low in common organic solvents like THF, DCM and ACN. It is good soluble only in DMF for performing the polymerization, rest of the conditions were kept identical to previous experiments (RT, C=1 M, inert atm, $n_{catalyst}/n_{initiator}$=1/1). Nevertheless, ROP of the N-boc–serine-β-lactone resulted in an oligomeric poly(N-boc-serine-β-lactone) (PNbocSL-1) formation which had a molecular weight of around 1210 g/mol according to GPC. Increasing polymerization time to 24 hours did not make any change on the molecular weight (PNbocSL-2) (Table 3-3). Due to the poor processability of N-boc–serine-β-lactone, NTSL was utilized for further polymerization investigation with organometallic zinc catalyst in the following parts.

According to Wei et al. [112,113], NTSL was polymerized with PEG and ε-caprolactone under the catalysis of $ZnEt_2$ (diethylzinc). After unsuccessfull polymerization attempts of serine with organic catalyst SIMes, this organometallic zinc compound was utilized for our system. PNTSL homopolymers were obtained in toluene at 90 °C under inert atmosphere by adjusting monomer and catalyst molar ratio to 100/1. Homopolymer **PNTSL-3** was obtained with a narrow polydispersity (1.18) within 20 minutes. When the polymerization time was extended to 24 hours, broadened molecular weight distribution was observed (**PNTSL-4**, PDI=1.77) (Table 3-4). The ^{1}H-NMR and FT-IR spectrum and corresponding signal assignments were consistent with the expected structure of PNTSL (see Appendix D: Supporting Information).

Table 3-4. Polymerization data for PNTSL and PLLA-*co*-PNTSL catalyzed by $ZnEt_2$

Polymer	$n_{monomer}/n_{catalyst}$	Time	Yield	M_n (GPC) (g/mol)	Đ
PNTSL-3	100/1	20 min	80%	25000	1.18
PNTSL-4	100/1	24 hours	80%	15600	1.77
PLLA-*co*-PNTSL (RC1)	200/1	15 min	81%	8800	1.37
PLLA-*co*-PNTSL (RC2)	200/1	18 hours	75%	9700	1.67

*Reactions at 90 °C in toluene; catalyst of $ZnEt_2$, $n_{lactide}/n_{NTSL}$=2.5/1

Random copolymer **(RC)** formation of NTSL with L-lactide was investigated in the same conditions with homopolymers. (Total monomer to catalyst ratio was 200/1 and $n_{lactide}/n_{NTSL}$=2.5/1). Random copolymers (**RC1** and **RC2**) were isolated after 15 minutes and 18 hours with good yields (75-81%). Again, broadened molecular weight distributions were observed with longer reaction times (1.37 to 1.67) (Table 3-4). Polymers were characterized by ^{1}H-NMR spectroscopy and block ratios were determined by the integration ratio of PLLA CH protons at 5.20 ppm and trityl aromatic protons at around 7.55-7.25 ppm. Integration ratios between the aromatic trityl protons and lactide's methine protons 4/1 (theoretical 3/1), which shows that 1 eq. serine monomer reacted with 2 eq. lactide instead of 2.5 eq. Here by these performed successful polymerizations, applicability of the $ZnEt_2$ catalyst was confirmed for our system. Block copolymer formation in the presence of alcohol functional macro-initiator will be investigated in the next part.

The thermal stability of PNTSL homopolymer and PLLA-*co*-PNTSL (RC1) random copolymer was investigated by TGA in nitrogen atmosphere with a heating rate of 10 ˚C/min range from RT to 600 ˚C as shown in Figure 3.4. PNTSL and random copolymer RC1 both show one step thermal decomposition. While PNTSL starts to decompose at 238 ^{o}C, RC1 starts at around 180 ^{o}C. It seems that aromatic polymer PNTSL is more stable against heating due to the rigidity of the phenyl groups. Glass transition temperatures (T_g) and melting temperatures (T_m) of the polymers were determined by DSC analysis, as second heating DSC curves were presented in Figure 3.4. T_g of the PNTSL was observed around 153 ^{o}C and no melting peak was determined till 200 ^{o}C, afterwards thermal decomposition starts. This behavior can be explained by π-π stacking and well-organization of the aromatic groups rather than the aliphatic polymer. In the random copolymer case, three peaks were observed at 72 ^{o}C, 126 and 136 ^{o}C. The peak at 72 ^{o}C is the T_g region of PLLA itself and the transition around of 126-136 ^{o}C are the glass transition region of the random copolymer. By incorporation of the PLLA units into PNTSL, T_g was decreased as we can see from the Figure 3.4.

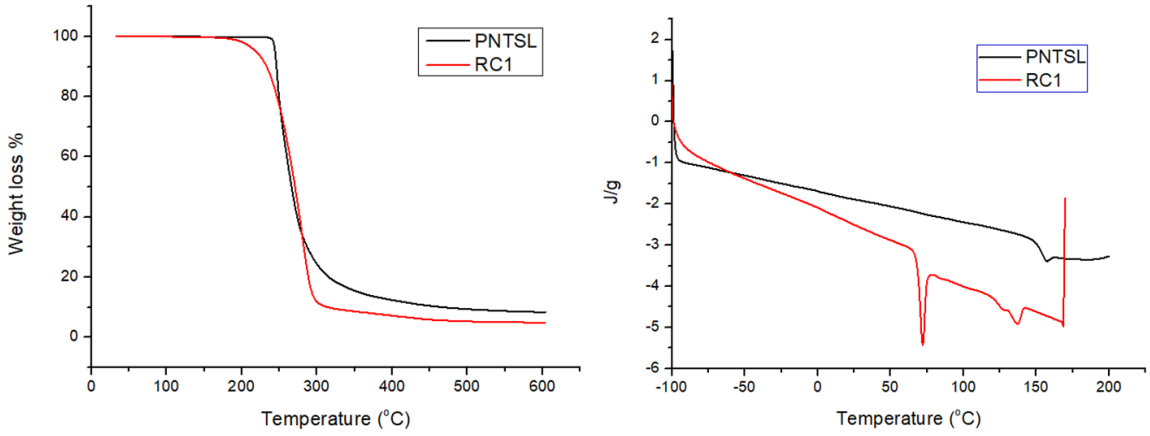

Figure 3.4. TGA and DSC graphs of PNTSL and RC1

3.2.4. Block Copolymer Formation

After achieving the polymerization of NTSL by $ZnEt_2$ catalysis, block copolymer formation was first investigated with commercially available CH_3O-PEG-OH (M_n=1200 g/mol) to understand the macro-initiator effect according to the literature to yield PEG-*b*-PNTSL as shown in Scheme 3.6.[112]

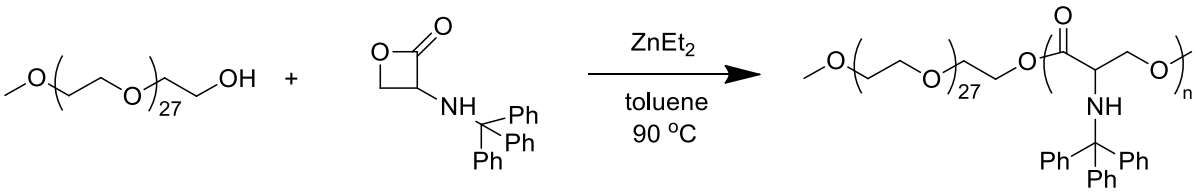

Scheme 3.6. Polymerization of NTSL with CH_3O-PEG-OH

Polymerization was carried out in toluene at 90 °C within 15 minutes resulted in PEG-*b*-PNTSL with 74% yield as a white solid (Table 3-5). Structure of the polymer was characterized by ^{1}H-NMR which showed all the corresponding peaks of the compound which are 7.44-7.05 ppm (Ar), 3.85 and 3.65 ppm (CH_2), 3.59 ppm (PEG's CH_2), 3.43 ppm (CH), 2.69 ppm (NH). Theoretical feeding ratio between monomer and initiator was 60:1 (27 H from one PEG unit to 60 repeating unit from serine) but on ^{1}H-NMR this ratio was calculated as 27 H of PEG attached to 46 repeating units of serine.

Table 3-5. Polymerization results of PEG-*b*-PNTSL

Polymer	$DP_{(theo)}$	n_{mon}/n_{cat}	$DP_{(exp)}$ [a]	M_n [b]	Đ [b]	Yield (%)
PEG-*b*-PNTSL	27/60	100/1	27/46	8700	1.11	74

(a) DP (exp) was calculated according to the ^{1}H-NMR end group analysis
(b) GPC against polystyrene standard, eluent THF

After successfully achieving the block copolymer by PEG (testing the macro-initiator effect), now polymerization of NTSL by using hydroxyl terminated PLLA as a macro-initiator was investigated in the same catalytic system.

Hydroxyl-terminated **PLLA (1-4)** with different DPs (30, 70, 95 and, 120) was used in the presence of $ZnEt_2$ to polymerize NTSL monomer (Scheme 3.7). Copolymers were synthesized within 15 minutes at 90 ˚C in toluene. While the monomer to catalyst ratio was adjusted to 100/1 by mol, initiator ratio was varied depending on the intended degree of polymerization. Precipitated polymers by methanol were further purified by gel permeation chromatography from the homopolymer residues. It is assumed that polymerization proceeds through coordination-insertion mechanism by the formation of zinc-alkoxide which initiates the polymerization of lactone by the cleavage of acyl-oxygen bond.[227,228]

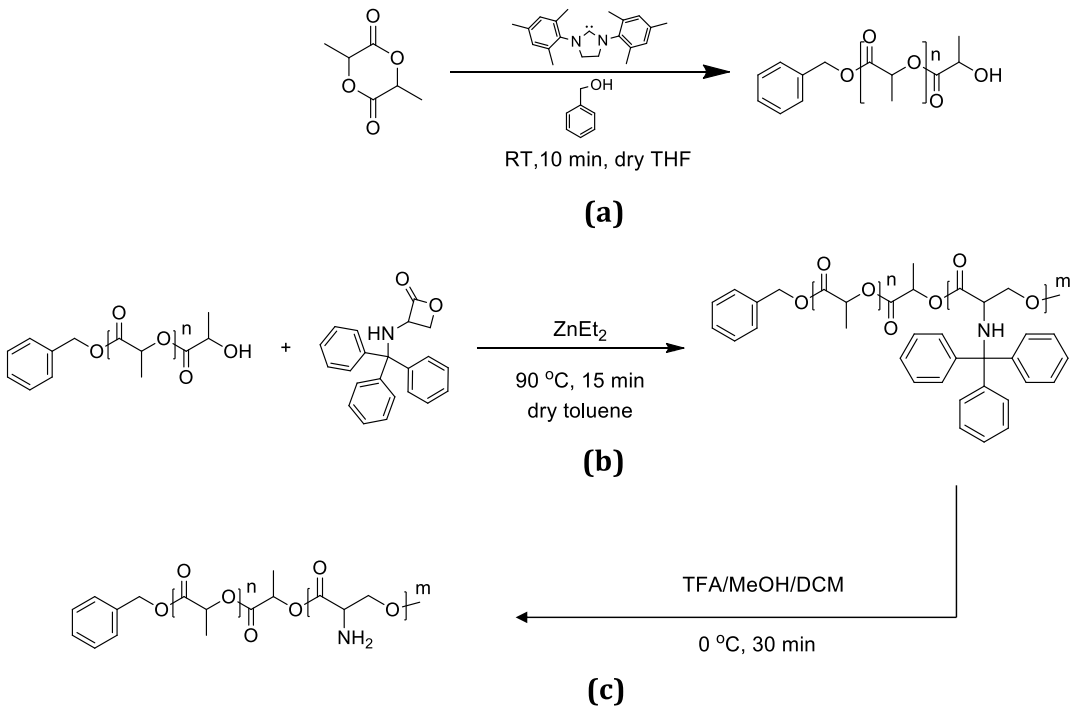

Scheme 3.7. (a) Synthesis of PLLA (b) Synthesis of PLLA-*b*-PNTSL (c) Removal of trityl group

To investigate the reaction kinetics in the presence of PLLA macro-initiator, polymerization of NTSL was monitored every 10 minutes. Block copolymer **BC1**, was synthesized with **PLLA-4** by $ZnEt_2$ ((n(serine)/n($ZnEt_2$)=100/1)) and, each 10 minutes an aliquot was analyzed by GPC and ^{1}H-NMR, at the same time monomer consumption was controlled by TLC. Figure 3.5 presents the molecular weight change by time during the polymerization. Black dash line shows the homopolymer PLLA-4 and the rest are the molecular weight curves of the copolymer by 10 minutes intervals. As seen from the graph, molecular weight does not change after 10 minutes and further during one hour. Additionally, the monomer spot on TLC does not change after 10 min, means conversion of monomer stops after this time which reduces the yield of the polymerization. Change on peak molecular weight versus reaction time was demonstrated in Figure 3.5.

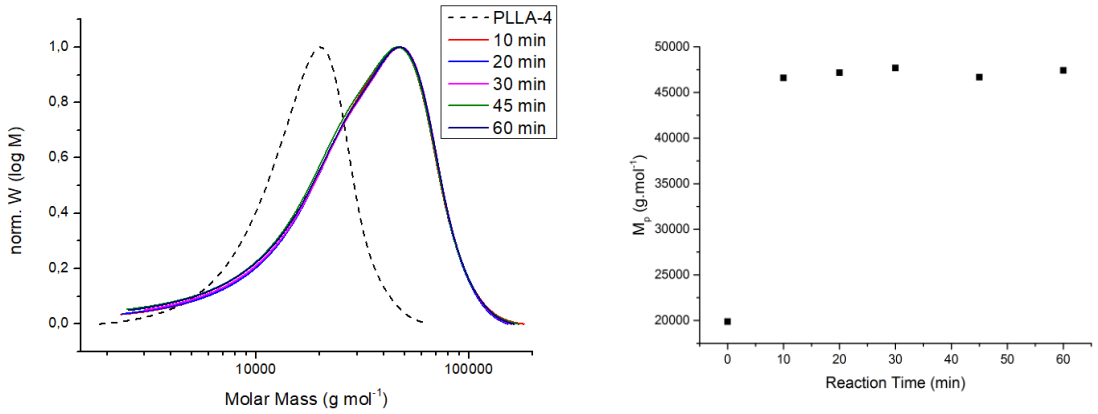

Figure 3.5. Monitoring the molecular weight by GPC in different time intervals and peak molecular weight versus reaction time (Final polymer (after 60 min): M_n=20600 g/mol, Đ=1.84) (THF, against PS)

After determining the reaction time, block copolymers with various chain lengths were synthesized and details are presented in Table 3-6. Before the polymerizations, PLLA macro-initiators were azeotropically dried in toluene. Reaction time was kept at 15 minutes under inert atmosphere and molar ratio of monomer to catalyst was 100/1 for all the polymerizations. Initiator amount was calculated for each block copolymer for intended degree of polymerization individually. Theoretical and experimental block ratios of the copolymers (calculated by ^{1}H-NMR) were presented together with the GPC results in Table 3-6. Yield of the polymerizations were between 56-82%. As mentioned before, certain percentage of the monomer stays unreacted as confirmed by TLC which reduces the yield of the reaction. The interaction of the carbonyl group of PLLA with $ZnEt_2$ metal catalyst might reduce the activity of $ZnEt_2$ thereby resulted in a low conversion.

Table 3-6. Polymerization data of PLLA-*b*-PNTSL block copolymers

Polymer	$DP_{(theo)}$ PLLA/PNTSL	GPC		Yield %	$DP_{(exp)}$ PLLA/PNTSL
		M_n (g/mol)	Đ		
BC2	70/70	14000	1.52	56	70/49
BC3	70/140	35000	1.48	72	70/140
BC4	70/210	55000	1.50	80	70/210
BC5	30/120	42400	1.44	68	30/120
BC6	120/240	43000	1.35	82	120/220
BC7	70/140	18000	1.93	-	70/175
BC8	70/210	34500	1.40	72	70/350
BC9	120/240	17000	1.78	-	120/120
BC10	120/240	14000	1.77	-	120/140

*Monomer/catalyst ratio was adjusted to 100/1, temperature 90 ^{o}C
*$DP_{(exp)}$was calculated by ^{1}H-NMR
*Reaction time is 15 minutes
*GPC against polystyrene standard, eluent THF

Structure of the block copolymers was fully characterized by the combination of ^{1}H, ^{13}C-apt, ^{1}H-DOSY NMRs and by FTIR techniques. Additional to the classical structural information obtained by NMRs and IR, ^{1}H-DOSY-diffusion ordered spectroscopy, which is a special technique, confirms the block copolymer formation in terms of covalent attachment of different blocks to each other.[229] The method is based on diffusion coefficients of the species, basically covalently attached species own the same diffusion coefficients, therefore unreacted polymer chains or other species in the material can be distinguished easily having another signal.[229] Figure 3.6 below shows the successful covalent linkage of two polymer blocks of PLLA-*b*-PNTSL by this technique. The diffusion coefficient signals of all components of the polymer were same, proving the pure block copolymer formation.

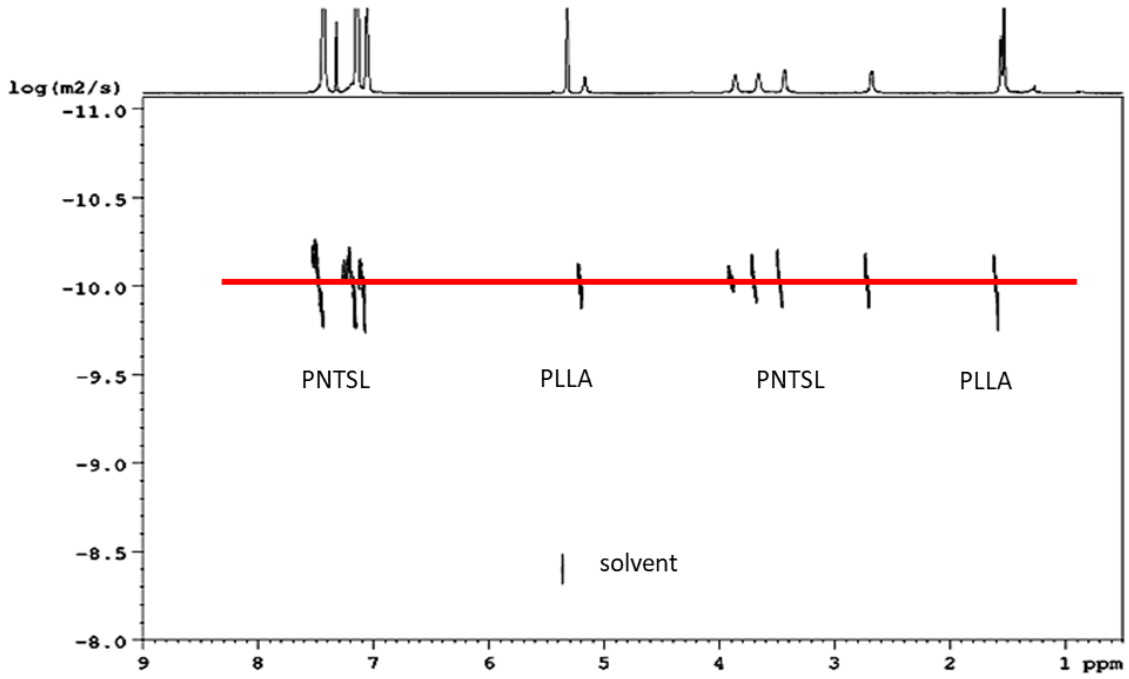

Figure 3.6. ^{1}H-DOSY spectrum of PLLA-*b*-PNTSL (BC6) (CD_2Cl_2, 700 MHz, 298 K)

In Figure 3.7, the peaks marked with letters from **a** to **f** in ^{1}H-NMR can be assigned to the characteristic signals of the protons in the copolymer for both PLLA and PNTSL blocks such as; **c** at 1.56 ppm CH_3 of PLLA**, b** at 5.16 ppm CH of PLLA, **d** at 3.86 and 3.66 ppm CH_2 of PNTSL, **e** at 3.43 ppm CH of PNTSL, **f** at 2.69 NH of PNTSL and **a** at 7.44-7.04 ppm corresponds to the aromatic protons of the PNTSL block.

Experimental block ratios of the copolymers were estimated from the relative area of the peak at 5.17 ppm **(b)** corresponding to the PLLA CH proton to those at 3.86 **(d),** or 3.44 **(e)** ppm corresponding to the CH_2 or CH proton of the PNTSL block. The chain lengths (DP) of the second block varied from 49 to 220. Likewise, ^{13}C-NMR also assigns all the corresponding carbons in the copolymer as shown in Figure 3.8.

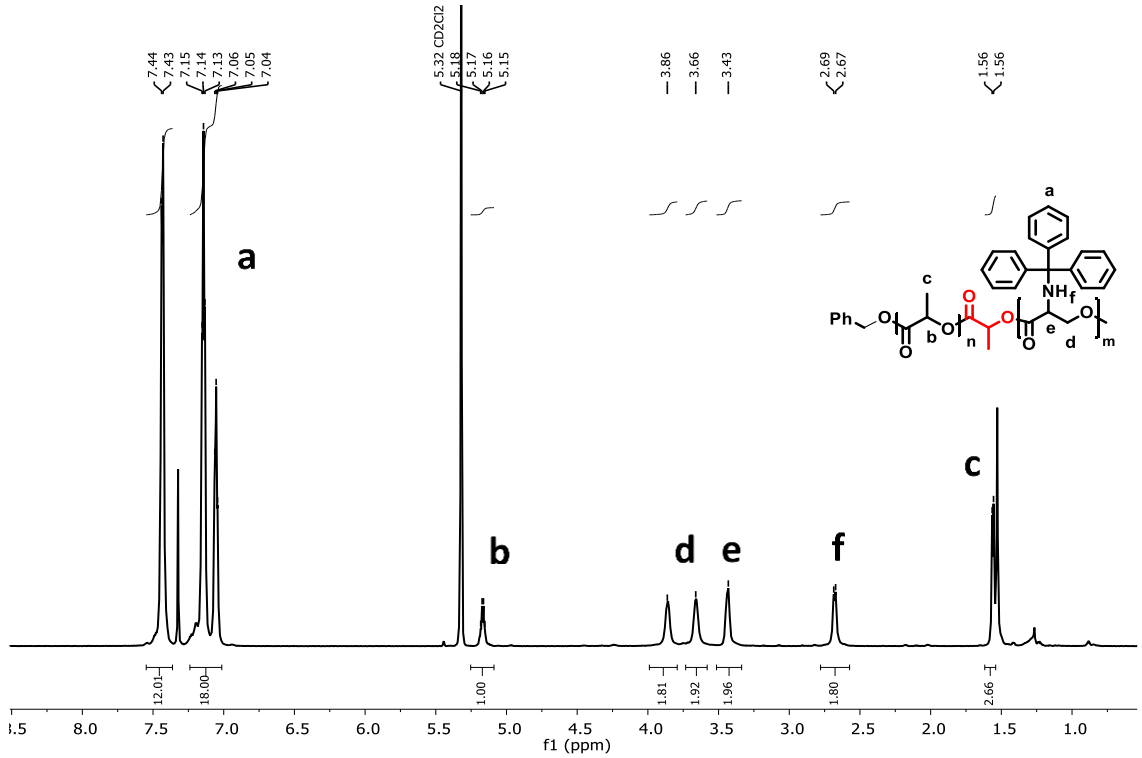

Figure 3.7. ^{1}H-NMR spectrum of PLLA-*b*-PNTSL block copolymer BC6 (CD_2Cl_2, 700 MHz, 298 K)

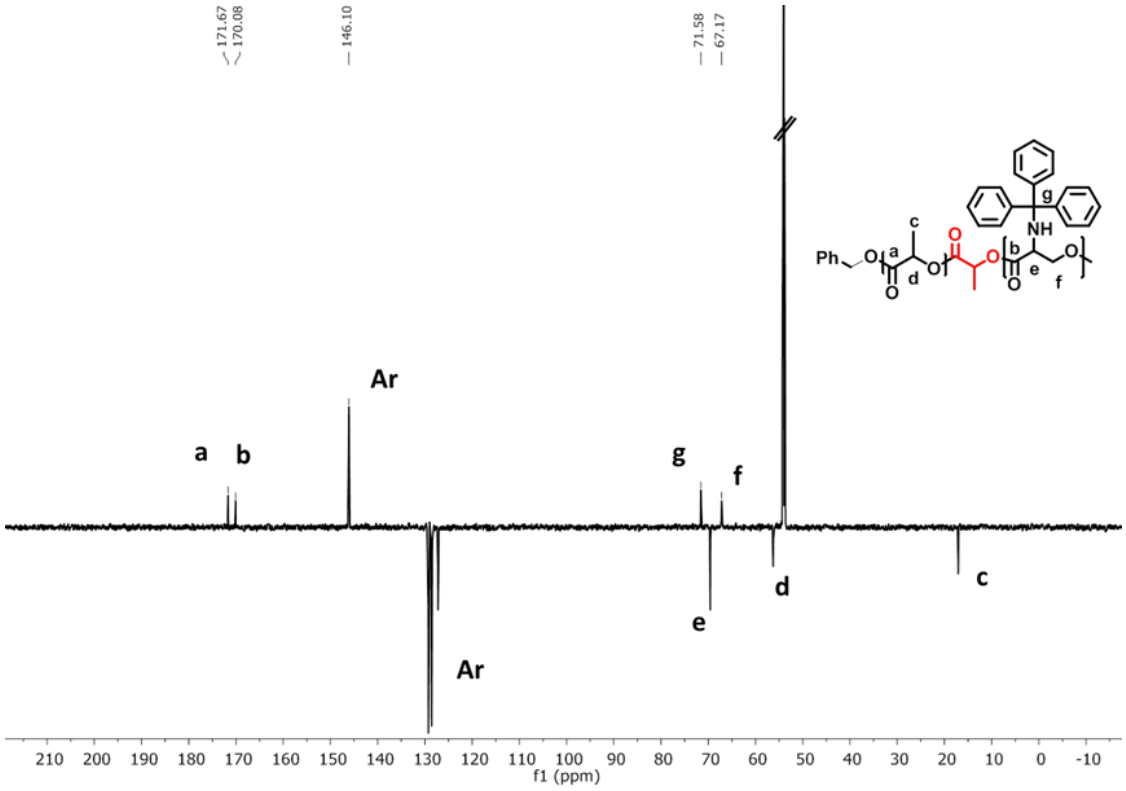

Figure 3.8. ^{13}C-apt NMR of the block copolymer BC6 (CD_2Cl_2, 75 MHz, 298 K)

Block copolymers are additionally characterized by FTIR as the spectrums of PLLA, PNTSL and block copolymer PLLA-*b*-PNTSL **(BC6)** are presented in Figure 3.9. As summarized as well in Table 3-7 and explained in previous sections, characteristic PLLA ester carbonyl stretch was observed at 1758 cm^{-1} whereas C-O-C asymmetric and symmetric stretch vibrations were formed at 1187 and 1088 cm^{-1}. In the spectrum of PNTSL, aromatic absorption peaks are CH stretches at 3056 and 3026 cm^{-1}, C=C stretches of the aromatic ring at 1489 and 1448 cm^{-1} and out of plane CH bending at 745 and 700 cm^{-1}. Additionally, NH bending at 1597 cm^{-1} and C-O-C asymmetric and symmetric stretching vibrations at 1138 and 1029 cm^{-1} describe the PNTSL.

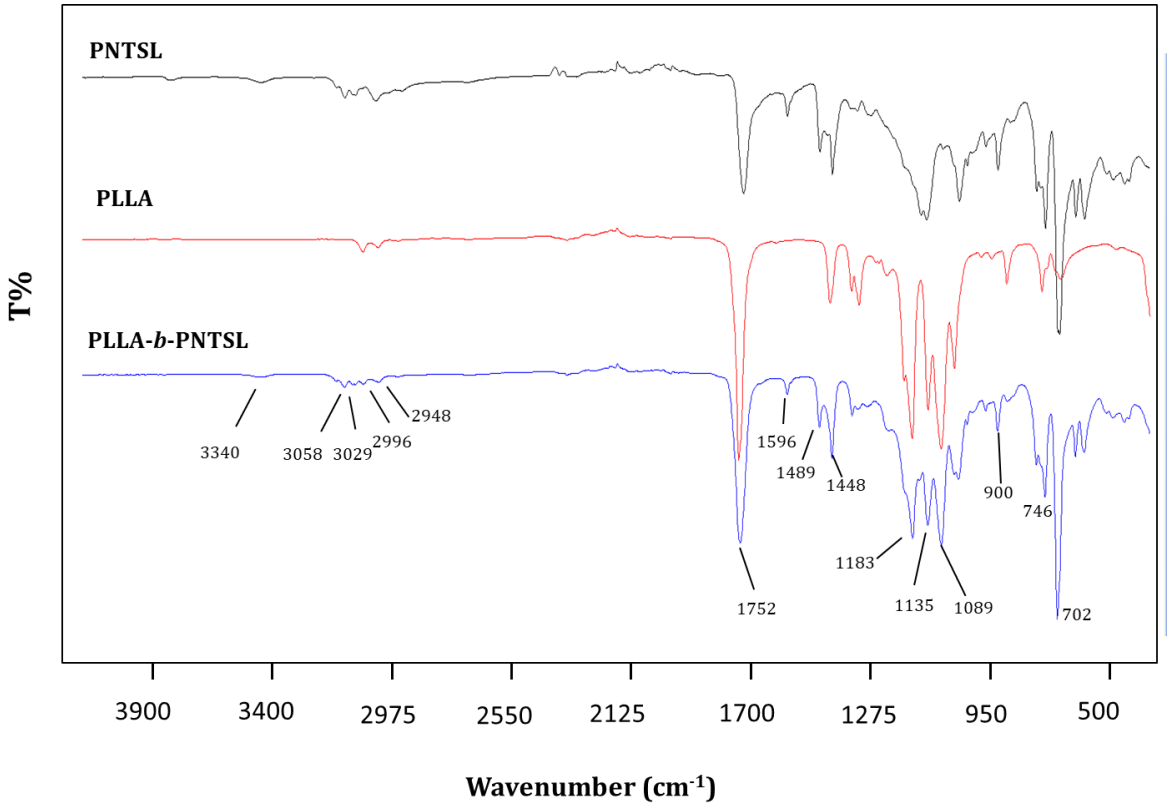

Figure 3.9. FTIR spectrum of PNTSL, PLLA and block copolymer BC6

FT-IR spectrum of block copolymer presents all the characteristic bands. Alkyl and aromatic CH stretches are observed in the region of 3058-2948 cm^{-1}. Carbonyl group of the block copolymer is shifted at 1752 cm^{-1} which is the middle point of two different carbonyl values. NH bending is seen at 1596 cm^{-1} and C-O-C ester stretches are observed

between 1183-1089 cm^{-1}. The C=C stretches of the aromatic ring are seen at 1489 and 1448 cm^{-1} and the out of plane C–H bending at 746 and 702 cm^{-1}.

Table 3-7. FT-IR bands of PLLA-4, PNTSL-1 and block copolymer BC6

Polymer	Wavenumber (cm^{-1})	Vibration type
PLLA-4	2999 and 2996 1456 and 1360 1758 1187-1088	*v* (-CH) δ ($-CH_3$) *v* (-C=O ester) *v* (-C-O-C ester)
PNTSL-1	3635 3336 3056 and 3026 2957 and 2870 1742 1597 1489 and 1448 1138-1029 745 and 700	*v* (-OH) *v* (-NH) *v* (-CH aromatics) *v* (-CH) *v* (-C=O ester) δ (-NH) *v* (C=C aromatics) *v* (-C-O-C ester) δ (-CH aromatics)
PLLA-*b*-PNTSL (BC6)	3340 3058 and 3029 2996 and 2948 1752 1596 1489 and 1448 1183-1089 746 and 702	*v* (-NH) *v* (-CH aromatics) *v* (-CH) *v* (-C=O ester) δ (-NH) *v* (C=C aromatics) *v* (-C-O-C ester) δ (-CH aromatics)

These presented three NMR techniques; ^{1}H, ^{13}C and ^{1}H-DOSY and FT-IR characterization together precisely confirms the structure of the block copolymers. Molecular weights and molecular weight distributions of the copolymers were determined by GPC against polystyrene standards using THF as eluent. By adjusting the molar ratio of the NTSL monomer to macro-initiator PLLA, block copolymers with various chain lengths which have the molecular weights in the range of 10000 to 55000 g/mol were successfully synthesized (Table 3-6). In the following, molecular weight analysis of the polymers is presented in detail.

Figure 3.10.a shows the elution volumes of the BC2, BC3 and BC4 block copolymers purified by precipitation right after the polymerization. As it is seen, distribution is almost monomodal but has a small shoulder on the lower molecular weight side of the elugram

which corresponds to the unreacted homopolymer residue, further eliminated by preparative GPC column. For example, polymer BC2 before and after the purification was shown in Figure 3.10.b and Figure 3.10.c presents the purified BC2 and BC4 in comparison.

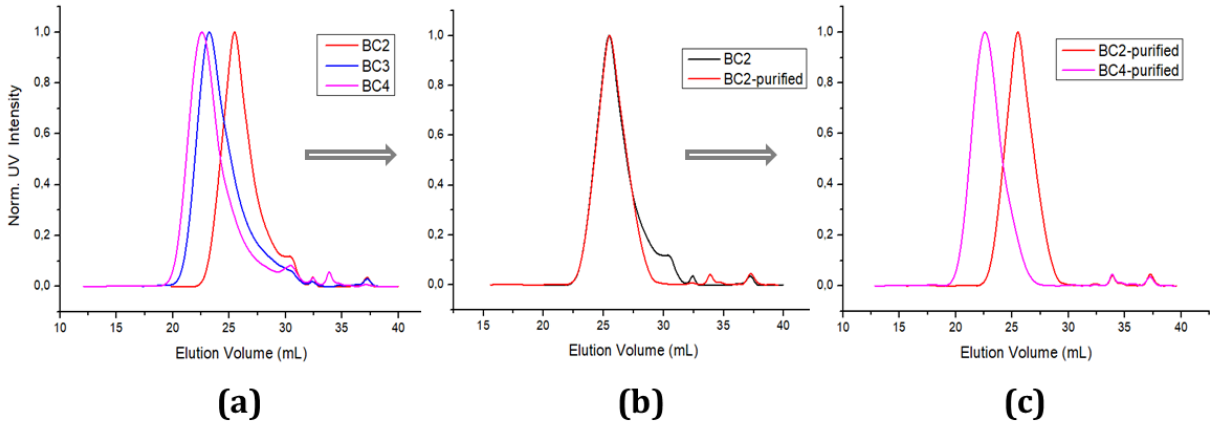

Figure 3.10. (a) Crude GPC elugrams of BC2, BC3 and BC4 (b) BC2-before and after preparative GPC (c) BC2 and BC4 after preparative GPC

After purifications, molecular weight distributions of **BC2** (block ratio= 70/49), **BC3** (block ratio= 70/140) and **BC4** (block ratio= 70/210) (they were all initiated by PLLA-2 (dash line) (PLLA/DP=70)) were obtained as demonstrated in Figure 3.11. By adjusting the initial PLLA amount, molecular weights can be controlled (see the shifts on the curves).

Polymer	DP (theo)	DP (exp)	M_n (g/mol)	Đ
PLLA-2	70	70	8500	1.15
BC2	70/70	70/49	14000	1.52
BC3	70/140	70/140	35000	1.48
BC4	70/210	70/210	55000	1.50

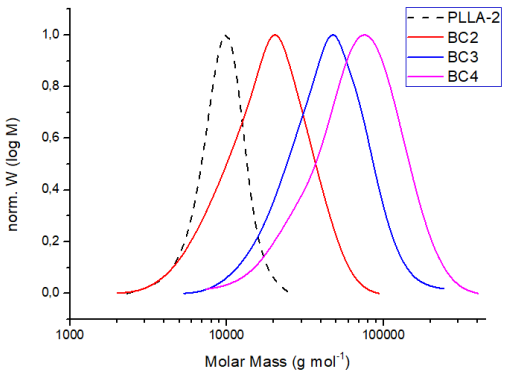

Figure 3.11. GPC curves of block copolymers BC2, BC3, BC4 and table of the polymerization data

Figure 3.12 presents the molecular weight distribution of the block copolymer BC5 which was initiated by PLLA-1 (dash line). A molecular weight of around 4200 g/mol was obtained with a polydispersity index of 1.44. Block ratio of BC5 was calculated by ^{1}H-NMR as 30/120, which corresponds to the theoretical degree of polymerization.

Polymer	DP $_{(theo)}$	DP $_{(exp)}$	M_n (g/mol)	Đ
PLLA-1	40	30	2800	1.28
BC5	30/120	30/120	42000	1.44

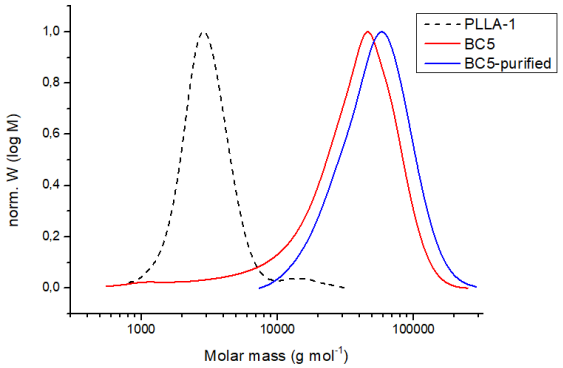

Figure 3.12. GPC curves of block copolymer BC5 and PLLA-1 homopolymer

Other block copolymers (Table 3-6) were also purified and analyzed by the same method. Figure 3.13 shows the molecular weight distributions of the copolymers BC6 to BC10.

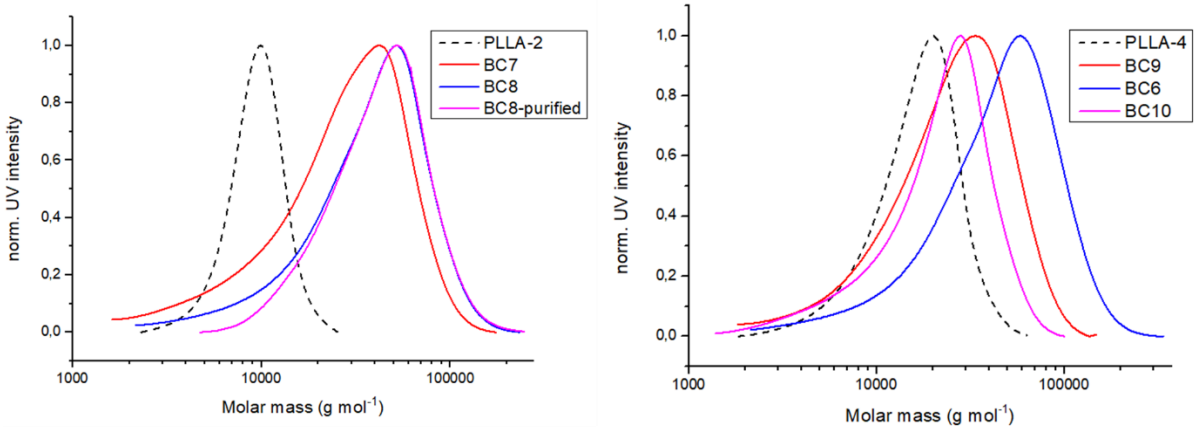

Figure 3.13. GPC curves of the copolymers BC6, BC7, BC8, BC9 and BC10

Thermal stability of the block copolymers was determined by TGA in a nitrogen atmosphere with a heating rate of 10 ˚C/min at a temperature range from RT to 600 ˚C as shown in Figure 3.14. Block copolymers demonstrated one step thermal degradation which starts around of 224-228 ºC.

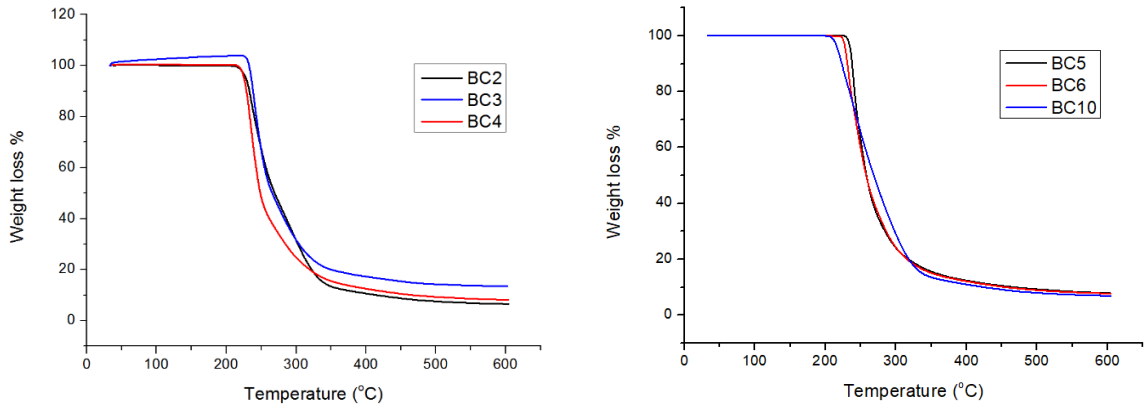

Figure 3.14. TGA graphs of the block copolymers

Glass transition (T_g) and melting temperatures (T_m) of the polymers were investigated by DSC, as second heating DSC curves were presented in Figure 3.15. Mostly two T_g values were observed due to the typical different phase behavior of the block copolymers. The analysis for BC2 revealed three different phase transition peaks. There is a slight slope around 73 °C which corresponds to the T_g of the first block PLLA-2 (homopolymer has T_g around 69 ˚C). Around 136 ˚C and 150 ˚C, two phase transitions were observed. It was assumed that one of is the T_g of the PNTSL block and other is the melting peak of the PLLA which was observed at 149 ˚C in the analysis of homopolymers (Section 3.2.2). Because PLLA/PNTSL repeating unit ratio is close to each other 70/49 in this BC2 block copolymer case, we could clearly see the melting of the PLLA block. In the analysis of BC3, the same behavior was observed except of the T_g of the PLLA. In the DSC curve of the BC4 which has the block ratio of 1/3, T_g of PNTSL block was clearly observed at around 161 ˚C. BC5 and BC6 showed T_g of PLLA around 70 ˚C and 74 ˚C, T_m of PLLA was around 142 ˚C (only in BC5) and T_g of PNTSL was about 141 and 154 ˚C.

Table 3-8. Thermal characterization of the block copolymers

Polymer	T_g 1(˚C)	T_m 1 (˚C)	T_g 2 (˚C)
BC2	73	150	149
BC3	-	-	143
BC4	83	-	161
BC5	70	-	141
BC6	74	-	154

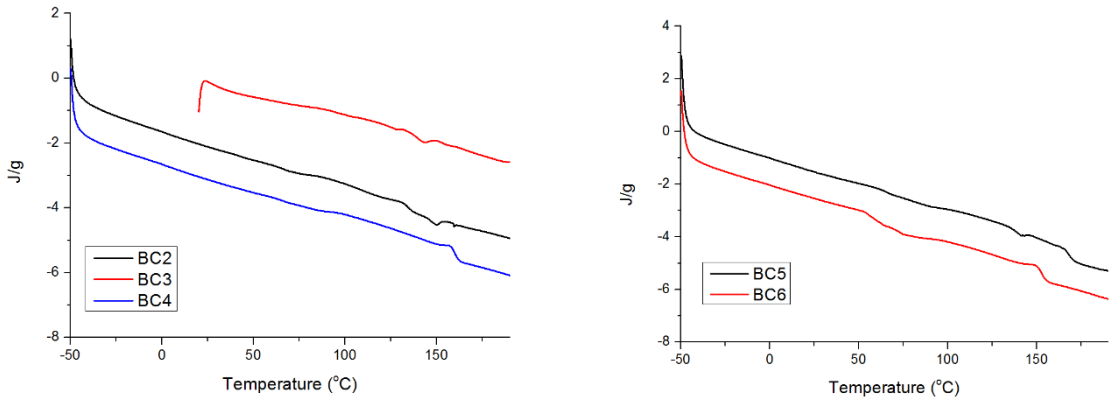

Figure 3.15. DSC graphs of the block copolymers

3.2.5. Deprotection of the Trityl Groups

Hydrophobic trityl groups of the block copolymers were removed by trifluoroethanol/methanol in DCM at 0 ˚C. Dilute acidic solution was used for the cleavage because of the acid sensitivity of the ester backbone of PLLA-*b*-PNTSL block copolymer. Deprotection was confirmed by ^{1}H-NMR by disappearance of the aromatic trityl peaks as it shown in Figure 3.16. Moreover, serine CH and CH_2 peaks are shifted up to the 4.82 ppm from 3.82-3.44 ppm.

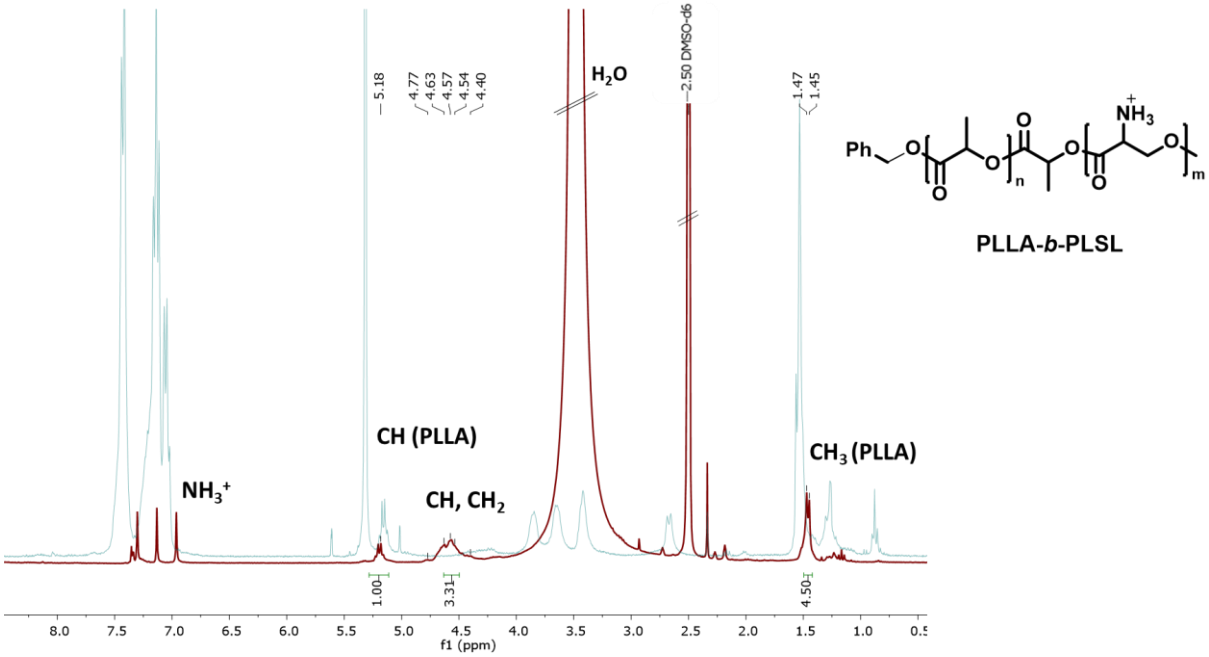

Figure 3.16. ^{1}H-NMR spectrum of block copolymer before (blue, CD_2Cl_2) and after (red, d6-DMSO) deprotection (700 MHz, 298 K)

Deprotection was further confirmed by FTIR spectroscopy as shown in Figure 3.17. Broad absorption band was formed around 2900 cm^{-1} after cleavage of the trityl due to the formation of NH_3^+ salts in the side chain of the block copolymer. New carbonyl stretching at 1669 cm^{-1} and absorptions at 836, 798 and 723 cm^{-1} attributed to CF_3COO^- formation. Moreover, out of plane C–H bending of aromatic rings seen at 746 and 702 cm^{-1} were disappeared in the spectrum of the deprotected polymer.

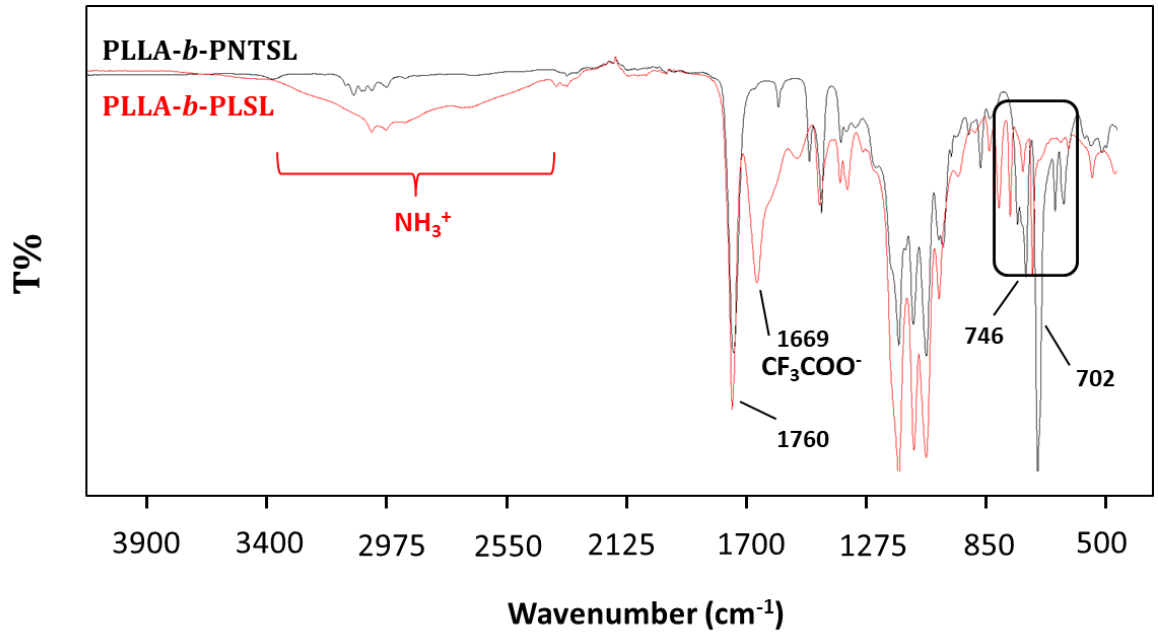

Figure 3.17. FTIR spectrum of block copolymer before (black) and after deprotection (red)

The yield of the deprotection reactions was quite low (max. 54%). Spassky[35] and Huang et al.[113] have observed the main chain scission beside the deprotection of the copolymers. This is probably the reason for low reaction yield. The problem remained even after the decrease of the temperature to the 0 ˚C during the deprotection. When diluted or less amount of acid was used, deprotection was not completed.

By this deprotection reaction, the polarity of the polymer has changed and the structure gained its amphiphilic character. At the same time, functional free amine groups were formed which is important for post-synthetic functionalization. These amphiphilic block copolymers were used for further self-assembly studies, discussed in the upcoming part.

3.2.6. Self-assembly Study of the Block Copolymers

Cleavage of the hydrophobic trityl groups of PLLA-*b*-PNTSL leads to the formation of amphiphilic Poly(L-lactide)-*b*-poly(L-serine lactone) (PLLA-*b*-PSL) block copolymers which can assembly into different morphologies in aqueous medium. In this research, polymeric micelles were prepared mainly by dialysis method which based on the dissolution of the copolymers in organic solvents and solvent replacement by diffusion.[230]

Amphiphilic PLLA-*b*-PSL block copolymers were dissolved in DMSO and dialyzed against water for 24 hours (MWCO=1000). By the slow diffusion of water through the membrane, the solvent was replaced. Obtained aqueous dispersions were sonicated for 2 hours. Removing the larger aggregates by centrifugation (12000 rpm) resulted in well-dispersed particles, further analyzed by Dynamic Light Scattering (DLS) and Transmission Electron Microscopy (TEM). As presented in detail in Table 3-9, the hydrodynamic radius of the polymers was around 83 to 206 nm as determined by DLS measurements.

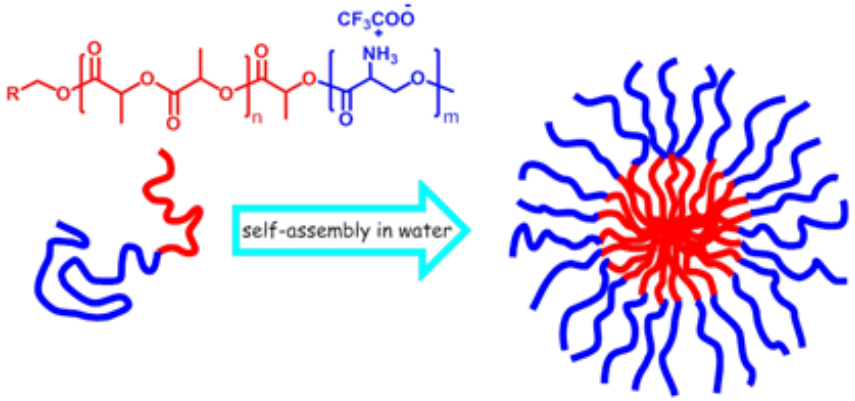

Table 3-9. DLS and CMC data of block copolymers in water

Polymer	D_h [nm] (water)	CMC (mg/mL)	Polymer	D_h [nm] (water)	CMC (mg/L)
BC2dp	206±7	-	**BC7dp**	83±7	-
BC3dp	83±7	0.01	**BC8dp**	95±5	0.029
BC4dp	143±0.6	-	**BC9dp**	88±11	0.072
BC5dp	193±5	0.032	**BC10dp**	-	-
BC6dp	164±0.8	0.031			

Furthermore, micelle formation was monitored by fluorescence spectroscopy by using pyrene as a hydrophobic probe at room temperature.[231] As it shown in

Figure **3.18**, while keeping the pyrene concentration constant in solution ($6x10^{-7}$ M), emission intensity of the pyrene was recorded (excited at 339 nm) in the presence of various amounts of micelles (1.00 mg/mL to 0.000125 mg/mL). Critical micelle concentration (CMC) was estimated by plotting intensity of the first peak at 375 nm of the emission spectra profile against of the logarithm of the micelle concentration.[146] CMC values were determined from the crossover point at low concentrations (Figure 3.23, Figure 3.21).

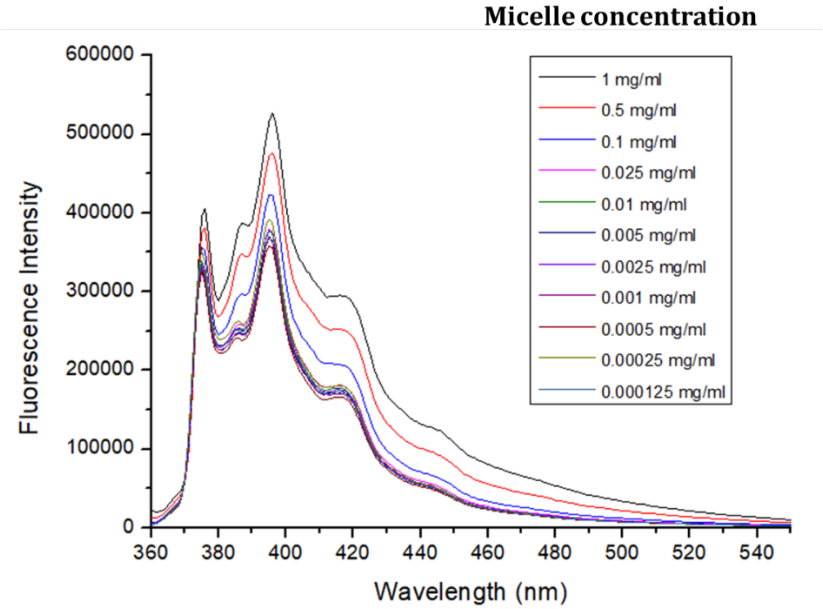

Figure 3.18. Fluorescence intensity of pyrene in various micelle concentrations for BC6dp

Morphology of the block copolymer aggregates were investigated by TEM analysis. Micelles were determined by dropping of the polymer solution onto the carbon grid after staining with uranyl acetate in trehalose.

Figure 3.19.a,b demonstrated the investigation of the morphology of BC2dp. The preparation of this micelle solution was difficult due to the longer hydrophobic block (PLLA/PSL=70/49). Therefore, this polymer tends to aggregate into the larger and undefined particles as we can see in the images. In a certain extent, 100 nm to 200 nm

long wormlike structures were also observed. Indeed, worm like micelles were expected because of the hydrophilic/hydrophobic ratio of the block copolymer. CMC could not be determined for BC2dp due to the heterogeneity of the system. According to the DLS measurements, BC2dp had an approximate diameter of 206 nm (Table 3-9), however larger aggregates around 500 nm were also observed which supports the TEM results.

When it comes to the TEM analysis of BC4dp which hydrophilic/hydrophobic block ratio is 1/3 (70/210), mainly spherical micelles around 50 nm were observed as it was expected from the theoretical point of view (Figure 3.19.c.d.) In DLS measurements, aggregates around 143 nm were observed. After several days of storage at room temperature, TEM image of the same sample was measured again as shown in Figure 3.19.e. It shows larger spherical micelles together with wormlike structures. It is assumed that the degradation of hydrophilic serine ester backbone of the block copolymer leads to the formation of these tubular aggregates in the solution due to the shortened hydrophilic part and changed hydrophile/hydrophobe balance in the solution.

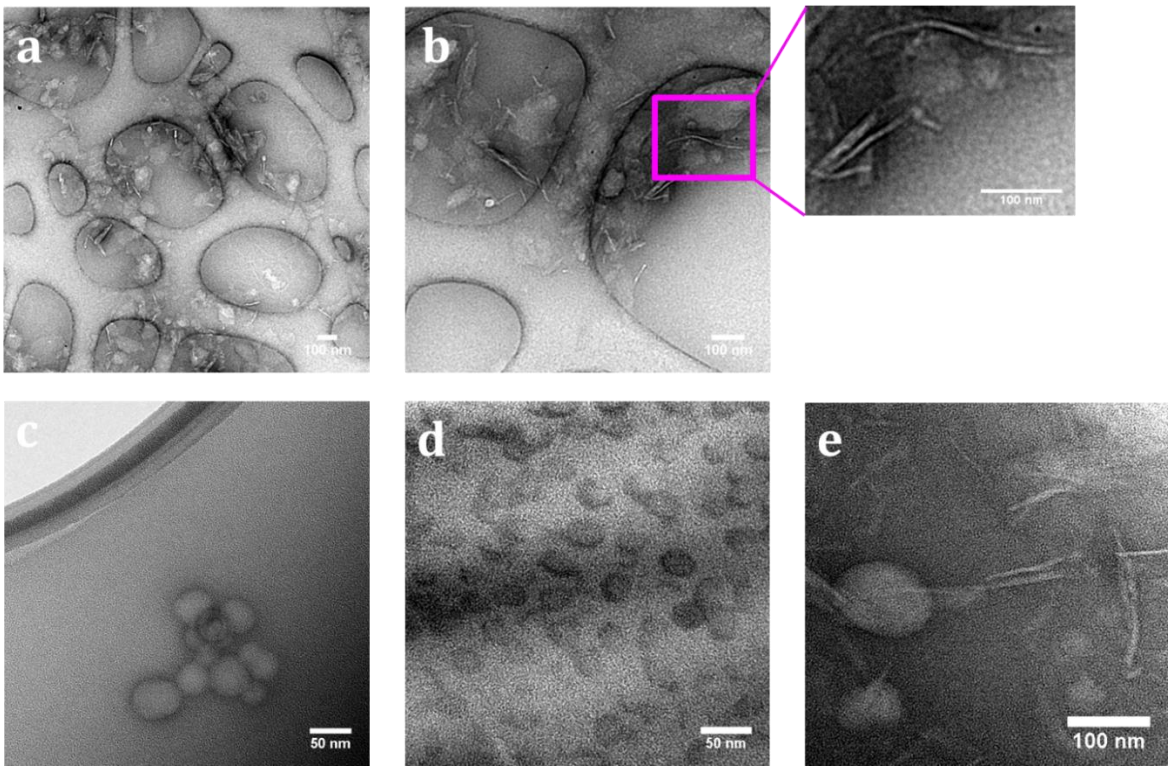

Figure 3.19. (a, b) TEM images of BC2dp and (c, d, e) TEM images of BC4dp

While block copolymer **BC3dp** demonstrates the spherical micelles around of 50-100 nm as shown in the TEM micrographs below in Figure 3.20.a,b, **BC8dp** forms different length of long bride tubes in solution (Figure 3.20.c). CMC values of these copolymers were determined as 0.01 mg/mL and 0.029 mg/mL, respectively (Figure 3.21).

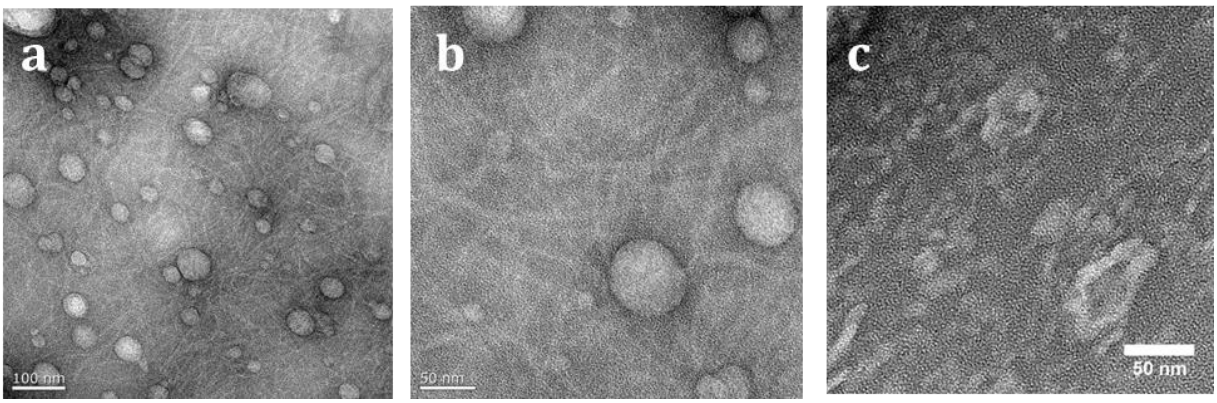

Figure 3.20. TEM images of (a, b) BC3dp and (c) BC8dp

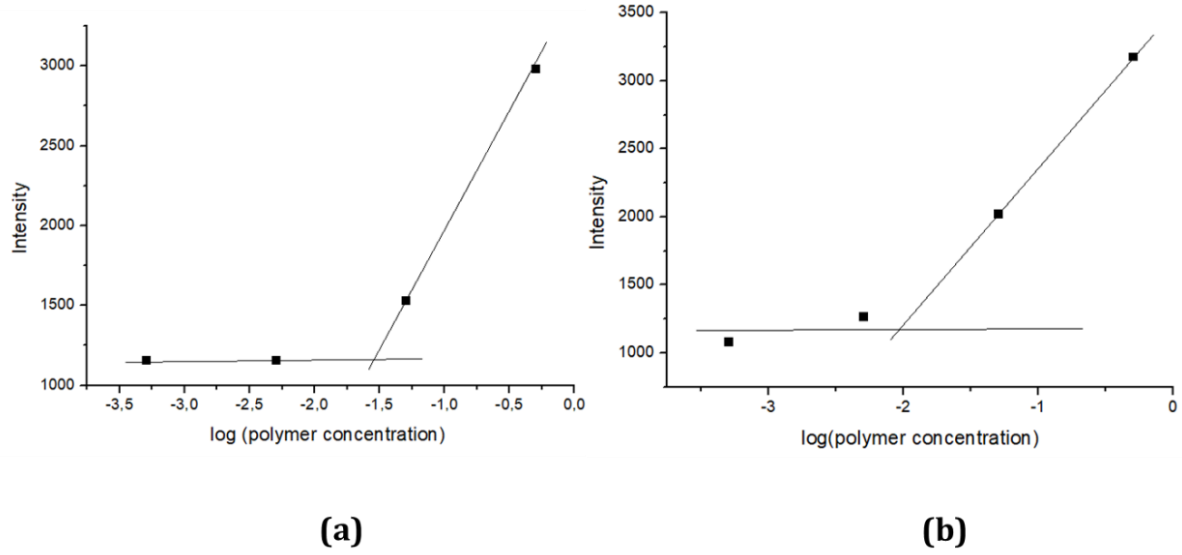

Figure 3.21. CMC determination of (a) BC8dp and (b) BC3dp

Block copolymer BC6dp (30/120) has a hydrodynamic radius of 193 nm according to the DLS analysis. TEM results demonstrated quite small (<50 nm) spherical particles as seen in Figure 3.22.b. Strong interaction of the polymer with electron beam during the measurements made analysis difficult. Figure 3.22.a was taken while this interaction. CMC

of the BC6dp and BC5dp block copolymers was determined as 0.031 mg/mL and 0.032 mg/mL in water, respectively (Figure 3.23).

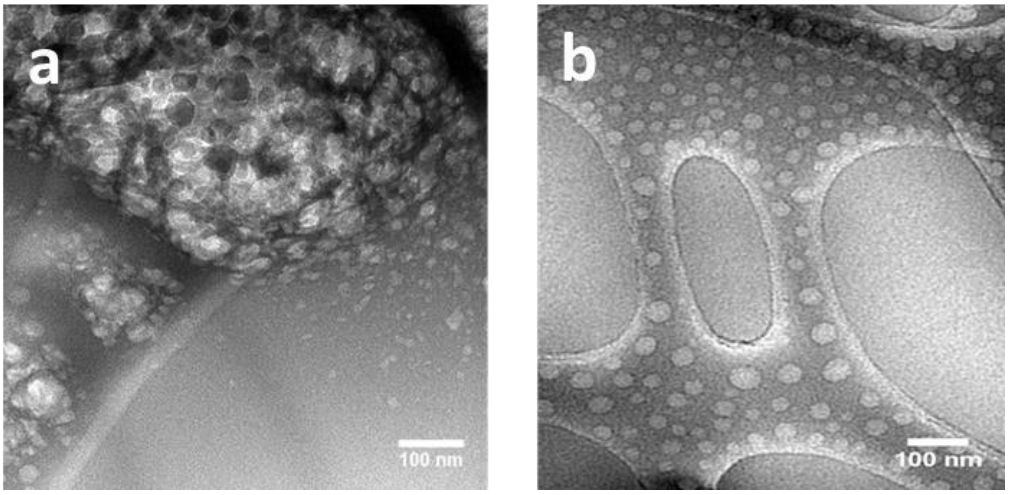

Figure 3.22. TEM investigation of BC6dp

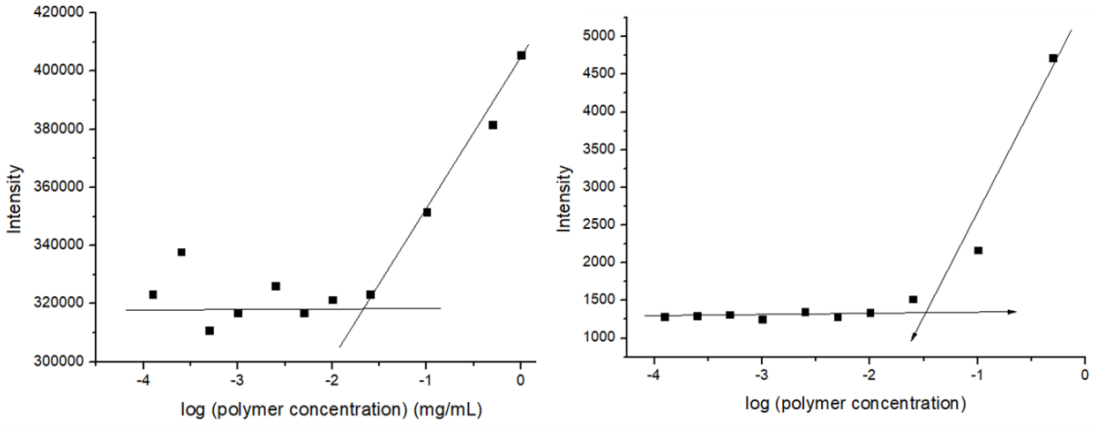

Figure 3.23. CMC determination of (a) BC6dp and (b) BC5dp

3.2.7. Cytotoxicity of the Polymeric Micelles

Cell viability studies of the PLLA-*b*-PLSL block copolymer micelles were performed on A549 human lung adenocarcinoma cell line. Different chain lengths of block copolymers

BC5dp (30/120), BC3dp (70/140) and BC6dp (120/220) were investigated to identify their biocompatibility *via* incubating them into the mentioned cell medium in various concentrations (0.2, 0.1 and 0.05 mg/mL). In order to investigate the difference of toxicity behavior of the amino-functional poly(α-amino acid) *vs.* pseudo-poly(amino acid), PEG_{45}-*b*-$polylysine_{90}$ were also synthesized and cell viability is studied. Data is expressed as % cell viability (proportion of living cells) and % standard deviation (Figure 3.24). As demonstrated below, all of the PLLA-*b*-PLSL micelles, even in the highest concentration, show no cytotoxicity. In contrast to that, PEG_{45}-*b*-$polylysine_{90}$ copolymer is very toxic even at lower concentrations.

These results clearly confirm that PLLA-*b*-poly(L-serine lactone) block copolymers are biocompatible materials and very promising for drug delivery applications. Further step can be the bio-investigation *in vivo.*

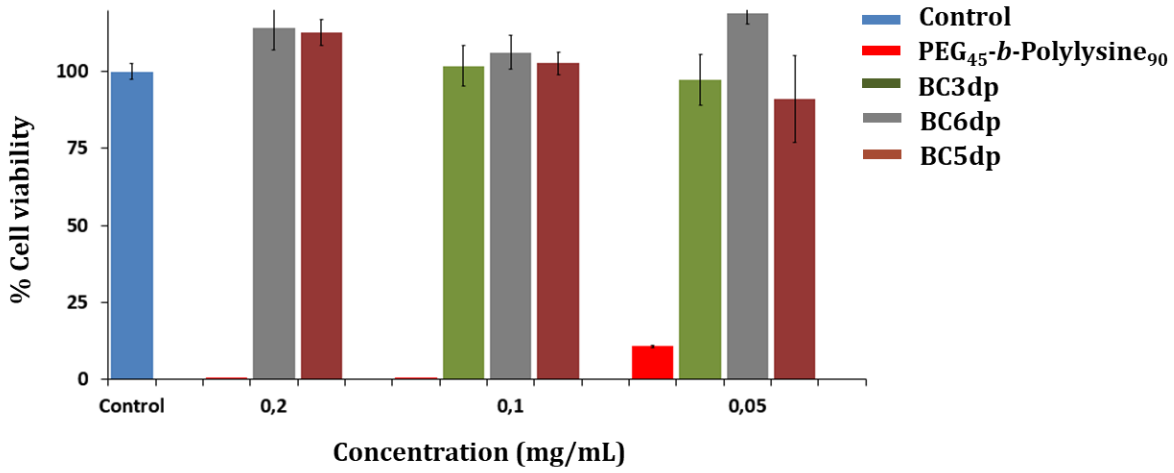

Figure 3.24. Cytotoxicity data of the BC3dp, BC6dp and BC5dp micelles with various concentrations (mg/mL)

3.3. Conclusion and Outlook

Synthesis of the novel biocompatible and amino-functional block copolymer of L-lactide and N-protected L-serine has been performed successfully by sequential ring-opening polymerization. Although various PLLA copolymers have been synthesized in the literature up to now; in our study, however, biocompatibility of the PLLA has been preserved by utilization of a N-protected derivative of inherently biocompatible amino acid "N-protected L-serine lactone" as a co-monomer.

PLLA with different chain lengths (DP= 40 to 200) were prepared by ROP of L-lactide using N-heterocyclic carbene, SIMes, as a catalyst at ambient temperature in 10 minutes with narrow polydispersity of around 1.2. Polymerization of N-trityl serine lactone was proceeded by SIMes as well, but only oligomerization was achieved. Further, it was demonstrated that PLLA macro-initiators with –OH end groups are able to initiate the ROP of N-trityl-L-serine lactone, catalyzed by $ZnEt_2$ in solution. All the copolymerization was carried out as described in two steps, purified by precipitation and further analyzed by GPC with number averaged molecular weights up to 55000 g/mol and with polydispersity of around 1.50. Characterization of the diblock copolymers was performed by NMR and IR spectroscopy and, number average molecular weights were calculated by the end group analysis in ^{1}H-NMR. The presence of all the building blocks and their covalent linkage was determined by the combination of ^{1}H- and ^{1}H-DOSY NMR. Existence of differing diffusion coefficients in this 2D spectrum could be assigned to any by-products that may have been formed. Thermal properties of the block copolymers were studied by TGA and DSC and, two glass transition temperatures were observed at around 75 °C and 145 °C. After the cleavage of trityl group under acidic conditions, the formation of PLLA-b-PLSL micelles was readily achieved in aqueous solution at ambient temperature by dialysis method. The generated micelles possess an average diameter of roughly 100 nm according to the DLS measurements. In order to assess the efficacy of these amphiphilic PLLA micelles as a cargo carrier system, pyrene loading into the aggregates were performed and critical micelle concentrations were investigated by Fluorescence spectroscopy. Their morphology was analyzed by TEM and showed wormlike or spherical aggregates depending on the block ratio of hydrophilic/hydrophobic parts and molecular

weights of the copolymers. Finally, cell experiments were demonstrated that the micelles are fully biocompatible in A549 human lung adenocarcinoma cell line.

Obtained PLLA-based amphiphilic block copolymers with unique properties such as biocompatibility, specific aggregate formations and amino functionality makes them a promising drug nanocarrier for further studies. In particular, PLLA hydrophobic core can be stabilized in water by the amino functional hydrophilic corona, leading to micellar structures with different morphologies. These surface properties of the aggregates are very important for increasing the blood circulation time and cell uptake properties of the materials *in vivo*. Moreover, the presence of amino groups offers great potential for further bio-conjugations with bio-active molecules such as vitamins, specific peptide sequences, carbohydrates, aptamers etc. for targeting delivery applications. Thus, the PLLA-based micelles can possess all necessary properties to consider them as an excellent alternative to commonly used drug delivery vehicles.

3.4. Experimental Part

3.4.1. Materials and Methods

Following chemicals were purchased from Sigma Aldrich and used as received: L-Serine, L-lactide, trityl chloride, trimethylsilylchloride (TMS-Cl), 1-pyrene butanol, benzyl alcohol, triethylamine (TEA), benzotriazol-1-yloxytris(dimethylamino)-phosphoniumhexafluoro phosphate (BOP), pyrene, diethyl zinc ($ZnEt_2$) 15% w/w toluene solution and trifluoroacetic acid (TFA). N-boc-serine β-lactone (Across Organics), methoxy-PEG-OH (M_n=1200 g/mol) (Rapp Polymer) and, 1,3-bis(2,4,6 trimethylphenyl)-2-imidazolidinylidene (SIMes) (ABCR) were stored under inert atmosphere in glovebox. All solvents were purchased from Sigma Aldrich if not stated otherwise. Toluene and THF were purified by distillation from sodium with benzophenone. Other solvents were of analytic grade and used as received.

3.4.2. Synthesis

N-trityl-L-serine

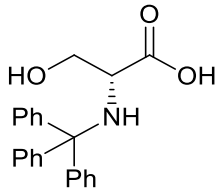

N-trityl-L-serine was synthesized according to the literature.[214] L-Serine (5.00 g, 47.60 mmol, 1.00 eq) was suspended in CH_2Cl_2 (80 mL) under argon. TMS-Cl (21.10 mL, 166.00 mmol, 3.50 eq) was added at RT and mixture was refluxed for 1 hour. After cooling to RT, 40 ml CH_2Cl_2 solution of TEA (23.30 mL, 166 mmol in 40 mL CH_2Cl_2, 3.50 eq) was added and solution refluxed again for one hour. Reaction mixture was cooled down to 0 ^oC and MeOH (3 mL) in CH_2Cl_2 (15 mL) was added. Afterwards, TEA (6.66 mL, 47.60 mmol, 1.00 eq) and trityl chloride (13.2 g, 47.60 mmol, 1.00 eq) were added over 15 min. The reaction was allowed to stir overnight. MeOH (10.0 mL) and TEA (8 mL) were then added, and the mixture was stirred for an additional 15 min. All solvents were removed under vacuum,

and the crude acid was dissolved in EtOAc (150 mL) and washed with a 5% citric acid solution and then with water. The organic layer was dried over $MgSO_4$, filtered, and concentrated, yielding yellow foam. The crude acid was purified by precipitation from $CHCl_3$, and the product was isolated as a white solid (8.60 g, 24.75 mmol, 52%).

^{1}H NMR (300 MHz, CD_2Cl_2) δ: 7.50 – 7.40 (m, 6H), 7.36 – 7.19 (m, 9H), 3.72 – 3.63 (m, 1H), 3.50 – 3.42 (m, 1H), 2.82 (dd, J = 11.0, 4.5 Hz, 1H) ppm.

N-trityl-L-serine lactone ((S)-3-(Tritylamino)oxetan-2-one) (NTSL)

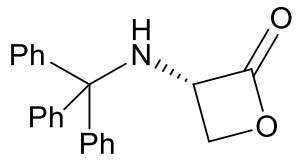

NTSL was synthesized as described in the literature.[214] N-trityl-L-serine (2.00 g, 5.76 mmol, 1.00 eq) was suspended in CH_2Cl_2 (40 mL) under argon atmosphere at ambient temperature. TEA (2.30 mL, 16.00 mmol, 2.78 eq) was added, and the mixture became homogeneous. BOP (3.56 g, 8.06 mmol, 1.40 eq) was added in two portions and the solution was stirred for two hours. Reaction mixture was diluted with water and stirred additional 30 min. The layers were separated, and the aqueous layer was extracted with CH_2Cl_2 (3x). Combined organic layers were dried over $MgSO_4$, filtered, and concentrated, yielding a yellow solid. The crude solid was purified using flash column chromatography on silica gel (petroleum ether/EtOAc 85:15) as a white solid (1.32 g, 4.01 mmol, 70%).

^{1}H NMR (300 MHz, CD_2Cl_2) δ: 7.50 (dd, J = 7.1, 1.6 Hz, 6H), 7.39 – 7.20 (m, 9H), 4.64 – 4.53 (m, 1H), 3.54 (s, 1H), 3.13 (s, 1H), 2.72 (d, J = 11.7 Hz, 1H) ppm.

^{13}C NMR (75 MHz, CD_2Cl_2) δ: 172.51, 145.79, 128.96, 128.84, 127.57, 71.25, 71.25, 71.17, 65.17 ppm.

Poly(L-lactide) (PLLA)

General polymerization procedure for the synthesis of PLLA is described below, using PLLA-4 as an example. Table 3-10 summarizes the synthetic details and results of all the polymerizations (PLLA-1 to PLLA-5).

Polymerization of L-lactide was carried out in the glovebox under N_2 atmosphere. In a typical procedure, 1 M solution of L-lactide (1.00 g, 6.94 mmol, 1.00 eq) was prepared with dry THF. SIMes (0.0212 g, $6.94x10^{-2}$ mmol, 0.01 eq) and benzyl alcohol ($6.94x10^{-2}$ mmol, 7.00 µL, 0.01 eq) were dissolved in a minimum amount of THF and added to the L-lactide solution. Polymerization proceeded for 10 minutes at room temperature and polymer was precipitated by cold methanol. PLLA was filtered and dried under vacuum as a white solid (PLLA-4, 0.85 g, 85%).

Table 3-10. Synthetic details and polymerization results of PLLA

Polymer	DP (theo)	M/Cat/I	L-lactide		Yield %	DP (exp) (^{1}H-NMR)	GPC	
			m (g)	n (mmol)			$M_{n\ (g/mol)}$	Đ
PLLA-1	40	20/1/1	0.5	3.47	32	30	2800	1.28
PLLA-2	70	35/1/1	1	6.94	88	70	8500	1.15
PLLA-3	80	40/1/1	0.5	3.47	81	95	8800	1.40
PLLA-4	200	100/1/1	1	6.94	85	120	13800	1.32
PLLA-5	200	100/1/1	0.5	3.47	88	190	13500	1.16

*M/Cat/I: molar ratio of monomer/catalyst/initiator: L-lactide/SIMes/Benzyl alcohol

^{1}H-NMR (δ (ppm) 500 MHz, CD_2Cl_2): 7.41 – 7.29 (m, 5H, Ph), 5.24 – 5.08 (q, J = 7.1 Hz, 1H, CH), 1.59 – 1.51 (d, J = 7.1 Hz, 3H, CH_3) ppm.

FT-IR (ATR): 2999, 2996 (*v* (-CH)), 1456, 1360 (δ (-CH_3)), 1758 (*v* (-C=O ester)), 1187-1088 (*v* (-C-O-C ester)) cm^{-1}.

GPC (THF as eluent, against PS): As g*iven in Table 3-10.*

Experimental degree of polymerizations (DP(exp)) were calculated by the end group analysis via ^{1}H-NMR (Table 3-10).

Synthesis of poly(N-trityl-L-serine lactone) (PNTSL), poly(N-boc-serine-β-lactone) (PNbocSL) and statistical PLLA-*co*-poly(N-trityl-L-serine lactone) (PLLA-*co*-PNTSL) by SIMes

General polymerization procedure is described below and applied to all these polymers with slight differences. Table 3-11 summarizes the synthetic details and polymerization results.

Polymerization was carried out in the glovebox under N_2 atmosphere at room temperature in different reaction times and solvents. In a typical procedure, 1 M solution of monomer (or monomers in the copolymer case) was prepared with dry solvent as a final concentration of 1M. SIMes and 1-pyrenebutanol were dissolved separately in a minimum amount of solvent and added to the monomer solution. Polymerization was proceeded for different time intervals and isolated by precipitation with cold methanol, followed by drying under vacuum.

Table 3-11. Synthetic details and polymerization results of PNTSL, PNbocSL and PLLA-*co*-PNTSL by SIMes

Polymer	M/Cat/I	L-lactide		NTSL or NbocSL		Time	Solvent	Yield %
		m (g)	n (mmol)	m (g)	n (mmol)			
PNTSL-1	50/1/1	-	-	0.25	0.76	15 min	THF	26
PNTSL-2	50/1/1	-	-	0.25	0.76	24 h	THF	30
PLLA-6	50/1/1	0.055	0.38	-	-	15 min	THF	82
PLLA-*co*-PNTSL	50/1/1	0.04	0.27	0.09	0.27	15 min	THF	39
PNbocSL-1	50/1/1	-	-	0.07	0.38	3 h	DMF	-
PNbocSL-2	50/1/1	-	-	0.07	0.38	24 h	DMF	-

PNTSL-1 and PNTSL-2:

^{1}H-NMR (δ (ppm) 700 MHz, CD_2Cl_2): δ 7.41 (d, J = 7.3 Hz, 6H), 7.25 - 7.17 (m, 9H), 4.56 – 4.46 (m, 1H), 3.46 (t, J = 5.8 Hz, 1H), 3.05 (dd, J = 5.6, 4.6 Hz, 1H), 2.63 (d, J = 11.7 Hz, 1H) ppm.

GPC (THF as eluent, against PS):

PNTSL-1; M_n=1600 g/mol; Đ = 1.18; ($M_{n(theoretical)}$=17000 g/mol)

PNTSL-2; M_n=1500 g/mol; Đ= 1.79; ($M_{n(theoretical)}$=17000 g/mol)

PLLA-6:

^{1}H-NMR (δ (ppm) 700 MHz, CD_2Cl_2): 8.36 – 7.64 (m, 9H, pyrene-Ar), 5.09 (q, J = 7.1 Hz, 1H, CH), 1.48 (d, J = 7.0 Hz, 3H, CH_3) ppm.

GPC (THF as eluent, against PS): M_n=8000 g/mol; Đ= 1.39; ($M_{n(theoretical)}$=7200 g/mol)

PLLA-co-PNTSL:

^{1}H-NMR (δ (ppm) 700 MHz, CD_2Cl_2): δ 8.31 – 7.85 (m, 9H, pyrene-Ar), 7.50 - 7.48 (t, J = 7.7 Hz, 6H-Ar), 7.33 - 7.26 (t, J = 7.3 Hz, 9H-Ar), 5.17 (q, J = 7.1 Hz, 1H, CH of PLLA), 4.58 (t, J = 11.1 Hz, 1H, CH_2 of PNTSL), 3.55 (t, J = 5.8 Hz, 1H, CH_2 of PNTSL), 3.13 (t, J = 5.1 Hz, 1H, CH of PNTSL), 2.72 (d, J = 11.6 Hz, 1H, NH), 1.56 (d, J = 7.1 Hz, 3H, CH_3 of PLLA) ppm.

GPC (THF as eluent, against PS): M_n=10000 g/mol, Đ= 1.55

PNbocSL-1 and PNbocSL-2:

^{1}H-NMR (δ (ppm) 500 MHz, CD_2Cl_2): Not characterizable

GPC (THF as eluent, against PS):
PNbocSL-1; M_n=1210 g/mol; Đ= 1.16; ($M_{n(theoretical)}$=9300 g/mol)
PNbocSL-2; M_n=1250 g/mol; Đ= 1.16; ($M_{n(theoretical)}$=9300 g/mol)

Synthesis of poly(N-trityl-L-serine lactone) (PNTSL) and statistical PLLA-*co*-poly(N-trityl-L-serine lactone) (PLLA-*co*-PNTSL) by $ZnEt_2$

General polymerization procedure used for the synthesis of PNTSL by $ZnEt_2$ is described below and in the literature.[112] *The same procedure was applied for the statistical copolymer of L-lactide and NTSL. Table 3-12 presents the synthetic details and results of all the polymerizations (PNTSL-3, PNTSL-4, PLLA-co-PNTSL (RC1) and (RC2)).*

In a typical procedure, NTSL (0.10 g, 0.03 mmol, 1.00 eq) (in the case of copolymer L-lactide and NTSL) was introduced into a flame dried, argon purged flask and dissolved in 1.50 mL of dry toluene under inert atmosphere at 90 ˚C. $ZnEt_2$ solution (3.00 µmol, 2.70

μL, 0.10 eq) was added and polymerization was carried out for 15 minutes. Reaction mixture was cooled down to 0 °C rapidly and toluene was evaporated. Copolymer was dissolved in THF, filtered and precipitated by cold methanol as a white solid.

Table 3-12. Synthetic details and polymerization results of PNTSL and PLLA-*co*-PNTSL by $ZnEt_2$

Polymer	M/Cat	L-lactide		NTSL		Time	Solvent	Yield %
		m (g)	n (mmol)	m (g)	n (mmol)			
PNTSL-3	100/1	-	-	0.1	0.03	20 min	toluene	80%
PNTSL-4	100/1	-	-	0.1	0.03	24 h	toluene	80%
PLLA-*co*-PNTSL (RC1)	200/1	0.12	0.87	0.11	0.35	15 min	toluene	81%
PLLA-*co*-PNTSL (RC2)	200/1	0.12	0.87	0.11	0.35	18 h	toluene	75%

PNTSL-3 and PNTSL-4:

^{1}H-NMR (δ (ppm) 700 MHz, $CDCl_3$): 7.68 – 7.07 (m, 15H), 4.03 (s, 1H, CH_2), 3.83 (s, 1H, CH_2), 3.60 (s, 1H, CH), 2.82 (s, 1H, NH) ppm.

GPC (THF as eluent, against PS):

PNTSL-3; M_n=25000 g/mol; Đ= 1.18

PNTSL-4; M_n=15600 g/mol; Đ= 1.77

PLLA-co-PNTSL:

^{1}H-NMR (δ (ppm) 700 MHz, CD_2Cl_2): 7.50-7.49 (6H-Ar), 7.31-7.12 (9H Ar), 5.16 (CH-PLLA), 4.41-4.17 (CH_2-PNTSL), 3.67 (CH-PNTSL), 2.51 (NH), 1.55 (CH_3-PLLA) ppm.

GPC (against PS, THF as eluent):

PLLA-*co*-PNTSL (RC1); M_n=8800 g/mol; Đ= 1.37

PLLA-*co*-PNTSL (RC2); M_n=9700 g/mol; Đ= 1.67

PEG-*block*-poly(N-trityl-L-serine lactone)(PEG-*b*-PNTSL)

PEG-*b*-PNTSL copolymer was synthesized according to the literature.[112] CH_3O-PEG-OH (M_n=1200 g/mol) (0.02 g, 0.01 mmol, 1.00 eq) was dried azeotropically by toluene and NTSL (0.30 g, 0.90 mmol, 90.00 eq) was added to this flame dried, argon purged flask. Solid was dissolved by 1 mL of dry toluene under inert atmosphere at 90 ˚C. $ZnEt_2$ solution (1.00 µmol, 1.00 µL) was added and polymerization was carried out for 15 minutes. Reaction mixture was cooled down to 0 ˚C rapidly and toluene was evaporated. Copolymer was dissolved in THF, filtered and precipitated by cold methanol as a white solid (0.27 g, 84%).

^{1}H-NMR (δ (ppm) 300 MHz, CD_2Cl_2): 7.43 - 7.09 (m, 15H, Ar), 3.85 (s, 1H, CH_2), 3.65 (s, 1H, CH_2), 3.60 (d, J = 1.1 Hz, CH_2CH_2O, PEG(CH_2)), 3.49 – 3.35 (m, 1H, CH), 2.67 (d, J = 9.8 Hz, 1H, NH) ppm.

GPC (THF as eluent, against PS): M_n=8700 g/mol; Đ= 1.11

Poly(L-lactide)-*block*-poly(N-trityl-L-serine lactone)(PLLA-*b*-PNTSL)

General polymerization procedure for the synthesis of PLLA-b-PNTSL block copolymers is described below using, BC3 as an example. Table 3-13 and Table 3-14 presents the synthetic details and results for all the polymerizations from BC2 to BC10.

In a typical procedure, NTSL (0.50 g, 1.50 mmol, 1.00 eq) and hydroxyl terminated-PLLA macro initiator (PLLA-2) (0.054 g, 10.80 µmol, 0.0072 eq) were introduced into a flame dried and argon purged flask and dissolved in 2.5 mL of dry toluene under inert atmosphere at 90 °C. $ZnEt_2$ solution (15.18 µmol, 14.00 µL) [n($ZnEt_2$)/n(NTSL)=1:100] was added and polymerization was carried out for 15 minutes. Reaction mixture was cooled down to 0 ˚C rapidly and toluene was evaporated. Copolymer was dissolved in THF, filtered and precipitated by cold methanol as a white solid (BC3, 0.36 g, 72%).

Table 3-13. Synthetic details of BC2 to BC10

Polymer	$DP_{(theo)}$ PLLA/PNTSL	NTSL		PLLA-OH		$ZnEt_2$ (µL)	toluene (mL)	Yield (%)
		m (g)	n (mmol)	m (g)	n (µmol)			
BC2	70/70	0.50	1.5	0.12	21.6	14	3	56
BC3	70/140	0.50	1.5	0.054	10.8	14	3	72
BC4	70/210	0.50	1.5	0.036	7.2	14	3	80
BC5	30/120	0.50	1.5	0.027	12.6	14	3	68
BC6	120/240	1.00	3.0	0.11	12.6	27.3	4.2-4.5	82
BC7	70/140	0.50	1.5	0.05	10	14	3	-
BC8	70/210	0.50	1.5	0.036	7.2	14	3	72
BC9	120/240	0.30	0.9	0.033	3.8	8.2	2.2	-
BC10	120/240	0.50	1.5	0.04	8	14	3	-

^{1}H-NMR (δ (ppm) 500 MHz, CD_2Cl_2): δ 7.51 – 7.37 (d, J = 7.0 Hz, 6H, Ar), 7.24 – 6.97 (dt, J = 62.2, 6.8 Hz, 9H), 5.23 – 5.11 (q, J = 6.8 Hz, 1H, CH(PLLA)), 3.99 – 3.78 (s, 1H, CH_2), 3.71 – 3.61 (s, 1H, CH_2), 3.51 – 3.29 (s, 1H, CH), 2.75 – 2.56 (d, J = 9.1 Hz, 1H, NH), 1.57 – 1.54 (d, J = 6.9 Hz, 3H, CH_3 (PLLA)) ppm.

^{13}C-NMR (δ (ppm) 75 MHz, CD_2Cl_2): 171.67, 170.08, 146.10, 129.25, 128.55, 127.20, 71.58, 69.58, 67.17, 56.23, 16.78 ppm.

FT-IR (ATR): 3340 (v (-NH)), 3058 and 3029 (v (-CH aromatics)), 2996, 2948 (v (-CH)), 1752 (v (-C=O ester)), 1596 (δ (-NH)), 1489, 1448 (v (C=C aromatics)), 1183-1089 (v (-C-O-C ester)), 746, 702 (δ (-CH aromatics)) cm^{-1}.

GPC (against PS, THF as eluent): As presented in Table 3-14.

Experimental degree of polymerizations (DP(exp)) were calculated by the end group analysis via ^{1}H-NMR (Table 3-14).

Table 3-14. Polymerization results of BC2 to BC10

Polymer	GPC		DP (exp) PLLA/PNTSL	Polymer	GPC		DP (exp) PLLA/PNTSL
	M_n (g/mol)	Đ			M_n (g/mol)	Đ	
BC2	14000	1.52	70/49	**BC7**	18000	1.93	70/175
BC3	35000	1.48	70/140	**BC8**	34500	1.40	70/350
BC4	55000	1.50	70/210	**BC9**	17000	1.78	120/120
BC5	42400	1.44	30/120	**BC10**	14000	1.77	120/140
BC6	43000	1.35	120/220				

Deprotection of the trityl groups of PLLA-*b*-PNTSL

General cleavage procedure of the trityl groups of PLLA-b-PNTSL block copolymers is described below. Table 3-15 summarizes the synthetic details for all the polymers from BC2dp to BC10dp.

In a typical reaction, block copolymer was dissolved in a dry CH_2Cl_2 (2 mL) at room temperature and purged with argon. Separately, cleavage cocktail TFA/methanol/DCM (1:2.5:36.5 v/v/v) was prepared as a stock solution. Polymer solution was cooled down to 0 ˚C and desired amount of cleavage solution was added *via* syringe in 0.1 mL portions every 5 minutes. After a total reaction time of 30-40 min reaction mixture was precipitated into cold diethyl ether. The precipitant was filtered, washed with diethyl ether and dried under vacuum as a white solid (Yield 54% - 75%).

^{1}H-NMR (δ (ppm) 500 MHz, CD_2Cl_2): δ 7.58 – 6.87 (m, Bn-Ar) (NH_3^+), 5.38 – 5.02 (q, J = 7.0 Hz, 1H, CH (PLLA)), 4.84 – 4.23 (m, 3H, PNTSL), 1.62 – 1.34 (d, J = 7.0 Hz, 3H, CH_3 (PLLA)) ppm.

FT-IR (ATR): 3350-2800 (v ($-NH_3^+$)), 2996, 2948 (v (-CH)), 1752 (v (-C=O ester)), 1669 (v (-C=O ester of CF_3COO^-)), 1183-1089 (v (-C-O-C ester)), 836, 798 and 723 cm^{-1}.

Table 3-15. Synthetic details of the cleavage of trityl groups

Pol.	Pol. (mg)	v(mL)	DCM (mL)	Time (min)	Pol.	Pol. (mg)	v(mL)	DCM (mL)	Time (min)
BC2	120	0.9	2	30	**BC7**	120	1.8	2	30
BC3	120	1.8	2	30	**BC8**	120	2	2	30
BC4	120	2.7	2	30	**BC9**	120	1	2	30
BC5	120	1.1	2	30	**BC10**	120	2	2	30
BC6	120	2	2	30					

*v (mL): volume of the cleavage cocktail: TFA/methanol/DCM: (1:2.5:36.5 v/v/v)

Preparation of polymeric micelles

Polymeric micelles were prepared by dialysis method. 20 mg of each block copolymer was dissolved in 5 mL of DMSO, filtered from 0.8 μm teflon syringe filter and transferred into the RC dialysis membrane (MWCO=1000 g/mol). Samples were dialyzed against water for 24 hours followed by 2 hours of sonication and centrifugation at 12000 rpm for 20 minutes. Resulted dispersion was used as a stock solution for micelle study (mass loss was neglected during the dialysis, final concentration was adjusted to 2 mg/mL). Only for BC2dp which has longer hydrophobic block (70/49), solution was freeze dried after centrifugation and redispersed in water in a concentration of 0.50 mg/mL.

For DLS and TEM analysis, polymeric dispersions were prepared in a concentration of 0.50 mg/mL by dilution from the stock solution. Samples were sonicated for 15 minutes and filtered from 0.8 μm syringe filter.

Critical micelle concentration (CMC) determination

$6*10^{-2}$ M stock solution of pyrene was prepared in acetone (1.2135 g pyrene, 100 mL acetone). 2 μL of this solution was added to the 100 mL of water and aceton was removed under vacuum in order to obtain $12*10^{-7}$ M pyrene/water solution for fluorescence measurements.

This water solution of pyrene was mixed with the polymeric micelle solutions in which concentration is ranged from 1.00 mg/mL to 0.000125 mg/mL. The final pyrene

concentration in each polymer solution was $6*10^{-7}$ M. Pyrene emission was recorded between 360-550 nm by excitation at 339 nm. CMC was estimated by plotting the intensity of the first band to the log of the micelle concentration.

Cytotoxicity of the polymeric micelles

Cell viability of the block copolymer micelles were tested on A549 human lung adenocarcinoma cell line. A549 Cells (German Collection of Microorganisms and Cell Cultures, Braunschweig) were cultured in high glucose DMEM supplemented with 10% FCS, 10% Penicillin/Streptomycin, 1% MEM non essential amino acid at 37 °C/5% CO_2. Passages of cells were made near confluency in a T-75 Flask using standard trypsination protocol using Trypsin LE Express (ThermoFisher Scientific).

A549 cells (5000 cells/well) in a white 96-well (half-area) microplate and left to adhere overnight in an incubator at 37 °C/5% CO_2. The cells were treated with the prescribed amount of polymers (0.05 – 0.2 mg/mL in DMEM) and were incubated for 24 h at 37 °C/5% CO_2. (Block copolymers BC3dp, BC5dp, BC6dp and PEG_{45}-*b*-poly(L-lysine)$_{90}$ (0.2, 0.1 and 0.05 mg/mL)). The cell viability was subsequently tested using CellTiter-Glo® Luminescence Cell Viability Assay (Promega) according to manufacturer's protocol. Cells without treatment are referenced as blank and the data is represented as % cell viability. All measurements were performed in triplicates.

CHAPTER 4

Design and Preparation of Stimuli-responsive Nanocarriers

4. Design and Preparation of Stimuli-responsive Nanocarriers

4.1. Introduction

Biocompatible nanoparticles have been of interest for many years due to their potential as drug delivery vehicles.[9,143,180,232] It is generally accepted that the defective vasculature of solid tumors results in the accumulation of macromolecules and nanoparticles in the tumor, a pharmacological phenomenon known as the Enhanced Permeability and Retention (EPR) effect.[233,234] A number of approaches have been explored to exploit this effect including polymer-based chemotherapy, micelles, liposomes, polymersomes, and nanoparticles (both inorganic and organic) made by various techniques.[235–237] Each of these classes of materials have advantages and disadvantages that are, to a certain extent, idiosyncratic. However, controlled drug release and general biodegradability have emerged as two of the most desired attributes of a given nanomedicine.

Tumor targeting includes more than simply accumulating into the targeted tissue. It also requires the selective release of a therapeutic payload only at the targeted site. Again, there have been many approaches to achieving this goal, but virtually all of the work in this area has used pH, redox, temperature, magnetic fields, tumor-specific enzymes, or light as the drug-release stimulus.[238–240] An approach utilizing a novel stimulus could potentially be a major breakthrough in this field. The challenge in designing a suitable drug-release mechanism is that it must be sufficiently stable in general circulation, but must be completely labile in the target environment.[236,238] Release mechanisms using tumor-specific enzymes[206] are arguably the most effective at achieving this goal: pH-sensitive groups hydrolyze to a certain extent in circulation, redox-active compounds also often react in off-target tissue, a temperature gradient between tumor tissue and the rest of the body is often difficult to achieve precisely, and light has a limited penetration depth (particularly at shorter wavelengths, which are often used to trigger release). In the context of drug release, proteases are often the class of enzyme employed.[19,241] The diversity within this enzyme class enables a number of protein sequences to be employed, cleaved by a number of different enzymes. Among the most commonly employed approaches is the use of the GFLG peptide linker, which is selectively cleaved by cathepsin B, a lysosomal cysteine protease overexpressed in many tumor cells. However, this

approach requires the delivery vehicle to enter the lysosome.[242] Our approach has been to target matrix metalloproteinases (MMPs), specifically MMP-2, which is present at the invasive front of many solid tumors.[243,244] Degradation begins as soon as the tumor is reached without requiring initial cell internalization of the entire carrier; MMPs are overexpressed in several cancers, potentially enabling more general therapeutic applications; diffusion throughout the tumor may be enhanced due to the fact that degradation takes place outside of an individual cell, potentially enhancing therapeutic efficacy.[245–247]

Previous work in our group by Dorresteijn et. al[248] demonstrated that the oligopeptide sequence PLGLAG can be incorporated into PLLA nanoparticles and subsequently degraded by MMP-2. This approach has the further advantage that PLLA itself is fully biodegradable and biocompatible. In addition to the material itself, the size of a drug-carrier is a key consideration. It must be large enough to avoid renal clearance, but small enough to avoid clearance from the bloodstream by Kupffer cells.[249–251] That study targeted a size around 100 nm, which fulfills both of these criteria.[248] These nanoparticles were synthesized by nonaqueous emulsion polymerization using PI-*b*-PEG as the emulsifier. As a result, the initially hydrophobic particles had to be transferred into aqueous media using Lutensol AP 20, a PEG-based surfactant, to stabilize the nanoparticles in water.[248] There are disadvantages to this surfactant approach, however. In particular, potential changes in particle morphology and masking the peptide from the target enzyme. Additionally, the polyisoprene portion of the emulsifier is non-biocompatible.

Because of these aforementioned drawbacks and challenges, herein, tailor-made fully biocompatible and biodegradable polymeric nanomaterials are aimed to be developed, meaning that no non-biocompatible elements exist either in the emulsifier or in the core of the nanoparticle. PEG-*block*-poly((1-pyrenyl methyl) glutamate) (PEG-*b*-PGlu(Pyr)) block copolymers should be considered as biocompatible emulsifiers to generate MMP-2 sensitive PLLA-*b*-peptide-*b*-PLLA nanoparticles *via* nonaqueous emulsion polymerization. Particle transfer from this organic platform into the aqueous system should be demonstrated by the polarity reversal of the particle surface *via* light-induced mechanism (Scheme 4.1).

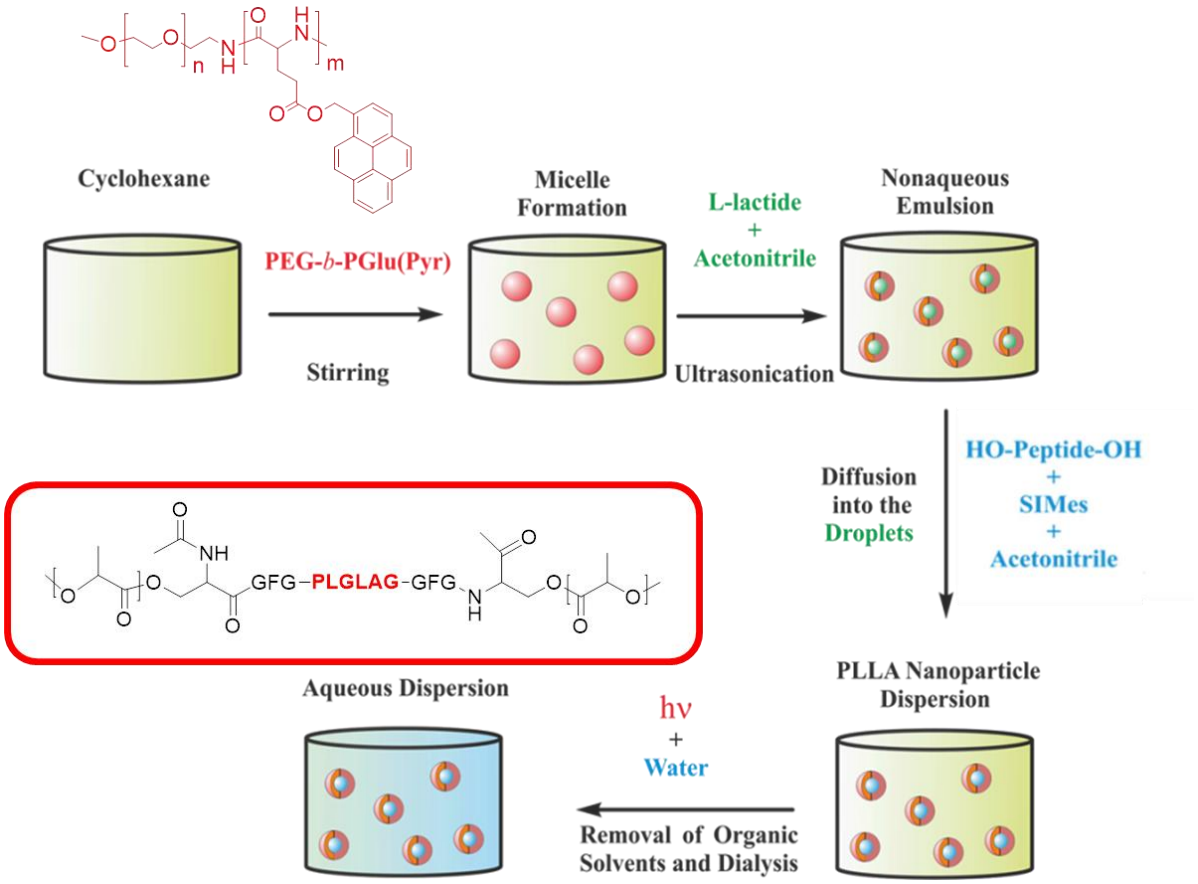

Scheme 4.1. Schematic illustration of the fabrication of smart nanocarrier

In the second part of this chapter, development of both enzyme (MMP-2) and photo-degradable triblock copolymer, PEG-*b*-peptide-*b*-poly((1-pyrenyl methyl) glutamate), is aimed as a novel bio- and photo-responsive material (Scheme 4.2). For designing such a system, new synthetic strategies should be developed. Post-polymerization modification is a commonly used route for block copolymer synthesis; however, the functional monomer approach is more promising in the presence of sensitive moieties e.g., peptides in order to avoid the degradation and challenging stepwise reactions and purifications. Therefore, the goal is the synthesis of novel pyrene-functional L-glutamic acid NCA monomer "γ-(1-pyrenylmethyl)-L-glutamate N-carboxyanhydride" (pyrene-Glu NCA). Designing and employing the PEG-modified MMP-2 degradable PEG-*b*-PLGLAG-NH_2 macro-initiators for the polymerization of pyrene-Glu NCA, new types of biocompatible block copolymers should be obtained. By these bio-responsive block copolymers, both, core and shell modified enzymatically and photolytically degradable smart copolymers

can be generated. Both of these elements are novel in themselves, and together they represent an interesting advance in the field of nanoparticles for drug delivery.

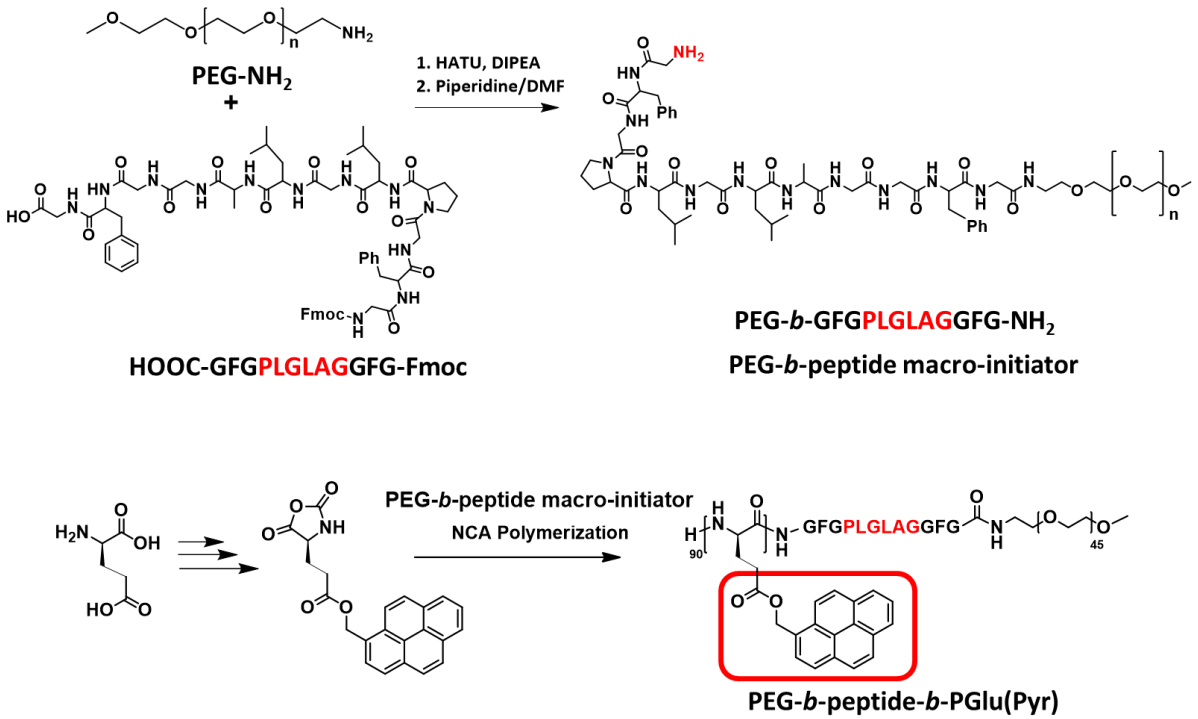

Scheme 4.2. Synthesis of smart triblock copolymers

4.2. Results and Discussion

Amphiphilic block copolymers are known by their phase separation phenomena which results in a nano- or micro-scale aggregates in solution.[114] Nonaqueous emulsion is an emerging platform which can be stabilized by AB type amphiphilic copolymers with certain solubility properties.[164] For the stabilization of such systems, PEG-*block*-poly((1-pyrenyl methyl) glutamate) (PEG-*b*-PGlu(Pyr)) copolymer was developed *via* post-polymerization modification method by my predecessor Robert Dorresteijn.[39] This emulsifier was used to generate PLLA nanoparticles *via* nonaqueous emulsion polymerization, further transferred the particles into water by light-induced hydrophilization of the particle surface.[39]

Post-polymerization modification is a stepwise approach for designing the functional copolymers as presented in Scheme 4.3. In the case of functional group interfering with the polymerization mechanism, this method is more suitable. In a typical approach, a protected NCA monomer is polymerized, followed by deprotection and subsequent modification with the desired moieties.[70,75]

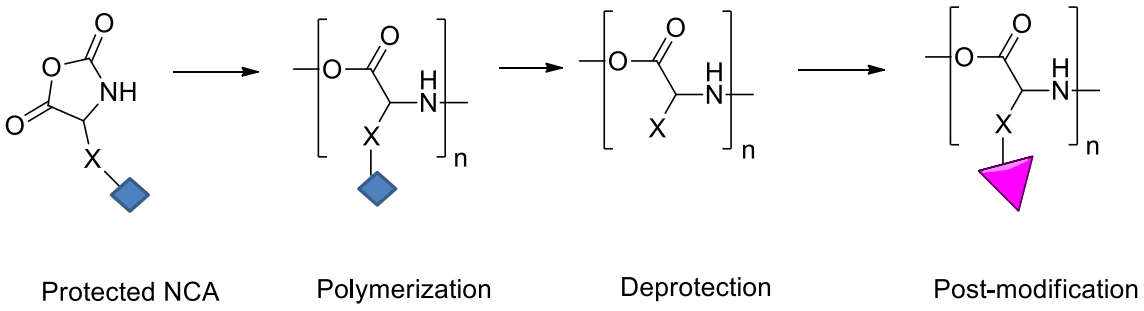

Scheme 4.3. Post-polymerization modification approach

Herein this study, PEG-*b*-PGlu(Pyr) photo-cleavable emulsifier is utilized for the generation of the enzyme cleavable PLLA-*b*-peptide-*b*-PLLA triblock copolymer nanoparticles. Before the particle study, however, some optimization on the synthetic procedure has to be made which will be described in the following section.

4.2.1. Synthesis of Photo-cleavable Block Copolymer by Post-polymerization Modification Approach

PEG-*b*-PGlu(Pyr) copolymer was synthesized by stepwise post-polymerization modification approach with a slightly modified procedure as described below in Scheme 4.4. γ-benzyl-L-glutamic acid-NCA (Glu(Bz)-NCA) (**5.1**) was prepared by Fuchs-Farthing method using triphosgene as a reagent in THF and purified by repeated crystallization from ethyl acetate/n-hexane with 80% yield. Polymerization of Glu(Bz)-NCA was performed according to the literature using methoxy-PEG-NH_2 (M_n=2000 or 5000 g/mol) in DMF in the presence of urea at RT, under argon flow in order to remove the released CO_2 from the reaction mixture. The versatility of the method, however, has been demonstrated by synthesizing copolymers having different block ratios which correspond to the theoretical degree of polymerizations as confirmed by GPC and ^{1}H-NMR end group analysis (Table 4-1). Block copolymers were obtained with a narrow polydispersity (1.27-1.43) except of BC20, which was synthesized in the absence of urea that leads to a conformational change during the polymerization and results in a broader molecular weight distribution.

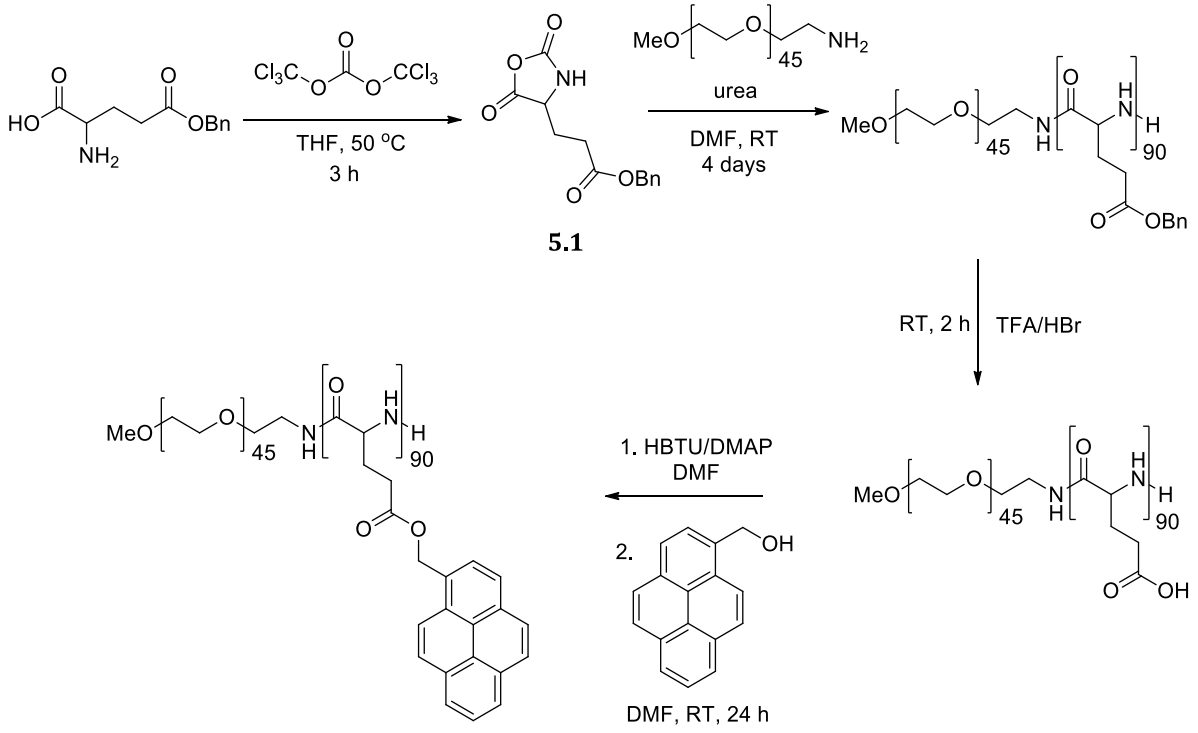

Scheme 4.4. Synthesis of photo-cleavable PEG-*b*-PGlu(Pyr) block copolymer by post-polymerization modification approach

Table 4-1. Polymerization results of PEG-*b*-PGlu(Bz) copolymer

Polymer	Block ratio (theo)	GPC		Block ratio (exp)
		M_n (g/mol)	Đ	
BC17	45/10	5600	1.31	45/10
BC18	45/45	7500	1.27	45/45
BC19	45/90	16500	1.43	45/90
BC20	112/60	9200	2.11	112/60

*GPC against PS standards, DMF as eluent (RID detector)
*Block ratio(exp) is determined by ^{1}H-NMR *via* end group analysis

Protecting benzyl groups of the block copolymer were cleaved fully by TFA/HBr/CH_3COOH mixture in 2 hours, which was published before by catalytic hydrogenation with Pd/H_2 in 4 days resulted in not fully deprotection (Figure 4.1).[39] An additional advantage of this approach is that the product could be recovered by precipitation into diethyl ether, rather than dialysis over an extended period of time. Consequently, this approach considerably reduces the time required to complete the entire synthesis.

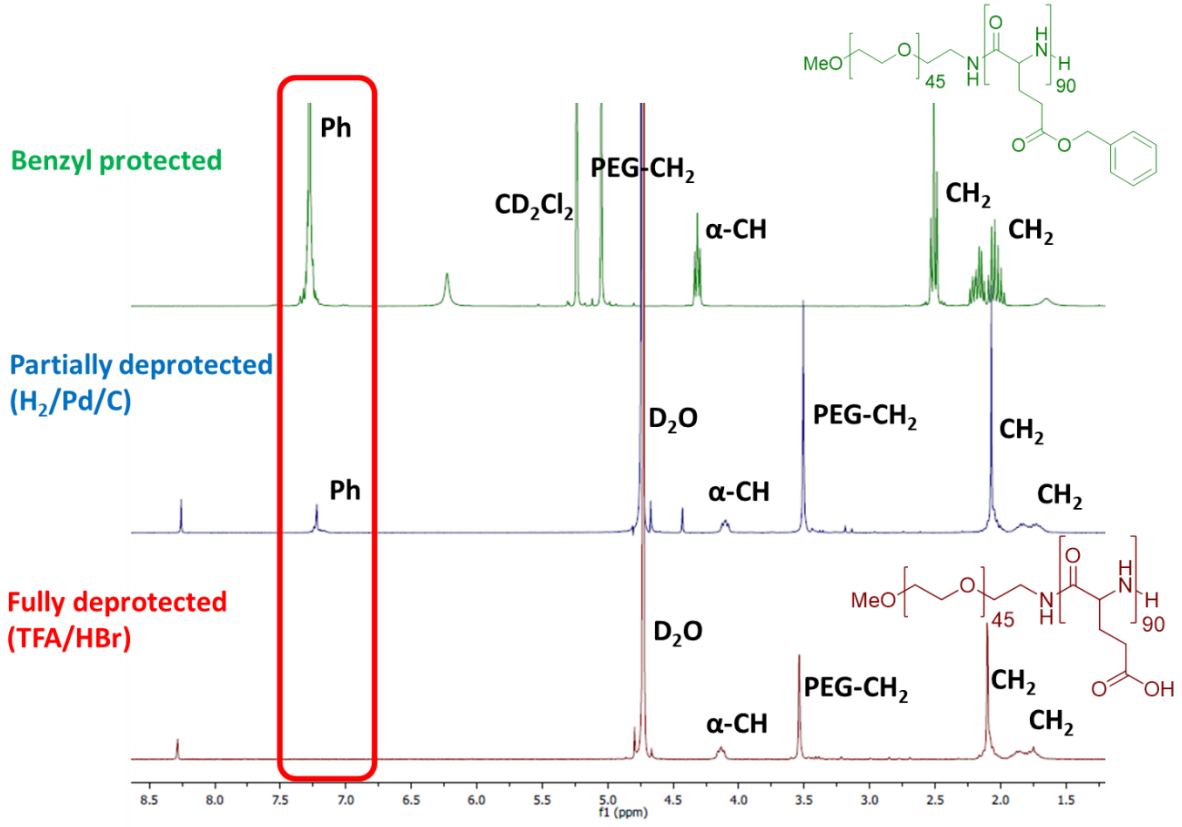

Figure 4.1. Comparison of deprotection strategies: Top (green): ^{1}H NMR spectra of benzyl-protected polymer in CD_2Cl_2; Center (blue): Spectra of the partially deprotected polymer after reacting with H_2, Pd/C for 4 days in D_20; Bottom (red): Fully deprotected polymer *via* reaction with TFA and HBr in D_20 (500 MHz, 298 K)

The final step of installing the pyrenyl units on the polypeptide block could benefit from further optimization. The conditions previously reported, involve conversion of the -COOH side groups to the acid chloride by reacting with PCl_3 for three days under reflux. However, the polymer is only partially soluble under the conditions described in the paper (80 mg polymer in 5.25 mL PCl_3).[39] This lack of solubility ultimately results in the diminished yield reported (61% yield, with 86% esterification). Nevertheless, the final polymer can be achieved via the current methodology by using HBTU/DMAP coupling agents with 85% yield, with 88% esterification degree. ^{1}H-DOSY measurements revealed the equal diffusion constant of both blocks and pyrene demonstrating the covalent attachment of the pyrene to the block copolymer (Figure 4.2).

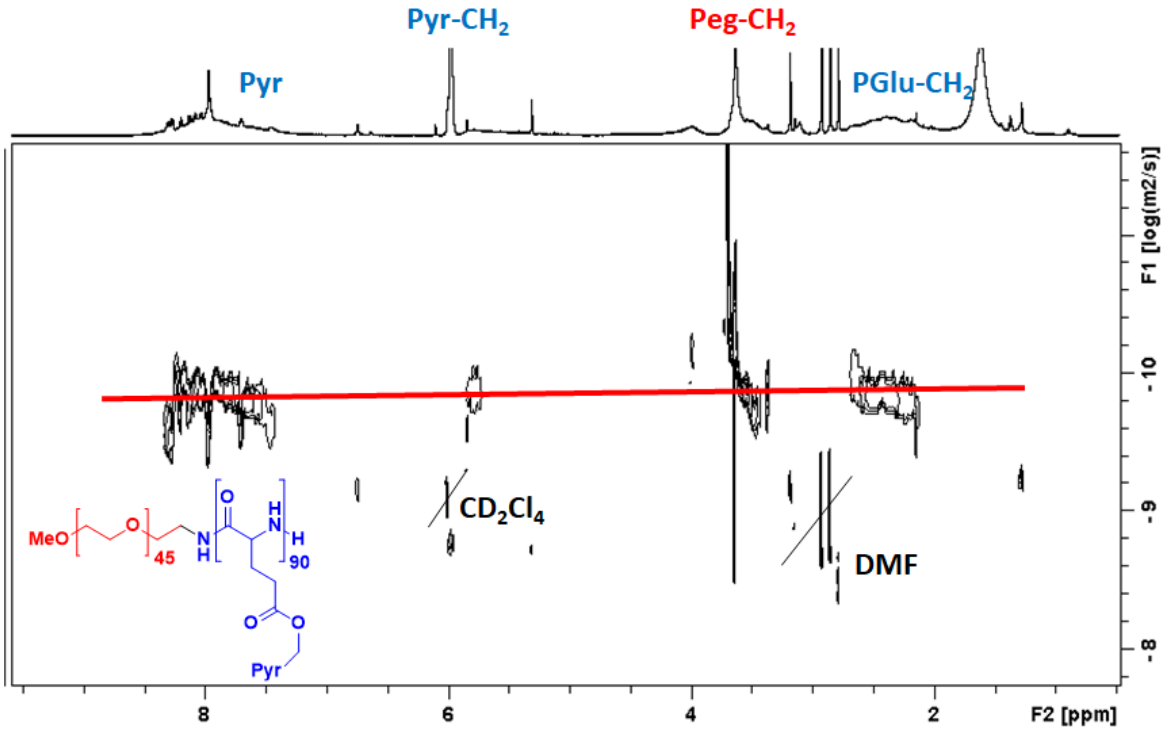

Figure 4.2. ^{1}H-DOSY spectrum of PEG-*b*-PGlu(Pyr) block copolymer (700 MHz, CD2Cl4, 298 K)

The final pyrene modified block copolymer will be used for the stabilization of nonaqueous emulsions of acetonitrile/cyclohexane. In order to achieve maximum emulsifying efficiency within this system, the molecular weight of the block copolymer should be bigger than 30000 g/mol with a 2:1 (hydrophobic:hydrophilic) molar block composition.[165,167,170] Therefore, pyrene functionalized **BC19** which has PEG (45) and PGlu (90) repeating unit is used for further nanoparticle study (M_n= 31000 g/mol).

4.2.2. Synthesis of MMP-2 Cleavable PLLA-*b*-peptide-*b*-PLLA Triblock Copolymer Nanoparticles

Nonaqueous emulsion polymerization is a versatile tool for generating nanoparticles in water-free environment in one pot reaction with a desirable size range as mentioned in detail in Section 1.3.2 (Scheme 4.5).[160,164,166] MMP-2 cleavable PLLA-*b*-peptide-*b*-PLLA triblock copolymer nanoparticles were prepared by this technique using PEG-*b*-PGlu(Pyr) as an emulsifier in acetonitrile/cyclohexane solvent system.

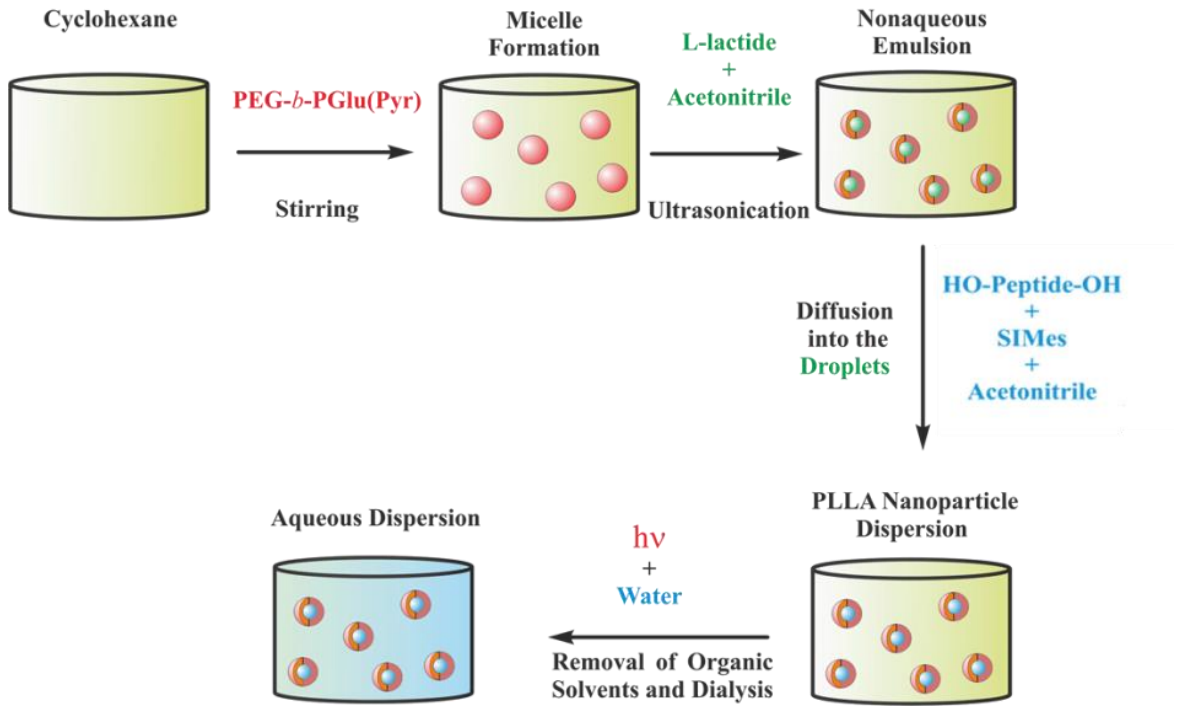

Scheme 4.5. Nonaqueous emulsion polymerization

PLGLAG bearing peptide sequence, Ac-Ser-Gly-Phe-Gly-**Pro-Leu-Gly-Leu-Ala-Gly**-Gly-Phe-Gly-Ser-NH_2 (Ac-SGFG**PLGLAG**GFGS-NH_2) which has two terminal serine units with free hydroxy groups, was used to initiate the ROP of L-lactide by SIMes catalyst (Scheme 4.6). Simultaneously, the scrambled peptide sequence, **LALGPG**, was also employed to synthesize triblock copolymer particles to have a control set for cargo release studies.

Triblock copolymer of PLLA-*b*-(Ac)SGFG-**PLGLAG**-GFGS-NH_2-*b*-PLLA was obtained with a number average molecular weight is around 10000 g/mol with a molecular weight distribution of 1.25. Overall synthesized copolymers were summarized in the Table 4-2.

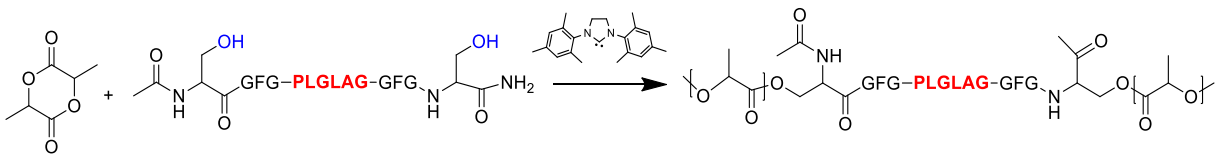

Scheme 4.6. Synthesis of PLLA-*b*-peptide-*b*-PLLA block copolymers

PLGLAG peptide sequence can be specifically bisected by MMP-2 which is an enzyme overexpressed in tumor tissues.[247,252,253] Incorporation of this specific peptide sequence

into PLLA polymer particle leads to a degradation of the particles by enzyme and release the physically loaded cargo molecule. In the previous work done in our group, MMP-2 degradable PLLA-*b*-peptide-*b*-PLLA triblock copolymer nanoparticles were prepared with the same technique but using PI-*b*-PEO emulsifier which is not biocompatible and fully hydrophobic. In order to transfer the particles to aqueous medium, additional surfactant Lutensol AP-20 was used.[248] Herein, photosensitive PEG-*b*-PGlu(Pyr) was employed to stabilize the emulsion which can further change the polarity of the nanoparticle surface with UV exposure. The photocleavage of the pyrene group enables the transfer of the particles in water as demonstrated in the literature.[39]

Two important challenges were achieved by combining of enzyme and UV-cleavable groups: fully biocompatible nanoparticles were obtained (either core or corona) and, with a practical, mild UV cleavage, particles dispersed in water without addition of a second surfactant layer or harsh deprotection conditions.

Table 4-2. Polymerization data of PLLA-b-peptide-b-PLLA triblock copolymers

Sample	Sequence	M/Cat/I	M_n (g/mol)	Đ	R_h (NAE)	R_h (water)
1*	PLGLAG	70/2/1	11200	1.25	-	-
2*	LALGPG		7000	2.27	-	-
3**	PLGLAG		7100	3.62	540±84 nm	300±184 nm
4**	LALGPG		9400	2.95	650±112 nm	295±23 nm

*Sample 1 and 2 were synthesized by solution polymerization in acetonitrile
**Sample 3 and 4 were synthesized by nonaqueous emulsion polymerization in acetonitrile/cyclohexane (cargo loaded)
*Hydrodynamic radius was determined by DLS

Processing of the PEG-*b*-PGlu(Pyr) copolymer is difficult due to the strong hydrophobicity and π-π stacking of pyrene in solution. Dispersing the polymer in cyclohexane or n-hexane requires long and strong stirring and sonication for 3.5-4 hours. Even though these treatments, precipitate formation was observed during the polymerization of L-lactide, which affected the size of the particles obtained *via* this emulsion.

PLLA-*b*-peptide-*b*-PLLA triblock copolymer nanoparticles were characterized by DLS and SEM right after the polymerization. At larger scales (45 mg emulsifier, 18.75 mL cyclohexane) particle size was obtained around of 540 nm in cyclohexane, revealed by

DLS. SEM pictures demonstrate micro-meter size ranged spherical particles in organic phase (Figure 4.3.a).

Hydrophobic pyrene groups were photolytically cleaved by UV exposure in cyclohexane/water mixture (λ=366 nm, P=4W, t=5 h) and by the resulted polarity reversal of the nanoparticle surface from pyrene to carboxylic acid, particles were transferred into the aqueous phase. After photolysis, the cyclohexane phase was evaporated, and the resulting aqueous dispersion was purified by dialysis. When they transferred into water by UV cleavage, aggregated and undefined particles were obtained as seen in Figure 4.3.b.

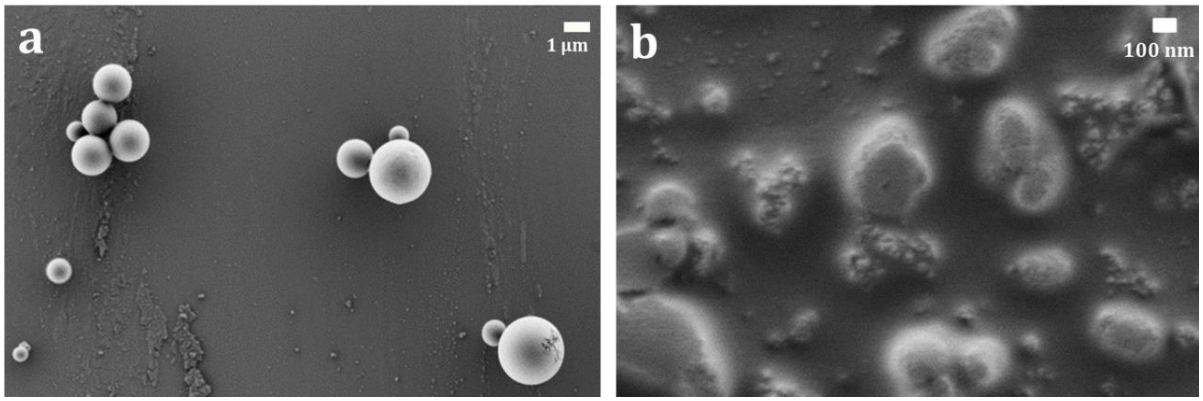

Figure 4.3. SEM image of PLLA-*b*-peptide-*b*-PLLA nanoparticles (a) in cyclohexane (b) in water

At small scales (6 mg emulsifier, 2.5 mL cyclohexane), the particles fall within the desired range in organic solvents (100-200 nm). After the cleavage, particles with a hydrodynamic radius of around 300 nm were obtained according to the DLS measurements. However, SEM micrographs of the particles demonstrated the strong aggregation as shown in Figure 4.4.

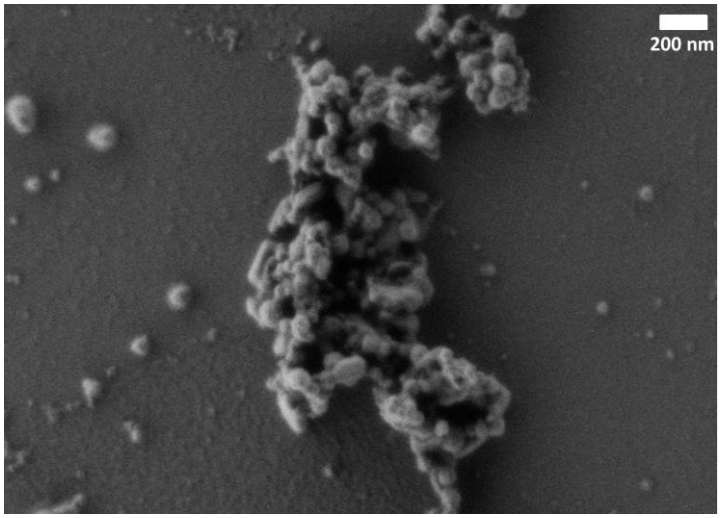

Figure 4.4. Triblock copolymer nanoparticles after photolytical cleavage and transfer to water

Evaluation of the enzyme degradability of the particles by MMP-2

Particles were loaded with the hydrophilic fluorescent probe 9-bromo-N-(2,5,8,11,15,18,21,24- octaoxapentacosan-13-yl)perylene-3,4-dicarboxy monoamide, PMI (Figure 4.5), and MMP-2 enzyme cleavage studies were performed with both cleavable (PLGLAG) and scrambled (LALGPG) sequences.

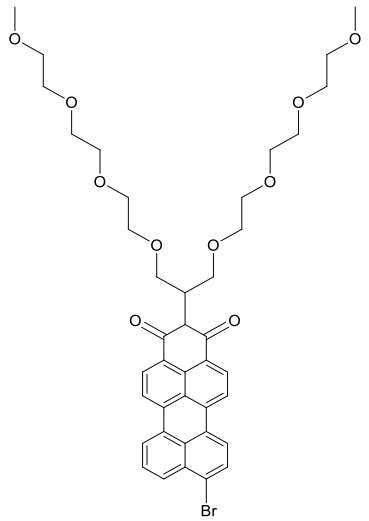

Figure 4.5. Structure of PMI dye used for encapsulation

15 sets of experiments were performed (including replicates and controls) by incubating the nanocarriers in MMP-2 solution at 37 ˚C. After 10 days of incubation, dye

concentration of the supernatant was determined by fluorescence spectrometry. Figure 4.6.a and b presents, respectively, the fluorescence spectra of the particles bearing cleavable sequence (PLGLAG-Sample 1 and 2) and the scrambled sequence (LALGPG-Sample 1, 2 and 3) in the polymer chain together with its control experiments.
As shown in Figure 4.6.a, upon 10 days of incubation, remarkable dye release was observed from the cleavable particles as fluorescence intensity is 60% higher in comparison to the control experiment. In contrast to that, scrambled ones showed almost no dye release as no difference was observed on the fluorescence intensities with control experiments (Figure 4.6.b).

These results already confirm that cleavage and dye release process work more efficient with biocompatible cleavable emulsifier rather than the PI-b-PEO/Lutensol system (Figure 4.6.c). In the previous publication only 20% of dye release was observed from the cleavable sequence bearing nanoparticles by MMP-2.[248] Eventhough processing of the biocompatible/photo-cleavable emulsifier is difficult due to the π-π stacking tendency, more efficient cargo release was obtained.

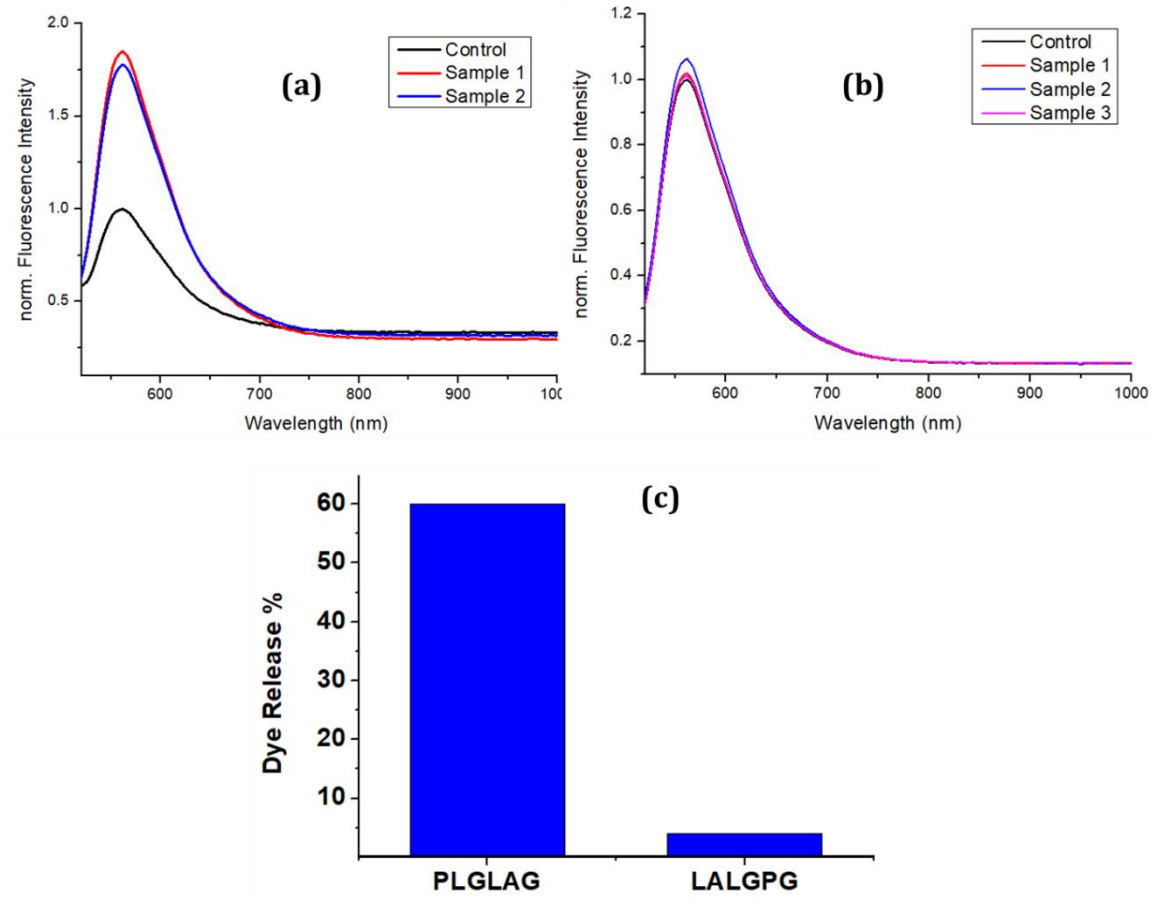

Figure 4.6. Dye release from nanocarriers bearing either (a) the cleavable sequence (PLGLAG) or (b) the scrambled sequence (LALGPG) in the polymer chain after 10 days of incubation time. (c) Comparison of % dye release of both particles. Each measurement is presented as % released relative to control specimens not incubated with MMP-2

One of the ultimate goals of this project is the delivery of chemotherapy agents that are selectively released at the tumor site. The current strategy is to physically incorporate chemotherapy agents into the nanoparticle, which are then released upon degradation. 5-fluorouracil (5-FU), a common chemotherapy agent, was used in proof-of-concept experiments. There are several advantages to this approach including nearly-complete drug release, as well as the facile method of incorporating the drug itself without requiring any chemical modification/covalent attachment. To determine the applicability of the both PLGLAG and LALGPG containing nanoparticles for drug delivery, 5-Fluorouracil loaded particles were incubated with C2C12 cells to check the cytotoxicity (Tests were performed by Sapun Parekh from Bonn Group). According to the assays, however, no cytotoxicity was observed. This was surprising because of the already observed dye

release *in vitro*. However here, several factors have to be considered. The dynamics of the cell culture is of course different and more complicated than just buffer system (where dye release study was conducted in). The emulsifier used to stabilize our particles is polypeptide, therefore in the cell medium, the surface of the particles can be coated by a protein layer due to the protein-protein interactions. This additional coating layer on the surface could prevent the interaction of the particles with MMP-2, thereby inhibition of the cleavage could be observed. The surface of the particles were negatively charged due to the -COOH groups of the poly(L-glutamic acid) after the photolytic degradation of the pyrene. The electrostatic repulsion of the nanoparticle surface with cell membrane could also inhibit the cleavage, thus drug release and cytotoxicity.

In this studied system, the negatively-charged emulsifier shell of the particle can prevent or slow down the interaction of the peptide sequence in the core with the MMP-2 enzyme which exists in the cancer medium. Additionally, in the presence of aforementioned problems, efficiency of the triggered release must be very low. What if the enzyme-cleavable particles are stabilized by enzyme and photo-cleavable emulsifiers?

4.2.3. Synthesis of Photo-cleavable Block Copolymer by Functional Monomer Approach

Poly(α-amino acid)s can be prepared also through direct polymerization of functionalized NCA monomers, called the "Functional Monomer Approach" (Scheme 4.7). The critical point of this strategy is that the functionality on the NCA side chain should not interfere with the polymerization reaction of NCA. However, it is a straightforward method and side reactions from repeated protection-deprotection steps can be eliminated, which increases the purity of the final product and the yield of the reaction.[70]

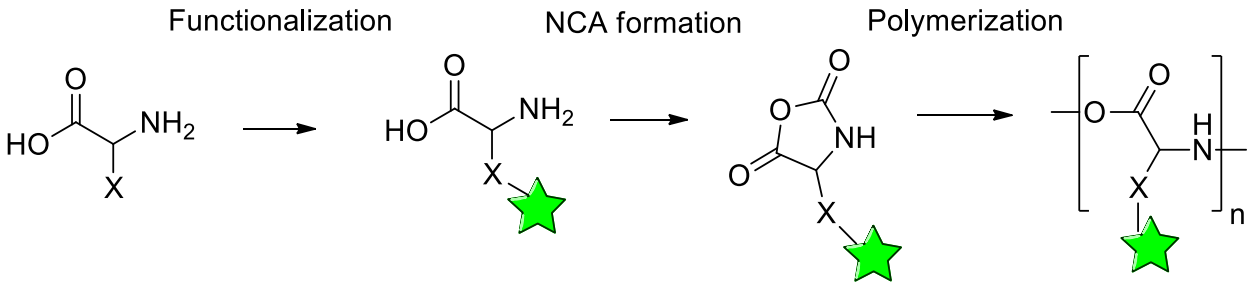

Scheme 4.7. Functional monomer approach

The most common functional NCA types studied in the literature are azide, alkyne or alkene functionalized NCAs because of their further click chemistry potential (Figure 4.7). Deming et al.[254] synthesized azido-L-lysine NCA monomers and showed that its polymerization yielded well-defined azidopolypeptides. Poly(γ-propargyl-L-glutamate) synthesized from the γ-propargyl-L-glutamate NCA was modified further with various amine azides and sugar azides.[255,256] Cheng et al.[257] reported the synthesis of poly(γ-(4-allyoxylbenzyl)-l-glutamate) from γ-(4-allyoxylbenzyl)-l-glutamate NCA monomer, modified with 2-aminoethanethiol via the thiol-ene approach.

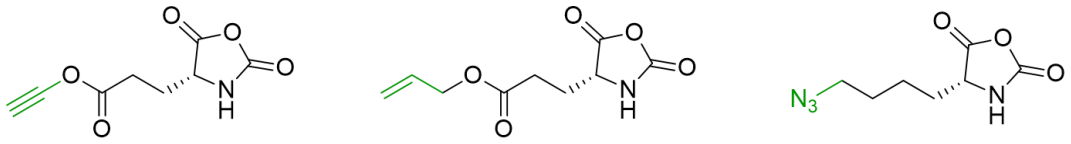

γ-propargyl-L-glutamate NCA γ-allyl-L-glutamate NCA azido-L-lysine NCA

Figure 4.7. Modified NCA monomers for click and thiol-ene reactions

Various oligo(ethylene glycol) (OEG) functional NCAs were synthesized by inspiration of the self-assembly and thermosensitive properties of PEG (Figure 4.8). Deming et al.[258], reported the diethylene glycol-functionalized PLys(poly(EG2-Lys)) and its block copolymer with leucine which forms spherical vesicles. OEG functionalized serine and cysteine monomers were also prepared and their polymerization behavior was studied by the same group.[259] NCA monomers such as cysteine and serine with saccharide functionalities were also reported in literature.[260] Glycosylated-L-lysine NCA monomers were synthesized using glucose, mannose and galactose and polymerized to yield well-defined high molecular weight polypeptides (Figure 4.8).[261]

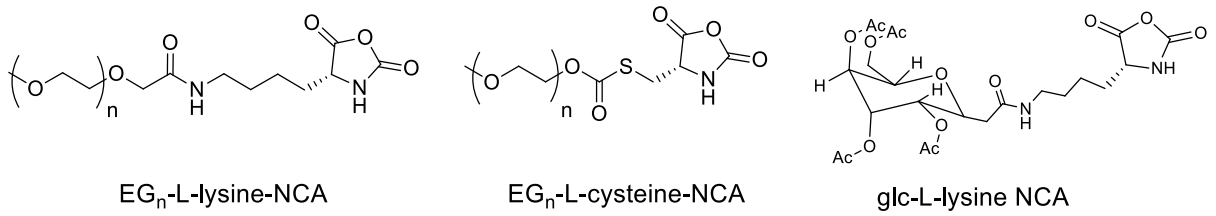

Figure 4.8. OEG functionalized NCA monomers and glucose modified lysine NCA

Additional to the aforementioned functionalities, NCA monomers with photosensitive chromophores were reported. Photosensitive PEG-*b*-poly(S-(o-nitrobenzyl)-l- cysteine) was synthesized from S-(o-nitrobenzyl)-l-cysteine NCA (Figure 4.9.a) by Dong et al.[262] to study the controlled drug release through UV irradiation. Ito et al.[263] reported anthracene and naphthalene functional glutamic acids NCA polymerizations to investigate monolayer properties (Figure 4.9.b). γ-cinnamyl-l-glutamate NCA monomer (Figure 4.9.c) was polymerized and photolytically crosslinked in order to form PEG-polypeptide micelles.[264]

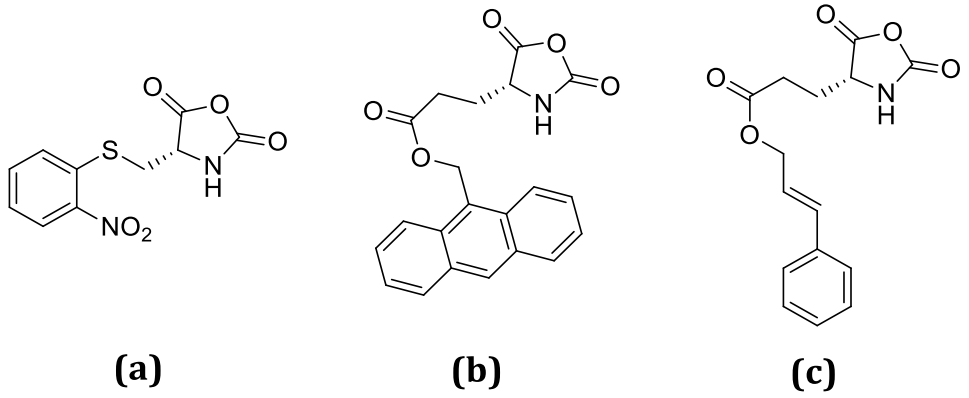

Figure 4.9. (a) Nitrobenzyl (b) antracene (c) cinnamyl modified NCAs

The synthesis of PEG-*block*-poly((1-pyrenyl methyl) glutamate) (PEG-*b*-PGlu(Pyr)) block copolymer by post-polymerization modification was a stepwise and challenging approach as described in the previous section.[39] Repeated steps i.e, polymerization, deprotection, modification and intense purification work up after each, decrease the overall yield of the reactions. Additionally, due to the harsh conditions of deprotection, this route cannot be applied in the presence of sensitive moieties. In order to avoid these complex issues, pyrene functional NCA monomer of L-glutamic acid was synthesized the first time in the

literature in this part of the study. Thanks to this novel photo-labile monomer, a wide variety of copolymers can be designed by employing suitable functional initiators without any complicated issue (Scheme 4.8).

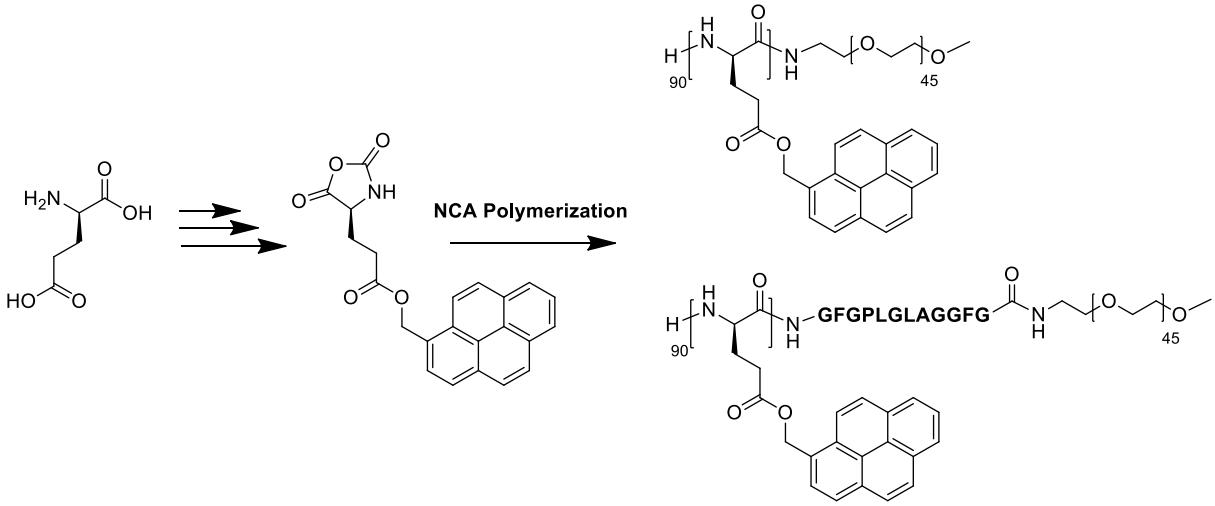

Scheme 4.8. Synthesis of photo-cleavable block copolymers by functional monomer approach

4.2.3.1. Synthesis of γ-(1-pyrenylmethyl)-L-glutamate N-carboxyanhydride

Pyrene functional monomer, γ-(1-pyrenylmethyl)-L-glutamate N-carboxyanhydride (pyrene-Glu-NCA), was synthesized in five steps as demonstrated in Scheme 4.9. For the preparation of γ-ester of L-glutamic acid, first of all, α–COOH and α–NH_2 is protected by means of copper complexation.[265] Compound **5.2** was prepared from the copper (II) acetate monohydrate and L-glutamic acid for 2 days at RT, resulted in blue solid precipitates. 1-pyrene bromide (**5.3**) was synthesized by the reaction of PBr_3 with 1-pyrene methanol in chloroform with 95% yield.[266] To functionalize the free γ-COOH of the L-glutamic acid copper complex (**5.2**), 1-pyrene bromide (**5.3**) was reacted in the presence of tetramethylguanidinium salts, yielding compound **5.4**. Immediate treatment with ethylenediamine tetraacetic acid (EDTA) was yielded to γ-(1-pyrenylmethyl)-L-glutamate (**5.5**). Final NCA monomer (**5.6**) was prepared with traditional Fuchs-Farthing method using triphosgene as a reagent in dry THF (86% yield).

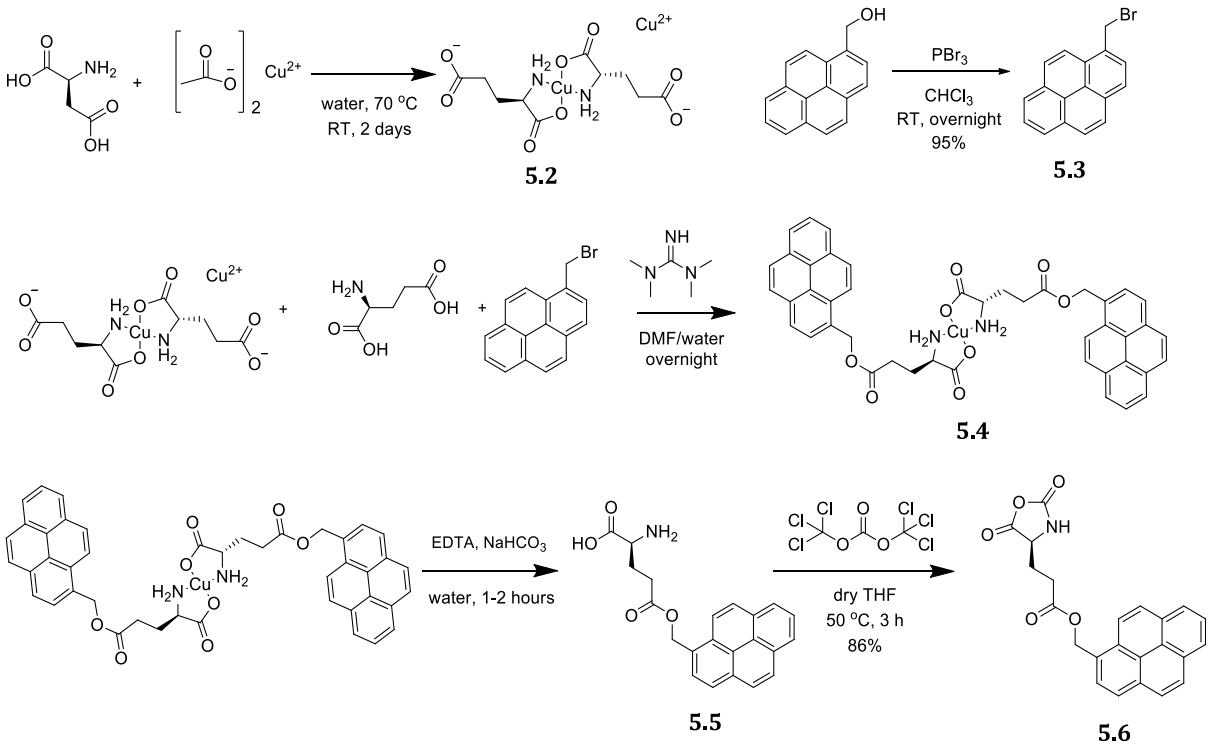

Scheme 4.9. Synthesis of γ-(1-pyrenylmethyl)-L-glutamate N-carboxyanhydride

The solubility of pyrene-Glu is very low, so spectrum has proceeded in DMF. However, by the NCA formation, well-soluble monomer was obtained in common organic solvents. The ^{1}H-NMR spectrum and corresponding signal assignments were consistent with the expected structure of pyrene-Glu-NCA. Especially the NH signal of the final NCA monomer at 6.3 ppm confirms the successful synthesis of the monomer (Figure 4.10).

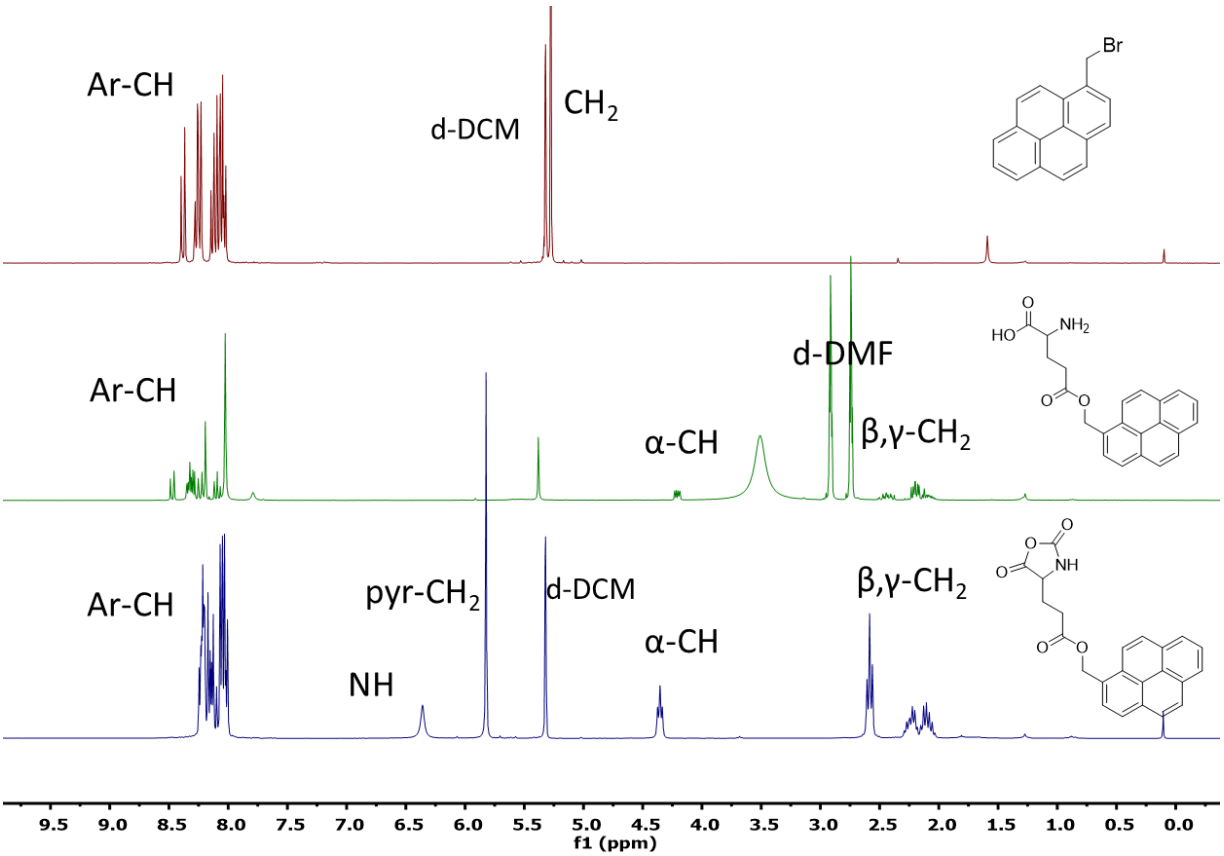

Figure 4.10. ^{1}H-NMR spectrum of top (red) 1-pyrene bromide (CD2Cl2), middle (green) pyrene-Glu (DMF-d7) and, bottom (blue) pyrene-Glu NCA (CD2Cl2) (300 MHz, 298 K)

4.2.3.2. Polymerization of γ-(1-pyrenylmethyl)-L-glutamate N-carboxyanhydride

Ring-opening polymerization of pyrene-Glu-NCA by nucleophilic PEG-NH_2 macro-initiator was investigated in different conditions (Scheme 4.10): various solvents and reaction temperatures were applied as presented in Table 4-3.

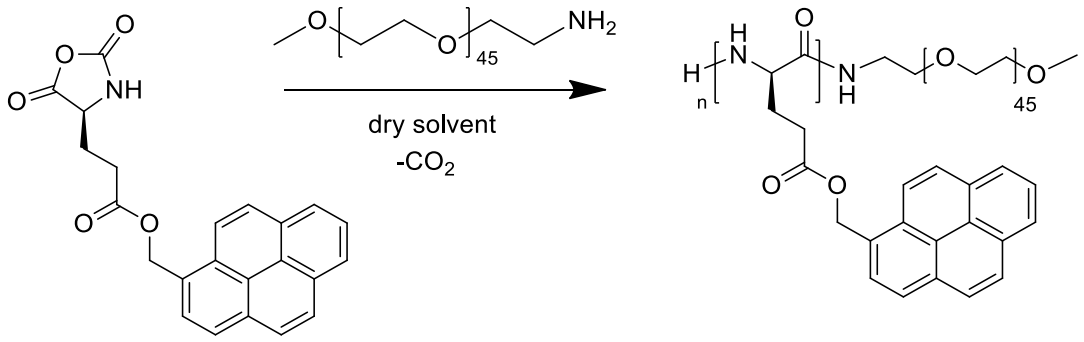

Scheme 4.10. Polymerization of pyrene-Glu-NCA with PEG-NH_2 macro-initiator

Table 4-3. Polymerization of pyrene-Glu-NCA by PEG-NH_2 (2000 g/mol) initiator

Polymer	DP (theo)	Solvent	T	Additive	Time	DP (exp)	Yield (%)
BC21	45/90	DMF	RT	urea	4 days	45/70	87
BC22		DCM	RT then 40 ˚C	-	1 day	45/180	91
BC23		THF	40 ˚C	LiCl	4 days	-	52
BC24		DMF	45 ˚C	urea	3 days	45/90	77
BC25		DMF/DCM (1/1=v/v)	35 ˚C	urea	3 days	45/90	85

Polymerization of pyrene-Glu-NCA was first proceeded in DMF **(BC21)** which is a common organic solvent for NCA polymerization in the presence of urea. Room temperature polymerization resulted in precipitation 1 hour after the start of the reaction. However, polymerization was conducted for 4 days under inert atmosphere and, purified by filtration followed by washing with diethyl ether.

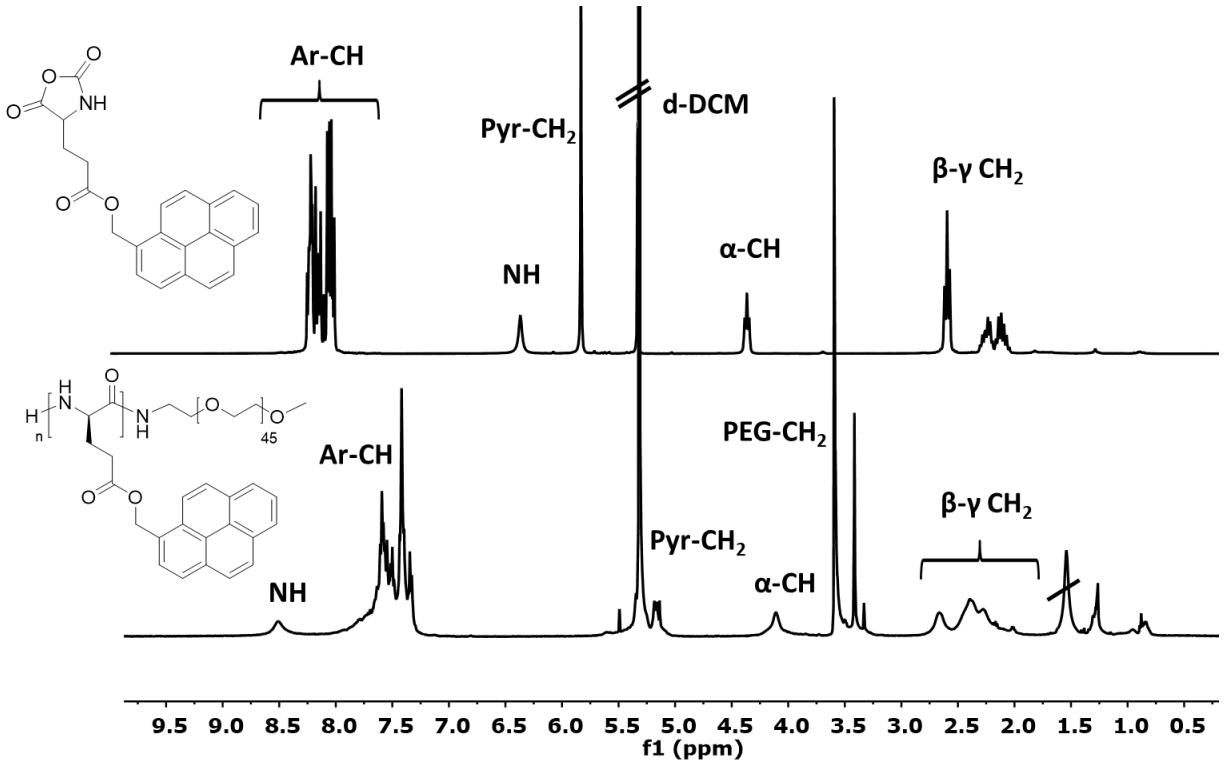

Figure 4.11. ^{1}H-NMR of pyrene-Glu-NCA and PEG-*b*-PGlu(Pyr) (**BC21**) in CD2Cl2 (700 MHz, 298 K)

As demonstrated by ^{1}H-NMR in Figure 4.11 with an ongoing polymerization; pyrene aromatic peaks were shifted from 8.50-8.00 to 8.00-7.00 ppm and getting broader. α-NH peak of the monomer at 6.30 ppm disappeared by the ring-opening and CH_2 peaks of the pyrene methanol shifts to 5.10 ppm. CH chiral proton was observed at 4.00 ppm and glutamic acid CH_2 peaks were between 3.00-2.00 ppm. PEG-CH_2 peaks were observed at 3.50 ppm and by the integrating this peak with the protons of the polymer, molar block ratio was calculated as 1/1.5 (means PEG/PGlu=45/70 repeating units). GPC analysis couldn't be performed due to the low solubility of the polymer in common organic solvents for GPC. ^{1}H-DOSY measurements confirmed the covalent attachment of the different blocks (Figure 4.12).

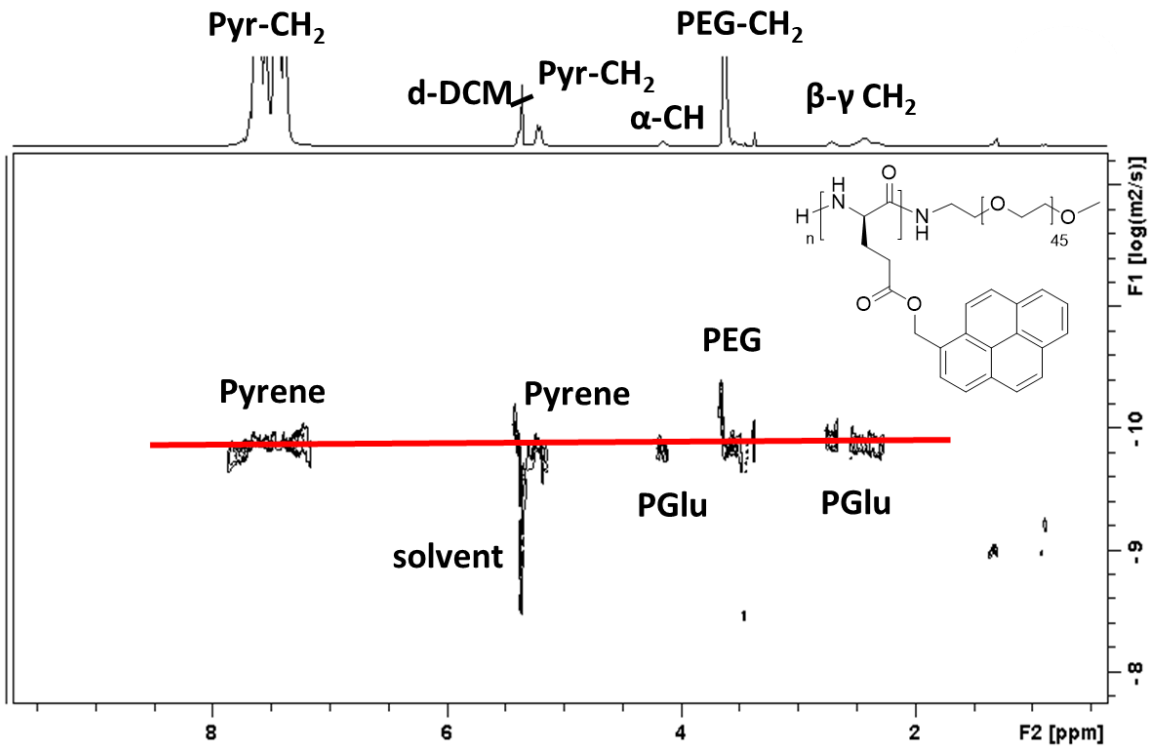

Figure 4.12. ^{1}H-DOSY spectrum of **BC21** (CD2Cl2, 700 MHz, 298 K)

To control over the precipitation issue during the polymerization, different solvent systems were investigated. Polymerization **(BC22)** was performed in DCM due to the better solubility of the material. Reaction was started at RT but became turbid after more or less 3 hours. Reaction mixture was then heated to 40 ˚C under reflux and, polymerization continued under these conditions for 24 hours. However, precipitation could not be avoided because of the π-π stacking. Polymerization was monitored by ^{1}H-NMR in different time intervals as seen below in Figure 4.13. Normally pyrene peaks of the monomer observed at 8.50-8.00 ppm. 10 minutes after the start of the polymerization, aromatics began to shift to 7.75-7.00 ppm. After 14.5 hours, the intensity of the shifted aromatic peaks was obviously high and its intensity did not change after 24 hours (see ^{1}H-NMR in Figure 4.13). Polymer was isolated by filtration and washing with diethyl ether (called insoluble fraction). Degree of polymerization was calculated by the integration ratio of PEG (CH_2 at 3.60 ppm) to PGlu (α-CH at 4.20 ppm) and the molar block ratio was determined as PEG/PGlu=1/4.

Soluble fraction (filtrate) was analyzed by ^{1}H-NMR as well and, molar block ratio was determined as PEG/PGlu=1/1. That means this soluble fraction contains unreacted monomer and lower molecular weight fractions of the polymer.

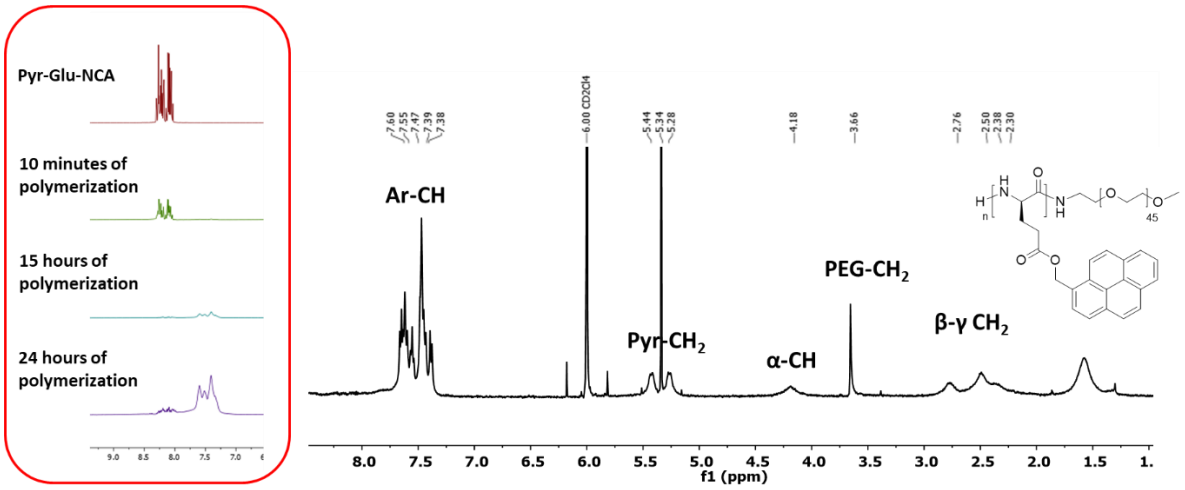

Figure 4.13. ^{1}H-NMR spectrum of purified **BC22** (insoluble fraction) and monitoring the polymerization by ^{1}H-NMR in different time intervals (region of 9.00-7.00 ppm, polymerization from 10 min to 24 hours) (CD2Cl4, 500 MHz, 333 K)

Polymerization in THF at 40 ˚C in the presence of LiCl also resulted in precipitation (**BC23**). The solubility of the polymer was worse in these conditions and no characterizable material was obtained after 4 days.

The last two polymerizations conducted in DMF at 45 ˚C in the presence of urea **(BC24)** and in DMF/DCM mixture at 35 ˚C in the presence of urea **(BC25)** were more stable against aggregation, where it started to precipitate after 1 day. As ^{1}H-NMR spectrum of BC25 was shown below in Figure 4.14, corresponding signal assignments were consistent with the expected structure. ^{1}H-DOSY measurement confirmed the covalent attachment of the different blocks and no unreacted PEG was observed as all the signals are narrow and at the same line. Molar block ratio was determined as 1:2 (45/90) which is in agreement with theoretical value. In spite of this polymerization study, unfortunately it was not possible to avoid precipitation due to the hydrophobic nature of the monomer. However, optimum conditions were determined for the polymerization of pyrene-Glu-NCA in order to obtain the polymer fits with a theoretical degree of polymerization.

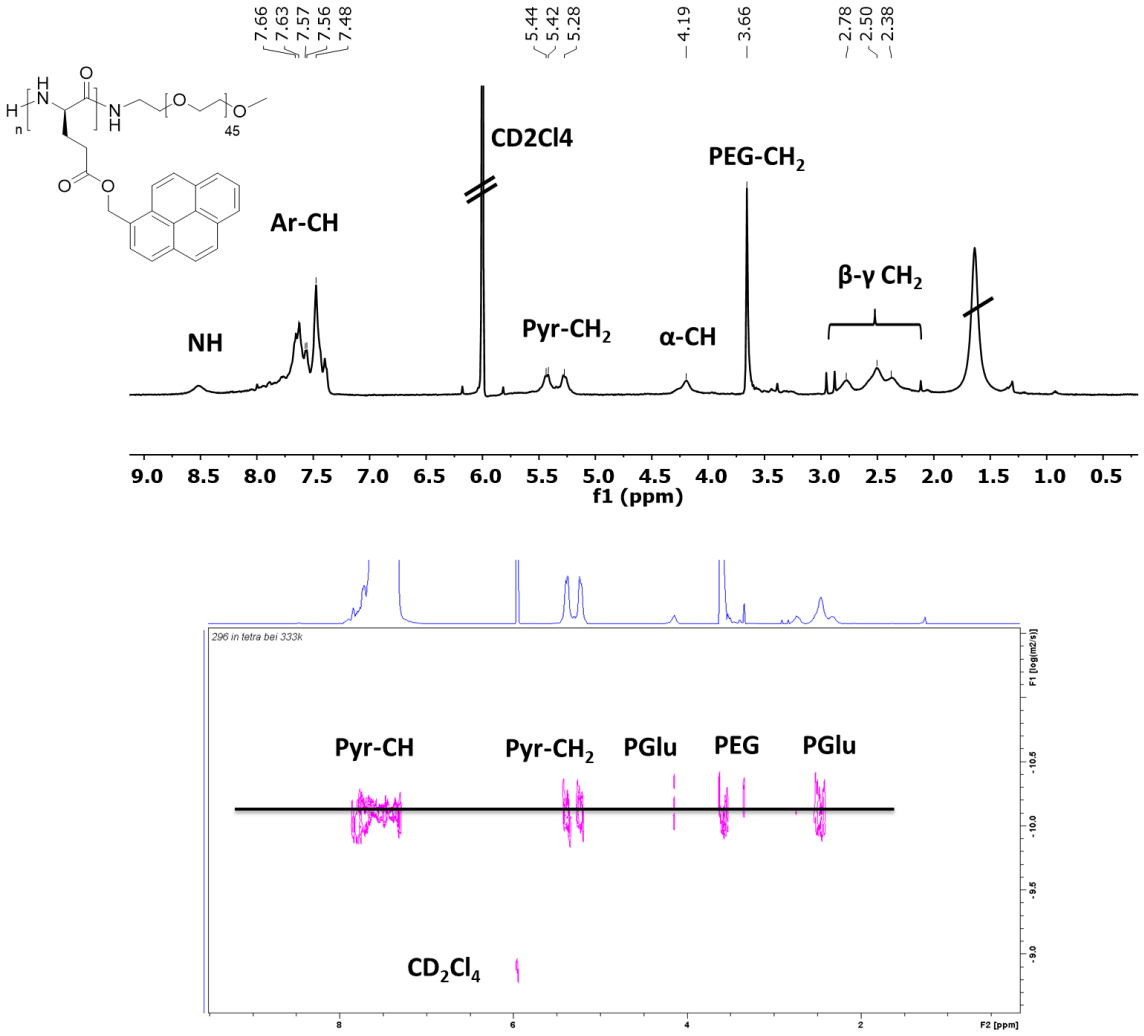

Figure 4.14. ^{1}H-NMR and ^{1}H-DOSY spectrum of **BC25** (CD2Cl4, 500 MHz, 333 K)

PLLA-*b*-peptide-*b*-PLLA nanoparticles by using BC25 as an emulsifier:

The self-assembly study of **BC25** in cyclohexane/acetonitrile was performed to control the aggregation behavior of the photo-cleavable polymer. Therefore, PLLA-*b*-peptide-*b*-PLLA nanoparticles were synthesized in this nano-reactor as all polymerization parameters were kept identical with previous studies. Processing of the PEG-*b*-PGlu(Pyr) was difficult as expected due to the strong π-π interactions. However, utilization of this polymer led to the formation of nanoparticles with better defined morphology then

previous ones as demonstrated in Figure 4.15. Moreover, smaller particles below 500 nm was obtained. This study supports the arguments of the cleaner process of functional monomer approach.

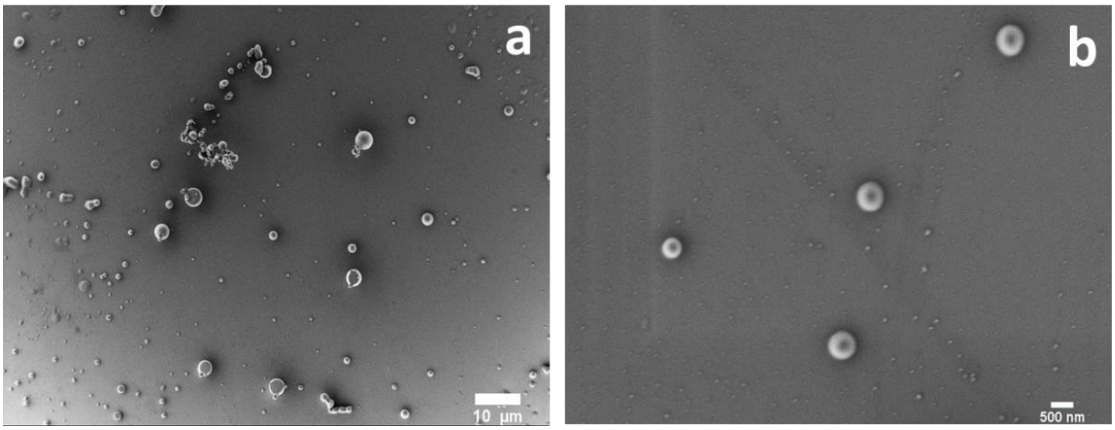

Figure 4.15. SEM micrographs of PLLA-*b*-peptide-*b*-PLLA nanoparticles emulsified by BC25 in cyclohexane

4.2.3.3. Synthesis of Smart PEG-*b*-peptide-poly((1-pyrenyl methyl) glutamate) Block Copolymer

After optimizing the polymerization conditions for pyrene-Glu-NCA by PEG-NH_2, MMP-2 cleavable PEG-PLGLAG-NH_2 conjugate was synthesized and used as an initiator for the polymerization of γ-(1-pyrenylmethyl)-L-glutamate N-carboxyanhydride in order to develop, enzyme degradable and photo-cleavable novel smart block copolymer. Since previous core MMP-2 cleavable nanoparticles did not show the cytotoxicity in cancer cells, it is assumed that the reason can be a shielding effect of the corona or the highly negative charged surface of the particles. The idea of this study is developed from this point of view to overcome these challenges by creating a fully-degradable system. Therefore herein, MMP-2- and photo-cleavable smart block copolymers were designed and synthesized (Figure 4.16). The obtained smart material can be used further as an emulsifier for nonaqueous emulsion polymerization to generate both core and shell MMP-2 cleavable moieties or self-assembly of itself can be studied in order to control the micelle or polymersome formation and further bio-degradations, etc. The fully degradable copolymer offers an important advantage by being located on the surface of the particle, and its cleavage will likely enhance the degradability of the entire nanoparticle.

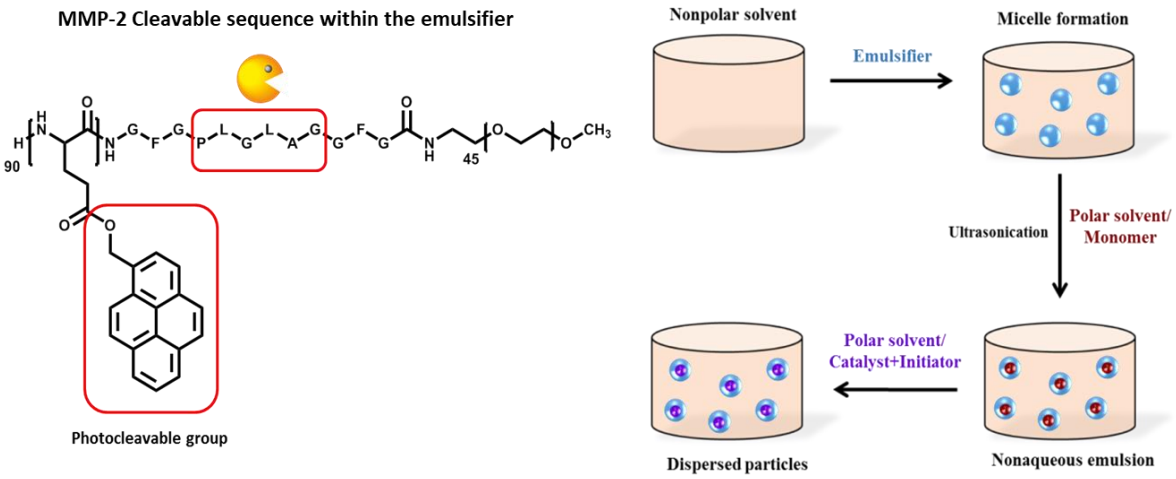

Figure 4.16. Enzyme degradable PEG-*b*-peptide-*b*-poly(glutamic acid-pyrenyl methyl)) triblock copolymer as emulsifier for the stabilization of PLLA-*b*-peptide-*b*-PLLA nanoparticles

Synthesis of macro-initiator PEG-GFGPLGLAGGFG-NH_2

Enzyme cleavable macro-initiator was synthesized by coupling of PEG-NH_2 and PLGLAG-COOH (Scheme 4.11). Amidation reaction between –NH_2 end groups of PEG and -COOH terminal groups of the peptide was performed through HATU coupling agent which proceeds the reaction *via* forming *in-situ* active esters of –COOH groups in basic conditions at RT. The average molecular weight and molecular weight distribution of the polymer was determined by GPC analysis.

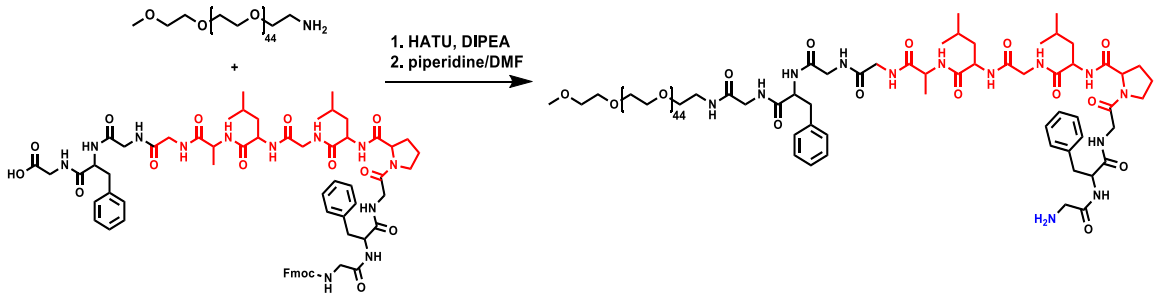

Scheme 4.11. Synthesis of enzyme cleavable macro-initiator PEG-GFGPLGLAGGFG-NH_2

In comparison with PEG-NH_2 as seen in Figure 4.17, molecular weight of the conjugate shifted to the higher values around of 4900 g/mol. Coupling product "PEG-*b*-peptide" has a monomodal molecular weight distribution as polydispersity index was determined as 1.27.

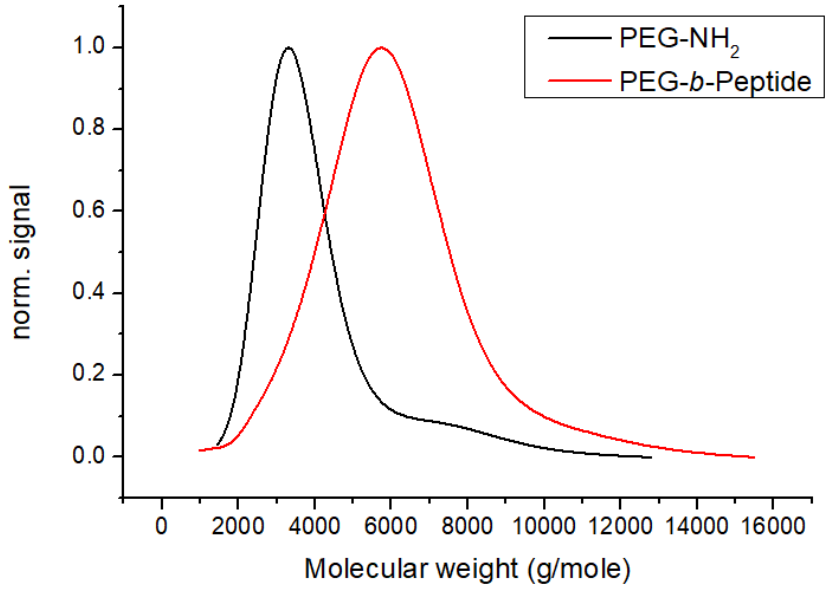

Figure 4.17. GPC curves of PEG-NH_2 and PEG-*b*-peptide (DMF, against PS standards)

The chemical structure of the bio-conjugate was characterized by ^{1}H-NMR (Figure 4.18, green spectra) as specific corresponding signal assignments were consistent with the expected structure of the conjugate. Specifically, the isopropyl and CH group of the leucine (14 H) was observed at around of 1-0.75 ppm. Total 29 H, coming from aromatics (10 H, benzyl groups of phenyl alanine, 8 H Fmoc group) and, NH groups (11 H) of the peptide backbone were in the region of 8.17-7.14 ppm. ^{1}H-DOSY measurement also confirmed the covalent attachment of two different blocks as seen in Figure 4.19. Fmoc group was cleaved with piperidine/DMF cleavage cocktail which was confirmed by ^{1}H-NMR (Figure 4.18, black spectra) by the disappearance of the Fmoc aromatics at 7.79-7.72, 7.68, 7.2 ppm and CH_2 of Fmoc at 4.35-4.24 ppm. By the cleavage additionally, integration ratio between leucine peaks and total aromatics decreased from 14H/29H to 14H/21H, in which the difference 8H corresponds to the Fmoc group.

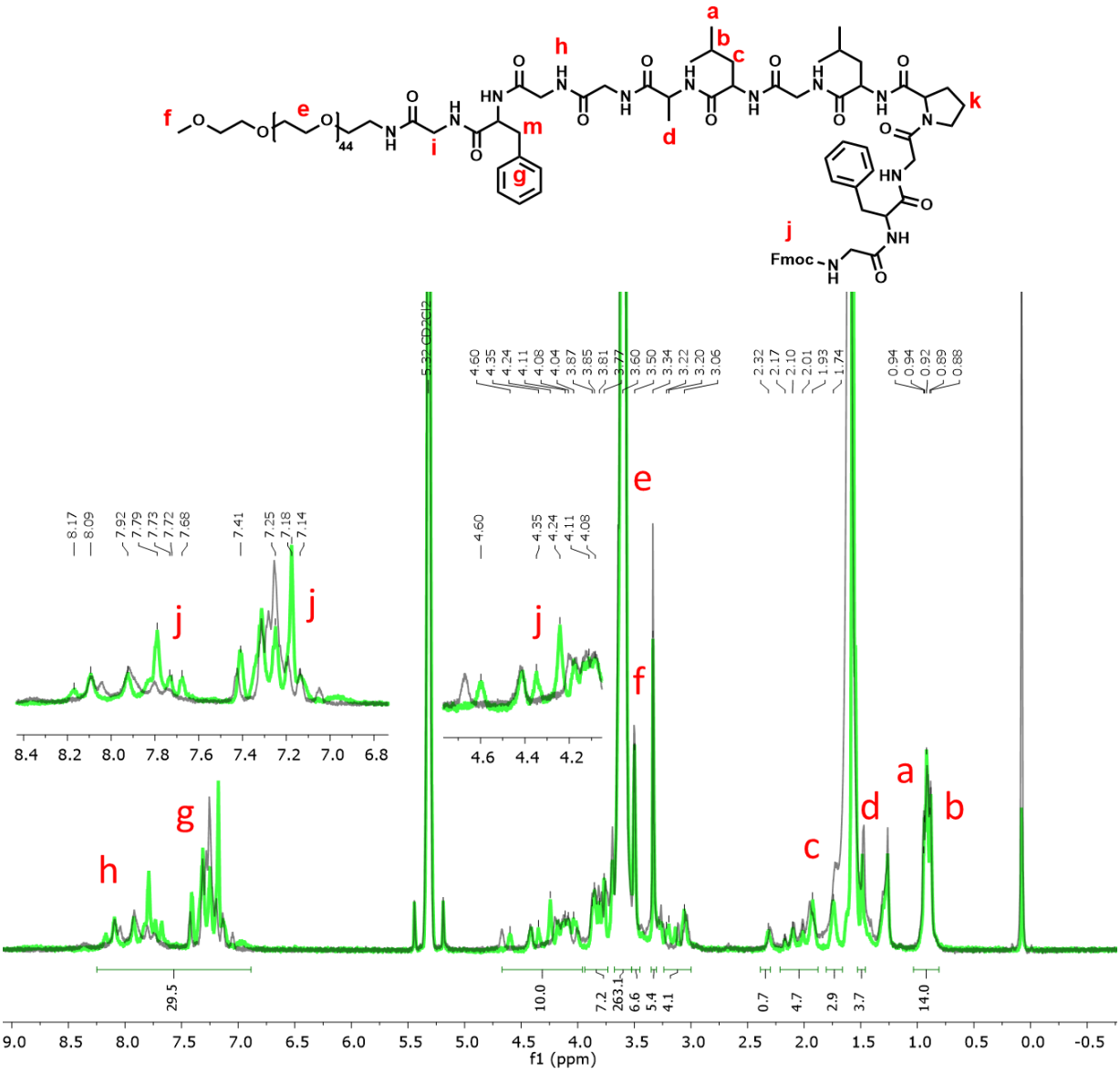

Figure 4.18. ^{1}H-NMR spectrums of PEG-*b*-peptide-Fmoc (green) and PEG-*b*-peptide (deprotected) (black) (CD2Cl2, 700 MHz, 298 K)

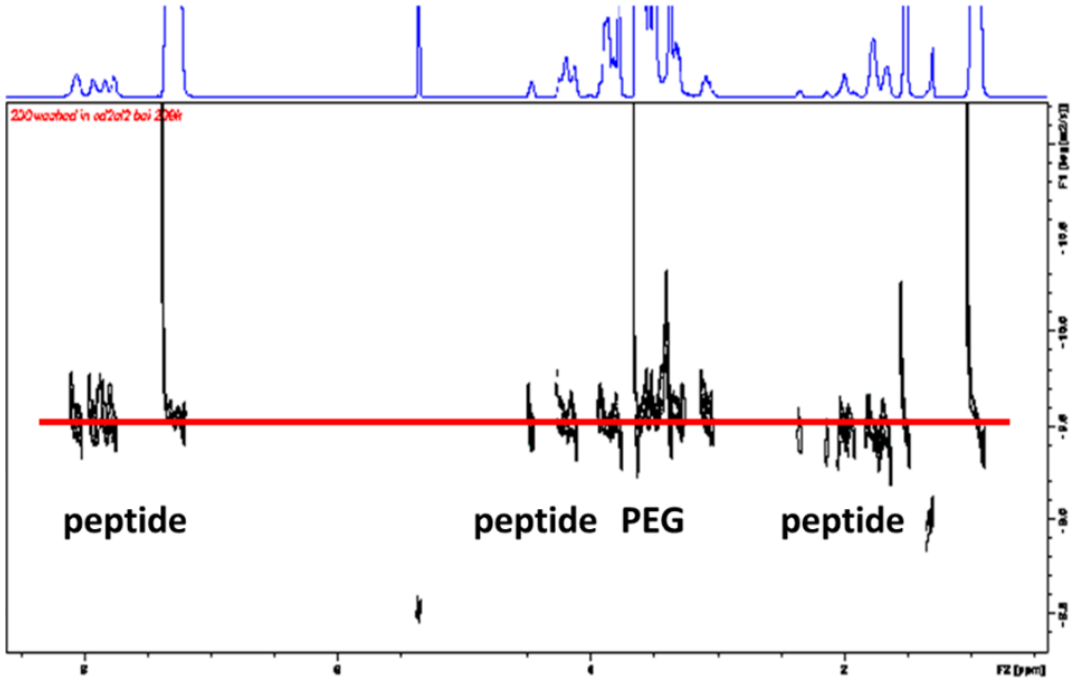

Figure 4.19. ^{1}H-DOSY spectrum of PEG-*b*-peptide bio-conjugate (CD2Cl2, 700 MHz, 298 K)

Polymerization of γ-(1-pyrenylmethyl)-L-glutamate N-carboxyanhydride by PEG-GFGPLGLAGGFG-NH_2 macro-initiator:

As polymerization conditions for pyrene-Glu-NCA was optimized in previous sections, herein DMF/DCM mixture was used as a solvent pair for the polymerization of photo-cleavable monomer by the macro-initiator PEG-*b*-peptide-NH_2 conjugate in the presence of urea (Scheme 4.12). Polymerization was proceeded at 35 ˚C for 4 days under schlenk conditions with a slow flow of argon. Precipitation occurred again 1 day after the start of the reaction.

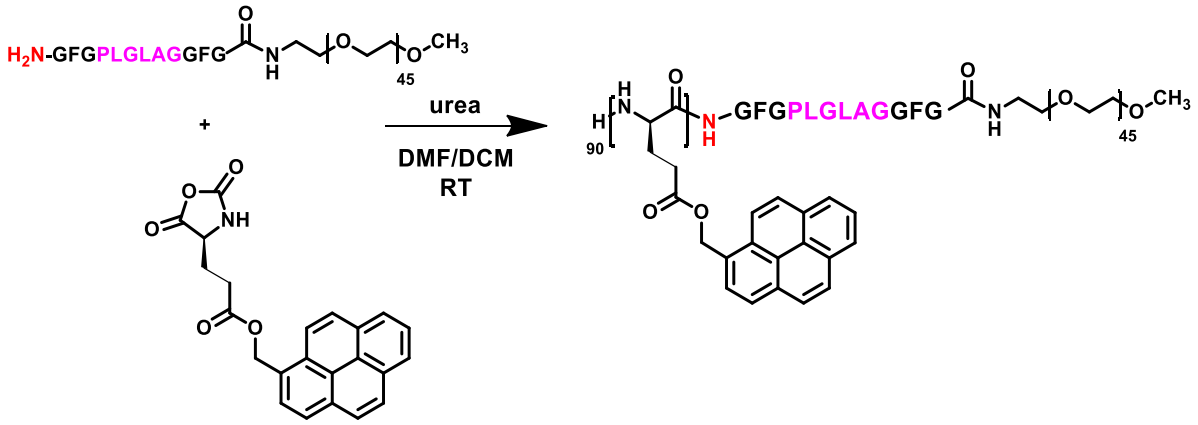

Scheme 4.12. Polymerization of pyrene-Glu-NCA by PEG-GFGPLGLAGGFG-NH_2

Obtained triblock copolymer PEG-*block*-GFGPLGLAGGFG-*block*-poly((1-pyrenyl methyl) glutamate) (PEG-*b*-PLGLAG-*b*-PGlu(Pyr)) was characterized by ^{1}H-NMR analysis as the spectrum was presented below in Figure 4.20. According to the ^{1}H-NMR spectra, corresponding signal assignments were consistent with the expected structure of the PEG and PGlu part of the copolymer. Peptide peaks could not be observed clearly due to the low amount and overlapping by the larger PGlu(pyrene) blocks. However, certain peaks of the peptide were detected as marked on the spectrum below. The most important evidence of the successful copolymerization was the repeated –CH_2 peaks of the PEG at 3.65 ppm which was used to determine the experimental degree of polymerization as 1:2 (45/90), matching exactly with the theoretically adjusted value.

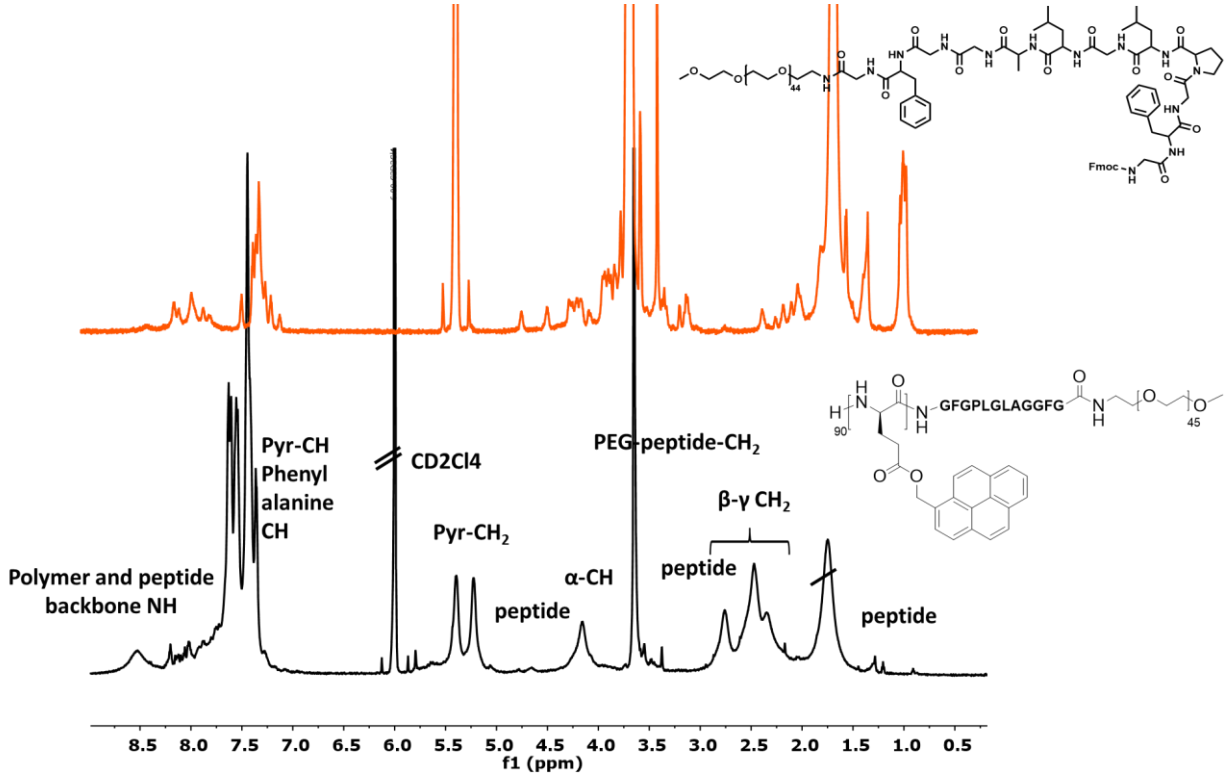

Figure 4.20. ^{1}H-NMR spectrum of PEG-*b*-GFGPLGLAGGFG-*b*-PGlu(Pyr))triblock copolymer (CD2Cl4, 700 MHz, 333 K)

Successfully synthesized enzyme and photo-cleavable PEG-*b*-PLGLAG-*b*-PGlu(Pyr) triblock copolymer can be utilized for the generation of PLLA-based nanoparticles *via* nonaqueous emulsion polymerization. This approach will lead to a formation of both core and shell enzyme degradable smart nanocarriers for cancer therapy. It is assumed that by that design; efficient triggered drug release will be observed.

4.3. Conclusion and Outlook

Enzyme-cleavable polylactide-*b*-peptide-*b*-polylactide (PLLA-*b*-peptide-*b*-PLLA) triblock copolymer nanoparticles were generated by fully biocompatible and photosensitive PEG-*block*-poly((1-pyrenyl methyl) glutamate) (PEG-*b*-PGlu(Pyr)) copolymer as a stabilizer *via* nonaqueous emulsion polymerization. Due to the strong aggregation tendency of the aromatic emulsifier, spherical but larger particles then expected were obtained with a diameter of around 500 nm in hydrophobic organic solvents. Polarity reversal of the emulsifier *via* UV stimuli lead to the transfer of the particles into aqueous medium followed by biodegradability study by MMP-2 enzyme. Dye loaded PLLA particles incorporated with enzyme sensitive peptide sequence "PLGLAG" and scrambled one "LALGPG" were incubated into MMP-2 medium and fluorescence measurements were performed from the supernatant of the particle solutions. Whereas cleavable particles demonstrated around 60% of dye release, scrambled ones show only 5% against control experiments. These results clearly show the effect of the emulsifier used to stabilize the nanoparticle system since previous studies in the literature showed only 20% dye release.

The block copolymer used in this approach was synthesized by post-polymerization modification method as described in the literature which is a stepwise and challenging approach in terms of practical point, yield and purity. Additionally, it is not a convenient approach in the presence of sensitive moieties, such as peptide sequences or acid sensitive groups in the backbone of the block copolymer. It should be noted that none of the amino acids in the enzyme-cleavable polypeptide sequence are likely to be extremely sensitive to the chemistry used to install the pyrene units by post-polymerization. Therefore, in the second part of the work, photocleavable block copolymer was synthesized by functional monomer approach by developing a novel pyrene functional NCA of L-glutamic acid. Novel monomer was successfully synthesized in several steps with 99% of purity. Polymerization study was carried out by PEG-NH_2 macro-initiator and optimum conditions were determined. By this approach, side reactions due to the stepwise synthesis can be eliminated and degradation risk of the sensitive polymeric parts is prevented.

Furthermore, MMP-2 cleavable PEG-peptide macro-initiator was synthesized by coupling reaction of PEG-NH_2 and HOOC-peptide-Fmoc sequence followed by the Fmoc-deprotection, leading to the formation of amino functional enzyme cleavable macro-initiator. Utilization of this enzyme cleavable peptide for the polymerization of pyrene-Glu-NCA was successfully performed to yield the enzyme and photo-degradable smart biomacromolecule.

Use of this smart biopolymer into emulsion systems will lead to the formation of enzyme degradable novel nanoparticulate systems for future drug delivery applications. The degradable emulsifier offers an important advantage by being located on the surface of the particle, and its degradation will likely enhance the degradability of the entire system. By using the designed smart triblock copolymer, some concerns about inhibition of the cleavage process of the particles due to the surface charge can be neglected. Having the enzyme-specific peptide sequence on the emulsifier will allow the direct contact of the particles with cancer cell medium. We assume that, this approach will increase the efficiency of the drug release dramatically and help to avoid the repulsion between cell medium and negative surface charge of the particles. Furthermore, using the pyrene moiety on the side chain of the glutamic acid will help to stabilize the organic nanoparticles in nonaqueous medium. By cleavage of the pyrene by UV-light, the particles will be transferred to the water due to the polarity change of the particle surface. This is the fast and easy approach to transfer the particles into the aqueous medium after synthesis without the need of a second surfactant layer.

4.4. Experimental Part

4.4.1. Materials and Methods

All solvents and reagents were purchased from Sigma Aldrich if not stated otherwise. α-methoxy-ω-amino poly(ethylene glycol) (PEG-NH_2) (M_n ~ 2000 g/mol and 5000 g/mol) was purchased from Rapp Polymere. 1,3-bis(2,4,6-trimethylphenyl)-2-imidazolidinylidene (SIMes) were purchased from ABCR and stored in glovebox. Peptides: Ac-SGFGPLGLAGGFGS-NH_2, Ac-SGFGLALGPG-GFGS-NH_2 and Fmoc-GFGPLGLAGGFG-COOH were obtained from Genosphere Biotechnologies. 9-bromo-N-(2,5,8,11,15,18,21,24-octaoxapentacosan-13-yl)perylene-3,4-dicarboxy monoimide (PMI) was kindly supplied by Robert Dorresteijn.

4.4.2. Synthesis

γ-benzyl-L-glutamic acid N-carboxyanhydride (Glu(Bz)-NCA)(5.1)

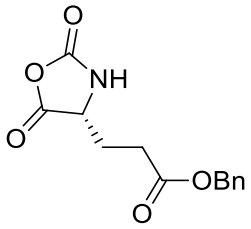

Glu(Bz)-NCA was synthesized as described in the literature.[39] γ-benzyl-α-glutamic acid (5.00 g, 21.10 mmol, 1.00 eq) was dissolved in dry THF (60 mL) under inert atmosphere. The suspension was heated to 50 ˚C under reflux and triphosgene solution (2.00 g in 10 mL dry THF, 7.00 mmol, 0.33 eq) was added dropwise. After 2 hours of stirring, additional triphosgene (0.60 g in 5 mL dry THF, 2.10 mmol, 0.01 eq) was added and suspension became clear solution within 1 hour. Reaction mixture was cooled down and stirred under the flow of inert gas for 2 hours into the NaOH bath. NCA was crystallized three times from THF/n-hexane, filtered and dried under vacuum to yield white fluffy solid, stored in the glovebox (4 g, 15.20 mmol, 80% yield).

^{1}H-NMR (δ (ppm) 300 MHz, CD2Cl2): δ 7.36 (m, 5H, ArH), 6.27 (s, 1H, NH), 5.13 (s, 2H, OCH2Ph), 4.39 (t, J=6.1 Hz, 1H, CHC(O)), 2.59 (m, 2H, CH2), 2.33-2.03 (m, 2H, CH2) ppm.

^{13}C-NMR (δ (ppm) 75 MHz, CD2Cl2): δ 173 (OC=O), 170.1 (OC=O), 152.2 (HNC=O), 136.2 (Ar), 129.2(Ar), 129.0 (Ar), 128.8 (Ar), 67.5 (CH2-Ar), 57.5 (CH), 30.3(CH2), 27.4 (CH2) ppm.

PEG-*block*-poly(γ-benzyl-L-glutamic acid) (PEG-*b*-PGlu(Bz))

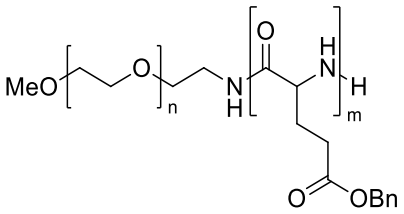

General polymerization procedure was described below according to the literature.[39] *Polymers with different degree of polymerizations were synthesized as synthetic details and characterization data were presented in Table 4-4 and Table 4-5, respectively.*

Glu(Bz)-NCA and urea were placed in a dry schlenk flask under inert atmosphere and dissolved in dry DMF. α-methoxy-ω-amino-PEG (PEG-NH_2) (M_n~2000 g/mol) was dissolved in a minimum amount of dry DMF and added to the monomer solution. Polymerization was conducted at RT for 4 days under slow argon flow. *(Only BC20 was polymerized with PEG-NH_2 (M_n~5000 g/mol)).* Polymers were precipitated by cold diethyl ether several times to yield as white solid.

Table 4-4. Polymerization data of Glu(Bz)-NCA with PEG-NH_2

Pol.	Block ratio (theo)	Glu(Bz)-NCA		PEG-NH_2		urea		DMF (mL)	Yield (%)
		m (g)	n (mmol)	m (g)	n (mmol)	m (g)	n (mmol)		
BC17	45/10	0.20	0.76	0.15	0.076	0.36	1.52	10	72
BC18	45/45	1.00	3.80	0.17	0.084	0.44	7.60	28	57
BC19	45/90	5.00	19.00	0.42	0.21	2.28	38.00	180	81
BC20	112/60	2.55	9.70	0.81	0.16	-	-	48	85

^{1}H-NMR (δ (ppm) 700 MHz, DMF): 8.51(1H, NH), 7.37 (m, 5H, Ar), 5.12 (m, 2H, CH2-Ar), 4.14 (1H, CH), 3.59 (s, 4H, OCH2CH2), 2.40-2.23 (m, 4H, CH2CH2) ppm.

GPC (against PS, DMF as eluent): As presented in Table 4-5.

Experimental degree of polymerizations (DP(exp)) were calculated by the end group analysis via ^{1}H-NMR (Table 4-5).

Table 4-5. Polymerization data of PEG-*b*-PGlu(Bz) copolymers

Polymer	Block ratio (theo)	GPC (RID)		Block ratio (exp)
		M_n (g/mol)	Đ	
BC17	45/10	5600	1.31	45/10
BC18	45/45	7500	1.27	45/45
BC19	45/90	16500	1.43	45/90
BC20	112/60	9200	2.11	112/60

*GPC against PS standards, DMF as eluent
*Experimental block ratio was determined by end group analysis *via* ^{1}H-NMR

PEG-*block*-poly(L-glutamic acid) (PEG-*b*-PGlu)

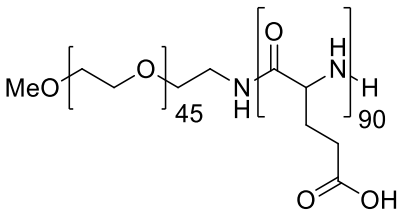

PEG-*b*-PGlu(Bz) copolymer (**BC19**) (1.60 g) was dissolved in trifluoroacetic acid (TFA) (14 mL) and 10 mL of HBr/CH_3COOH solution was added slowly. Mixture was stirred for 2.5 h under inert atmosphere and precipitated with diethyl ether. Polymer was washed with diethyl ether, filtered and dried under vacuum. For further purification, deprotected polymer was dissolved in water and dialyzed against water (MWCO=1000 g/mol) for 2 days (0.94 g, 94% yield).

^{1}H-NMR (δ (ppm) 700 MHz, D2O): 8.45 (s, 1H, NH), 4.31 (m, 1H, CH), 3.70 (s, 4H, OCH2CH2), 2.20 (m, 2H, CH2CH2) ppm.

PEG-*block*-poly((1-pyrenyl methyl) glutamate) (PEG-*b*-PGlu(Pyr))

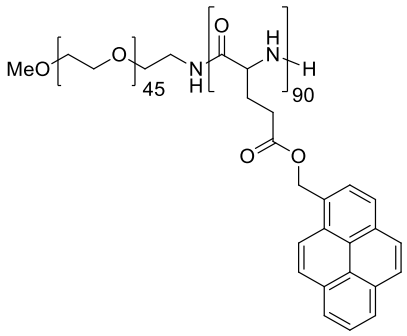

PEG-*b*-PGlu copolymer (0.60 g, 4.01 mmol, 1.00 eq), HBTU (2.30 g, 6.06 mmol, 1.51 eq) and 4-dimethylaminopyridine (0.74 g, 6.06 mmol, 1.51 eq) were weighed in a schlenk flask and pulled vacuum for 1 hour. 7 ml dry DMF was added and followed the addition of 3 mL of N,N-Diisopropylethylamine (DIPEA, 2.23 g, 17.22 mmol, 4.30 eq) (solution is a bit cloudy). After 10 min of stirring, 1.40 g (6.06 mmol, 1.51 eq) 1-pyrene methanol (dissolved in 3 ml dry DMF) was added to the main solution. Reaction was covered with Al folie and stirred for 24 h. Polymer was precipitated by cold diethyl ether three times to yield grey solid product (1.23 g, 85% yield).

^{1}H-NMR (δ (ppm) 700 MHz, C2D2Cl4): 8.20 (m, 9H, Ar-pyrene), 5.53 (2H, Ar-CH2), 4.01 (2H, CH), 3.57 (s, 4H, OCH2CH2), 3.31 (s, 3H, OCH3), 2.30 (m, 8H, CH2CH2).

M_n (determined by end group analysis *via* ^{1}H-NMR, 86% esterification) **=** 31000 g/mol.

PLLA-*b*-peptite-*b*-PLLA Nanoparticles

PLLA-*b*-peptite-*b*-PLLA nanoparticles were synthesized as described in the literature.[39] PEG-*b*-PGlu(Pyr) copolymer (45.00 mg) was magnetically stirred in cyclohexane (14.40 g) at room temperature. L-Lactide (76.00 mg, 0.53 mmol, 1.00 eq) was dissolved in acetonitrile (0.203 g). The emulsion was formed by dropwise addition of the monomer solution into the cyclohexane/PI-*b*-PGlu(Pyr) dispersion and subsequent treatment with sonication for 5 min using a Bandelin Sonorex RK255H ultrasonic bath operating at 640 W. SIMes (4.68 mg, 15.30 µmol, 0.03 eq) and the 1-pyrenyl butanol (4.20 mg, 15.30 µmol, 0.03 eq) were dissolved in acetonitrile (0.203 g) and added dropwise to the emulsion under inert atmosphere. The emulsion was stirred for 15 min at RT to produce PLLA nanoparticles. A sample was taken out of the emulsion to analyze the particle size and

morphology *via* DLS and SEM. To the remaining emulsion, water (18.5 mL) was added. After UV irradiation (366 nm) and vigorous stirring for 3 h at RT, the organic solvent was removed in vacuo, and the dispersion was isolated from the precipitated 1-pyrenyl methanol *via* filtration. The remaining aqueous dispersion was dialyzed against water for 3 days (MWCO=1000 g/mol).

1-(Bromomethyl) pyrene (5.3)

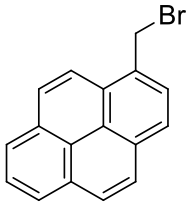

1-(Bromomethyl) pyrene was synthesized according to the literature.[266] 1-pyrenemethanol (2.00 g, 8.60 mmol, 1.00 eq) was dissolved in dry chloroform (30 mL) under inert atmosphere. Phosphorus tribromide (0.82 mL, 8.60 mmol, 1.00 eq) was added dropwise over a period of 30 min under ice-cold conditions and reaction mixture was stirred overnight at RT. Solution was neutralized slowly with saturated sodium bicarbonate solution and extracted. Organic phase was washed with water/sodium chloride solution and dried over $MgSO_4$. Solution was filtered and dried under vacuum to yield yellow solid (2.40 g, 8.13 mmol, 95% yield).

^{1}H-NMR (δ (ppm) 300 MHz, CD2Cl2): δ 8.38 (d, J = 9.3 Hz, 1H), 8.31 – 8.21 (m, 4H), 8.16 – 7.98 (m, 5H), 5.28 (s, 2H) ppm.

^{13}C-NMR (δ (ppm) 75 MHz, CD2Cl2): δ 132.0 (Ph), 131.3 (Ph), 130.8 (Ph), 130.6 (Ph), 129.1 (Ph), 128.3 (Ph), 128.1 (Ph), 127.8 (Ph), 127.4 (Ph), 126.3 (Ph), 125.7 (Ph), 125.6 (Ph), 125.2 (Cq,Ph), 124.9 (Ph), 124.7 (Ph), 122.9 (Ph), 32.3 (CH2) ppm.

γ-(1-pyrenylmethyl)-L-glutamate N-carboxyanhydride (pyrene-Glu-NCA) (5.6)

Pyrene-Glu-NCA was synthesized by described stepwise approach below;

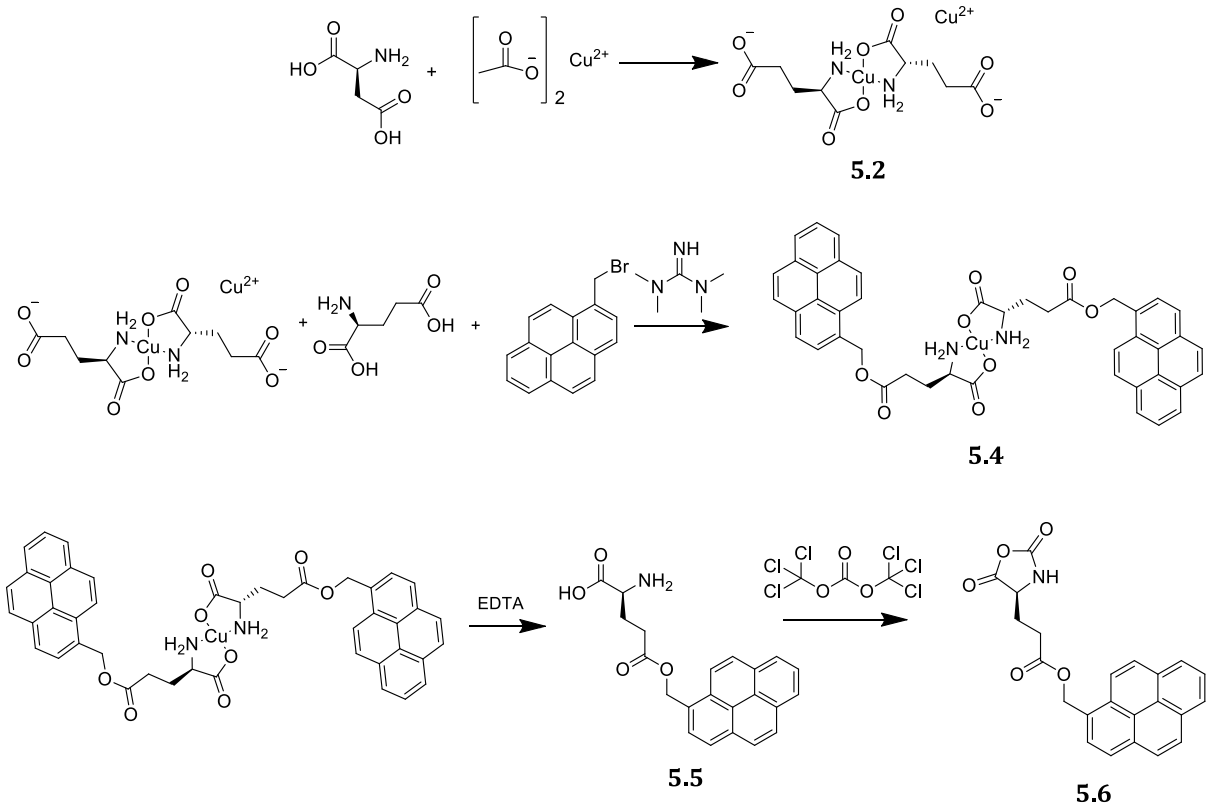

Copper complex of L-glutamic acid **(5.2)** was synthesized as described in the literature.[265] Copper (II) acetate monohydrate (14.00 g, 70.00 mmol, 1.00 eq) was dissolved in water (255 mL) and added dropwise to the L-glutamic acid solution (10.00 g in 255 mL water, 68.00 mmol, 0.97 eq) at 70 ˚C. Reaction mixture was stirred at RT for 2 days to complete the formation of L-glutamic acid-copper complex as blue precipitates. Solid was filtered, washed with water, ethanol and diethyl ether and dried under vacuo. Obtained insoluble complex was directly used for second step (12.00 g, 24.50 mmol, 85% yield).

L-glutamic acid copper complex **(5.2)** (2.40 g, 4.90 mmol, 1.00 eq) and L-glutamic acid (1.44 g, 9.80 mmol, 2.00 eq) were suspended in DMF/water mixture (9 mL/1.5 mL) and N,N,N',N'-tetramethylguanidine (2.45 mL, 19.6 mmol, 4.00 eq) was added slowly (30 min) to a stirred mixture. All solid was dissolved after 2 h of stirring and addition of 15 mL of DMF/water (v/v=9/1) lead to a formation of deep blue solution. 1-pyrenebromide **(5.3)**, (6.10 g, 20.00 mmol, 4.08 eq) was added directly to the solution, resulted in a highly viscous suspension. Addition of 5 mL of DMF was followed by overnight stirring. 50 mL of acetone was added and stirred vigorously around 1 hour until fine precipitate was obtained. Solid was washed with repeated centrifugation in acetone. Obtained solid was

suspended in water, centrifuged and washed several times with water by repeated centrifugation yielded to compound **5.4**. Procedure then followed subsequently with the next deprotection step:

The supersaturated aqueous solution of EDTA disodium salt (Na_2EDTA) was prepared by slow addition of EDTA (1.60 g) to a $NaHCO_3$ (0.90 g in 11 mL water) solution. The wet cake compound **5.4** was immediately treated with this solution resulted in a highly viscous slurry. Addition of 30 mL of water followed by stirring until compound 5.4 has decomposed. The mixture was cooled down and vacuum filtered. Stirred again with 50 mL of water and filtered. Washed with 20 mL of acetone and placed under vacuum to dry to obtain compound **5.5** (2.81 g, 7.78 mmol, 74 % yield).

^{1}H-NMR (δ (ppm) 300 MHz, DMF-d7): δ 8.60 – 7.85 (m, 9H), 7.79 (s, 1H, NH), 5.38 (s, 2H), 4.21 (m, 1H, α-CH), 2.53 – 2.33 (m, 1H), 2.28 – 1.98 (m, 3H) ppm.

γ-(1-pyrenylmethyl)-L-glutamate N-carboxyanhydride (Pyrene-Glu-NCA) **(5.6**) was synthesized by the traditional Fuchs-Farthing method used for NCA preparations in this thesis.[38,267] Pyrene-Glu (500 mg, 1.38 mmol, 1.00 eq) was suspended in 30 mL of dry THF and α-pinene (0.43 mL, 2.76 mmol, 2.00 eq) was added. The suspension was heated to 50 ˚C under reflux and subsequently treated with triphosgene (178.50 mg, 0.60 mmol, 0.43 eq). After 1.5 h of stirring, additional triphosgene (178.50 mg, 0.60 mmol, 0.43 eq) was added and the suspension became a solution after a total reaction time of 3 h. The reaction mixture was cooled down to room temperature and filtered. Monomer was purified by repeated crystallization from THF/n-hexane and ethyl acetate/n-hexane, respectively, to get pure yellowish solid product, dried under vacuum and stored under inert gas in glovebox (0.46 g, 1.19 mmol, 86% yield).

^{1}H-NMR (δ (ppm) 300 MHz, CD2Cl2): δ 8.37 – 7.87 (m, 9H), 6.36 (s, 1H), 5.82 (s, 2H), 4.35 (t, J = 6.1 Hz, 1H), 2.58 (t, J = 6.9 Hz, 2H), 2.32 – 2.00 (m, 2H) ppm.

^{13}C NMR (δ (ppm), 176 MHz, CD2Cl2): δ 172.99, 170.08, 151.80, 132.40, 131.74, 131.20, 130.06, 129.00, 128.86, 128.85, 128.48, 128.42, 127.83, 126.78, 126.20, 126.10, 125.29, 125.16, 125.03, 123.29, 65.91, 57.55, 30.50, 27.50 ppm.

Polymerization of NCA-Pyrene-L-glutamic acid

PEG-b-PGlu(Pyr) block copolymers BC21, BC22, BC23, BC24 and BC25 with a theoretical molar block ratio of 1:2 were synthesized according to the procedure below as synthetic details were presented in Table 4-6.

Pyrene-Glu-NCA **(5.6)** (200.00 mg, 0.52 mmol, 1.00 eq) was transferred from glovebox to schlenk flask and 10 ml of dry solvent (various solvents used, listed below in Table 4-6) was added under inert atmosphere. Urea (11.60 mg, 0.19 mmol, 0.36 eq) or LiCl (11.60 mg, 0.27 mmol, 0.52 eq) was added to the solution. Initiator PEG-NH_2 (11.50 mg, $5.75*10^{-3}$ mmol, 0.011 eq) with a number average molecular weight is around of 2000 g/mol was dissolved in minimum amount of dry solvent and added to the monomer solution. Polymerization was run in different temperatures and time intervals (precipitate forms during the all polymerizations) as described in Table 4-6. Polymers were filtrated, washed with diethyl ether and dried under vacuo to yield yellow solid.

Table 4-6. Synthetic details of PEG-NH_2 (2000 g/mol) initiated pyrene-Glu-NCA polymerization

Pol.	Add.	DP (theo)	Solvent	T (°C)	Time	Yield %	DP (exp)
BC21	urea	45/90	DMF	RT	4 days	87	45/70
BC22	-	45/90	DCM	RT then 40	1day	91	45/180
BC23	LiCl	45/90	THF	40	4 days	52	-
BC24	urea	45/90	DMF	45	3 days	77	45/90
BC25	urea	45/90	DMF/DCM (1/1=v/v)	35	3 days	85	45/90

*DP(exp) was calculated from ^{1}H-NMR end group analysis
*GPC could not be measured due to the low solubility of the polymers

Except of BC23, all the polymers were characterizable by ^{1}H-NMR, as they have a same chemical structure, ^{1}H-NMR of BC25 was presented here as a presentative example:

^{1}H NMR (δ (ppm) 500 MHz, CD2Cl4): 8.55-8.49 (s, 1H, NH), 7.90-7.40 (m, 9H-pyrene), 5.42 (m, 1H, CH2), 5.27 (m, 1H, CH2), 4.19 (s, 1H, α-CH2), 2.79-2.38 (m, 4H, β, γ-CH2) ppm.

Experimental block ratios were calculated by the end group analysis *via* ^{1}H-NMR as presented in Table 4-6.

Synthesis of PEG-GFGPLGLAGGFG-NH_2 Conjugate

HOOC-GFGPLGLAGGFG-Fmoc (80.00 mg, 62.92 μmol, 1.00 eq) and HATU (O-(7-Azabenzotriazole-1-yl)-N,N,N,N'-tetramethyluronium hexafluorophosphate) (28.71 mg, 75.51 μmol, 1.20 eq.) was dissolved in 5 mL of dry DMF and stirred for 15 minutes under inert atmosphere at RT. PEG-NH_2 (M_n=2000 g/mol) (129.46 mg, 2.92 μmol, 1.00 eq) was dissolved in 5 mL of dry DMF and injected to the main solution. The resulting yellow mixture was stirred for 20 min before N,N-diisopropylethylamine (DIPEA) (189.00 μmol, 0.032 ml, 3.00 eq) was added by syringe. The mixture was stirred for 72 hours at RT and precipitated by cold diethyl ether. Dried under vacuum as a white solid (147 mg, 70% yield).

^{1}H NMR (δ (ppm) 700 MHz, CD2Cl2): δ 8.13 (d, J = 54.8 Hz, 2H), 7.92 (s, 1H), 7.86 – 7.58 (m, 16H), 7.45 – 7.03 (m, 15H), 4.60 (s, 1H), 4.38 (d, J = 47.0 Hz, 1H), 4.24 (s, 2H), 4.06 (d, J = 30.0 Hz, 1H), 3.83 (dd, J = 52.1, 22.9 Hz, 6H), 3.60 (s, 81H), 3.34 (s, 2H), 3.20 (s, 0H), 3.14 (s, 0H), 3.06 (s, 2H), 2.32 (s, 1H), 2.01 (d, J = 123.8 Hz, 5H), 1.74 (s, 2H), 1.01 – 0.79 (m, 14H) ppm.

GPC (DMF as eluent, against PS, RID): M_n=4400 g/mol; Đ= 1.21

<u>Fmoc deprotection</u>:

PEG-GFGPLGLAGGFG-Fmoc (50.00 mg, 15.10 μmol, 1.00 eq) was dissolved in 3 ml of dry DMF and 2 ml solution of 40% piperidine in DMF (1.29 mg, 15.10 μmol piperidine, 1.00 eq) was added under strong stirring and inert atmosphere. Deprotection was proceeded for 3 hours at RT. Clear solution is filtered and precipitated by cold diethyl ether to yield light yellowish solid. Additionally, polymer was washed with $CHCl_3$/MeOH (1/10) to remove if there is unreacted PEG residue (38.00 mg, 82% yield).

^{1}H NMR (δ (ppm) 700 MHz, CD2Cl2): δ 8.18 – 7.63 (m, 7H), 7.43 (s, 1H), 7.35 – 7.03 (m, 14H), 4.67 (s, 1H), 4.42 (s, 1H), 4.27 – 3.96 (m, 5H), 3.93 – 3.73 (m, 4H), 3.60 (d, J = 4.5 Hz, 283H), 3.33 (d, J = 4.2 Hz, 5H), 3.15 – 2.94 (m, 2H), 2.30 (s, 1H), 2.21 – 1.85 (m, 4H), 1.03 – 0.80 (m, 14H) ppm.

Polymerization of pyrene-Glu-NCA by PEG-peptide-NH_2 initiator

Pyrene-Glu-NCA **(5.6)** (200.00 mg, 0.52 mmol, 1.00 eq) was transferred from glovebox to schlenk flask and dissolved in 6 ml of dry DMF and 3 ml of dry DCM under inert atmosphere. Urea (10.00 mg, 0.17 mmol, 0.33 eq) was added to the solution. Initiator PEG-Peptide-NH_2 (18.00 mg, $5.9*10^{-3}$ mmol) with a number average molecular weight is around of 3050 g/mol was dissolved in minimum amount of dry solvent and added to the monomer solution. Polymerization was conducted at 35 ˚C for four days. Polymers were isolated by filtration, washing with diethyl ether and, drying under vacuo (132 mg, 84%).

^{1}H NMR (δ (ppm) 500 MHz, CD2Cl4): δ 8.53 (s, NH), 8.02 (m, H), 7.89 – 7.20 (m, 18H), 5.63 (m, H), 5.31 (d, J = 119.5 Hz, 4H), 4.72 (m, H), 4.38 – 3.93 (m, 2H), 3.72 – 3.52 (m, 4H), 3.00 – 2.08 (m, 4H, β, γ-CH2) ppm.

M_n (g/mol) (^{1}H-NMR end group analysis): 33000 g/mol.

Cleavage study of particle dispersions

250 µL of PMI-loaded particle dispersion was mixed with 250 µL of buffer solution (100 mM Tris, 10 mM calcium chloride, and 150 mM sodium chloride, pH 8.0). From a stock solution of MMP-2 (100 µg/mL in 100 mM Tris, 10 mM calcium chloride, 150 mM sodium chloride, pH 8.0), 15.6 µL was activated with 1mM APMA for 2 h at 37 °C under 300 revolutions per minute agitation. After activation, MMP-2 was added to the particle dispersions in a ratio of 150 µL particles: 250 ng of activated MMP-2. This reaction was incubated in a 300 µL total volume of TCNB buffer (50 mM Tris, 10 mM calcium chloride, 150 mM sodium chloride, pH 7.5) for 10 days at 37 °C under 300 revolutions per minute agitation. Following this incubation, the reaction was centrifuged at 13.4 rpm for 20 min. 200 µL of the supernatant was analyzed via fluorescence spectroscopy in order to determine the concentration of released dye during incubation. Control reactions in which no MMP-2 was used were run in parallel and analyzed in the same way.

CHAPTER 5

N-carboxyanhydride (NCA) Polymerization: A Versatile Tool for Fluorescent Polypeptides

5. N-carboxyanhydride (NCA) Polymerization: A Versatile Tool for Fluorescent Polypeptides

5.1. Introduction

Proteins and natural peptides are significant materials for biological applications such as gene delivery,[268] drug delivery,[269] tissue engineering, or regenerative medicine.[270] Polypeptides derived from natural amino acids are inherently biocompatible and enzyme-degradable materials. When one considers a structural variety of amino acids, tailor-made polymers can be designed.[71,271,272] Special properties like pH sensitivity and folding into secondary structures increase the range of possible applications and therefore the demand for this class of polymers.[273,274] Polypeptides mainly can be synthesized by two methods, solid-phase peptide synthesis (SPPS) and α-amino acid N-carboxyanhydride (NCA) polymerization (Section 1.1.2).[86] Latter approach is necessary for large-scale synthesis of high molecular weight peptides.[87,275] In recent years, a tremendous amount of research has been conducted on NCA polymerization to develop hybrid materials with diverse architectures (random, block, graft, star, or dendritic copolymers) for drug delivery or bio-imaging. Some applications may require the side chains to remain free in order to retain the material properties with respect to conformation, solubility, cell-penetrating, etc. In such a case, one may revert to functionalizing the termini. Polymerization of NCAs most likely proceeds by conventional amine mechanism when primary amine initiators are used, which allows making C-terminal modification of poly(α-amino acid)s. Using dual initiators for NCA and controlled radical polymerizations (CRP) i.e atom transfer radical polymerization (ATRP), reversible addition-fragmentation chain-transfer (RAFT), and nitroxide-mediated polymerization (NMP), α-chain end functionalized polypeptides are obtained. For example, synthesis of poly(L-benzyl glutamate) and poly(Cbz-L-lysine) polymers were reported by using 2-bromo-N-(2-aminethyl)-2-methylpropionamide as an initiator to enable subsequent ATR Polymerization (Scheme 5.1.a).[276] Zhang et al.[277] also performed polymerization of NIPAM and BLG-NCA using an amino-functionalized RAFT agent as dual initiator (Scheme 5.1.b). Finally, NMP too can be combined with NCA-ROP, as represented in Scheme 5.1.c.[278]

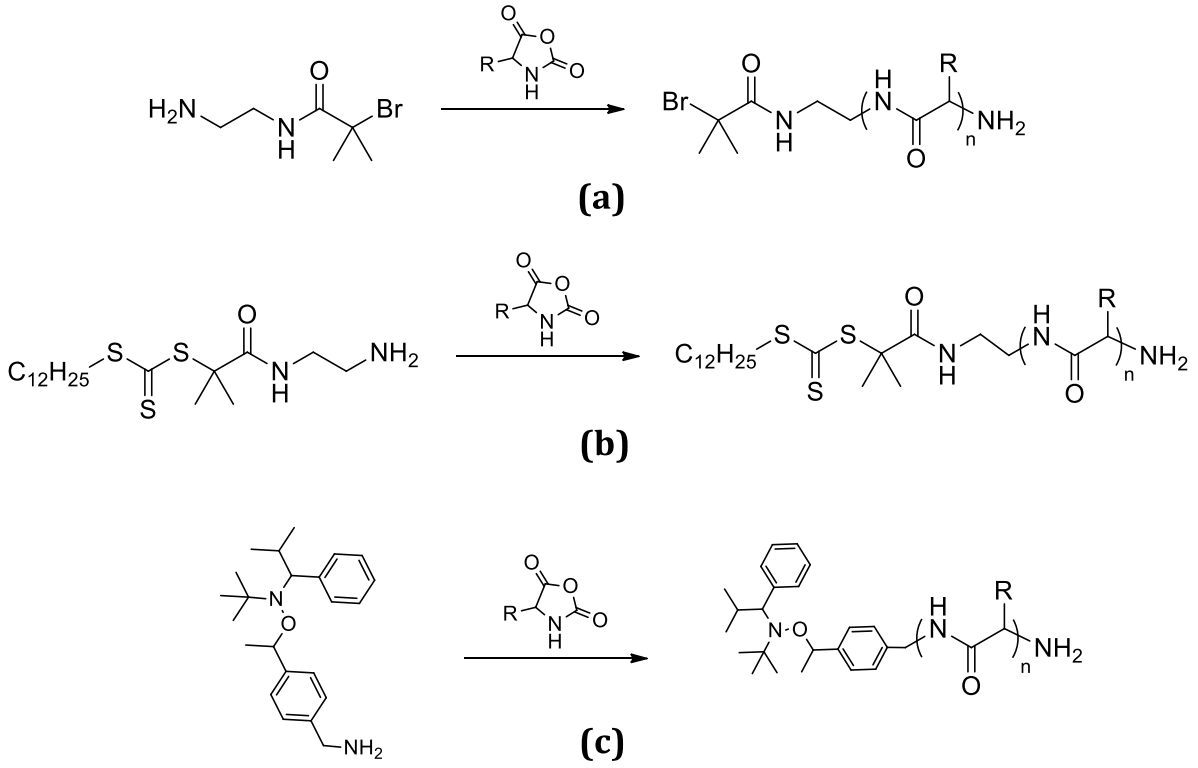

Scheme 5.1. Dual initiators for CRP and NCA ROP (a) ATRP (b) RAFT (c) NMP

Alkyne and azido functional initiators for the ROP of NCAs lead to further click reaction possibilities *via* the chain ends of the polymers.[279] Allyl end functional polypeptides were also reported for further thiol-ene reactions.[280] This approach is, therefore, very important that peptides can be modified with various kinds of molecules such as dyes, drugs, complexes, dendrimers, and bioactive agents, etc. Further polymerizations *via* end groups lead to the formation of block copolymers, which are crucial materials for many applications such as membranes, photonics, solar cells, additives, and pharmaceutical fields.[71,117,136] Moreover, obtained free N-terminal polypeptide can be used to initiate further NCA polymerizations in order to generate amphiphilic block polypeptides. These structures demonstrate unique self-assembly behavior and form special aggregates in solution i.e vesicles, wormlike or spherical micelles, or polymersomes (Figure **5.1**).[70,124,281]

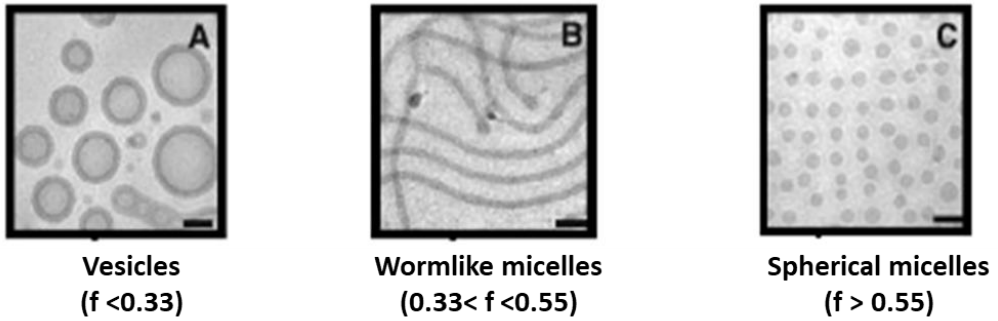

Figure 5.1. Cyro-TEM images of (A) vesicles, (B) wormlike micelles, and (C) spherical micelles[282]

Bioimaging based on luminescent techniques showed a special interest in self-assembled nano-structures in past decades.[283–287] Fluorescent probes are important tools to investigate the dynamic behavior of the materials and tracking them in biological systems. For example, investigation of protein-protein interactions *via* fluorescence spectroscopy requires labelling of the protein with a fluorescent molecule.[288] Auto-fluorescent proteins or water-soluble quantum dots can be used for such purposes. Especially green fluorescent proteins (GFP) were a popular alternative to synthetic dyes because of their high quantum yield (~0.8).[289] However, the main disadvantage of GFPs is their high molecular weight (~27 000 Da) which can affect the natural dynamics of the studied protein. Besides, complex photo-physical properties and fast photo-bleaching restrict its utilization.[290] Water soluble quantum dots are also useful tools because of the reduced spectral width in comparison to the organic fluorophores, high stability against photo-bleaching and high fluorescence intensity. Unfortunately, there is one major drawback, that the degree of covalent modification cannot be controlled quantitatively, because more than one protein molecule is attached to a single particle (usually 2-5 protein molecules).[291,292] Consequently, classic fluorescent molecules are still commonly used in biological investigation of living cells.

Fluorescent particles are used in drug and gene delivery systems for monitoring the distribution and localization of the materials. Such nanoparticles can be prepared either by physical encapsulation of fluorescent molecule in nano-container or covalent attachment of fluorescent probe to the polymer.[183,184,293,294] The latter approach requires certain functionality to link the dye molecule to polymer. Generally, this is the reactive

side chain of the polymer and normally gives an even distribution of dye labels on the surface of the nanocarrier. In contrast, modification of polymer end groups allows the preparation of uniformed nanoparticles with strictly defined localization and a precise number of fluorescent molecules. Additionally, native functions and properties of the polymers can be preserved by employment of this method.[77]

The main requirements of fluorescent molecules for bioimaging studies *in vivo* are cell permeability, chemical and photo stability, low toxicity, specific reactivity, and a wide spectrum of colors. Perylene diimide chromophores demonstrate excellent photo-physical properties and stability, high molar absorptivity and high fluorescence quantum yield.[185,295] Additionally, maximum excitation and emission wavelengths of the perylene derivatives are longer than 550 nm which is crucial to avoid overlapping with the autofluorescence of cells, tissues, and biological fluids.[186] Therefore, perylene chromophores are suitable candidates for the labelling of nanocarriers for *in vivo* studies. In recent years, many researchers have been investigating polymeric particles with covalently-attached PDI-molecules for pharmaceutical applications. Fan et al.[296] synthesized a perylene diimide zwitterionic polymer *via* ATRP for photodynamic therapy. The same group also reported perylene diimide coated nanoparticles consisting of high density glycol polymers as tumor targeted photoacoustic imaging and photo-thermal therapy.[297] Fluorescent probes should be naturally water-soluble for investigations in biological medium. Quante[298] reported hydrophilic, negatively charged tetrasulfonyl perylenetetracarboxydiimides (Figure **5.2**.a). As shown in Figure 5.2.b, water-soluble 1,6,7,12-tetra(4-sulfophenoxy)-N,N'-(2,6-diisopropylphenyl)-perylene-3,4:9,10-tetra carboxydiimide was synthesized by Kohl.[299] Later on by Peneva, various functional PDI derivatives were developed for biomolecule labelling studies.[300]

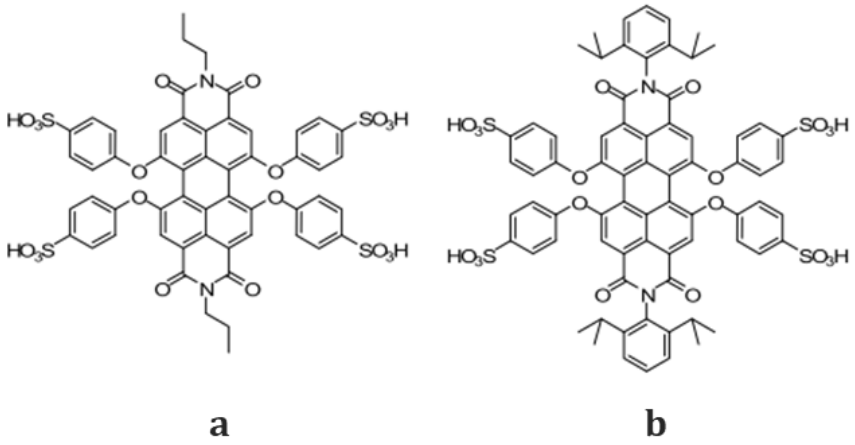

Figure 5.2. Structures of water-soluble PDI derivatives

Another possibility for designing a water-soluble fluorescent-labelled system is covalent modification of hydrophobic perylene derivatives with hydrophilic polymers. Polypeptides can be synthesized by using fluorophore or photosynthesizer initiators to directly obtain C-terminal modified systems. A tetra-amino substituted perylene dye, for example, was employed as initiator for the polymerization of glutamic acid and lysine. The resulting four-arm star shaped polymers were water-soluble and strongly fluorescent materials (Figure 5.3.a).[301] Linear water-solubilized perylene monoimide derivatives were prepared by Yin et al.[302] through functionalization with poly(amino ethyl methacrylate) for the investigation of pH-induced self-assembly (Figure 5.3.b). This approach is convenient in terms of keeping the dye fully inert within the system in order to avoid any side interaction with the cell environment. Additionally, photosensitizing porphyrin-based amine initiators can be used to initiate the polymerization of lysine and leucine to form amphiphilic diblock copolymers for photodynamic therapy with a high fluorescence quantum yield.[295] Moreover, di-sulfide functionalized PBLG *via* NCA polymerization of BLG-NCA was reported by Gupta et al.[303] ω-chain end groups of the polypeptides can be functionalized *via* the post-polymerization modification approach. Polypeptides obtained by NCA polymerization have amine terminal groups which can be used for further polymerization of NCA in order to prepare block copolymers.[38,75,136] Furthermore, block copolymers can be obtained by the coupling of amine end group of polypeptides *via* isocyanates.[304] ω-chain end groups of the polypeptides can be also functionalized with fluorescent molecules *via* post-polymerization method. Fluorescein isothiocyanate, for example, was used to label the ω-amino end of mPEG-SS-PLeu

copolymer, which self-assembled into micelles in water and was used for cell-imaging via confocal laser scanning microscopy (CLSM).[305]

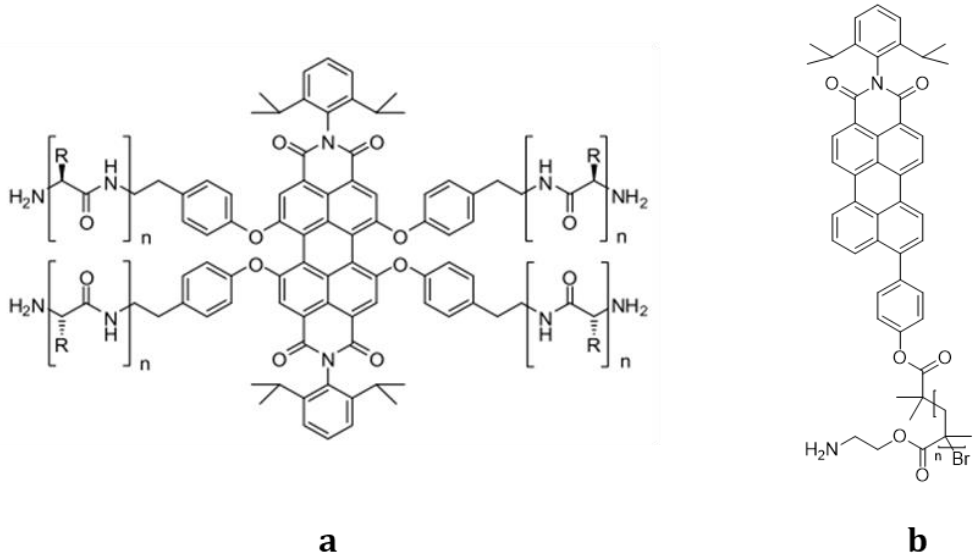

Figure 5.3. (a) Fluorescent star-shaped polypeptides (b) Fluorescent poly(amino ethyl methacrylate)

In this chapter, design and synthesis of C-terminal covalently fluorescence-labeled, polypeptide pH sensors and drug-nanocarriers are aimed. Structural diversity and pH-stimuli responsivity of the polypeptides should be combined with fluorescence-modified tools which is required for monitoring the distribution and localization of the particles in cells or tissues.[297,306] These functions are overall very critical for designing smart drug delivery vehicles suitable for particle tracking and bioimaging *in vivo*. In the way of reaching these goals, the following objectives are addressed:

(i) The synthesis of amphiphile forming, pH sensitive, C-terminal fluorescence-modified poly(L-lysine) derivatives for possible pH sensor applications,

(ii) Fluorescent amino-functional amphiphilic block copolymers *via* sequential NCA polymerization: Self-assembly of the cationic micelles as nanocontainers, biocompatibility, cell uptake and visualization studies.

Dye molecules that are only physically bound to a carrier are more likely to leach in solution environment than those that are covalently attached. Therefore, covalent modification of the macromolecules with fluorescent probes should be considered. Highly photo- and chemically stable, amino-functional perylene diimide derivatives (PDI-NH_2)

should be used as fluorescent initiators for the ROP of Lysine-NCA (Scheme 5.2). These fluorescent homopolymers might be of interest as pH sensor for monitoring the pH fluctuations in living systems with good water solubility, high fluorescence quantum yield and photostability.

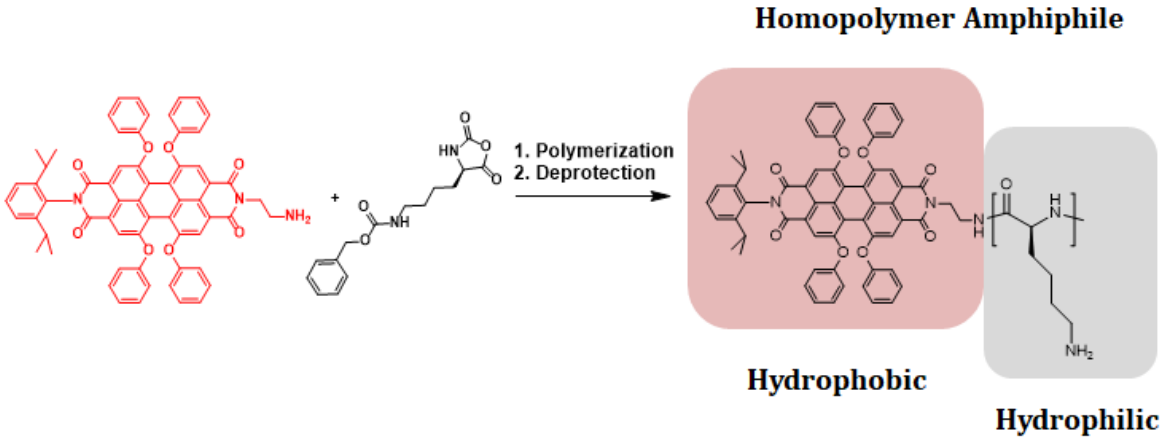

Scheme 5.2. Preparation of fluorescent homopolymer amphiphile

In the second part of this chapter, fluorescent amphiphilic block copolymer nanocarriers are aimed to develop. Smart nanoparticle drug delivery systems suitable for bioimaging process must have certain requirements such as:

- Fluorescence for the detection,
- Biocompatibility,
- Ability to self-assemble into nanoobjects around 100 nm for cell uptake,
- Surface charge for better interaction with the cell membrane,
- Functionality on the surface of particles for post-modification with bio-active molecules for targeted delivery.

To fulfill all these above-mentioned requirements; synthesis of micelle forming, surface amino-functional, fluorescent and biocompatible block polypeptides i.e PDI-poly(L-lysine)-*b*-poly(L-leucine) and PDI-poly(L-lysine)-*b*-poly(L-phenylalanine) are aimed to develop as nano-containers for drug delivery and bioimaging applications (Scheme **5.3**). Confocal Laser Scanning Microscopy (CLSM) offers the possibility to investigate potential utilization of the fluorescent particles *in vitro.*

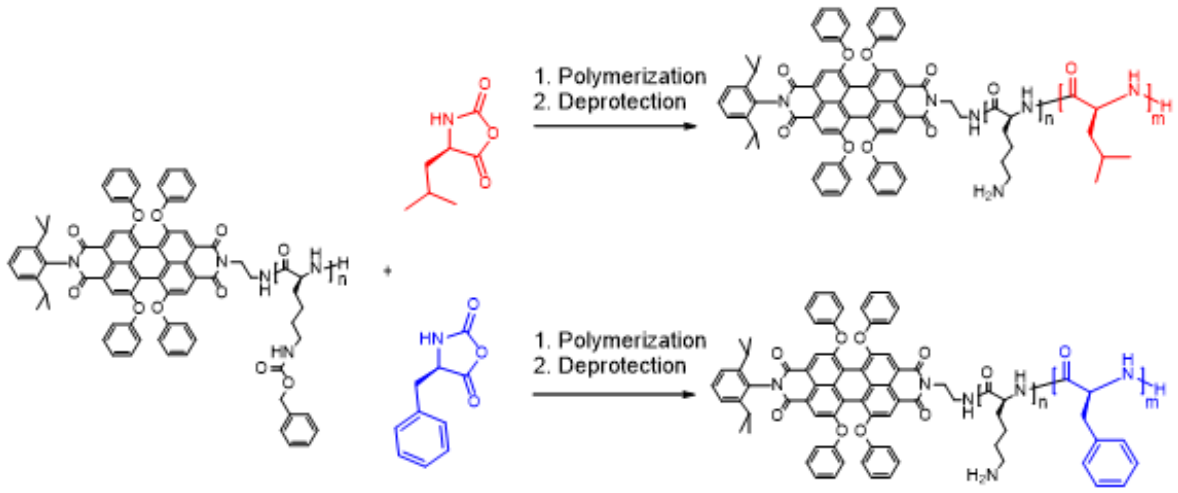

Scheme 5.3. Formation of block copolymer micelles

5.2. Results and Discussion

5.2.1. Synthesis of NCA monomers

All the poly(α-amino acid)s used in this research were synthesized by conventional ROP of amino acid NCAs. Synthesis of this type of monomers were first explored by Leuchs in 1906 using thionyl chloride, phosphorous pentachloride or phosphorus tribromide as halogenating agents with N-carbamoyl α-amino acids (Scheme 5.4.a).[307] The second approach for the NCA synthesis, which is commonly used due to the good yield, lack of racemization and better purity, is based on the phosgenation of α-amino acids by phosgene derivatives such as diphosgene or triphosgene (called Fuchs-Farthing method) (Scheme 5.4.b).[308,309]

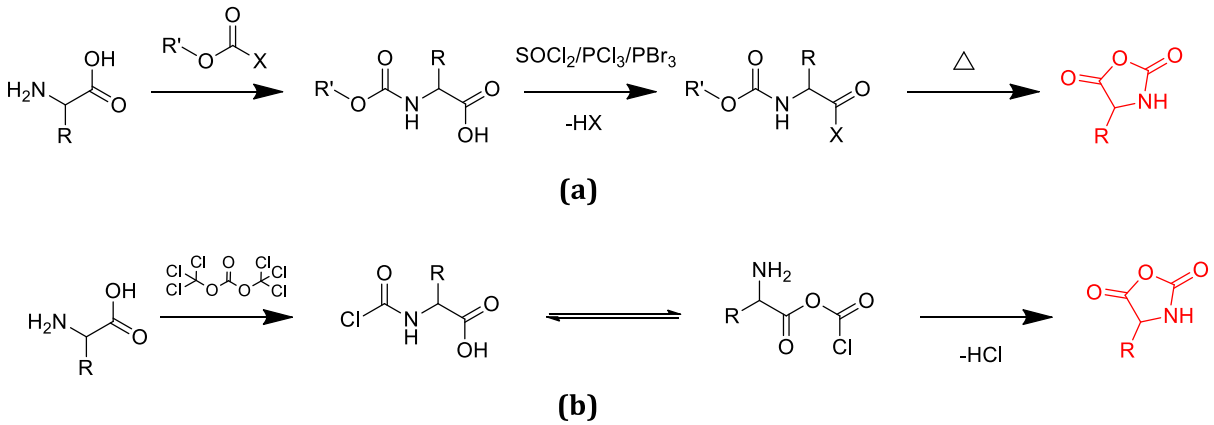

Scheme 5.4. Synthesis of α-amino acid NCA by (a) Leuchs method (b) Fuchs-Farthing method

Herein, NCA monomers (Figure **5.4**) were prepared by the Fuchs-Farthing method using triphosgene as a reagent in inert polar solvents such as ethyl acetate or THF under argon atmosphere as described in the literature (Scheme 5.5).[38,267,309] Addition of the carbonyl group of triphosgene to the corresponding amino acid results in an intramolecular cyclization and formation of NCA monomer.

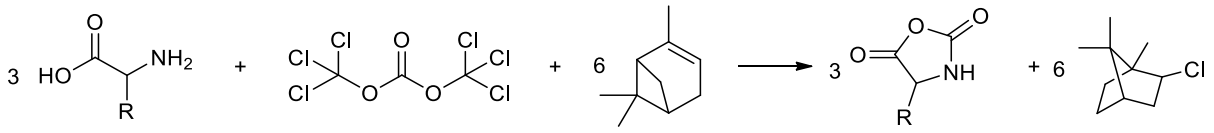

Scheme 5.5. Preparation of NCA monomer by Fuchs-Farthing method

Using a HCl scavenger during the reaction is necessary to prevent the formation of isocyanic acid chloride by the decomposition of the NCA monomer due to high concentrations of HCl (Scheme 5.6).[38]

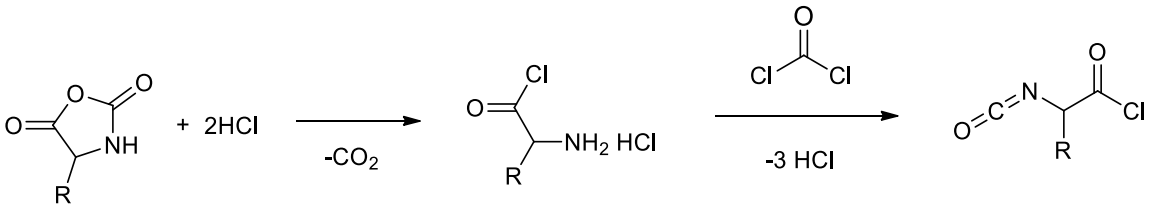

Scheme 5.6. Decomposition of NCAs to isocyanic acid chloride by high concentration of HCl

Purification is mostly possible by repeated crystallization, although some NCAs are very difficult to crystallize, washing with $NaHCO_3$ and rapid drying or flash column chromatography can be applied in these cases before crystallization.[267,310,311] If the monomer tends to crystallize easily like Lysine-NCA, it can be obtained with high yields (94-80%) and purity (>98%) after three recrystallization cycles. NCAs like leucine and phenyl alanine require several times of filtration through a silica plug to remove the chlorinated residues. Repeated precipitation from ethyl acetate/n-hexane eventually results in a clean white powder (purity>95%)(Yields 64-70%).[311]

L-Lysine NCA, synthesized with the two different protecting groups N-ε-fluorenylmethoxycarbonyl-L-lysine-N-carboxyanhydride (Fmoc-Lysine NCA, 4.1) and N-ε-carbobenzyloxy-L-lysine-NCA (Cbz-Lysine NCA, 4.2), L-leucine NCA (4.3) and L-phenyl alanine NCA (4.4) were synthesized and characterized by ^{1}H and ^{13}C-NMR spectroscopy (Figure 5.4)(Section 5.4.2).

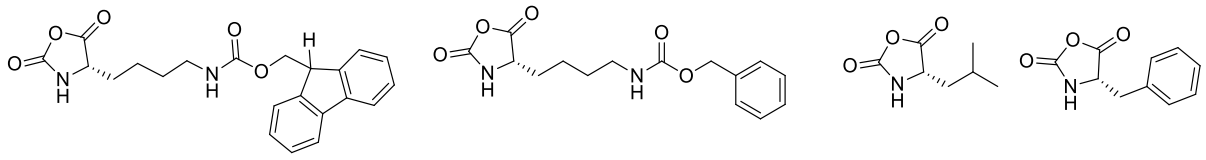

(4.1) (4.2) (4.3) (4.4)

Figure 5.4. Structures of synthesized NCA monomers

5.2.2. Synthesis of Terminal Fluorescence Labelled Polymers

The amino acid NCAs can be polymerized by conventional ROP using nucleophilic initiators as described in detail in Section 1.1.2. Primary amines are suitable initiators that lead the polymerization by "normal amine mechanism (NAM)" which is a nucleophilic ROP where the polymer chain grows linearly with the monomer conversion. The sterically less hindered primary amines are more nucleophilic compared to the ω-amino groups of the propagating chains; therefore, initiation is faster than propagation, leading to a higher degree of control of polymer chain formation with low polydispersity index. In the absence of side reactions, the polymerization proceeds as shown in Scheme 5.7.[88,89]

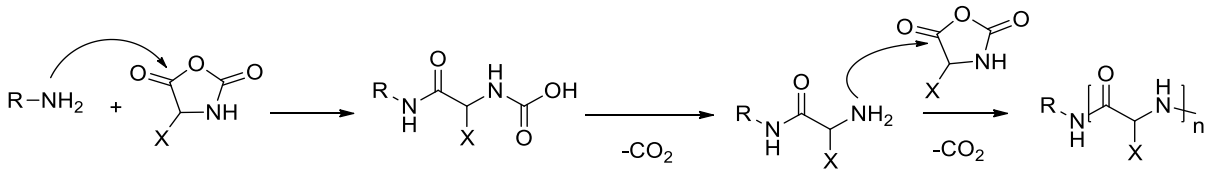

Scheme 5.7. ROP of NCA via normal amine mechanism

C-terminal modification of polypeptides is achieved by this approach. The reactivity of chain ends can be controlled by decreasing the reaction temperature to 0 ˚C, so free -NH_2 ended polymers are obtained. In that case, N-terminal modification of the polypeptides is possible as well by further reactions with intended species. In this research, primary amine initiators were applied for the polymerization of NCAs. Two different methods were employed for the C-and N-terminal florescence functionalization of the polypeptides:

- Post-polymerization end group functionalization
- Direct initiation approach by specially designed initiators

5.2.2.1. Post-polymerization End Group Functionalization Approach

In this approach, polypeptides were synthesized by double functional small initiators for further post-modifications via end group functionalities (Scheme 5.8). Keeping the pH sensitivity of the polypeptide side chains in mind, materials obtained by this approach can be considered as "pH switchable linkers" for further modification with dyes, dendrimers, bio-active molecules, polymers, nanoparticles etc.

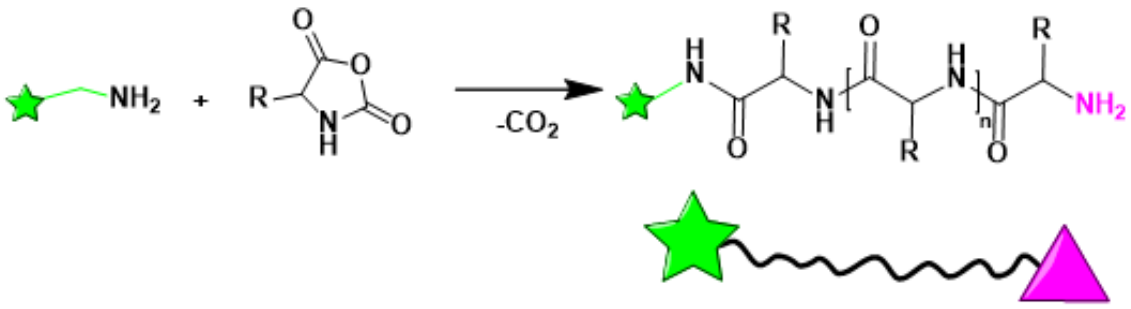

Scheme 5.8. Synthesis of functional end group containing polypeptides

Polymerization of the ε-amine protected Lysine NCA was performed by using several double functional initiators to obtain different end functional polymeric linkers. For that purpose, polymerizations with N-boc-1,6-hexanediamine, propargyl amine and N-Boc-ethylenediamine were investigated as shown in Scheme 5.9 (Table 5-1).

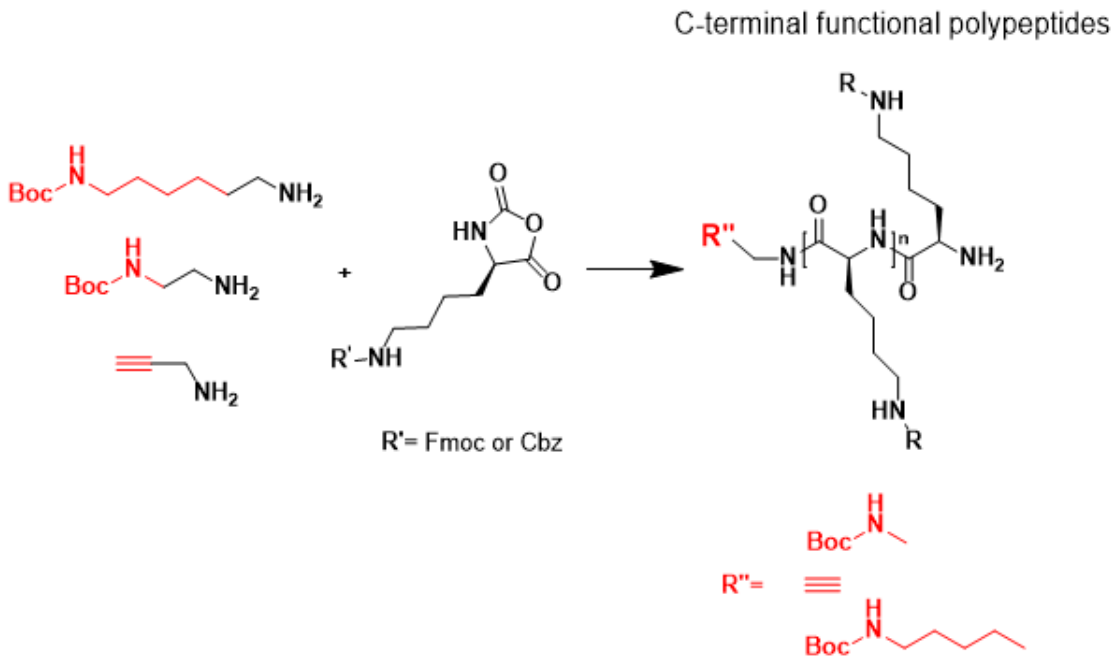

Scheme 5.9. Polymerization of Lysine-NCA with small functional initiators

Table 5-1. Polymerization data of Lysine-NCA with small functional initiators

Pol.	Monomer	T (°C)	Initiator	DP (theo)	DP (exp)	Yield (%)	GPC	
							M_n (g/mol)	Đ
PLL-1	Fmoc-L-Lysine-NCA	RT	N-Boc-1,6-hexanediamine	40	-	-	-	-
PLL-2	Cbz-L-Lysine-NCA	RT	Propargyl amine	40	12	45	3700	1.42
PLL-3		RT	N-Boc-1,6-hexanediamine	40	20	73	5400	1.32
PLL-4		RT	N-Boc-ethylenediamine	40	39	80	10300	1.19
PLL-5				40	46	82	12500	1.38
PLL-6		0 °C		30	25	40	6700	1.24

*GPC analysis was performed using DMF as eluent against Polystyrene standards
*DP_{exp} was calculated according to GPC
*DP_{exp} of PLL-2 was calculated by NMR via end group analysis

It is important to mention that Fmoc-Lysine NCA is not stable under this polymerization conditions. Synthesis of **PLL-1** was performed in DMF using N-Boc-1,6-hexanediamine at RT, which resulted in the formation of a hardly soluble precipitate in any organic solvents. ^{1}H-NMR analysis, conducted from the small soluble fraction of the reaction mixture,

showed the peaks of Fmoc and some undefined species. It is known in the literature that Fmoc groups can be cleaved in basic conditions.[312] So apparently here, the Fmoc group was cleaved by the initiator and free side chain amino groups led to graft polymerization, resulting in insoluble network formation. Klok et al.[313] reported a similar problem during the polymerization of Fmoc-Lysine NCA with n-hexylamine. Their five days of polymerization resulted in the formation of precipitate which could not be dissolved, neither in organic nor in water-based solvents.[313] To avoid this cleavage of the Fmoc group, the monomer type was changed to Cbz-Lysine-NCA which is fully stable under basic conditions.

Cbz-Lysine NCA was polymerized with different amine initiators as summarized in Table 5-1. First round of polymerizations (**PLL-2, PLL-3, PLL-4** and **PLL-5**) were proceeded at RT for four days under inert atmosphere via schlenk technique. Keeping slow argon flow was important during the polymerization to remove the released CO_2 in order to prevent possible side effects such as backbiting.[70,88] In contrast to Fmoc-Lysine NCA, no precipitation from the reaction mixture were observed during any of the polymerizations and obtained products were fully soluble in common organic solvents. Structures of all the polymers were successfully determined by ^{1}H-NMR spectroscopy as given in Section 5.4.2. Determination of the chain lengths by the end group analysis via NMR was difficult due to the overlapping of the initiators by broad polymer peaks. However, average degree of polymerizations were calculated by the molecular weights which was determined by GPC.

Polymerization of Cbz-Lysine NCA with N-Boc-1,6-hexanediamine with a theoretical degree of polymerization (DP) 40, resulted in a well-characterized polymer with a number average molecular weight of 5400 g/mol (**PLL-3,** 73% yield, PDI: 1.32, DP_{exp}: 20). Further polymerization of Cbz-Lysine NCA with propargylamine resulted in a number average molecular weight of around 3700 g/mol and PDI of 1.42 (**PLL-2**). Nevertheless, distribution was bimodal, and lower molecular weight than calculated value was obtained with a DP of 12 (DP_{theo} is 40). Finally, **PLL-4** and **PLL-5** obtained by the polymerization of Cbz-Lysine-NCA by *N*-Boc-ethylenediamine initiator resulted in consistent degree of polymerizations with theoretical values with narrow dispersities (PDI: 1.1-1.38) and yields over 80% as given in Table 5-1. Therefore, in the upcoming part, one of these

polymers, **PLL-5**, is used for the further functionalization with carboxylic acid functional perylene derivative via terminal amine groups (Scheme 5.10, compound **4.5**).

N-terminus dye modification of poly(Cbz-L-lysine)

Amino terminal groups of poly(Cbz-L-lysine) were modified with "N-(2,6-diisopropylphenyl)-N'-(4-aminoethyl)-1,6,7,12-tetra(4-sulfonylphenoxy)-perylene-3,4:9,10-tetracarboxydiimide" **(SO_3H-PDI-COOH, Compound 4.5)** in order to obtain a fluorescent biopolymer. SO_3H-PDI-COOH was kindly synthesized and provided by Sebastian Stappert. Polymers overall used for the dye modification were summarized below in Table 5-2.

Table 5-2. N-terminal modification of PLL-5 and PLL-6 with SO_3H-PDI-COOH

Polymer	GPC		Modified polymer	GPC	
	M_n (g/mol)	Đ		M_n (g/mol)	Đ
PLL-5 (synthesized at RT)	12500	1.38	**PLL-5-PDI-SO_3H**	17500	1.54
PLL-6 (synthesized at 0 °C)	6700	1.24	**PLL-6-PDI-SO_3H**	6200	1.38

*GPC analysis was performed using DMF as eluent, against Polystyrene standards

Amidation reaction between **PLL-5** and **SO_3H-PDI-COOH** was performed in the presence of HBTU coupling agent (2-(1H-benzotriazol-1-yl)-1,1,3,3-tetramethyluronium hexafluorophosphate) which proceeds the reaction *via* forming *in situ* active esters of –COOH groups in basic conditions at RT (Scheme 5.10).[314,315] Coupling product **PLL-5-PDI-SO_3H** was purified by repeated precipitation with diethyl ether. Excess amount of dye was removed by intense washing and reddish powder was obtained.

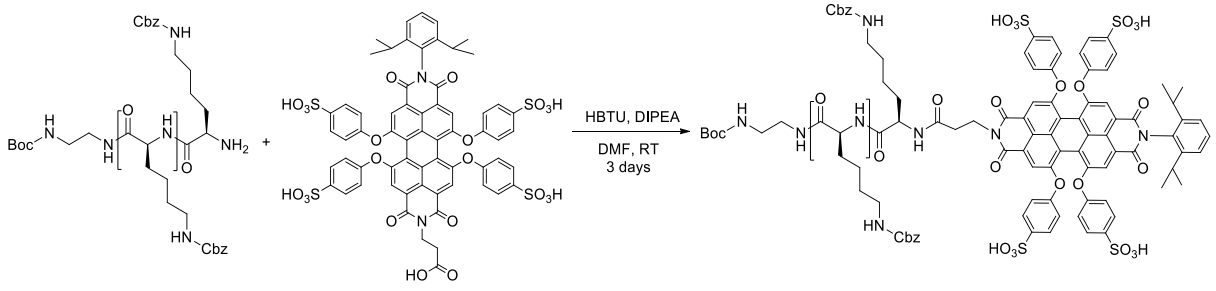

PLL-5 **Compound 4.5**

Scheme 5.10. N-terminal functionalization of PLL-5 with SO_3H-PDI-COOH

^{1}H-NMR of SO_3H-PDI-COOH, PLL-5 and coupling product **PLL-5-PDI-SO_3H** were presented in Figure 5.5.a. Dye peaks were marked as pink area, which are δ = 0.94 ppm (12H of isopropyl groups) and δ = 6.73, 6.90-6.95, 7.56-7.61, 7.85-7.87 ppm (aromatics of dye). ^{1}H-DOSY measurements were also performed to confirm the covalent attachment of the species. As it seen from Figure 5.5.b, peaks of the dye molecules are not in the same line with those of polymer peaks, means that, species of dye and polymer have different diffusion coefficients. To have a control study, PLL-5 and PDI-SO_3H was physically mixed and analyzed by ^{1}H-DOSY. Superposition of the spectrum of the physical mixture and the coupling product is presented in Figure 5.5.c, exactly the same signal values at the same position were observed. That means, no chemical attachment occurred by this technique or yield of the covalent modification was very low.

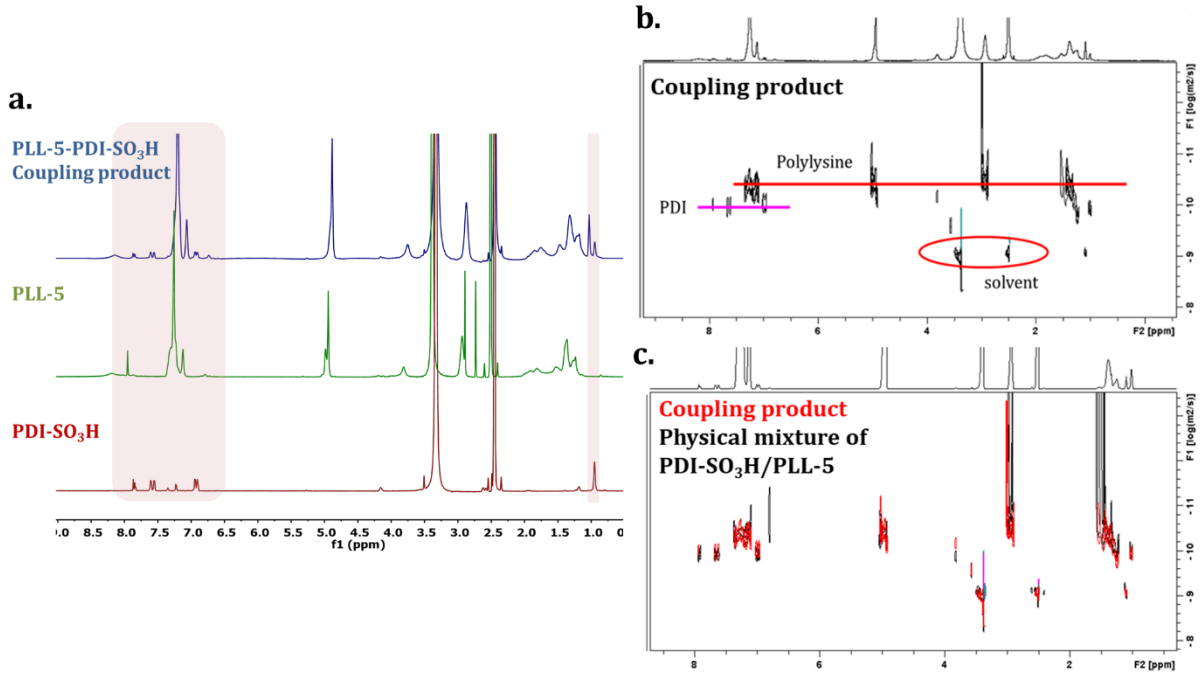

Figure 5.5. (a) ^{1}H-NMR of SO_3H-PDI-COOH, PLL-5 and PLL-5-PDI-SO_3H (b) ^{1}H-DOSY of PLL-5-PDI-SO_3H and (c) Superposition of ^{1}H-DOSY of coupling product (PLL-5-PDI-SO_3H) (red signals) and ^{1}H-DOSY of physical mixture of SO_3H-PDI-COOH and PLL-5 (black signals) (700 MHz, DMSO-d6, 298 K)

In the literature, Giani et al.[98] studied the temperature controlled polymerization (from RT to 0 ˚C) of ε-trifluoroacetyl-L-lysine NCA in DMF and investigated the polymer end groups by nonaqueous capillary electrophoresis to detect the living (-NH_2) and dead

(carboxylate and formyl) chain ends (Section 1.1.2). Analysis of the polymer synthesized at RT resulted in only 22% of the living terminal -NH_2 groups. When the polymerization temperature was reduced to 0 ˚C, 99% of the chain ends were determined as living –NH_2 groups. Additional research of Heise and coworkers also confirmed by MALDI-TOF-MS technique that polymerization of NCAs at RT results in end group blocked polymers.[38] This issue is most likely the reason of failure in the performed coupling reaction.

Therefore, poly(Cbz-L-lysine) **(PLL-6)** was synthesized with the same initiator (N-boc-ethylenediamine) at 0 ˚C for four days (Table 5-1). Yield of the polymerization was quite low (around of 40%) but molecular weight of the obtained polymer was 6700 g/mol with PDI of 1.24 (against PS standard, in DMF, fits to the theoretical DP=30). Terminal amine groups of PLL-6 were coupled with SO_3H-PDI-COOH in the presence of HBTU and DIPEA for three days. Same reaction conditions were applied as in the previous coupling attempt to yield **PLL-6-PDI-SO_3H.** After the reaction, polymer was intensively washed with water to remove unreacted water-soluble dye and additionally dialyzed against THF and then water. After intensive purification, ^{1}H-NMR and ^{1}H-DOSY measurements were performed in order to analyze the chemical structure and the covalent bounding of the dye to the N-terminus of the polymer. ^{1}H-DOSY measurement showed the same diffusion coefficients for all the species as shown in Figure 5.6 which proves the covalent modification of the polymer with fluorescence label. The coupling ratio was determined by the integration ratio of the aromatic peaks of PDI-SO_3H at δ = 7.62-7.53 ppm (8H) to CH proton of polylysine at 4.21-3.65 ppm (157H) as 19% dye attachment to the polymer.

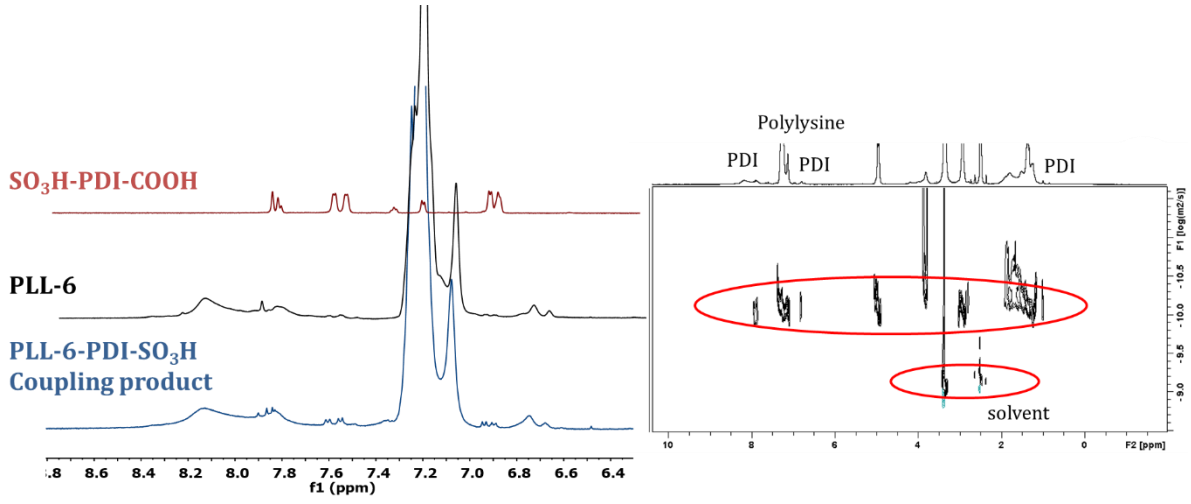

Figure 5.6. ^{1}H-NMR (between 9-6 ppm) of PLL-6, SO_3H-PDI-COOH and PLL-6-PDI-SO_3H coupling product, and ^{1}H-DOSY of **PLL-6-PDI-SO_3H** (700 MHz, DMSO-d6, 298 K)

The coupling ratio was additionally calculated by means of optoelectronic properties of the materials as UV-*vis* and emission spectra of PLL-6-PDI-SO_3H in DMF are depicted in Figure 5.7. There are three absorption maxima at 446, 536 and 575 nm, respectively. Fluorescence spectrum was recorded by excitation at 570 nm, resulted in an emission maximum at 607 nm. The dye modification ratio was estimated under the assumption that polymer attachment to dye does not affect its optoelectronic properties and all dye molecules are attached to polymer. Measurements of the DMF solutions of pure SO_3H-PDI-COOH and coupling product were performed and the ratio of PLL-6-SO_3H-PDI (dye attached) to PLL-6 (non-attached) was calculated as ~1:5 by means of the Lambert-Beer law. That means, around 20% of the polymer is labelled by the fluorescence molecule which is consistent with the coupling ratio calculated by ^{1}H-NMR technique.

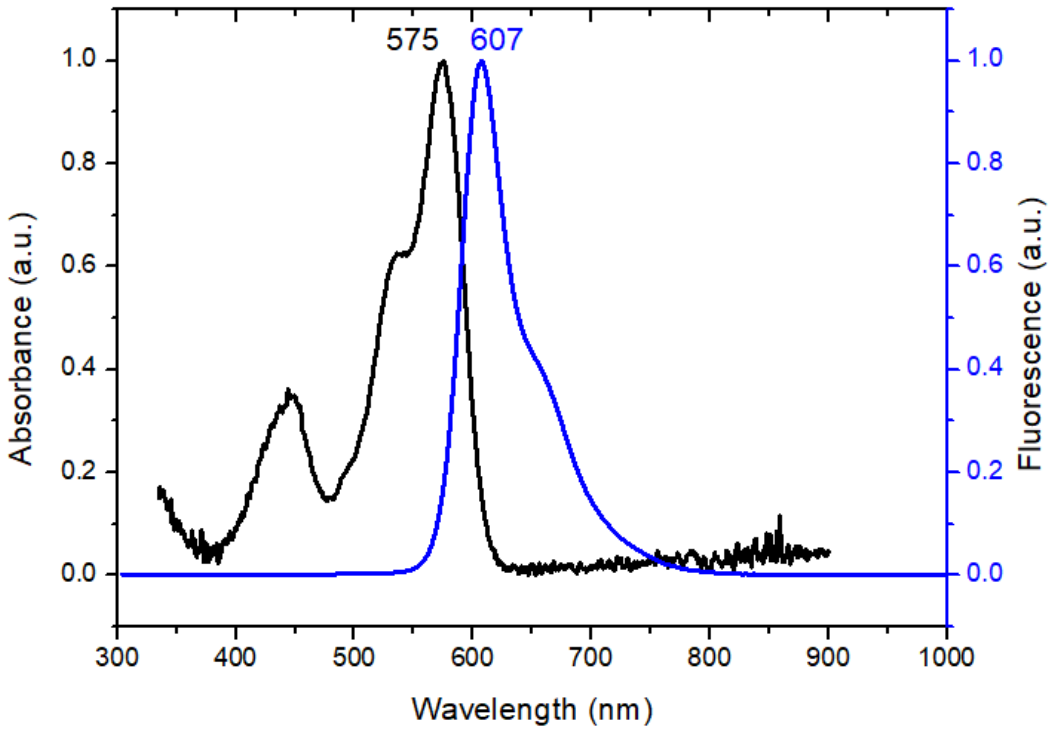

Figure 5.7. Normalized UV-*vis* (black) and Fluorescence (blue) spectra of PLL-6-PDI-SO_3H in DMF

Consequently, end group modification of poly(Cbz-L-lysine) with SO_3H-PDI-COOH *via* HBTU coupling was more successful when the polymerization was performed at 0 ˚C.

However, coupling yield was still low (~20%) and purification from unreacted dye was problematic in some cases. This situation might cause a problem on further self-assembly of the material due to the polydispersity in micelle environment. Therefore, the synthetic route of the project was changed to direct initiation of NCA monomer with specifically designed amine functional PDI derivatives as explained in the next section.

5.2.2.2. Direct initiation approach by designed initiators

Due to the described problems, we faced in the previous method, direct initiation approach is used in this part of the study. The functional dye molecule which is intended to modify the polymer is directly used to initiate the polymerization of the NCA monomer. Thus, C-terminal functionalization of the polypeptide could be achieved.[70] It is a more convenient way to avoid the chain termination problem during the N-terminus modification of the polymer chain. Therefore, amino functional N-(2,6-diisopropylphenyl)-N'-(4-aminoethyl)-1,6,7,12-tetraphenoxyperylene-3,4:9,10 tetracarboxy diimide (PDI-NH_2) was synthesized and employed as an initiator for the ROP of Cbz-L-lysine NCA. Using focal point modified perylene derivatives for C-terminal modification of linear polypeptides is a very useful approach in order to obtain well-defined fluorescent polymers with free side chain functionalities.

Synthesis of the initiator PDI-NH_2

Compound **4.9**, N-(2,6-diisopropylphenyl)-N'-(4-amino ethyl)-1,6,7,12-tetraphenoxy perylene-3,4:9,10-tetracarboxydiimide (PDI-NH_2), was synthesized according to the reported literature with slightly modified conditions (Scheme 5.11).[300,316]

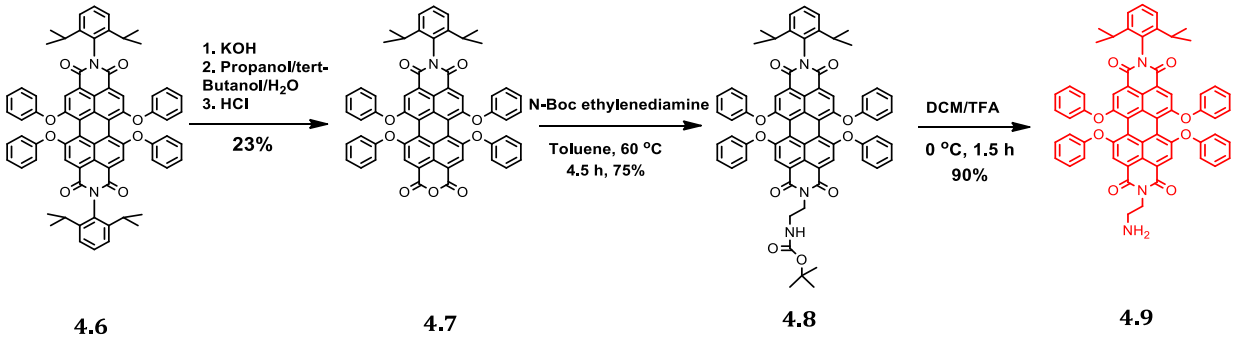

4.6 **4.7** **4.8** **4.9**

Scheme 5.11. Synthesis of PDI-NH_2 initiator

The synthesis of **4.9** was started with compound **4.6**, a commercially available product from BASF. Monosaponification to yield perylene monoimidemonoanhydride (**4.7**) was performed under strong basic conditions with potassium hydroxide. The process was controlled by TLC to minimize the completely saponified perylenedianhydride byproduct. To obtain clean **4.7**, the crude product was purified by silica chromatography using DCM as eluent with a 23% yield.[316] Characterization was performed by NMR spectroscopy (purity 96%). Subsequently, imidiziation was performed at 60 ˚C for 4.5 h by using N-Boc-ethylenediamine instead of ethylenediamine to avoid the formation of ethylene bridged bisperylene side products.[300] After silica chromatography using DCM/acetone (100/1) as eluent, **4.8** was obtained as a red solid with 75% yield. In the final step, Boc protecting group was cleaved by TFA to yield the desired amine functional perylene derivative **4.9**, whose structure was confirmed by NMR spectroscopy (Section 5.4.2). Optical properties of the PDI-NH_2 in DCM were investigated by UV-*vis* and Fluorescence measurements (Figure 5.8). UV spectrum of PDI-NH_2 shows three absorption maxima; 444 nm, 536 nm and 575 nm respectively. Solution was excited at 536 nm and emission maximum was recorded at 609 nm.

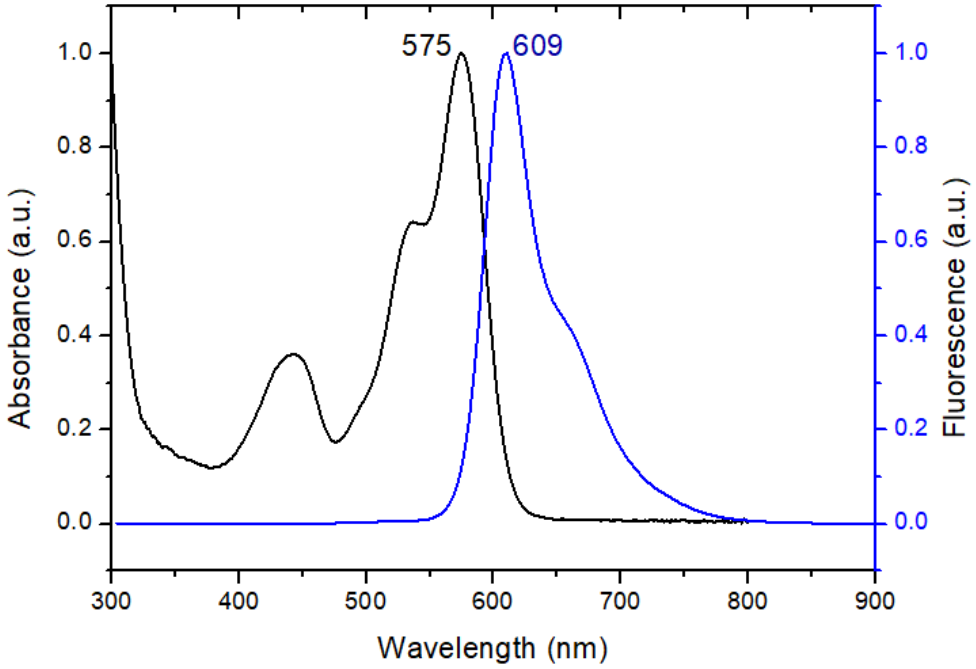

Figure 5.8. UV-*vis* and Fluorescence spectra of PDI-NH_2 (**4.9**) in DCM

Synthesis of the fluorescent poly(L-lysine)

Compound **4.9-**PDI-NH_2, was used as an initiator for ROP of Cbz-Lysine-NCA (Scheme 5.12). Three fluorescent polymers with different chain lengths were obtained with good yields (>80%) and narrow polydispersity, as summarized in Table 5-3. As discussed in the previous section, reducing the polymerization temperature has a dramatic effect on the polymerization mechanism, in terms of preventing the blockage of the terminal amine groups of the obtained polymer by NCA anion or the solvent DMF.[38,96] Therefore, polymerizations were performed at low temperature (0 ˚C for 4 days under inert atmosphere) for further utilization of free amino terminal polymers as macro-initiators.

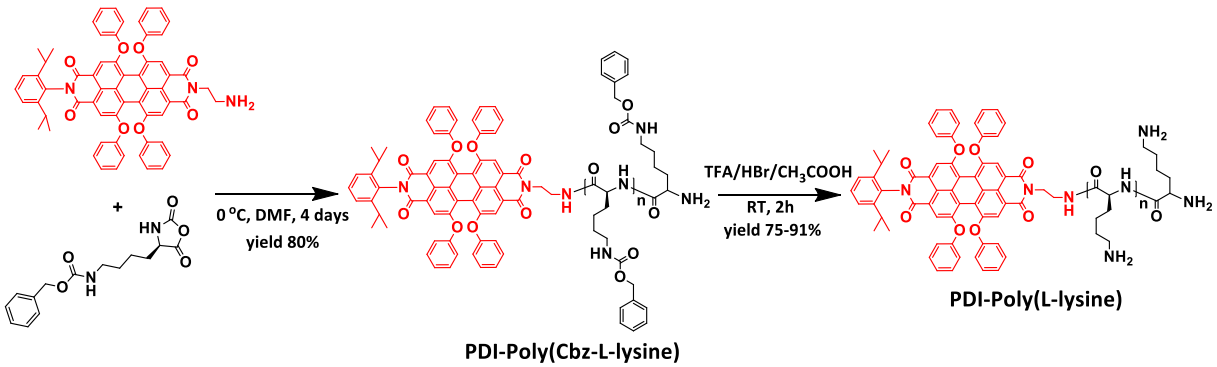

Scheme 5.12. Polymerization of Cbz-Lysine NCA by PDI-NH_2 and deprotection of Cbz groups

Poly(Cbz-L-lysine)s with a degree of polymerization of 20, 40 and 60 were obtained with narrow polydispersity in the range of 1.27-1.30. Average molecular weight and molecular weight distributions of the polymers were determined by GPC using two different detectors, i.e., RID and UV at 520 nm, respectively (Table 5-3). The wavelength of 520 nm corresponds to the absorption region of PDI-NH_2. Thus, the determined polymer at this wavelength is covalently PDI modified.

Table 5-3. Polymerization data of PDI-NH_2 modified Poly(Cbz-L-lysine) by direct initiation method

Pol.	DP (theo)	GPC (RID)			GPC (520 nm)			DP** (exp)	Yield %
		M_n	n*	Đ	M_n	n*	Đ		
PLL-7	20	6000	22	1.37	5100	19	1.31	23	98
PLL-8	40	10200	39	1.22	8700	33	1.27	40	91
PLL-9	60	10700	41	1.28	9600	37	1.27	60	65

*n is the degree of polymerization calculated by M_n from GPC
*GPC is measured DMF as eluent, against polystyrene standards
**DP(exp) is the degree of polymerization determined by ^{1}H-NMR

^{1}H-NMR of the **Compound 4.9-PDI-NH_2** and **PLL-8** are shown below in Figure 5.9 as representative examples. The corresponding peaks of all the protons of the PLL-8 were determined, and by the integration of the isopropyl peaks of the dye (12H) at δ=1.07 ppm (peak **a**) to α-CH (δ=3.8 ppm) or CH_2 (δ= 5.1 ppm) peaks of the polymer, chain lengths were determined as given in Table 5-3 as DP(exp). Experimental DPs were consistent with the theoretical values for all the fluorescence polymers. As all these characteristic results

revealed, C-terminal functionalization of poly(Cbz-L-lysine) with PDI fluorescent probe by direct initiation method was successfully achieved.

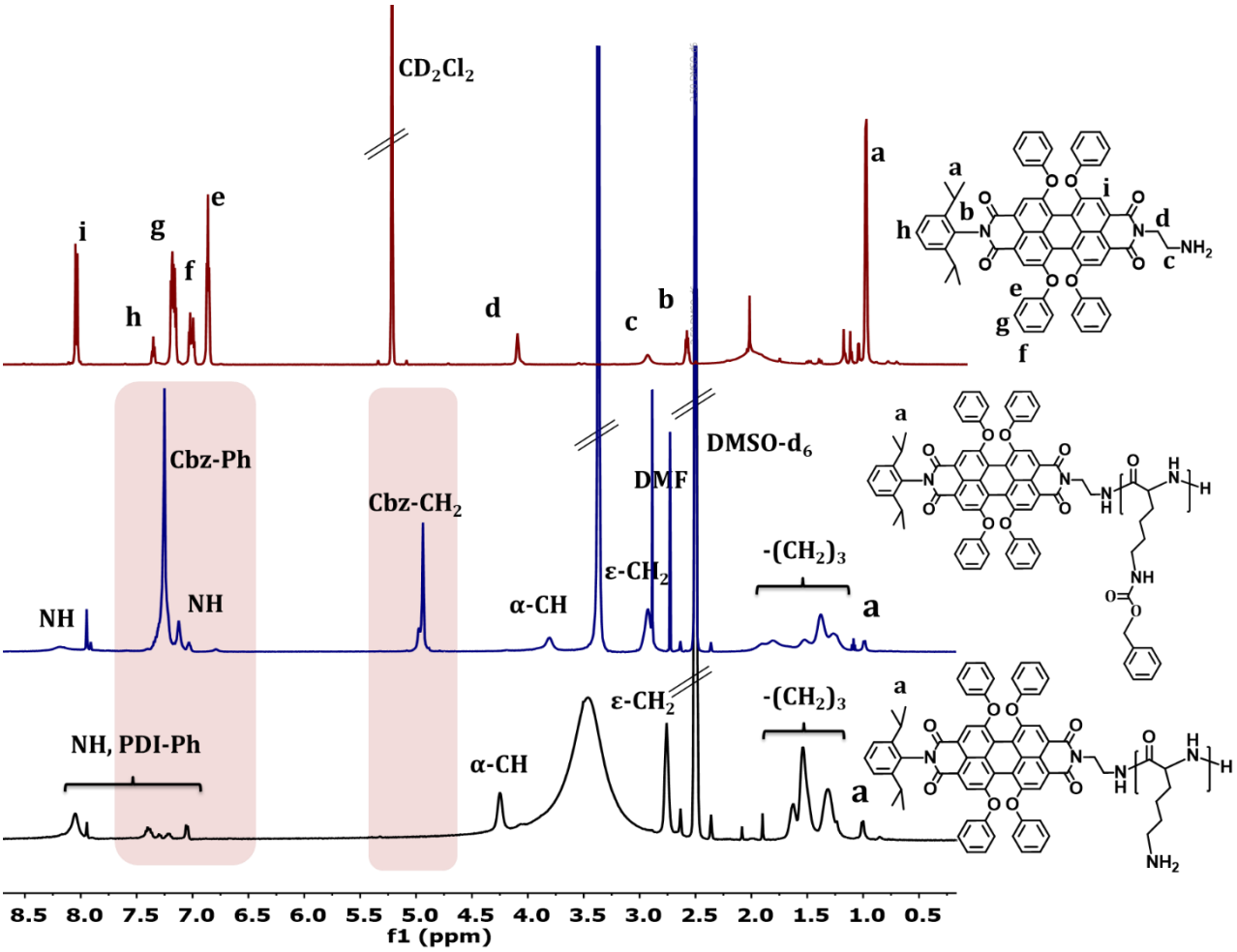

Figure 5.9. ^{1}H-NMR spectrum of Compound 4.9-PDI-NH_2 (red), PLL-8 (blue) and PLL-8dp (black) (500 MHz, 298 K, DMSO-d6)

In order to have an amino functional fluorescence polypeptide, the Cbz protecting group of the polymer side chain was cleaved under strongly acidic conditions by HBr/CH_3COOH in trifluoroacetic acid (TFA) at RT for 2 h.[136] The target polymers were isolated by precipitation with diethyl ether and dialyzed against water for three days to remove the excess of the acid and other impurities. The final free amine containing fluorescent polymers PLL-7dp, PLL-8dp and PLL-9dp with DP=20, 40 and 60 were obtained, respectively (Scheme 5.12).

Complete cleavage was confirmed by ^{1}H-NMR by disappearance of the Cbz phenyl peaks at around δ = 7.49 – 6.99 (m, 5H-Ar), and CH_2 peaks at around δ = 5.08 – 4.86 (m, 2H, Cbz-CH_2), demonstrated as pink regions in Figure 5.9. Aromatic PDI peaks arose clearly in the region of δ = 7.5-7.0 ppm after the removal of Cbz.

Besides NMR characterization, FT-IR spectra of the polymers have also confirmed the cleavage of Cbz as presented in Figure 5.10. The broadband at the region of 3200-2500 cm^{-1} in the FTIR spectrum of deprotected polymer shows the formation of free amine/ammonium salts. Additionally, the disappearance of the Cbz groups C=O amide band at 1690 cm^{-1} confirms the complete deprotection.

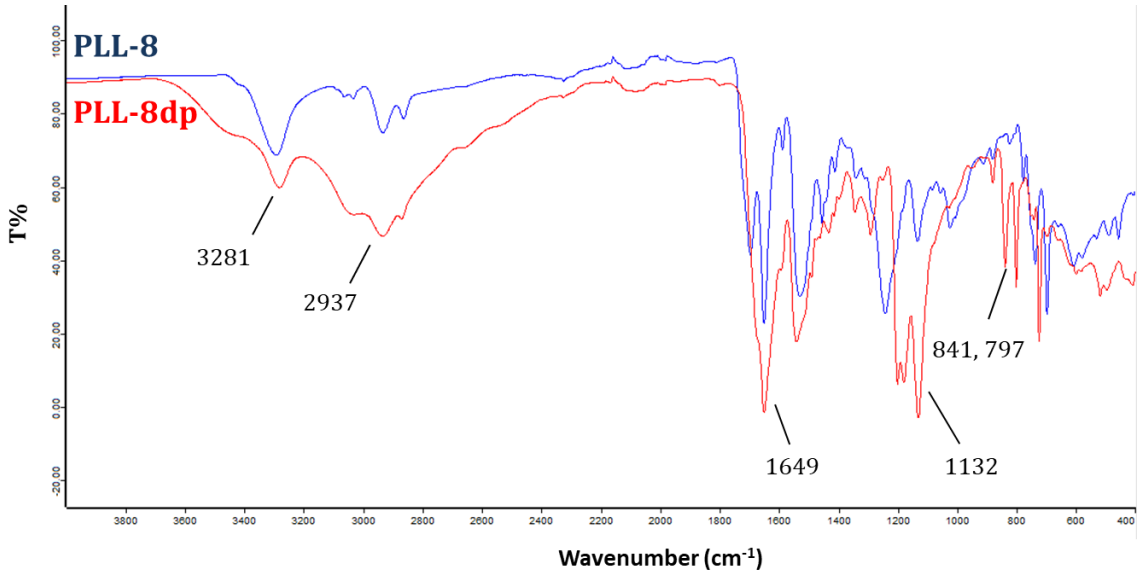

Figure 5.10. FTIR spectrum of protected PLL-8 (blue) and deprotected PLL-8dp (red) polymer

5.2.3. Supramolecular Assembly of Homopolymer Amphiphiles

Owing to the fact that proteins and polypeptides are essential for living organisms, investigation of their conformational behavior is getting great attention, which is important for the function of the material.[317–319] Poly(L-lysine) is a water-soluble polypeptide with free side chain amine groups, which can be used as a pH sensor through pH dependent conformational changes such as random coil at low pH and, α-helix at high pH.[320,321] In addition to that, C-terminal PDI functionalization makes poly(L-lysine) a

unique material which can behave as supramolecular fluorescent "pH-sensor" (Figure 5.11).

Fluorescence is one of the most widely used technique for determination of protein folding and conformational dynamics due to its sensitivity against the environment of the probe and a high signal-to-noise ratio even with a small amount of the material.[322–324] However, it is strongly influenced by the structure and therefore, it has to be correlated by an additional method such as circular dichroism (CD).[323] The conformational behavior of polypeptides containing intrinsically fluorescent amino acids, most importantly tryptophan, can be investigated by exciting at 295 nm or above, without the need of labeling with an additional fluorescent probe.[322] However, it is still not useful for bio-imaging studies. In this point, of course, fluorescently labelled probes are necessarily used for visualizing intracellular processes and molecular interactions at the level of single cells. Therefore herein, pH-responsive supramolecular assembly of PDI-poly(L-lysine) was investigated by UV-*vis* absorption and fluorescence techniques and obtained data was correlated with CD measurements. The size of the aggregates was analyzed by dynamic light scattering (DLS) or fluorescence correlation spectroscopy (FCS). Furthermore, biocompatibility and cell interaction behavior of the fluorescent polymers were investigated by confocal microscopy as a proof of concept.

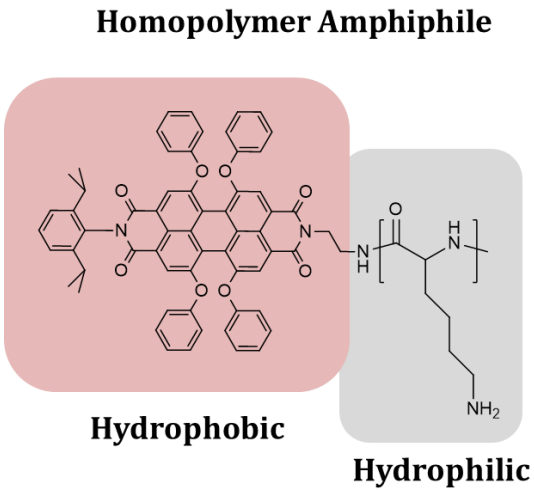

Figure 5.11. Structure of PDI-Poly(L-lysine) homopolymer amphiphile

In principle, a polymer chain bound to the fluorescent molecule can affect the luminescent properties of the label. Herein additionally, the water solubilization of the hydrophobic

PDI by hydrophilic poly(L-lysine) might have an influence on the behavior of the dye. Therefore, fluorescent poly(L-lysine)s with different chain lengths were first investigated by means of optoelectronic properties.

PDI-NH_2 is a typical fluorophore with three absorption maxima at 444 nm, 536 nm and 575 nm and emission maxima at 609 nm in DCM as described before (Figure 5.8). The absorbance and fluorescence spectra of PLL-7dp, which is PDI attached poly(L-lysine) (DP=20), in water was presented in Figure 5.12. Two electronic transitions are visible in the absorbance spectrum, the S0-S1 transition is situated at around 580 nm, and S0-S2 transition appears at 455 nm. Intensity of the absorption maxima at 536 nm of PDI-NH_2 (in DCM) decreased and became like a little shoulder in water solution of PLL-7dp around of 546 nm. Emission maxima of the PDI-NH_2 was bathochromically shifted (around 30 nm) from 609 nm (λ_{ex}= 536 nm) to 636 nm (λ_{ex}= 580 nm) by water solubilization. Therefore, around 536 nm wavelength can be used to excite this dye in the cell environment by fluorescence microscopic techniques, obtaining a good signal/noise ratio due to the reduced auto-fluorescence of cell medium.[186] The bathochromic shift on emission spectrum reflects the changes in the environment surrounding the perylene chromophore. Because there is no common solvent for hydrophobic PDI and amphiphilic PDI-attached poly(L-lysine); these changes can be attributed either to the different solvents used (DCM and water) or aggregation behavior of the amphiphile in aqueous medium. Chain length of the polymer does not affect the absorption and emission wavelengths as measurements revealed.

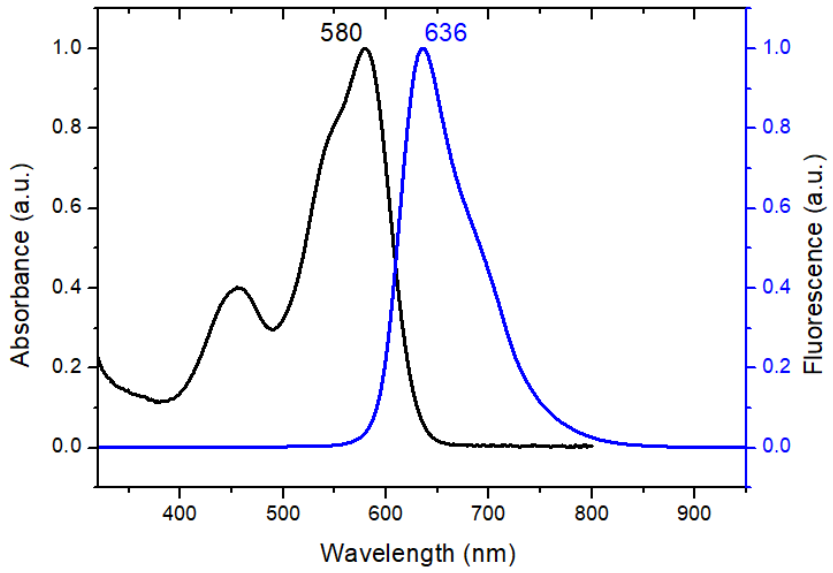

Figure 5.12. Normalized UV-*vis* and Fluorescence spectra of PLL-7dp in water

Aggregation is a general encountered phenomenon in dye chemistry. According to the molecular excitonic theory, mainly H- and J-aggregations can be observed. By parallel stacking of the molecules H-aggregates are formed whereas head-to-tail assembly results in a formation of J-aggregates. In H-aggregates, the absorption maximum is blue-shifted with respect to the isolated chromophore and the fluorescence is normally quenched. However, J-aggregates usually show fluorescence, and both the absorption and emission maxima are red-shifted.[325,326] So far, different solvents had to be used for PDI and the polymer, 30 nm red-shift on emission spectrum cannot be attributed to these mentioned phenomena.

Before investigating the pH responsive behavior of the materials, concentration dependent aggregation profile of the polymers was studied as absorbance and emission spectra of PLL-7dp were presented in Figure 5.13 and Figure 5.14 as a representative example. No abrupt change was observed on either absorption or emission values which can denote the critical aggregation concentration from 0.1 mg/mL to 0.025 mg/mL concentration range of PLL-7dp.

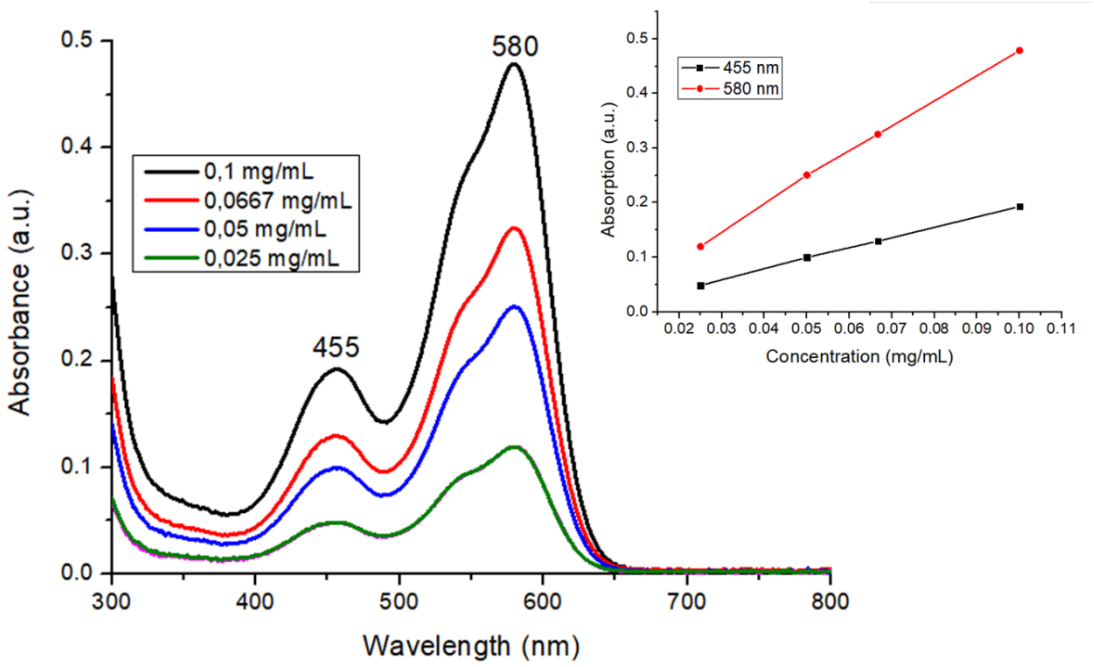

Figure 5.13. (a) Concentration dependent UV-*vis* spectra and absorption maxima (at 455 and 580 nm) plotted against concentration of the PLL-7dp

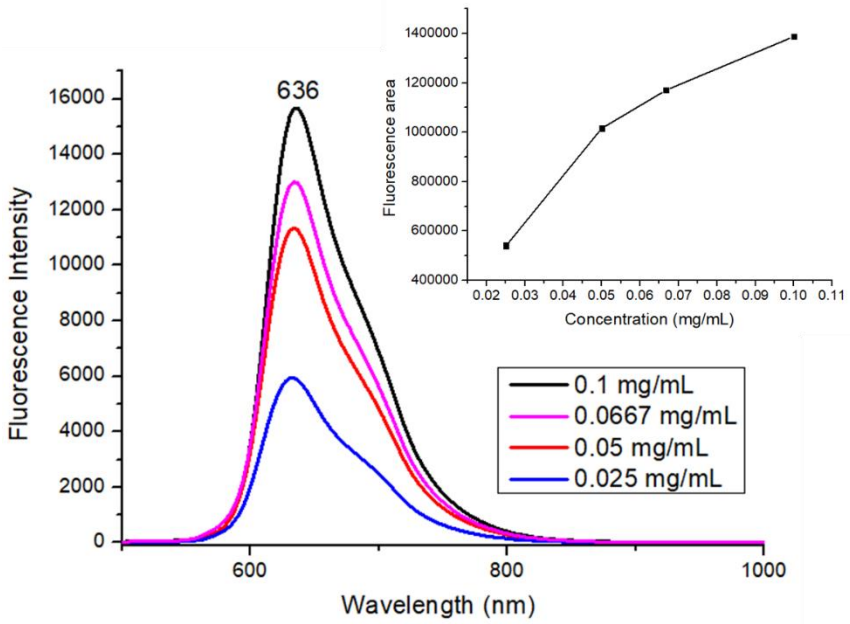

Figure 5.14. (a) Concentration dependent fluorescence spectra (λ_{ex}= 580, λ_{em}= 636 nm) and fluorescence area plotted against concentration of the PLL-7dp

Dynamic light scattering (DLS) is one of the commonly applied techniques to investigate the aggregation phenomena.[327] Thus, particle sizes of PDI modified polymers were

measured and the hydrodynamic radius of the polymers was found around 46 nm, 61 nm and 97 nm for PLL-7dp, PLL-8dp and PLL-9dp, respectively, as summarized in Table 5-4. By increase of the hydrophilic polymer length, the size of the aggregates increased due to the stronger association of water-soluble amine/ammonium side chains with the polar environment. Further investigations showed that DLS is not every time the suitable technique for our system to detect the hydrodynamic radius because of the strong fluorescence of the PDI at the wavelength set up of our Zetasizers in house (632 nm). TEM analysis by uranyl acetate staining technique was attempted to visualize the amphiphile aggregates of PLL-7dp in water. As shown in Figure 4.15, spherical aggregates around 20 nm were observed. The particle size detected by TEM was smaller than from DLS. Furthermore, no π-π stacking occurred as XRD measurements revealed.

Table 5-4. DLS results of PDI-modified poly(L-lysine)s

Polymer	Size (nm)
PLL-7dp	46 ± 9
PLL-8dp	61 ± 18
PLL-9dp	97 ± 40

Figure 5.15. TEM image of PLL-7dp in water

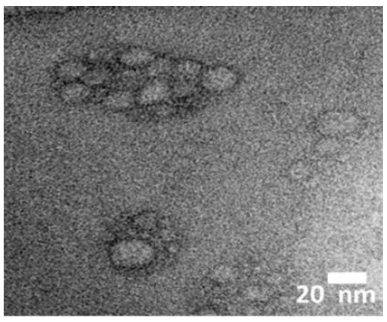

Investigation of the pH responsive properties of the fluorescent polymers

Poly(L-lysine) is an inherently pH responsive material which exists in a random-coil formation at low pH, α-helix at a pH above 10.6, and transforms into β-sheet when the α-helix is heated.[328] In order to investigate the effect of those properties on optoelectronic behavior of the dye labelled poly(L-lysine), aqueous solutions of different chain length fluorescent polymers (PLL-7dp, PLL-8dp and PLL-9dp) were prepared in TRIS-HCl buffer in various pH values (from 2 to 10) and their absorption and emission spectra were recorded. Buffer has no additional effect on absorption and emission properties of the polymers as control experiments revealed (Appendix D: Supporting Information).

The typical absorption spectrum of PLL-7dp in water has two maxima at 580 and 455 nm and a shoulder around of 546 nm as presented above (Figure 5.13). When pH was adjusted to 2, the intensity of the shoulder at 546 nm increases and becomes the main absorption peak at pH 2, however, no shift on the maximum wavelength was observed as seen in Figure 5.16.a. When the pH was increased from 2 to 12, the intensity of the maximum absorption peak at 546 nm decreased gradually by slow deprotonation of ε-amine groups. There is no obvious shift on the peak maximum at 580 nm by pH stimuli but the absorption maxima at 456 nm is slightly shifting to 450 nm. Protonation of ε-amino groups of poly(L-lysine) in an acidic environment induces the formation of a random coil polypeptide which is increasing the solubility of the polymer. In that way, intramolecular amphiphilic balance is changing within the whole system which might encourage aggregation phenomena.

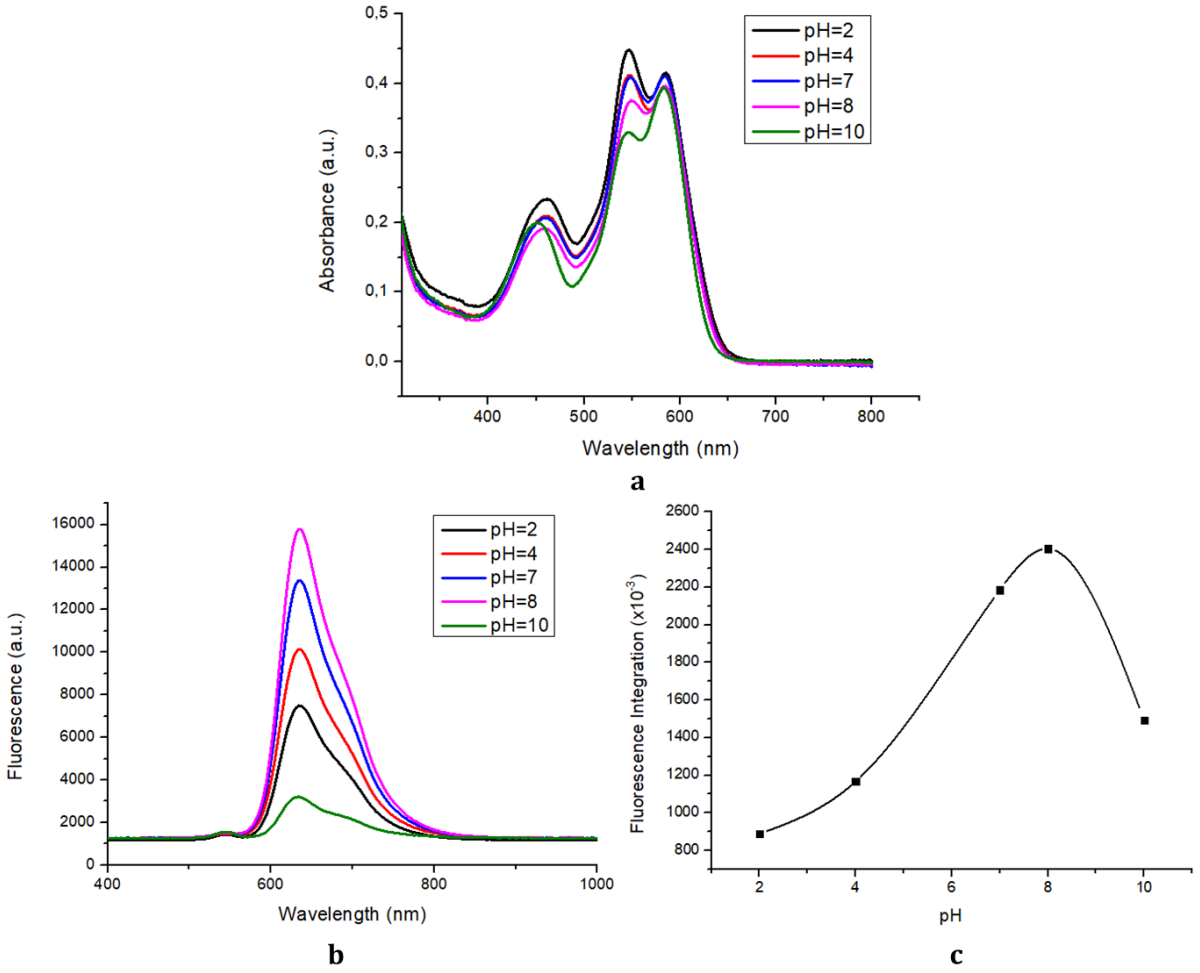

Figure 5.16. (a) UV-*vis* spectra of PLL-7dp in TRIS-HCl buffer with different pH values (b) Fluorescence spectra of PLL-7dp in TRIS-HCl buffer (λ_{ex}= 547 nm, λ_{em}= 636 nm) and (c) fluorescence integration plotted against pH

Figure 5.16.b exhibits the fluorescence emission spectra of PLL-7dp that were measured at different pH values upon excitation at 546 nm, demonstrating the pH dependency of the fluorescent polypeptide amphiphile.

The highest intensity of fluorescence was observed at pH 8 which is around the pK_a of poly(L-lysine). By acidic treatment, the intensity of the emission spectrum decreased gradually, which can be attributed to the molecular aggregation. A supporting evidence was detected in absorption spectrum as explained above that the intensity of the band at 546 nm was increased towards acidic medium. When the pH was increased from 8 to 10, fluorescence intensity was sharply decreased, means quenched (Figure 5.16.c). This behavior can be explained by the folding of the polypeptide in basic environment. Poly(L-

lysine) adopts to random coil at low pH and α-helix at high pH values as determined by CD which will be explained in detail in the upcoming section. Enhancing hydrogen bonding by deprotonation of amino groups of the polypeptide at pH 10, folded polypeptides in helical conformation were fabricated. By this helical assembly, C-terminal PDI moieties automatically come closer and due to this π-π interaction of aromatic systems, the fluorescence has been quenched dramatically. Decreasing solubility at higher pH values would also effect the formation of aggregates thereby quenching.[329]

In general, the same behavior was observed against pH for the longer fluorescent polypeptide chains as UV-*vis* and Fluorescence measurements revealed for PLL-8dp (DP=40) and PLL-9dp (DP=60) (Figure 5.17 and Figure 5.18). Only little intensity changes were observed at the absorbance maximum at 580 nm for PLL-9dp as seen in Figure 5.18.a. Emission intensities of the polymers decreased as well in very acidic (pH=2) and very basic (pH=10) conditions (Figure 5.17.b.c and Figure 5.18.b.c). It is known in the literature that α-helix transitions are easily observed in longer polypeptides, because 3.6 repeating units make one turn of helix in the structure.[330] Indeed, tendency to helical folding is expected to be more dominant for PLL-9dp (DP=60) in comparison to PLL7-dp (DP=20). The maximum fluorescence intensity of three polymers in buffer is at 15000, 19000 and 24000 a.u., respectively from PLL-7dp to PLL-9dp. It can be attributed that fluorescence intensity is increasing with the increased chain lengths because of the better solubilizing effect of the hydrophilic polymer chains to the core formed hydrophobic perylene moiety.

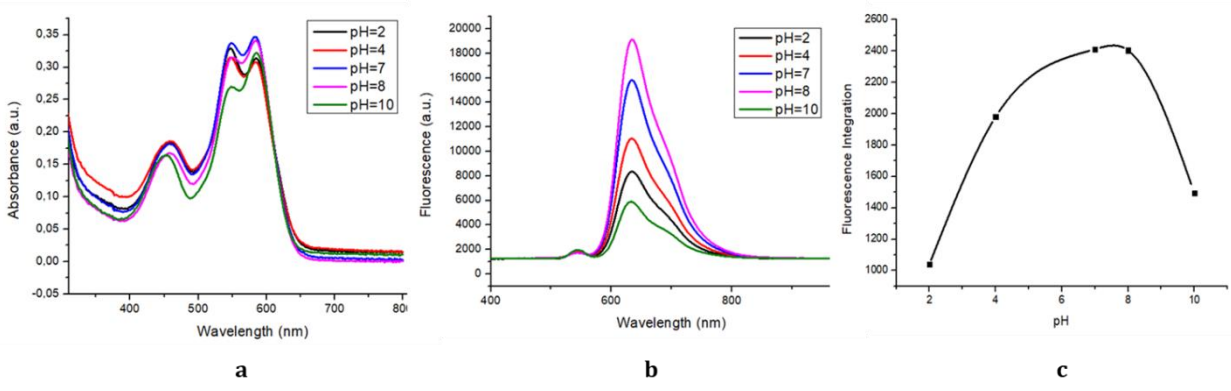

Figure 5.17. (a) UV-*vis* spectra of PLL-8dp in TRIS-HCl buffer (b) Fluorescence spectra of PLL-8dp in TRIS-HCl buffer ((λ_{ex}= 547 nm, λ_{em}= 636 nm) (c) fluoresc. integration plotted against pH

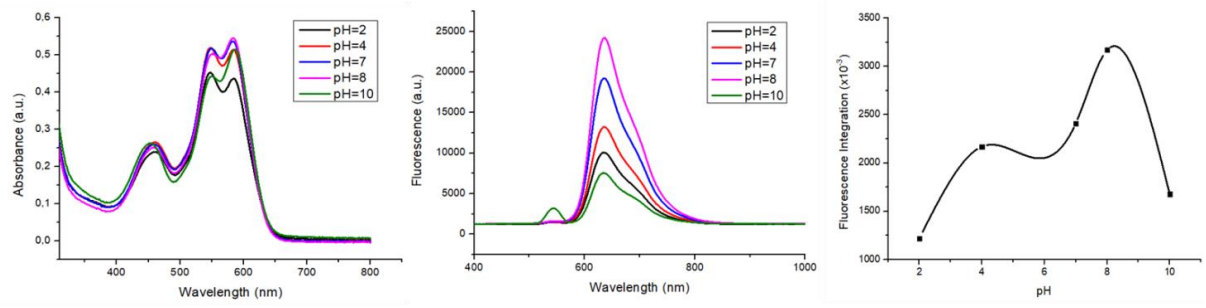

Figure 5.18. (a) UV-*vis* spectra of PLL-9dp in TRIS-HCl buffer (b) Fluorescence spectra of PLL-9dp in TRIS-HCl buffer ((λ_{ex}= 547 nm, λ_{em}= 636 nm) (c) fluoresc. integration plotted against pH

Further, Fluorescence Correlation Spectroscopy (FCS) was attempted to be applied for understanding the aggregation phenomena for PLL-9dp which should have more response to pH due to the longest chain length (Table 5-5).

Table 5-5. FCS results of PLL-9dp in water with different pH values

Sample	**Concentration**	**Size (nm)**		
		pH=2	pH=7	pH=10
PLL-9dp	10^{-7} mol/L	9.2 nm (I=6,3 kHz) (Aggregates)	2.3 nm (I=2 kHz)	1.86 nm (I=0,9 kHz)

*FCS data give us general information about aggregation but not for comparing of closer values certain by numbers due to the 15 % of error bar.

As we can see in Table 5-5, aggregates around 9.2 nm were observed at pH 2. When pH was increased to 7 (around pK_a of PLL), single chains of 2.3 nm were detected and further pH increase to 12 resulted in chains of 1.86 nm. This measurement supports the argumentation on aggregation behavior of the polymers obtained by other methods. Aggregation at acidic pH was expected due to the high protonation rate of the peptide side chain. In basic environment no large aggregates were observed according to the FCS, which means folding of the single polypeptide chains push the aromatic π-π systems closer together and therefore quench themselves.

Circular Dichroism (CD) investigation

Circular dichroism (CD) is a phenomenon which is a differential absorption of left-handed (L-CPL) and right-handed circularly polarized light (R-CPL).[331] When optically active molecule-light interaction occurs, velocity of right and left polarizations and molar absorption coefficients differ from each other ($c_L \neq c_R$) due to different refractive indices of L-CPL and R-CPL. This difference of $\Delta\varepsilon = \varepsilon_L - \varepsilon_R$, means different optical rotation which defines as circular dichroism. Electric and magnetic fields of circularly polarized light beam interact differently with the chiral center of the molecule. In a typical CD experiment, an asymmetrical sample is exposed to equal amounts of left and right circularly polarized light and a sample absorbs right and left-handed circularly polarized light to different extents, yielding CD spectra. Due to the interaction with the molecule, the electric field vector of the light traces out an elliptical path after passing through the sample. The units of CD are mean residue ellipticity (degree cm^2 $dmol^{-1}$) and the difference in molar extinction coefficients called the molar circular dichroism or Δε (liter mol^{-1} cm^{-1}). ($[\theta] = 3298(\Delta\varepsilon)$).[331,332]

The technique CD spectroscopy is therefore very sensitive for structural characterization of polypeptides and proteins such as determination of secondary structures (α-helix, random coil and β-sheet) and conformational changes by any stimuli, binding, denaturation etc. CD absorption spectrum in the range of 180 and 260 nm is used to investigate various conformations of biomaterials. CD spectra of protein in general (Figure 5.19.a) demonstrates π-π* and n-π* transitions of the amide groups. A random coil shows a negative band at 197 nm (π-π* - transition) and a weak positive band at 210-220 nm which is the lowest energy transition in the peptide chromophore and is assigned to the n-π* transition. α-helix exhibits two π-π* transitions with positive Δε at 190 nm and an n-π* transition with negative Δε at around of 208 nm and 222 nm. β-sheet structures have a positive transition at 198 nm (π-π*) and a negative band at 215 nm (n-π*). Often there are several secondary structures in a protein, so that the obtained CD spectrum shows an additive superposition of the individual structures.[333,334] It is important to note that, in the presence of aromatic side chains for example in the case of phenylalanine, tyrosine or tryptophan, they might have an absorption bands in UV spectrum.[322] Nevertheless contribution to the CD spectra in the near UV is usually negligible.

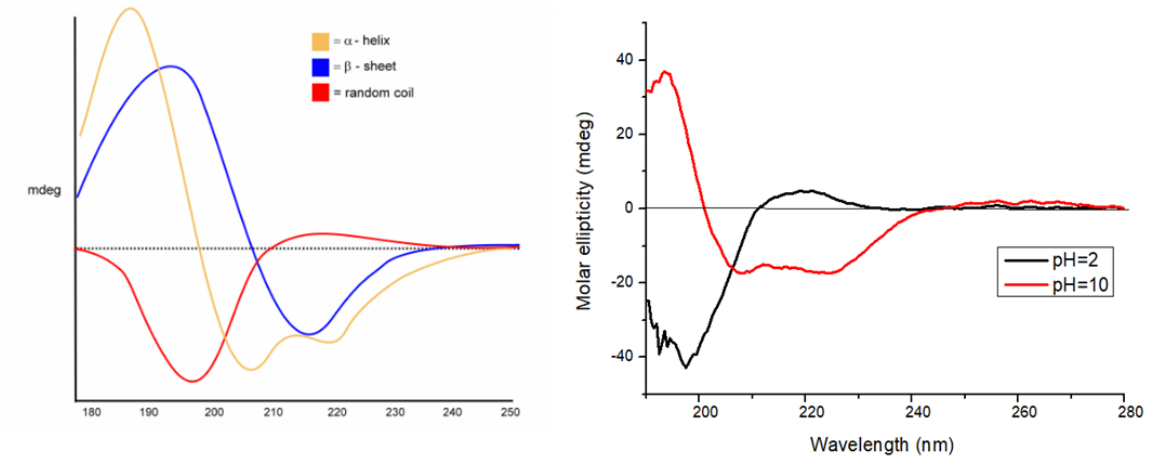

Figure 5.19. (a) General CD spectra of polypeptides (b) CD spectra of PLL-9dp at pH 2 and 10

The secondary structure estimation of fluorescent poly(L-lysine) was determined by CD spectroscopy in order to investigate the pH responsivity and support the hypothesis above on optical investigations. First of all, it is clearly seen from the Figure 5.19.b that, PLL-9dp shows obvious transition of random coil to α-helix by pH change from 2 to 10.

PLL-7dp and PLL-9dp solutions with a concentration of $3*10^{-5}$ M were prepared in water and the pH of the solutions was adjusted by HCl/NaOH solutions. Conformational changes of polypeptide were induced by electrostatic repulsions within the polypeptide chain due to ionization of side chains by pH stimuli. Polymers, at different pH values from 2 to 12, were analyzed by CD spectroscopy. Here below in Figure 5.20.a and b, CD spectra of the shortest (PLL-7dp, DP=20) and the longest (PLL-9dp, DP=60) polypeptides are demonstrated. As seen for both spectra, the proportion of α-helix increases with increasing pH value. The fluorescent polypeptides are mainly in random coil formation between pH 2-8 (negative band at 197 nm, positive at 210-220 nm), and adopts α-helix at pH 10 and 12 (positive peak at 194 nm, negative peak at 210 and 220 nm). However, further increase of the pH results in a precipitation.

Even though the spectrum of PLL-7dp is noisy and curves are not smooth, the change of the conformation by pH can be seen clearly. This is probably due to the length of the polypeptide which might be too short to form a clear helical structure, and therefore is not oscillating regularly. For PLL-9dp (DP=60), the concentration of the samples is the

same ($c=3*10^{-5}$ M), except of the one in pure water which is more concentrated ($c=6*10^{-5}$ M). Therefore, the negative signal, which corresponds to the random coil chain at 196 nm, is more intense. As mentioned above, α-helix formation increases by pH raise.

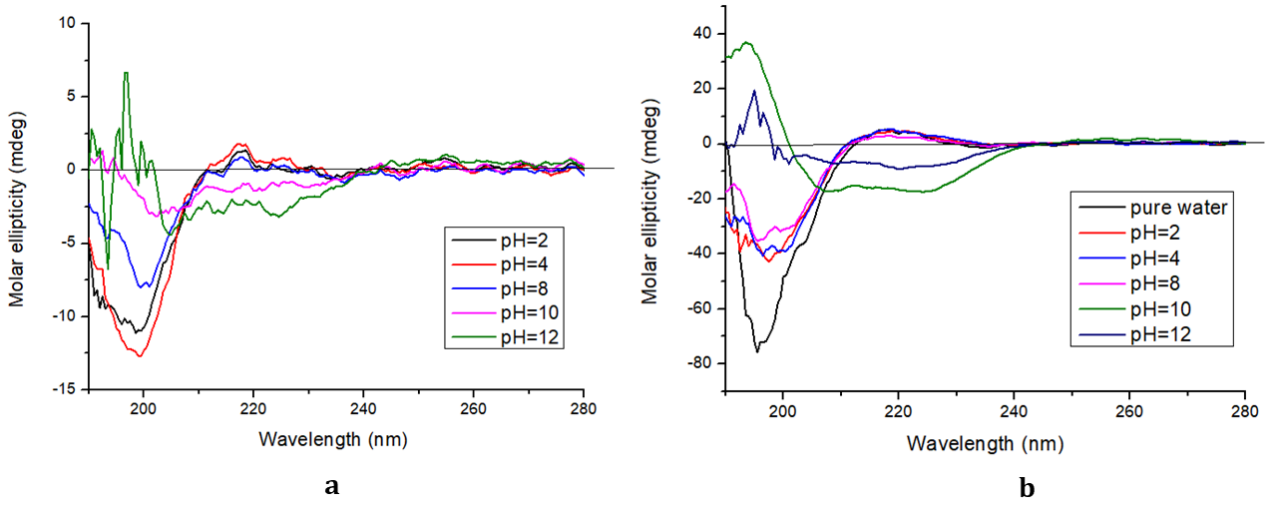

Figure 5.20. CD spectra of (a) PLL-7dp (b) PLL-9dp in various pH in water

As it discussed before, emission measurements revealed fluorescence quenching at basic pH values which was attributed to the conformational changes. By CD measurements, the helical formation was experimentally demonstrated and as assumed before, quenching of fluorescence is observed because of the closer distance of the perylene units to each other (the π-π systems) by folding of the polypeptide. Additionally, due to the more rigid structure and lower solubility of the helical peptide chain, perylene units are not able to be solubilized enough in water, therefore quenching the fluorescence intensity.

5.2.4. Investigation of the Cell Viability and Visualization of the Fluorescent Homopolymers by Confocal Techniques

In order to investigate the applicability of the fluorescent homopolymers in the biological medium, cytotoxicity experiments were proceeded. The cell viability study of the polymers was performed on A549 human lung adenocarcinoma cell line. PLL-7dp was chosen for the cell viability tests in order to better understand the effect of the dye onto toxicity because of the higher mass fraction of the dye in this homopolymer. PLL-7dp with

a degree of polymerization of 20, was incubated into the cell medium in two different concentrations (0.1 and 0.05 mg/mL). Additionally, as a comparison study, PEG/PLL which is PEG-*b*-Poly(L-lysine) copolymer (no dye) and homopolymer of poly(L-lysine) was also tested. Data is expressed as % cell viability (proportion of living cells) and % standard deviation. As Figure 5.21.a demonstrates, fluorescent polymer is quite cytotoxic at the concentration of 0.1 mg/mL, and 55% biocompatible when it is diluted (0.05 mg/mL). Actually, it is the expected result due to the highly positive charge of poly(L-lysine) which causes cytotoxicity. Measurements of PLL which is a homopolymer of poly(L-lysine) without dye is fully cytotoxic at 0.1 mg/mL and only showed 12% cell viability at 0.05 mg/mL. The PEG-*b*-poly(L-lysine) copolymer behaved the same. Thus, we could see that cytotoxicity is not caused by the dye, but is occurring due to the highly charged polymer chain. Even dye incorporation to the PLL has positive impact on biocompatibility of the polymer.

Cell uptake of the PLL-7dp was investigated via CLSM by incubation of the particles in macrophage medium. The polymer showed instantaneous attachment to the cell membrane upon incubation with macrophages (Figure 5.21.b). Most of the fluorescence was detected inside of the cell boundaries within 20 minutes (Figure 5.21.c.d). By these results we decided to go further to fluorescent block copolymer synthesis. By the incorporation of hydrophobic block into the fluorescent polypeptide, we assume that aggregation properties will be improved and cytotoxicity of the polymers will be reduced due to the decreasing molar percentage of the highly charged polylysine overall in the amphiphilic block copolymer.

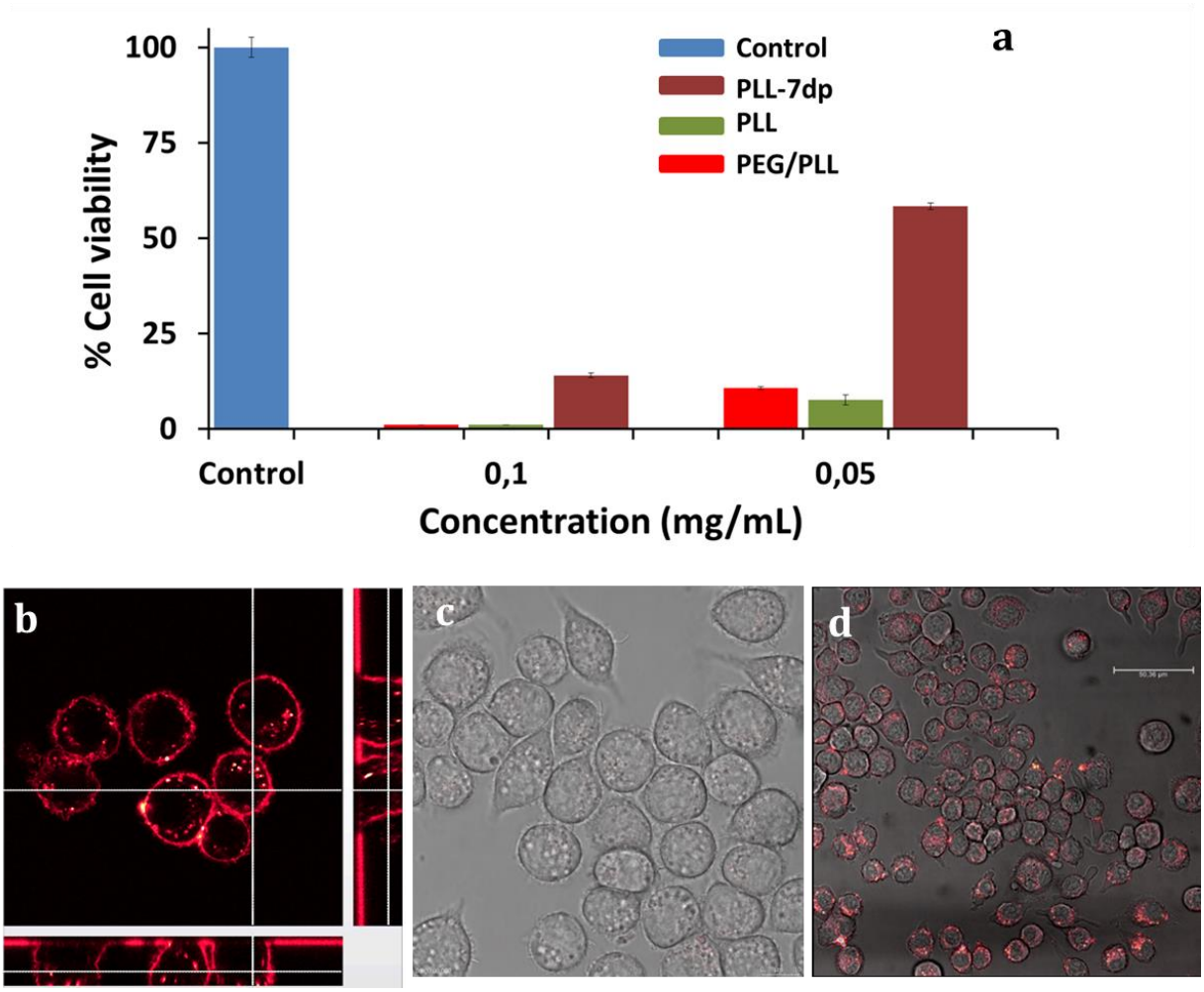

Figure 5.21 (a) Cytotoxicity data of PLL-7dp and reference samples (b) CLSM fluorescence and transmission images of particles upon incubation (c, d) CLSM fluorescence and transmission images of incubated particles after 20 minutes

5.2.5. Synthesis of Fluorescent Amphiphilic Block Copolymers

Polypeptide block copolymers can be designed as stimuli responsive smart biomaterials what makes them potential nanocarrier candidates for drug delivery applications. In this part of the study, we focus on the preparation of fluorescent amphiphilic block polypeptides, their self-assembly in aqueous medium and investigation of the obtained micelles for cell-imaging applications.

Previously synthesized poly(Cbz-L-lysine) is a C-terminal fluorescence modified homopolymer with free N-terminus which can act as a macro-initiator for further ring

opening polymerization of NCAs. From this point of view, two different block copolymers of L-lysine with L-leucine and L-phenyl alanine, respectively, are generated by sequential NCA polymerization *via* PDI-poly(Cbz-L-lysine) as macro-initiator. PDI-poly(Cbz-L-lysine) (DP=20, 40 and 60) was particularly synthesized at 0 ˚C in order to reduce the end group termination which strongly occurs at room or higher temperature during NCA polymerizations as it was explained in Section 1.1.2 and 5.2.2.2.[96,335,336] Obtained homopolymers containing free terminal $-NH_2$ groups initiated the polymerization of L-leucine and L-phenyl alanine as the suggested strategy is depicted in Scheme 5.13.

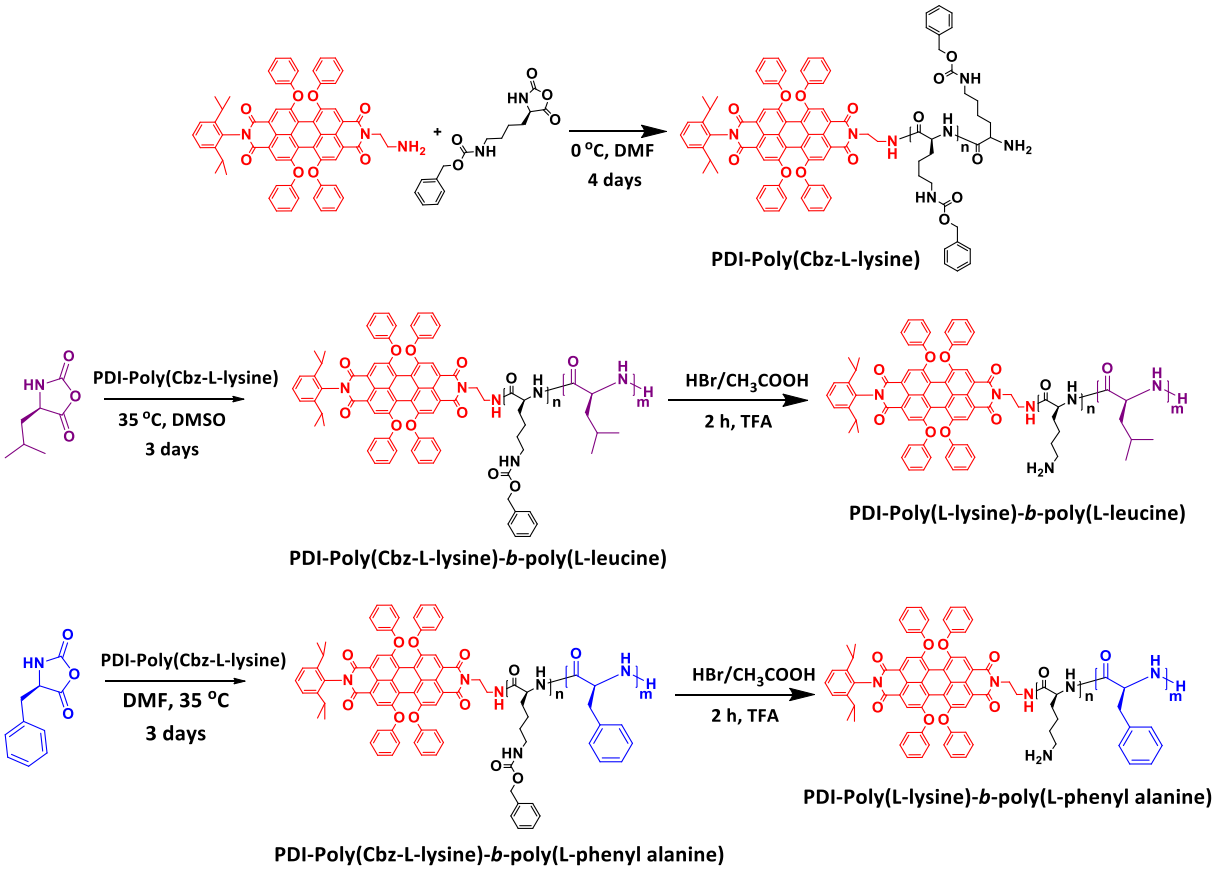

Scheme 5.13. Synthesis of the dye labelled-block copolymers; poly(Cbz-L-lysine)-*block*-poly(L-leucine) and poly(Cbz-L-lysine)-*block*-poly(L-phenyl alanine)

Polymerization of phenylalanine NCA is performed in dry DMF at 35 ˚C for 3 days under slow flow of argon. Gas flow is important to remove the generated CO_2 from the system during the polymerization. Polymerization of L-leucine NCA was first attempted in DMF

as well in the same conditions, but the solution became instantaneously cloudy. While working on the optimization of the proper reaction conditions, dry DMSO was employed and the polymer stayed mostly soluble for 3 days at 35 ˚C.[77] It is well established in literature that polypeptide polymers are typically recovered by precipitation in cold ether, due to the peptides' insolubility.[38] Synthesized different chain length copolymers and characterization details are presented below in Table 5-6.

Table 5-6. Molecular characteristics of fluorescent block copolymers

Polymer		$DP_{(theo)}$ PLL/PX	$DP_{(exp)}$	$M_{n\,(exp)}$ (g/mol)	Đ	Yield %
BC11	PDI-Poly(Cbz-L-lysine)-*b*-poly(L-leucine)	20/40	23/11	7550	1.22	76
BC12		40/40	40/-	-	1.44	75
BC13		60/20	60/15	18400	1.39	68
BC14	PDI-Poly(Cbz-L-lysine)-*b*-poly(L-phenylalanine)	20/40	23/11	7850	1.40	88
BC15		40/40	40/16	14000	1.35	78
BC16		60/20	60/12	18500	1.36	83

*PX: poly(L-leucine) or poly(L-phenylalanine)
*PDI was determined by GPC in DMF at 520 nm, calibration against PS standard
*$DP_{(exp)}$ and $M_{n(exp)}$ were calculated by ^{1}H-NMR

Structural characterization of the block copolymers was performed by ^{1}H-NMR and ^{1}H-DOSY analysis. ^{1}H NMR for Poly(Cbz-L-lysine)-*b*-poly(L-leucine) (**BC11**) and the macro-initiator (PLL-7) is shown in Figure 5.22 with the given peak assignments, which is representative for the polymers synthesized via sequential NCA addition. NH peptide backbone of the copolymer is observed as usual at around of 8.18-7.90 ppm. The corresponding peaks of PDI-poly(Cbz-L-lysine) block are; Cbz-Ar at 7.25-7.03 ppm, CH_2 of Cbz group at 4.93 ppm is, α-CH of PLL at 3.80 ppm, ε-CH_2 of PLL at 2.92, CH_2 of PLL at 1.94-1.23 ppm, PDI-isopropyl groups at 0.99 ppm. The peaks assigned to the poly(L-leucine) block are; α-CH at 4.18 ppm, and the peak at 0.86 ppm corresponds to isopropyl groups. An attempt to determine the actual polymer composition was made by the integration ratio below:

$$I_{\beta\text{-CH2 of PLL-7 (2.92 ppm)}} / I_{\alpha\text{-CH backbone of polyleucine (4.18 ppm)}}$$

But the integrations of the macroinitiator to hydrophobic peptide are not congruent as given in Table 5-6. First reason is the broader peaks of the blocks which does not allow to calculate the block ratio accurately. Second, this can be caused by the aggregation of helix forming peptides altering the peak integrations.

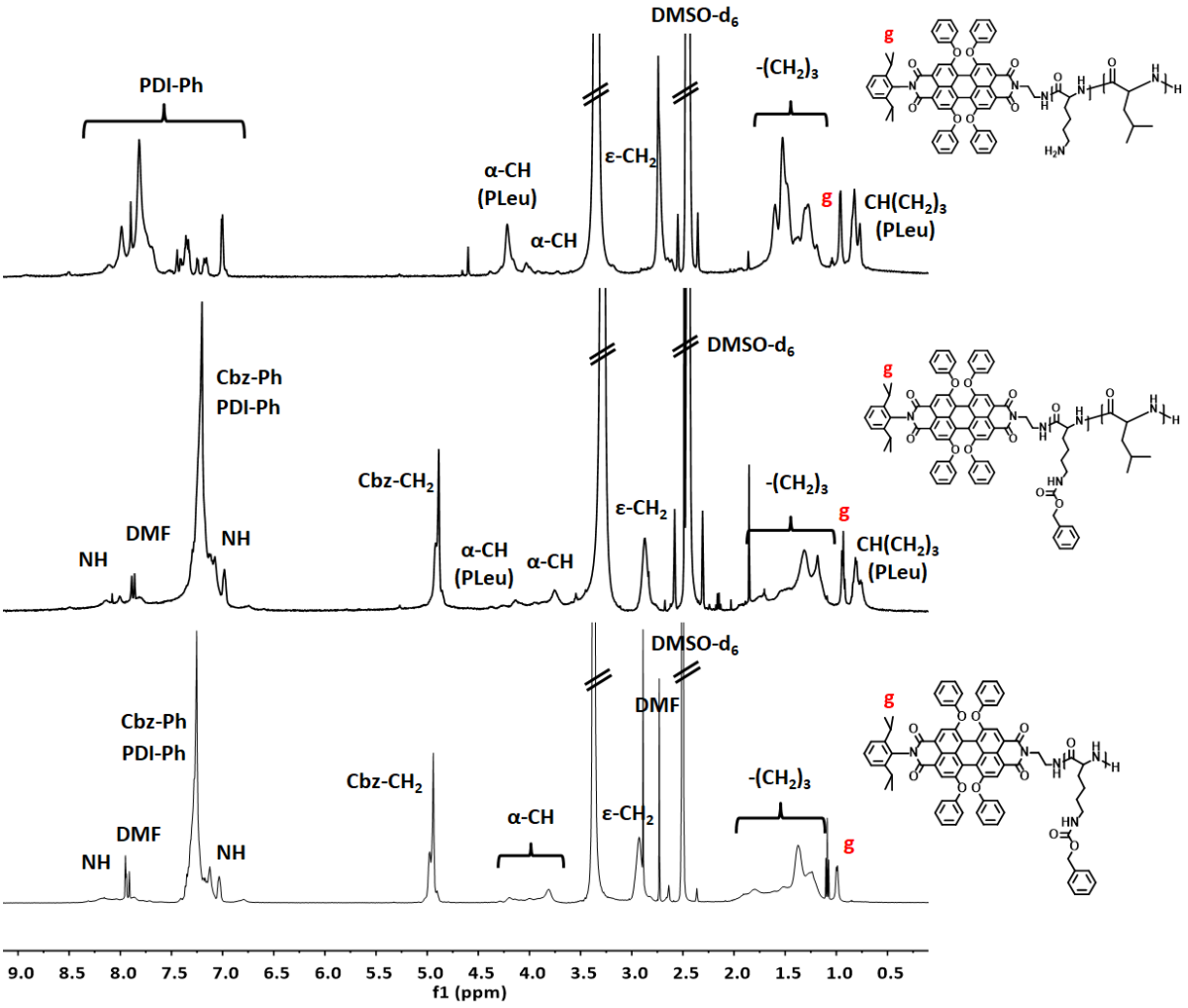

Figure 5.22. ^{1}H-NMR spectra of PDI-Poly(Cbz-L-lysine), BC11/PDI-Poly(Cbz-L-lysine)-*b*-poly(L-leucine) and BC11dp/PDI-Poly(L-lysine)-*b*-poly(L-leucine) (700 MHz, DMSO-d_6, 298 K)

In order to have evidence for the covalent attachment of the two different polymer blocks, ^{1}H-DOSY was measured which combines diffusion coefficients with proton signals. As the measurement reveals, all the species have the same diffusion coefficient, confirming the block copolymer formation Figure 5.23.

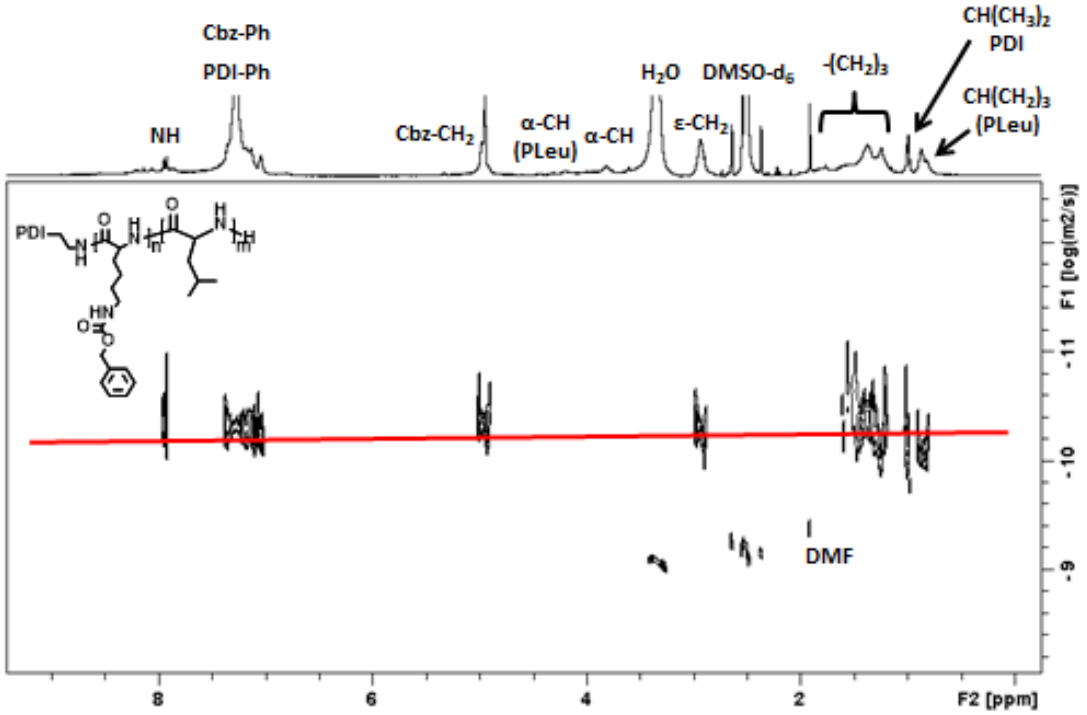

Figure 5.23. ^{1}H-DOSY spectrum of BC11/PDI-Poly(Cbz-L-lysine)-*b*-poly(L-leucine) (700 MHz, DMSO-d_6, 298 K)

Structural characterization of the Poly(Cbz-L-lysine)-*b*-poly(L-phenylalanine) (BC14) copolymer was made by ^{1}H-DOSY and ^{1}H-NMR as well which is presented in Figure 5.25 and Figure 5.24. The corresponding peaks of all the defined species were determined and block copolymer formation was confirmed by ^{1}H-DOSY analysis by observing the same diffusion coefficient for corresponding signals of the polyphenylalanine block (α-CH at 4.5 ppm) and the rest of the polymer. Block ratios were determined by the integration ratio of the peak of CH_2 of PLL-7 at 2.8 ppm and CH peak of poly(L-phenylalanine) at 4.5 ppm as given in Table 5-6.

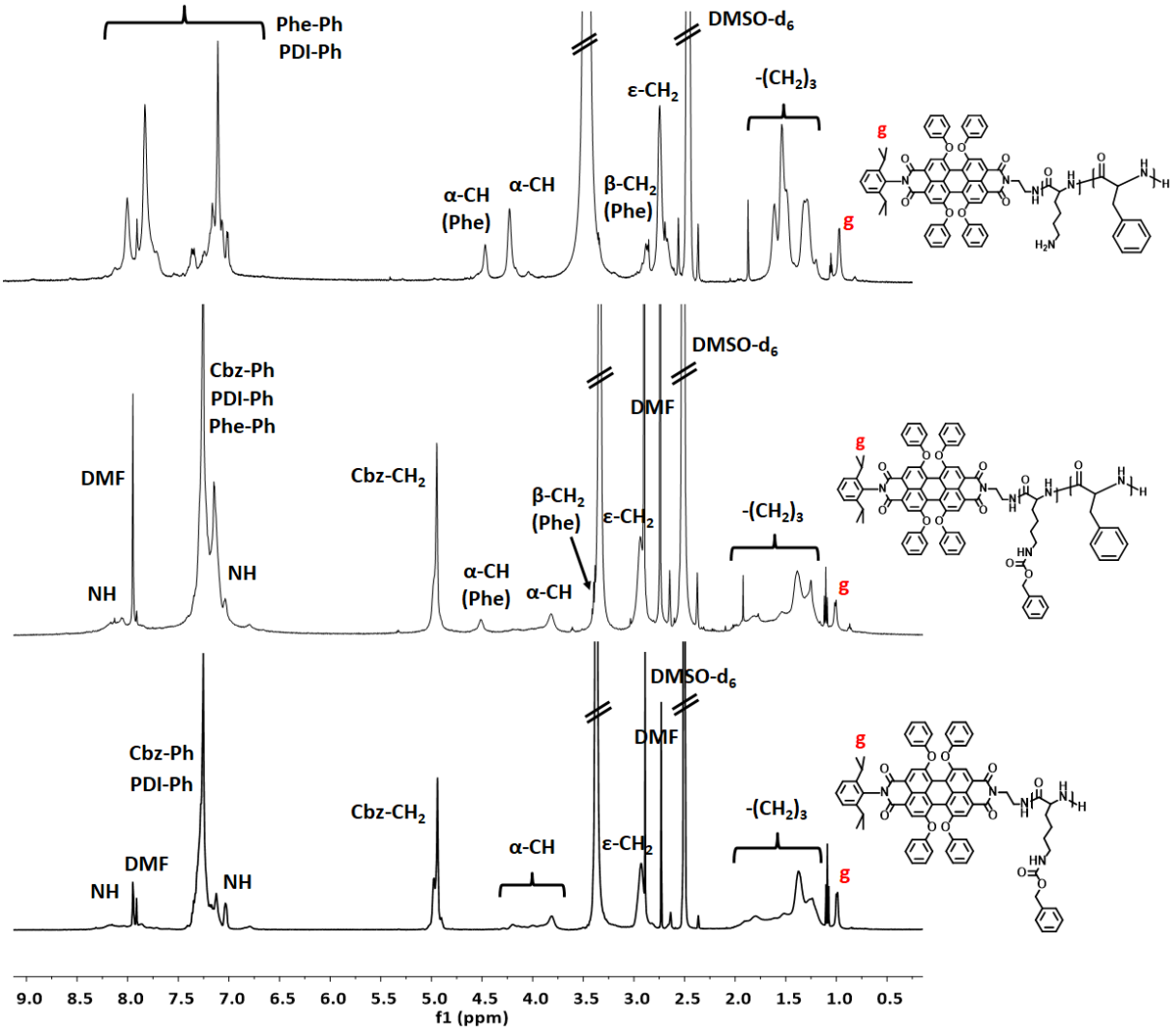

Figure 5.24. ^{1}H-NMR spectra of PLL-7/PDI-Poly(Cbz-L-lysine), BC14/ PDI-Poly(Cbz-L-lysine)-*b*-poly(L-phenylalanine) and BC14dp/PDI-Poly(L-lysine)-*b*-poly(L-phenylalanine) (700 MHz, DMSO-d_6, 298 K)

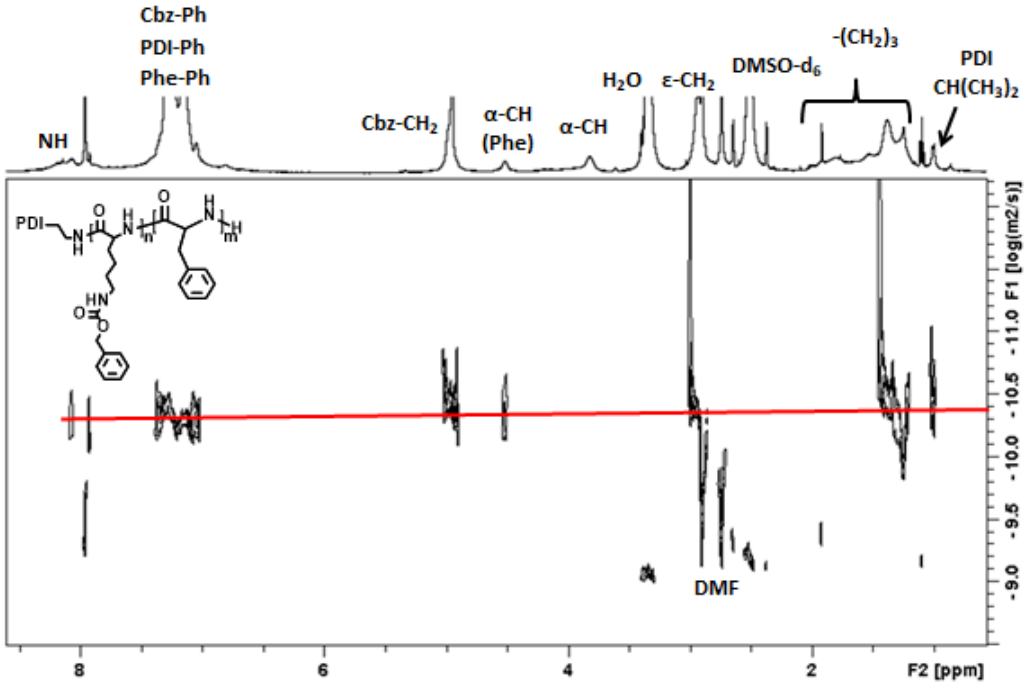

Figure 5.25. ^{1}H-DOSY spectra of BC14/PDI-Poly(Cbz-L-lysine)-*b*-poly(L-phenylalanine) (700 MHz, DMSO-d_6, 298 K)

Average molecular weights and molecular weight distributions of the block copolymers were attempted to be analyzed by GPC and exhibit narrow polydispersity (<1.49) (Table 5-6). While the determination, an interesting peak at very low retention times was observed for both PDI-poly(Cbz-L-lysine)-*b*-poly(L-leucine)(BC11 and BC12) and PDI-poly(Cbz-L-lysine)-*b*-poly(L-phenyl alanine) (BC14 and BC15) copolymers that correspond to M_n values greater than $2*10^5$ g/mole and $6*10^5$ g/mole, respectively (Figure 5.26). These peaks could only be explained as a consequence of the aggregation (self-assembly) of the block copolymers.[211]. During the GPC analysis of the BC15 and BC16 copolymers which have the longest hydrophilic polylysine chains, we did not face with this aggregation issue. Therefore, we determined the number average molecular weights by the end group analysis *via* ^{1}H-NMR even though that might be affected by the aggregation phenomena as well, presented in Table 5-6. Degrees of polymerization of hydrophobic blocks were lower than theoretical values for all the polymerizations.

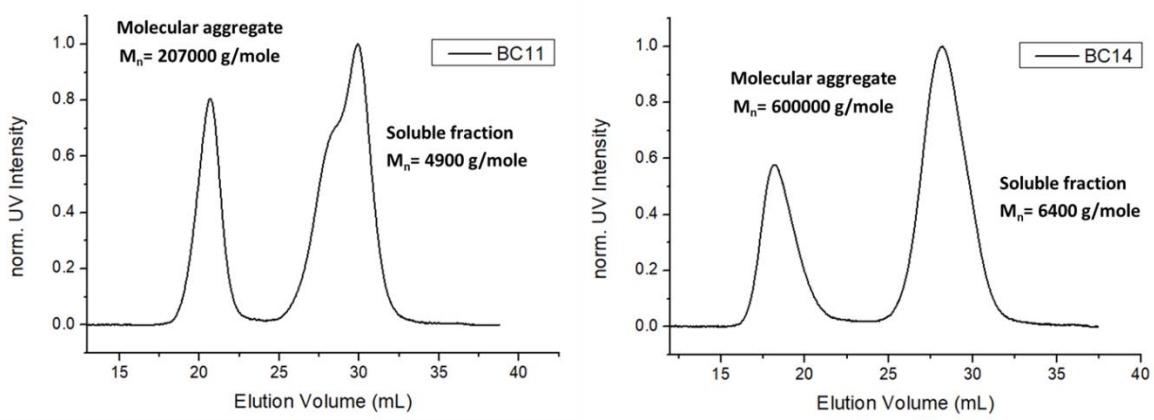

Figure 5.26. Aggregation phenomena encountered during GPC measurements

Thermal stability of the fluorescent polymers was evaluated by thermogravimetric analysis (TGA) by heating to 600 ˚C with a heating rate of 10 ˚C/min under inert atmosphere. Glass transition (T_g) and melting temperatures (T_m) were determined by differential scanning calorimetry (DSC), as second heating DSC curves were presented in Figure 5.27.b. Here below, TGA and DSC curves of PLL-7 macro-initiator together with BC11 and BC14 block copolymers are presented (Figure 5.27.a.b.). Decomposition of all the peptide backbone polymers starts at around of 250 ˚C. Homopolymer PLL-7 shows one step thermal degradation as expected. T_g of the polymer is observed at around of 44 ˚C. No melting peak was determined. For the block copolymers, one step thermal degradation was observed, because of the same chemical structure of the corresponding blocks.

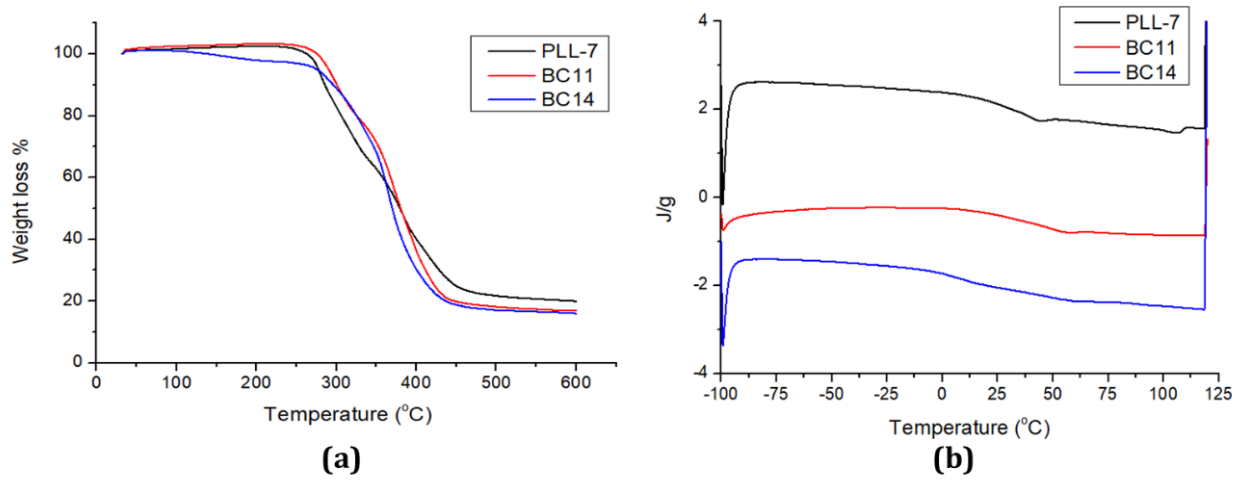

Figure 5.27. (a) TGA and (b) DSC curves of the fluorescent polymers

The Cbz groups of the Polylysine in all block copolymers were deprotected in order to obtain amphiphilic block copolymers for further self-assembly studies as presented in Scheme 5.13. Cbz protecting groups of the lysine were cleaved at strong acidic conditions by HBr/CH_3COOH in TFA at RT within two hours and purified by precipitation in cold diethyl ether followed by intense dialysis against water for 2 days. Obtained polymers are stored as freeze dried. By the deprotection reactions, free amine containing block copolymers were obtained.

Complete removal of the Cbz groups of the poly(Cbz-L-lysine)-*b*-poly(L-phenylalanine) copolymers (BC14, BC15 and BC16) was confirmed by ^{1}H-NMR by disappearance of the phenyl peaks at 7.49 – 6.99 ppm (m, 5H-Ar), and CH_2 peaks at 5.08 – 4.86 ppm (m, 2H, Cbz-CH_2), demonstrated in Figure 5.24. Aromatic peaks of phenylalanine can be clearly observed after the cleavage. Deprotection reaction for Poly(Cbz-L-lysine)-*b*-poly(L-leucine) copolymers (BC11, BC12 and BC13) are shown in general Scheme 5.13. Complete cleavage was confirmed by ^{1}H-NMR by disappearance of the phenyl peaks at 7.6 – 6.95 ppm (m, 5H-Ar), and CH_2 peaks at 5.08 – 4.86 ppm (m, 2H, Cbz-CH_2), demonstrated in Figure 5.22. By the removal of Cbz, aromatic PDI peaks arose clearly in the region of 7.5-7.0 ppm.

Consequently, ^{1}H-NMR, ^{1}H-DOSY and GPC measurements overall reveal that PDI-poly(Cbz-L-lysine) macro-initiator was able to generate fluorescent block copolymers with L-leucine and L-phenyl alanine. Chain lengths of the second hydrophobic blocks are lower than the theoretically adjusted values for all the polymerizations. This is the general encountered problem especially for the L-leucine monomer which does not tend to polymerize as lysine or glutamic acid. At the end, several different chain length block copolymers are obtained and their deprotection reaction leads to the formation of amphiphilic fluorescent block copolymers.

5.2.6. Self-assembly of the Amphiphilic Block Copolymers

Synthetic polypeptide block copolymers with amphiphilic character can adopt certain ordered conformations depending on the amino acid side chain. They can self-assemble into precisely defined bio-mimic structures through molecular interactions.[121,337] Herein, the polymers in Table 5-7 are used for further studies.

Table 5-7. Samples used for self-assembly and bio-imaging applications

Polymer		$DP_{(theo)}$	$DP_{(exp)}$	Đ
BC11dp	PDI-Poly(L-lysine)-*b*-poly(L-leucine)	20/40	23/11	1.22
BC14dp	PDI-Poly(L-lysine)-*b*-poly(L-phenylalanine)	20/40	23/11	1.40

Both amphiphilic fluorescent block copolymers; poly(L-lysine)-*b*-poly(L-phenylalanine) and poly(L-lysine)-*b*-poly(L-leucine), have a tendency to aggregate in aqueous systems as demonstrated by NMR analysis.

Normally, poly(L-lysine)-*b*-poly(L-phenylalanine) is very good soluble in DMSO. Thereof in the ^{1}H-NMR spectra of **BC14dp** in DMSO, all the corresponding peaks of the copolymer are observed (Figure 5.28.b). However, in the spectrum of the polymer in D_20, the peaks which correspond to the hydrophobic moieties, i.e phenyl protons of phenylalanine and perylene aromatic protons at around of 6.5 to 8 ppm, are not observed as shown in Figure 5.28.c. By the comparison of ^{1}H-DOSY spectrums of those two samples (Figure 5.28.a, BC14dp in DMSO-d6-black one and BC14dp in D_2O-red one), aggregation in water can be clearly observed as diffusion signals of the hydrophobic regions in the polymer disappeared. The same behavior is observed for poly(L-lysine)-*b*-poly(L-leucine) (**BC11dp**) block copolymer as well, as ^{1}H-NMR spectrums in DMSO-d6 and D_2O are shown in Figure 5.29.a and b.

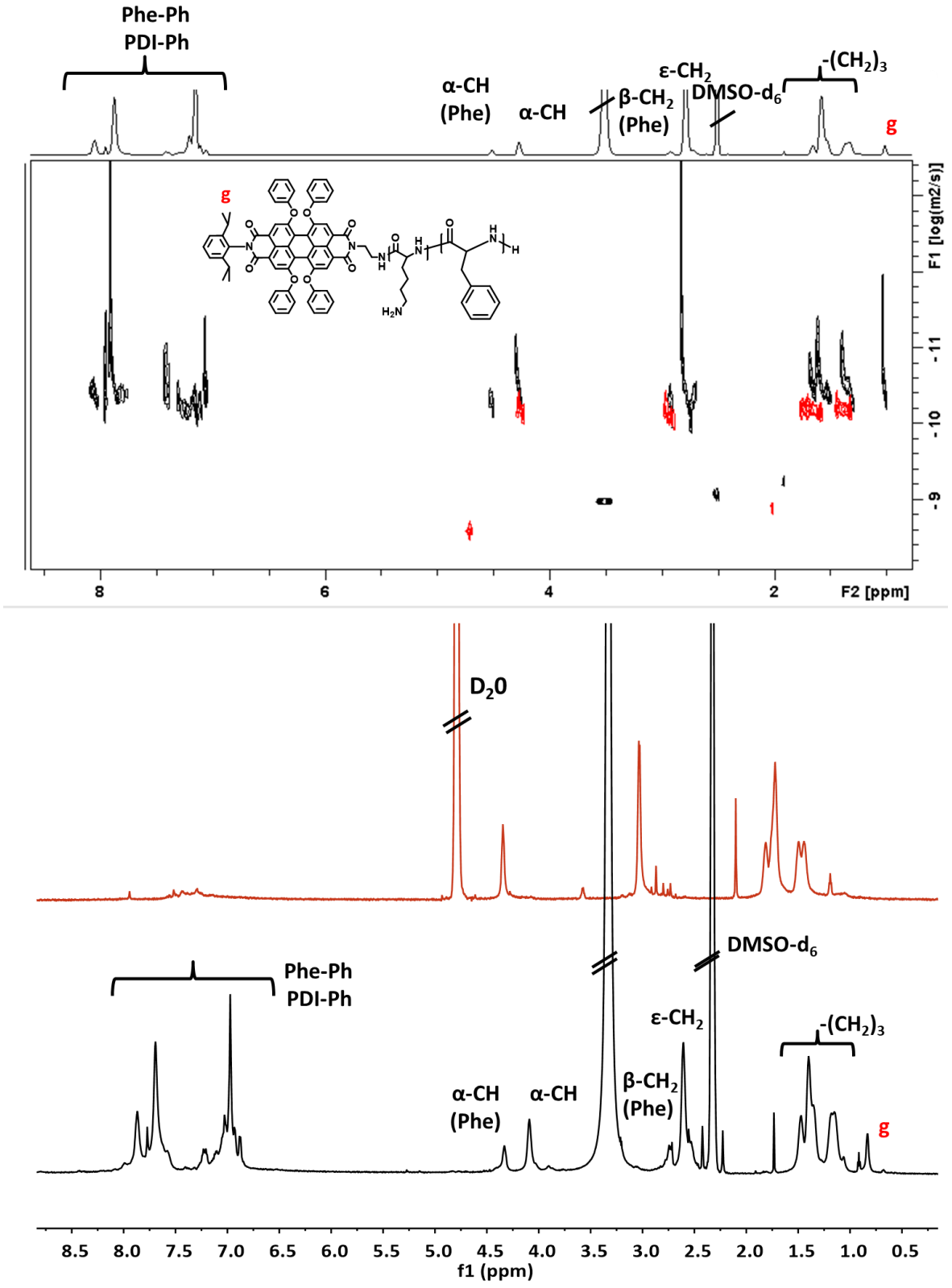

Figure 5.28. (a) Superposition of ^{1}H-DOSY spectrums of BC14dp in DMSO-d6 (black one) and BC14dp in D_2O (red one) (b) ^{1}H-NMR spectrum of BC14dp in DMSO-d6 (c) ^{1}H-NMR spectrum of BC14dp in D_20 (700 MHz, 298 K)

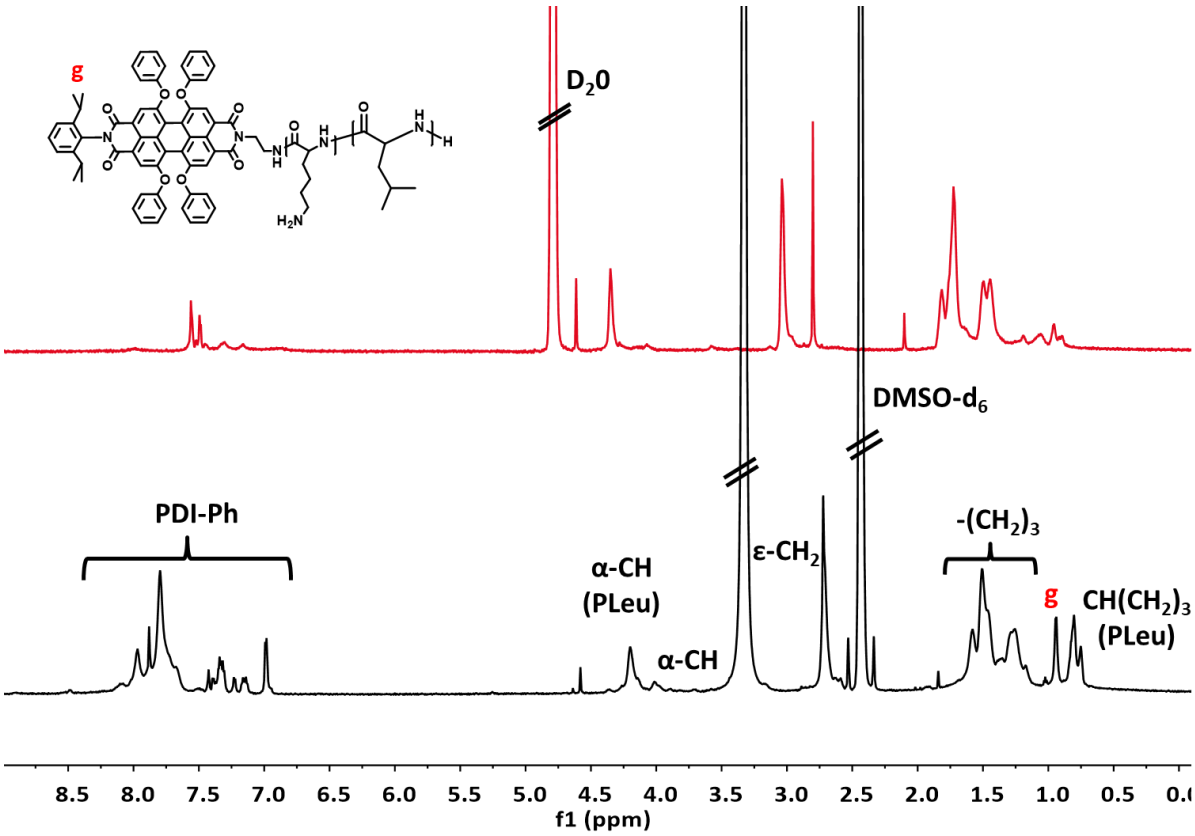

Figure 5.29. ^{1}H-NMR of BC11dp in DMSO-d6 (black one) and in D_20 (red) (700 MHz, 298 K)

Morphology of the particles can vary depending on the preparation method. We observed the aggregate formation as discussed above during the NMR investigation where the samples were prepared by direct dissolution in solvents. Herein additionally, thin film formation method is also applied for the sample preparation to control if better ordered and stable structures can be formed.

In the direct dissolution method, block copolymers were dissolved directly in water with a concentration of 1 mg/mL, sonicated for 2 hours, filtered through a 0.8 µm syringe filter and left to stir at RT for 1 week. In contrast to that, to prepare the samples by thin film formation, block copolymers were dissolved in DMSO and the solvent was removed under vacuum to form a thin film layer of the polymer at the bottom of the flask. Then the polymers were hydrated with water (final concentration is adjusted to 1 mg/mL) and left to stir at RT for 1 week.

Block copolymer solutions prepared by two different methods were analyzed by TEM in order to investigate the morphology of the aggregates. Sample analysis was performed for different time intervals to control over the stability. Additionally, the block copolymers in water were analyzed by Circular Dichroism Spectroscopy (CD) to control the conformation of the polypeptide in water which is important to understand the morphology. According to the CD curves, both copolymers were detected in a helical shape where two peak maxima at 210 and 222 nm for BC11dp, and 218 and 222 nm for BC14dp were observed (Figure 5.30).

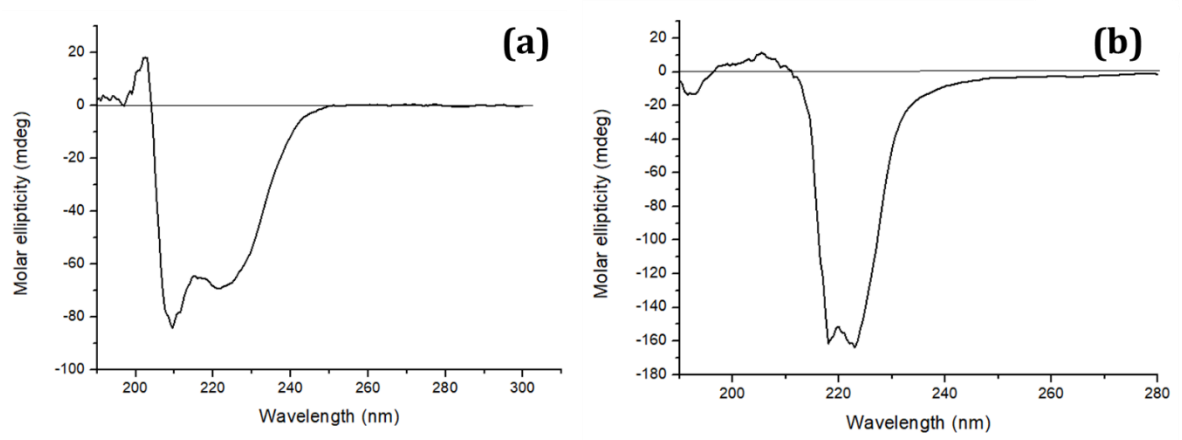

Figure 5.30. CD spectra of (a) BC11dp and (b) BC14dp in water

TEM investigation of the **BC11dp** (poly(L-lysine)-*b*-poly(L-leucine)) in water prepared by direct dissolution (DD) and thin film formation (TFF) method is shown in Figure 5.31. By the self-assembly of the rigid helical amphiphilic block copolymers, fibrillated wormlike micelles are formed. As the aggregation phenomenon was already seen by NMR, block copolymers are expected to assemble like the segregated hydrophobic poly(L-leucine) core which is surrounded by the hydrophilic poly(L-lysine) chains. Another important influence on the morphology is the hydrophobic perylene units that are connected to the α-end of the poly(L-lysine) chain. As already indicated by NMR, hydrophobic dye signals disappeared in D_20 (Figure 5.29). This hydrophobic nature of the dye can orient the polymer chains to wormlike structures rather than spherical ones. Micelles prepared by the direct dissolution method are clearly less ordered than the samples prepared by thin film formation (Figure 5.31). Micelles are better organized and distributed in solution by

time as seen from the micrographs after 4 weeks (Figure 5.31.e.f). As overall conclusion from the images, thin film formation seems to be the more suitable method for the preparation of well organized (poly(L-lysine)-*b*-poly(L-leucine)) block copolymer micelles in water. Fibrillated wormlike nano-structures were formed by the self-assembly of the block copolymer in water which have various lengths between 50-100 nm long.

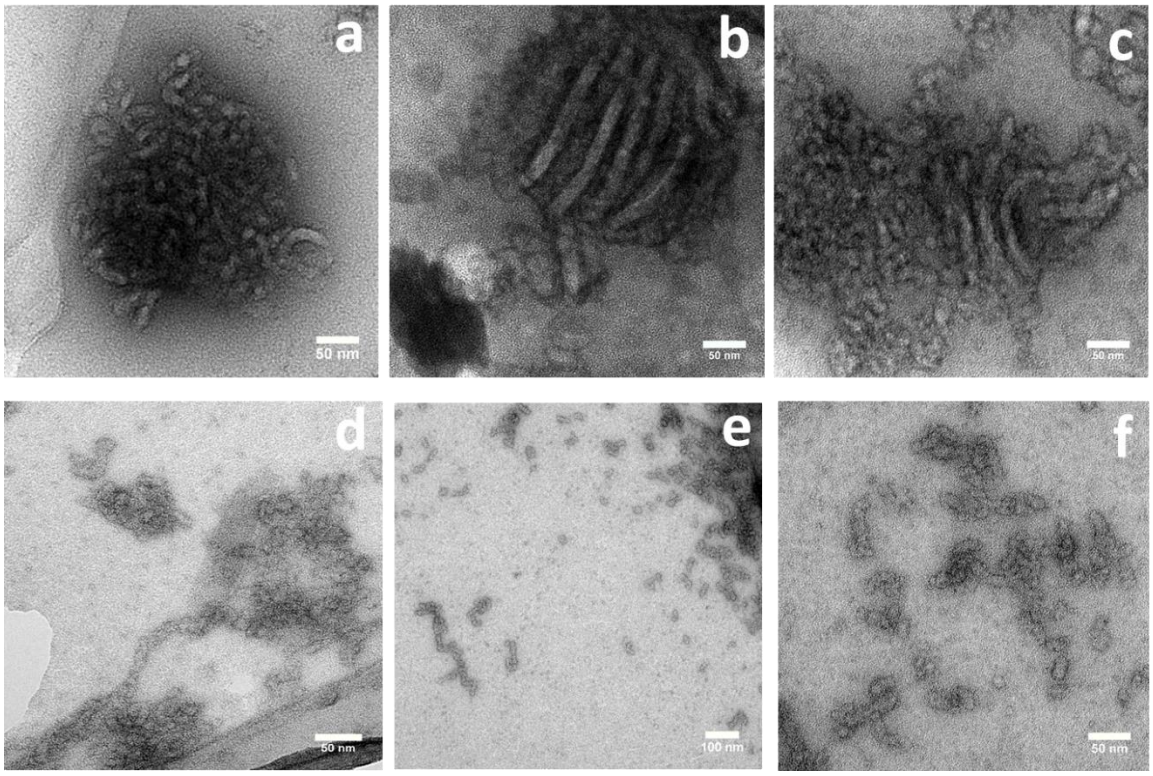

Figure 5.31. TEM images of BC11dp (poly(L-lysine)-*b*-poly(L-leucine)) in water (a) right after the sample preparation by DD (b, c) 2 weeks after the sample preparation by DD (d) 1 week after the sample preparation by TFF (e, f) 4 weeks after the sample preparation by TFF

TEM investigation of the **BC14dp** (poly(L-lysine)-*b*-poly(L-phenylalanine)) in water prepared by direct dissolution (DD) and thin film formation (TFF) method is shown in Figure 5.32. By the self-assembly of the helical polypeptide, fibrillated wormlike micelles were formed with various lengths between 50-100 nm long. We expect a similar aggregation behavior as BC11dp, except the effect of π-π stacking interactions due to the phenyl alanine in the core of the micelles. As seen from the micrographs below, better organized fibrillated worms are clearly observed due to the π-π stacking of phenyl groups and hydrophobic interactions with aromatic dye, especially when the micelles are

prepared by the thin film formation method (Figure 5.32). These micelles were already well-ordered after 2 weeks and still stable for 4 weeks.

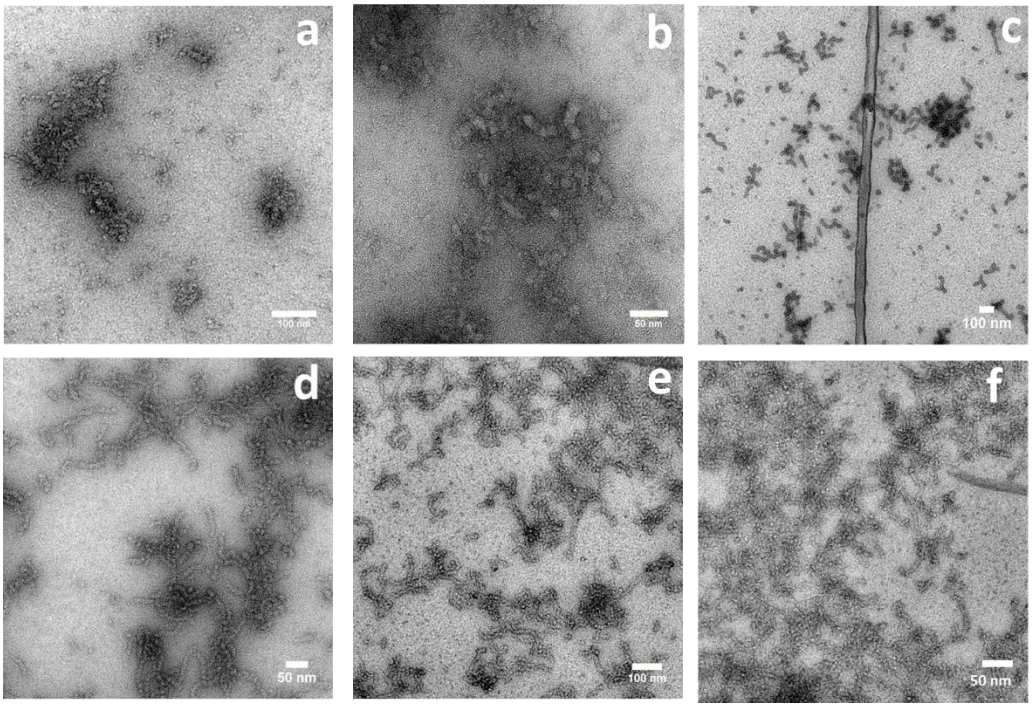

Figure 5.32. TEM images of BC14dp in water (a) right after the sample preparation by DD (b) 2 weeks after the sample preparation by DD (c, d) 1 week after the sample preparation by TFF (e, f) 4 weeks after the preparation by TFF

Due to the fluorescence of the perylene dye at the same wavelength as the light scattering by zetasizer, reliable DLS measurements could not be achieved. Therefore, as a representative example, FCS has been employed for BC14dp ((poly(L-lysine)-*b*-poly(L-phenylalanine)) to investigate the particle size of fluorescent macromolecular aggregates. According to the FCS measurements in extremely diluted water environment, a particle size of 44 nm was observed for 85% of the particles in total volume. The size of the small portion of the particles (15% of the total volume) was detected as 2.7 nm which is possibly the unreacted free PDI-poly(L-lysine) homopolymer impurity of the system. By that method, we could characterize the particle size in a reliable way and also determined the unreacted free macro-initiator in the system, which was not able to be detected before.

5.2.7. Investigation of the Cell Viability and Visualization of the Particles by Confocal Techniques

In this part of study, the potential of the fluorescent micelles for bio-imaging applications was evaluated by the Confocal Laser Scanning Microscopy technique (CLSM).

Covalently dye modified PDI-poly(L-lysine)-*b*-poly(L-leucine) **(BC11dp)** and PDI-poly(L-lysine)-*b*-poly(L-phenyl alanine) **(BC14dp)** polymeric micelles with different concentrations (0.2, 0.1 and 0.05 mg/mL) were incubated for 24 hours in A549 human lung adenocarcinoma cell line for the cell viability investigation. Data is expressed as % cell viability (proportion of living cells) and % standard deviation (Figure 5.33). As explained in Section 5.2.4 before, PLL-7dp (PDI-poly(L-lysine)) homopolymer was very toxic even at low concentrations. When this polymer was modified with the hydrophobic and uncharged poly(L-leucine) block (**BC11dp)**, no toxicity was observed in the cell medium at 0.05 mg/mL concentration. In comparison to that, block copolymer with poly(L-phenyl alanine) **(BC14dp)** is more toxic at high concentrations but the cell viability is observed as 85% at 0.05 mg/mL concentration.

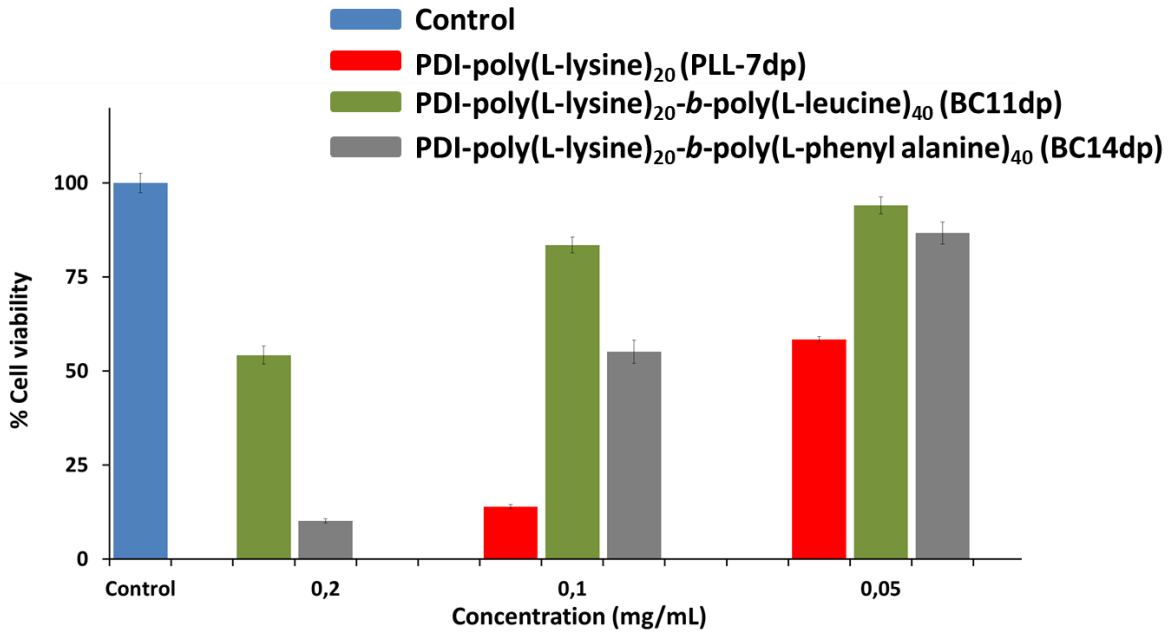

Figure 5.33. Cell viability study of the block copolymers

In conclusion, PDI-poly(L-lysine)-*b*-poly(L-leucine) (BC11dp) was more biocompatible than PDI-poly(L-lysine)-*b*-poly(L-phenyl alanine) (BC14dp) micelles as intrinsic toxicity of the phenyl alanine is higher.[338] However, in general, insertion of the hydrophobic block into fluorescence poly(L-lysine) lower the toxicity of the overall material as expected and aimed from the beginning of the research.

Fibrillated wormlike micelles of BC14dp were visualized by TEM analysis as discussed in previous section. Here below in Figure 5.34, a correlation study of TEM and CLSM was performed and studies demonstrated that the aggregates observed in TEM (picture **b**) are indeed the fluorescent particles as they show strong fluorescence in CLSM (picture **a,c**).

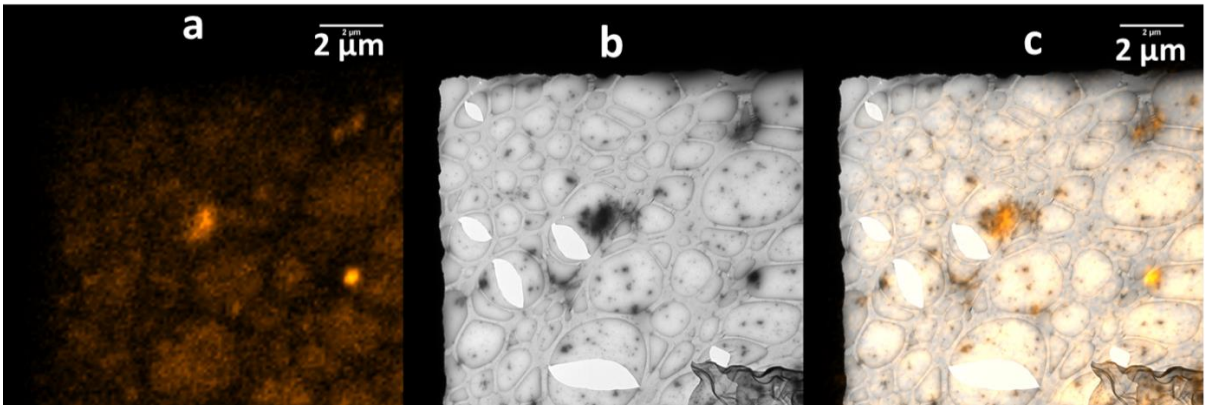

Figure 5.34. (a) CLSM (b) TEM and (c) overlay of TEM and CLSM images of BC14dp

Fluorescent micelles of BC14dp were then incubated with the macrophage cell medium and instantaneous attachment of the micelles to the cell membrane is observed in the first 20 minutes. The fluorescence and transmission image of the particles in cell medium shows the membrane attachment and uptake of the particles (Figure 5.35.a.b). The cells incubated with fluorescent particles were fixated by Johanna Simon after 24 hours and, confocal images were recorded again. As demonstrated in Figure 5.35.c, micelles were fully internalized into the cell as the polymer which adsorbed to the outer membrane of the cell is no longer visible.

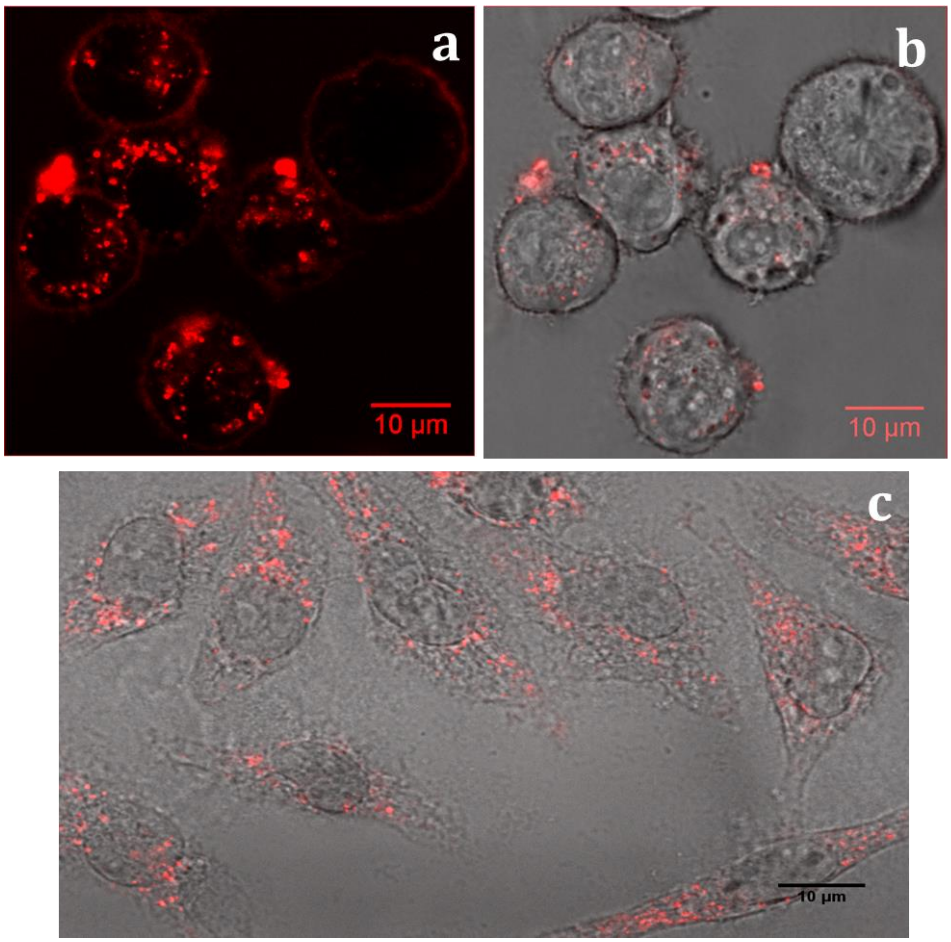

Figure 5.35. Cell uptake of BC14dp micelles by macrophages (a) CLSM image (b) Overlay of fluorescence and transmission image (c) CLSM image of fixed cells after staining and EPON embedding

Another technique used to visualize the micelles in cell medium was correlation of light and electron microscopy. Fixated cell medium incubated with fluorescent nanoparticles were analyzed by correlation of confocal (overlay of fluorescence and transmission channel) with SEM images by using two different detectors is shown below in Figure 5.36. As images reveal, successful uptake and visualization of the fluorescent polypeptide micelles was achieved.

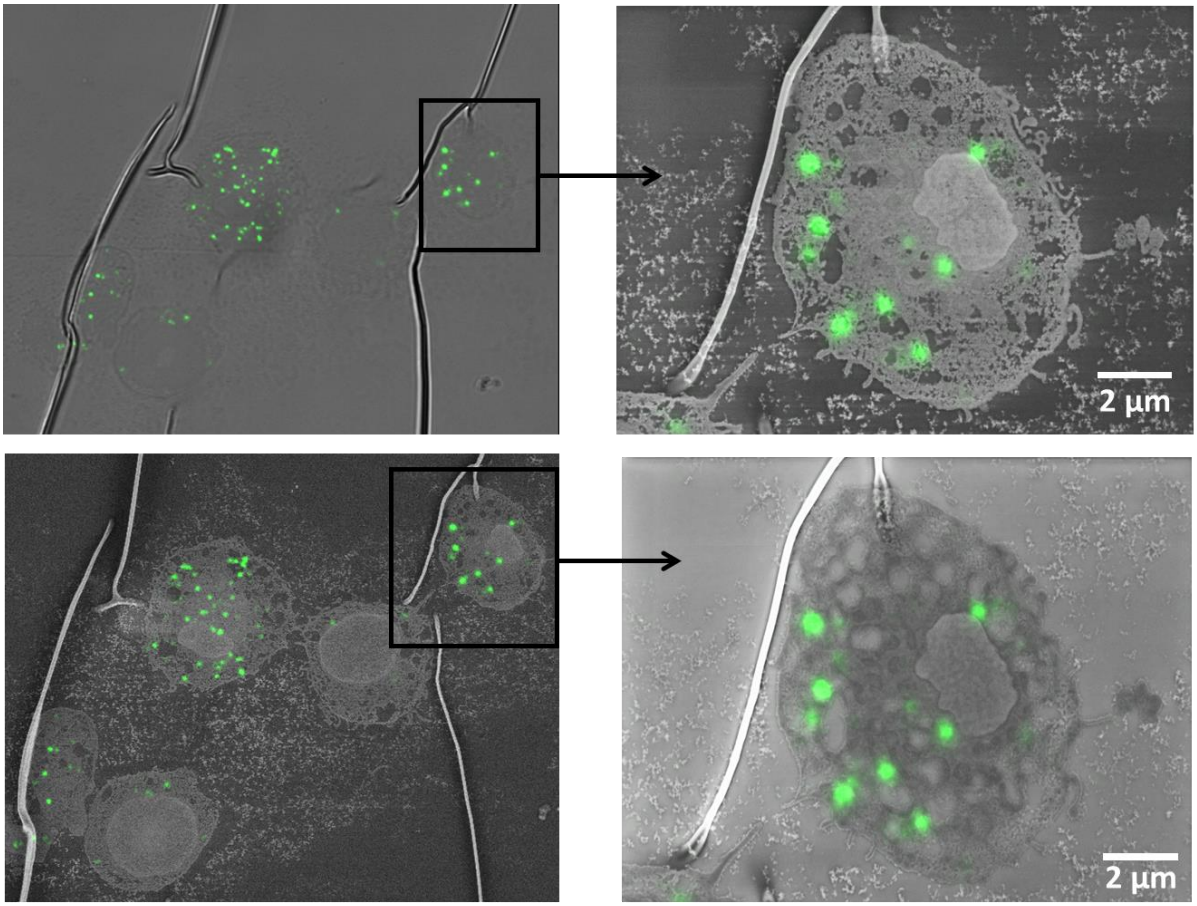

Figure 5.36. Correlation of confocal (overlay of fluo. and transmission channel) with SEM

To summarize overall the bioimaging studies of the fluorescent polypeptide micelles, first of all, fibrillated wormlike micelles were detected by TEM and were identified as fluorescent polymer aggregates by the correlation with CLSM. Homopolymer PLL-7dp and block copolymer BC14dp were successfully uptaken by the macrophages and, by the correlation of the confocal technique to SEM, successful visualization of the micelles was achieved. However, no assignment to dedicated organelles was found.

5.3. Conclusion and Outlook

The development of covalently fluorescence-labeled, pH sensitive polypeptides in the scope of biomedical applications is the key point of this study. These functions are very important for designing the drug delivery vehicle suitable for nanoparticle tracking and bioimaging *in vivo*. Therefore, this study aimed to develop fluorescence and multifunctional polymeric micelles possessing pH sensitivity as well as many reactive groups to be used as smart nanomaterials. In this manner, the main features of the developed polymeric micelles are;

- C-terminal fluorescence-labeled biocompatible polypeptides,
- Native functions of the polypeptides are preserved and suitable for introducing multiple targeting ligands through covalent and non-covalent conjugations,
- Conformation, size and optoelectronic properties of the particle is pH-dependent,
- Uniformed nanoparticles with strictly defined localization and a precise number of fluorescent molecules,
- No dye leakage out of the particle.

Each of these findings were shown at different stages of the whole research period. These are fulfilling the sub-objectives of the thesis to reach the overall goal. In this context, the starting point of this work was the synthesis of C-terminal fluorescence-labeled homo- and block polypeptides via sequential NCA polymerization with a controlled manner.

C- or N-terminus dye modification of the polymers was attempted by two approaches i.e post-polymerization modification and direct initiation by designed initiators. By post-polymerization modification method, Cbz-L-lysine-NCA was first polymerized by bifunctional amines such as N-Boc-ethylenediamine in order to have double functionality at the both ends of the polymer chain (PLL-5, PLL-6). These type of polymers in general can act as a pH sensitive linker and can be applied in various systems for example; combination with dyes acts as a pH sensor for monitoring the pH fluctuations in living systems or co-operation with FRET couples, energy transfer mechanisms can be studied etc. Further, N-terminal amine groups of the polymer were modified by –COOH functional fluorescent perylene derivative *via* amidation reaction. Nevertheless, modification yield was around 20% and purification was challenging due to the uncontrolled NCA

polymerization which mostly results in end blocked polymer chains. Therefore, second approach "direct initiation by designed initiators" was employed. Within this strategy; a tetraphenoxy perylenediimide modified in peri-position with ethylene diamine "N-(2,6-diisopropylphenyl)-N'-(4-aminoethyl)-1,6,7,12-tetra-phenoxyperylene-3,4,9,10 tetracarboxydiimide" (**PDI-NH_2**, Compound 4.9) was synthesized and used as an initiator for the ROP of Cbz-L-lysine-NCA. Three different chain lengths of PDI-poly(Cbz-L-lysine)s: **PLL-7** (DP=20), **PLL-8** (DP=40), **PLL-9** (DP=60) were prepared at 0 °C in order to avoid chain termination reactions. Thus, C-terminal PDI modified poly(Cbz-L-lysine)s were successfully obtained with a narrow molecular weight distribution (1.27-1.31) in one pot with good yields (65-98%) and high purity as ^{1}H-NMR spectra indicated. Deprotection of the Cbz groups led to the formation of a hydrophilic homopolymer with hydrophobic bulky perylene units at C-terminal, thereof, investigation of the supramolecular assembly was very interesting for understanding the conformational dynamics of the system. Water solubilized fluorescent PDI can be utilized as pH sensor in order to monitor the physiological changes of biological systems, therefore, its pH responsive behavior was investigated. DLS measurements revealed that the hydrodynamic radius was increasing from 41 nm (PLL-7dp) to 97 nm (PLL-9dp) by increased chain length of the poly(L-lysine)s. pH-stimuli behavior of the polymers was examined by means of optoelectronic properties of the perylene *via* UV-vis, Fluorescence spectroscopy and by the correlation of Circular Dichroism (CD) spectroscopy. Conformational changes of the polypeptide from random coil to α-helix in different pH environments, affect the optoelectronic behavior of the material. Poly(L-lysine) exist as random coil state in low pH, whereas folding to α-helix in basic environment (Figure 5.19). The similar behavior was observed for different molecular weight polymers. The highest fluorescence intensity was determined around the pKa value of pol(L-lysine) which is around pH 8. By acidic treatment, fluorescence intensity decreased due to the molecular aggregation, whereas fluorescence quenched at pH around 10 due to the helical folding of the polypeptide.

In order to check the potential utilization of the materials for pharmaceutical applications biocompatibility was also investigated (Figure 5.21). Cell viability of the A549 human lung adenocarcinoma cells against fluorescent polymers was around 50% (for 0.05 mg/mL concentration) which is still better than homopolymer of poly(L-lysine) itself which has only 10% viability. That's mean PDI-NH_2 itself is reducing the toxicity of the materials

because of the reduced mass fraction of the high cationically charged poly(L-lysine) segment. The cell uptake study of the fluorescent homopolymers was performed by macrophage incubation and successful visualization of the particles in biological medium by CLSM was achieved (Figure 5.21).

In the second part of this study, block copolymer synthesis and micellar self-assembly of the fluorescent polypeptides were investigated. Two main objectives were targeted for this extended study:

- Improving the aggregation properties of the polypeptides to obtain stable nanoparticles applicable for drug delivery and bio-imaging applications,
- Decreasing the toxicity of the material to be applied safely to the biological systems.

While revising the existing system accordingly to the aforementioned purposes; requirements were fulfilled for the novel smart nanoparticulate drug delivery systems which are:

- Biocompatibility,
- Ability to self-assemble into nanoobjects around or below 100 nm for cell uptake,
- Fluorescence for the detection,
- Functionality on the surface of particles for further post-modification with bio-active molecules for targeted delivery,
- Surface charge for better interaction with the cell membrane.

For the achievement of these goals, hydrophobic polypeptides were subsequently incorporated to the fluorescent PDI-poly(Cbz-L-lysine) homopolymers. The synthesis of two different block copolymers: PDI-poly(L-lysine)-*b*-poly(L-leucine) and PDI-poly(L-lysine)-*b*-poly(L-phenylalanine) were successfully carried out *via* sequential NCA polymerization of L-leucine NCA and L-phenylalanine NCA, respectively, followed by deprotection of Cbz groups (BC11dp to BC16dp). The success of all polymerization and deprotection steps was monitored by NMR spectroscopy. Moreover, covalent attachment of two different peptide blocks was demonstrated by DOSY-NMR which combines diffusion coefficients of the species with proton signals. As the measurement reveals, all the species have same diffusion coefficient, means confirming the block copolymer

formation. Additionally, relatively narrow molecular weight distributions around 1.22-1.40 were determined by GPC.

Aggregation tendency of the amphiphilic polypeptides was first determined basically by ^{1}H-NMR and ^{1}H-DOSY spectra in water. Normally observed peaks of the hydrophobic moieties such as phenyl groups of poly(L-phenylalanine) or isopropyl groups of poly(L-leucine) in ^{1}H-NMR or ^{1}H-DOSY in DMSO, could not be determined in the measured spectra in water due to the segregation and burning out of the hydrophobic groups into the core of the micelles. Hydrophobic PDI peaks were also disappeared in the NMR spectra of block copolymers in water.

Another important outcome from this further extend process was that the fibrillated wormlike micelles were fabricated which is a great drug delivery candidate due to the lower toxicity *in vitro*. Block copolymer micelles of BC11dp/PDI-Poly(L-lysine)-*b*-poly(L-leucine) (DP: 23/11) and BC14dp/ PDI-Poly(L-lysine)-*b*-poly(L-phenylalanine) (DP: 23/11) were prepared by two different methods i.e direct dissolution method and thin-film formation method for further self-assembly study. Both block copolymers were assembled to fibrillated wormlike micelles in aqueous medium as demonstrated by TEM measurements in various lengths between 50-100 nm long. Block copolymers were assembled like segregated poly(L-leucine) or poly(L-phenylalanine) in inner core and surrounded by the water-soluble poly(L-lysine) forming the outer shell. As seen from the micrographs, better organized fibrillated worms were observed for BC14dp/ PDI-Poly(L-lysine)-*b*-poly(L-phenylalanine) due to the π-π stacking of phenyl groups and hydrophobic interactions with aromatic PDI. Hydrophobic PDI units that are connected to the α-end of the poly(L-lysine) chain also segregated into the inner core as demonstrated already by NMR spectroscopy. This double segregation of C-terminal PDI and N-terminal hydrophobic blocks of poly(L-lysine) can orient the polymer chains to wormlike micelles in water. In both cases, micelles prepared by thin-film formation was better organized and stable for long term (min. 4 weeks). Polymeric micelles preserved their shape and stability throughout the whole steps as confirmed by TEM visualization. The cell uptake studies confirmed that the particles are eager to be uptaken into the cells and can be visualized by CLSM techniques.

Biocompatibility of the wormlike fibrillated nanocontainers of both BC11dp/PDI-Poly(L-lysine)-*b*-poly(L-leucine) and BC14dp/ PDI-Poly(L-lysine)-*b*-poly(L-phenylalanine) copolymers were tested in A549 human lung adenocarcinoma cell line. As previously revealed PLL-7dp/PDI-poly(L-lysine) homopolymer was quite toxic even at low concentrations (0.05 mg/mL). In the same concentration of BC11dp/poly(L-leucine), no cytotoxicity was observed. In comparison to that, cell viability of the BC14dp/poly(L-phenylalanine) copolymer was measured as 85% in the identical conditions.

In the final part of this work, the potential of the fluorescent micelles for bio-imaging applications was evaluated by the Confocal Laser Scanning Microscopy technique (CLSM). As a representative example, fluorescent BC14dp/PDI-poly(L-lysine)-*b*-poly(L-phenylalanine) copolymer micelles were incubated in macrophage medium and visualization and cell uptake process was monitored by CLSM. After 24 h incubation time, successful internalization of the particles into cell boundaries were visualized by the correlation of SEM or TEM with CLSM, however, no specific organelle attachment was observed. This was a complementary study to understand the applicability of the of the established aggregates from the perspective of drug delivery applications is indeed necessary for the applicability in biomedical science.

Based on the achieved goals, this work is demonstrating the potential of these fluorescence, multifunctional and stimuli-responsive nanoobjects and can be extended on further directions as smart systems for many biological applications. In fact, incorporation of various functional materials such as biologically active small molecules like vitamins; curcumin, selegilin, carbohydrates like galactose, laktose; peptides or proteins like CPPs or a special enzyme cleavable peptide sequences for example MMP type, enzymes, antibodies, aptamers etc. into the certain number of native amine functions of the polypeptide can widen the design and application area to targeted drug delivery field. Covalent modification either before self-assembly or further post-surface functionalization can be performed at the corona according to the needs. These modifications is not limited and will enhance the affinity and selectivity of the polymeric aggregates and provides potential for the wide range of pharmaceutical applications.

Another potential is the utilization of C- and N-terminus double functional, pH shrinkable polypeptides as linker in between different systems. By pH stimuli the distance between

separated moieties changes, for example FRET systems can be studied by that design i.e one side PDI modified polymer would be modified further by TDI from the N-terminal or gold or iron nanoparticles can be incorporated in fluorescent systems.

5.4. Experimental Part

5.4.1. Materials and Methods

Materials were purchased from Sigma Aldrich if not otherwise stated. H-Lys(Fmoc)-OH (Compound **4.1**) and N,N'-bis(2,6-diisopropylphenyl)-1,6,7,12-tetraphenoxyperylene-3,4:9,10-tetracarboxy diimide (Compound **4.6**) were purchased from Bachem and BASF, respectively. All solvents were purchased from Sigma Aldrich if not stated otherwise. Toluene and THF were purified by distillation from sodium with benzophenone. Other solvents were of analytic grade and used as received. Polymerizations were performed by glovebox and schlenk techniques under inert atmosphere. 0 ˚C polymerizations were performed, additionally, using Cryostat cooling system under schlenk line.

5.4.2. Synthesis

N-ε-fluorenylmethoxycarbonyl-L-lysine-N-carboxyanhydride (Fmoc-Lysine-NCA) (4.1)

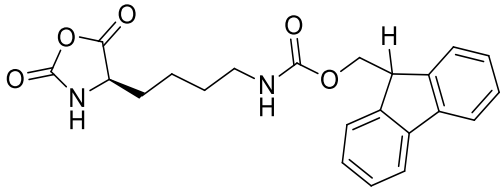

Fmoc-Lysine NCA was synthesized as described in the literature.[38] N-ε-fluorenylmethoxycarbonyl-L-lysine (5.00 g, 13.60 mmol, 1.00 eq) was suspended in 60 mL of dry ethyl acetate and α-pinene (4.98 mL, 31.40 mmol, 2.31 eq) was added. The reaction mixture was refluxed at 95 ˚C. Triphosgene (2.72 g, 9.17 mmol, 0.67 eq) was dissolved in 20 ml of ethyl acetate and added slowly once the reflux started. After 2 h of reflux, reaction became 80% clear and to complete the reaction 0.8 g of triphosgene (2.69 mmol, 0.20 eq) in ethyl acetate was added slowly. After 1 hour, the solution became fully clear, shows the reaction is completed. The reaction mixture was cooled down to room temperature and filtered. Monomer was purified by repeated crystallization from ethyl

acetate/n-hexane to get a pure white solid product, dried under vacuum and stored under inert gas in glovebox (4.28 g, 0.01 mol, 80% yield).

^{1}H-NMR (δ (ppm) 300 MHz, CD_2Cl_2): δ 7.78 (d, J = 7.8 Hz, 2H), 7.60 (s, 2H), 7.41 (s, 2H), 7.33 (s, 2H), 6.34 (s, 1H), 4.91 (s, 1H), 4.44 (d, J = 8.8 Hz, 2H), 4.30 (s, 1H), 4.23 (d, J = 7.6 Hz, 1H), 3.16 (t, J = 6.7 Hz, 2H), 1.97 (s, 1H), 1.82 (s, 1H), 1.43 (d, J = 56.7 Hz, 4H) ppm.

^{13}C-NMR (δ (ppm) 75 MHz, CD_2Cl_2): 169.9, 153.8, 152.5, 143.8, 141.3, 127.7, 127.1, 125.0, 120.0, 66.7, 57.4, 47.2, 40.0, 30.8, 21.3 ppm.

ε-Carboxybenzyl-L-Lysine-N-carboxyanhydride (Cbz-Lysine-NCA) (4.2)

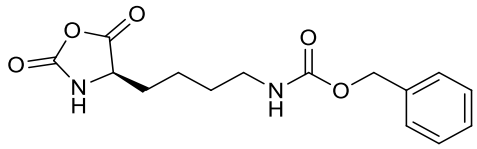

Cbz-Lysine NCA was synthesized as described in the literature.[311] H-Lys(CBz)-OH (5.00 g, 18.00 mmol, 1.00 eq) was suspended in dry ethyl acetate (60 mL) and α-pinene (6.5 mL, 41.00 mmol, 2.28 eq) was added under argon atmosphere. The reaction mixture was refluxed at 90 ˚C and triphosgene (7.90 g, 26.00 mmol, 1.44 eq) in 20 mL of ethyl acetate was added slowly. After 2-3 hours, the homogenous reaction mixture was cooled to room temperature, bubbled with argon to remove unreacted phosgene and HCl, and concentrated in vacuo. The monomer was three times crystallized from ethyl acetate/n-hexane to get pure white product (5.02 g, 16.00 mmol, 94% yield).

^{1}H-NMR (δ (ppm) 300 MHz, CD_2Cl_2): δ 7.36 (d, J = 3.5 Hz, 5H), 6.39 (s, 1H), 5.09 (d, J = 2.1 Hz, 2H), 4.94 (s, 1H), 4.30 (dd, J = 7.2, 4.8 Hz, 1H), 3.29 – 3.08 (m, 2H), 1.98 (ddt, J = 15.0, 9.9, 4.9 Hz, 1H), 1.83 (d, J = 10.4 Hz, 1H), 1.56 (dd, J = 10.7, 4.3 Hz, 4H) ppm.

^{13}C-NMR (δ (ppm) 75 MHz, CD_2Cl_2): 171.5, 156.0, 151.8, 137.1, 128.2, 127.6, 65.0, 56.9, 30.6, 28.7, 21.5 ppm.

L-Leucine-N-carboxyanhydride (Leucine NCA) (4.3)

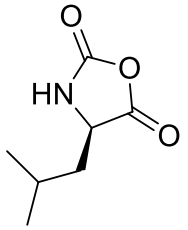

L-leucine NCA was synthesized as described in the literature.[42] L-leucine (6.00 g, 45.70 mmol, 1.00 eq) was suspended in dry THF (60 mL) and α-pinene (8 mL, 50.50 mmol, 1.11 eq) was added under argon atmosphere. The reaction mixture was refluxed at 70 °C and triphosgene (5.46 g, 18.40 mmol, 0.40 eq) in 25 mL of THF was added slowly. After 3 hours, the homogenous reaction mixture was cooled down to room temperature, bubbled with argon to remove unreacted phosgene and HCl, and concentrated in vacuo. The monomer was several times filtered through silica plug and at least five times precipitated from ethyl acetate/n-hexane to get pure white product (5.00 g, 31.81 mmol, 70% yield).

^{1}H-NMR (δ (ppm) 300 MHz, CD_2Cl_2): δ 6.78 – 6.38 (m, 1H), 4.35 (dd, J = 8.9, 4.2 Hz, 1H), 1.94 – 1.61 (m, 3H), 0.98 (t, J = 6.0 Hz, 6H) ppm.

^{13}C-NMR (δ (ppm) 75 MHz, CD_2Cl_2): δ 170.73, 152.85, 56.74, 41.33, 25.62, 22.99, 21.86 ppm.

L-Phenylalanine-N-carboxyanhydride (4.4)

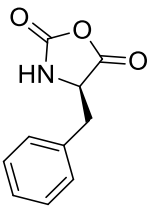

L-Phenylalanine NCA was synthesized as described in the literature.[339] L-Phenylalanine (8.00 g, 48.43 mmol, 1.00 eq) was suspended in dry THF (80 mL) and α-pinene (8 mL, 50.50 mmol, 1.04 eq) was added under argon atmosphere. The reaction mixture was refluxed at 80 °C and triphosgene (5.75 g, 19.37 mmol, 0.40 eq) in 25 mL of THF was added

slowly. After 5 hours, reaction mixture became clear and cooled down to room temperature, bubbled with argon to remove unreacted phosgene and HCl, and concentrated in vacuo. The monomer was several times filtered through silica plug and at least five times precipitated from ethyl acetate/n-hexane to get pure white product (6.00 g, 31.38 mmol, 64% yield).

^{1}H-NMR (δ (ppm) 300 MHz, CD_2Cl_2): δ 7.54 – 7.14 (m, 5H), 5.92 (s, 1H), 4.57 (dd, J = 8.3, 4.3 Hz, 1H), 3.27 (dd, J = 14.1, 4.3 Hz, 1H), 3.01 (dd, J = 14.1, 8.2 Hz, 1H) ppm.

^{13}C-NMR (δ (ppm) 75 MHz, CD_2Cl_2): δ 169.43, 151.94, 134.77, 129.79, 129.66, 128.40, 59.37, 38.31 ppm.

N-(2,6-diisopropylphenyl)-N'-(3-carboxyethyl)-1,6,7,12-tetra(4- sulfo phenoxy)-perylene-3,4:9,10-tetracarboxydiimide (SO_3H-PDI-COOH) (4.5)

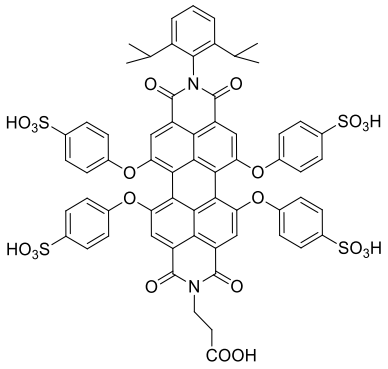

This compound was kindly synthesized by Sebastian Stappert as described in the literature.[300]

^{1}H NMR (300 MHz, DMSO-d6): δ 7.92 (s, 2H), 7.89 (d, J = 4.1 Hz, 2H), 7.63 (dd, J = 14.9, 8.3 Hz, 8H), 7.39 (d, J = 7.6 Hz, 1H), 7.27 (d, J = 7.7 Hz, 2H), 6.97 (t, J = 8.5 Hz, 8H), 4.14 (d, J = 24.2 Hz, 2H), 2.71 (dd, J = 9.0, 6.3 Hz, 2H), 1.25 (d, J = 7.7 Hz, 2H), 0.99 (d, J = 6.9 Hz, 12H) ppm.

^{13}C-NMR (300 MHz, DMSO-d6): δ 172.25, 162.51, 162.14, 155.26, 155.07, 154.78, 145.43, 144.86, 132.33, 132.03, 130.45, 127.72, 127.69, 123.59, 122.48, 119.87, 119.08, 118.99, 118.88, 31.99, 28.19, 23.64 ppm.

UV-Vis (H_2O): λ_{max} (ε) = 450 (11 454), 534 (22 510), 564 (25 059) nm

Fluorescence (H_2O, excitation 566 nm): λ_{max} = 622 nm

N-(2,6-diisopropylphenyl)-1,6,7,12-tetraphenoxyperylene-3,4:9,10-tetra carboxy-9,10- monoanhydride-3,4-monoimide (4.7)

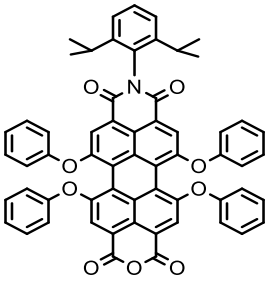

Compound **4.7** was synthesized as described in the literature.[316] N,N'-bis(2,6-diisopropylphenyl)-1,6,7,12-tetraphenoxyperylene-3,4:9,10-tetracarboxy diimide (Compound **4.6**) (2.46 g, 2.28 mmol, 1.00 eq) was dissolved in 250 mL of 2-propanol:tert-butanol (1:1) mixture. KOH (63.94 g, 1.14 mmol, 0.50 eq) was dissolved in 75 mL water and added to the dye solution. The reaction mixture was refluxed under argon atmosphere at 110 ˚C by following with TLC in DCM for 40 minutes. After cooling to room temperature, the solution was poured into water (0.5 L) and HCl (conc. 37%) added until color changed from green to red-brownish precipitate while cooling down in ice-bath. Precipitate was filtered and dried under vacuum at 60 ˚C. The solid was dissolved in glacial acetic acid (200 mL) and refluxed at 80 ˚C for 30 minutes and precipitated with water. Filtrate dried under vacuum and purified by column chromatography using DCM as eluent (0.48 g, 0.52 mmol, 23% yield, red solid).

^{1}H-NMR (δ (ppm) 300 MHz, CD_2Cl_2): δ 8.17 (s, 2H), 8.15 (s, 2H), 7.47 (d, J = 7.8 Hz, 1H), 7.38 – 7.25 (m, 10H), 7.24 – 7.10 (m, 4H), 7.06 – 6.94 (m, 8H), 2.79 – 2.57 (m, 2H), 1.07 (d, J = 6.8 Hz, 12H) ppm.

^{13}C-NMR (δ (ppm) 75 MHz, CD_2Cl_2): δ 163.73, 160.37, 156.91, 156.36, 155.78, 146.52, 130.69, 130.61, 125.47, 125.36, 124.58, 123.88, 122.68, 122.15, 120.75, 120.58, 120.52, 118.97, 29.61, 24.24 ppm.

UV-Vis (CH_2Cl_2): λ max (ε) = 443 (19500), 537 (30926), 575 (49363) nm
Fluorescence (CH_2Cl_2, excitation 536 nm): λ max = 610 nm

N-(2,6-diisopropylphenyl)-N'-(N-boc-4-aminoethyl)-1,6,7,12-tetraphenoxy perylene-3,4:9,10 tetracarboxydiimide (4.8)

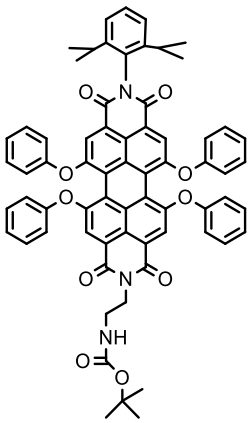

Compound **4.8** was synthesized with a slightly different procedure then as described in the literature.[300] Compound **4.7** (0.80 g, 0.87 mmol, 1.00 eq) and N-boc-ethylenediamine (167.2 mg, 1.04 mmol, 1.20 eq) were dissolved in toluene (60 mL). The reaction mixture was stirred under argon at 60 °C for 4.5 h. Following the reduction of the solvent, the material was purified over silica gel using DCM: acetone (100:1) as eluent, resulting in 0.85 g as a red solid (0.80 mmol, 75% yield).

^{1}H-NMR (δ (ppm) 300 MHz, CD_2Cl_2): δ 8.16 (s, 2H), 8.15 (s, 2H), 7.49 – 7.41 (m, 1H), 7.37 – 7.24 (m, 10H), 7.20 – 7.09 (m, 4H), 7.0-6.98 (ddt, J = 8.4, 2.7, 1.3 Hz, 8H), 4.24 (t, J = 5.7

Hz, 2H), 4.09-4.07 (m, 1H), 3.42-3.40 (q, J = 5.8 Hz, 2H), 2.70 – 2.68 (m, 2H), 1.26 (s, 9H), 1.09-1.07 (d, J = 6.8 Hz, 12H) ppm.

^{13}C-NMR (δ (ppm) 75 MHz, CD_2Cl_2): 180.07, 166.93, 164.00, 163.83, 156.44, 156.30, 156.09, 155.99, 146.55, 140.10, 131.62, 130.54, 125.14, 125.11, 124.55, 123.30, 121.47, 120.79, 120.72, 120.58, 120.48, 120.46, 118.75, 116.29, 40.75, 39.86, 29.60, 28.50, 26.76, 26.70, 24.23 ppm.

UV-Vis (CH_2Cl_2): λ max (ε) = 444 (14300), 535 (26320), 575 (41919) nm
Fluorescence (CH_2Cl_2, excitation 536 nm): λ max = 608 nm

N-(2,6-diisopropylphenyl)-N'-(4-aminoethyl)-1,6,7,12-tetra phenoxyperylene-3,4:9,10 tetracarboxydiimide (PDI-NH_2) (4.9)

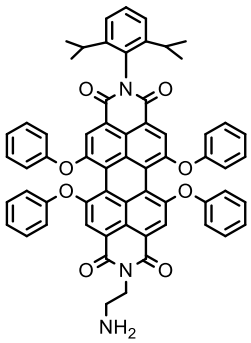

0.40 g (0.38 mmol, 1.00 eq) compound **4.8** was put into a 100 mL schlenk flask and dissolved in 5 mL DCM. Solution was cooled down to 0 ˚C in ice bath. 5 mL of TFA (65.34 mmol) was added slowly with a syringe and stirred 1 hour at 0 ˚C and another 30 min at RT. The solution was concentrated in vacuo to dryness. The remaining residue is dissolved in dioxane with addition of 25 % aqueous ammonia solution and again concentrated in vacuo to half of the volume. By further addition of aqueous ammonia solution, the product is precipitated and filtered through a glass filter. The precipitate was washed with water until the filtrate is neutral. The precipitated red solid was dried under vacuum (0.33 g, 0.34 mmol, 90% yield).

^{1}H-NMR (δ (ppm) 300 MHz, CD_2Cl_2): δ 8.15 (s, 2H), 8.13 (s, 2H), 7.46 (t, J = 7.8 Hz, 1H), 7.36 – 7.24 (m, 10H), 7.11 (dt, J = 18.6, 7.4 Hz, 4H), 6.97 (t, J = 7.2 Hz, 8H), 4.30 – 4.12 (m, 2H), 3.03 (s, 2H), 2.73 – 2.63 (m, 2H), 1.08 (d, J = 6.8 Hz, 12H) ppm.

^{13}C-NMR (δ (ppm) 75 MHz, CD_2Cl_2): δ 163.95, 163.82, 156.47, 156.26, 146.54, 133.53, 131.60, 130.86, 130.55, 130.51, 130.47, 129.96, 125.17, 124.55, 121.52, 120.70, 120.51, 29.60, 25.79, 24.23 ppm.

UV-Vis (CH_2Cl_2): λ max (ε) = 444 (13460), 536 (24300), 575 (37900) nm
Fluorescence (CH_2Cl_2, excitation 536 nm): λ max = 609 nm

General Lysine-NCA homopolymerization (PLL-1 to PLL-6)

Fmoc-Lysine NCA **(4.1)** or Cbz-Lysine NCA **(4.2)** was transferred from glovebox to schlenk line in schlenk flask and dry DMF was added under inert atmosphere as final concentration of monomer was adjusted to 0.5 M. To this a solution of desired amount of initiator in minimum amount of dry DMF was added. The reaction was left to stir in a cold salt/water bath of 0 ˚C or at room temperature for 4 days under argon atmosphere. The solution was precipitated in diethyl ether and polymer was filtered, dried in vacuo.

P.S.: Cryostat was used in the case of 0 ˚C polymerizations.

Synthetic details and polymerization results were presented in Table 5-8.

Table 5-8. Synthetic details of PLL-1 to PLL-6

Pol.	DP (theo)	Monomer		Initiator			T	DP (exp)	Yield %
		m (g)	n (mmol)	type	v (mL)	n (mmol)			
PLL-1	40	0.73	1.85	N-Boc-1,6-hexanediamine	0.01	0.046	RT	-	-
PLL-2	40	0.2	0.65	Propargyl amine	$1.04*10^{-3}$	0.016	RT	12	45
PLL-3	40	0.53	1.73	N-Boc-1,6-hexanediamine	$9.7*10^{-3}$	$4.33*10^{-3}$	RT	20	73
PLL-4	40	0.20	0.65	N-Boc-ethylenediamine	$2.57*10^{-3}$	$1.62*10^{-3}$	RT	39	80
PLL-5								46	82
PLL-6	30	0.50	1.63		$8.61*10^{-3}$	$5.44*10^{-2}$	0 ˚C	25	40

*Monomer is Fmoc-Lysine-NCA for PLL-1, Cbz-Lysine-NCA for the rest of the polymerization

PLL-1 *(N-Boc-1,6-hexanediamine initiated Poly(Fmoc-L-lysine));* Polymerization was resulted in a precipitation, product was not characterizable due to the non-solubility.

PLL-2 *(Propargylamine initiated Poly(Cbz-L-lysine)) (45% yield);*

^{1}H-NMR (δ (ppm) 850 MHz, DMSO-d6): δ 8.24 (s, 1H, NH), 7.49 – 7.09 (m, 5H, Ar), 6.81 (s, 1H, NH), 5.08 – 4.87 (m, 2H, Cbz-CH_2), 4.35 – 3.75 (m, 1H, α-CH), 3.07 (s, 1H, CH≡), 2.94 (s, 2H, ε-CH_2), 2.03 – 1.12 (m, 6H, α-γ-CH_2) ppm.

^{13}C NMR (214 MHz, DMSO): δ 156.06, 137.24, 128.32, 127.70, 65.12, 40.20, 39.15, 29.14, 27.89, 22.50 ppm.

GPC (DMF as eluent, against PS): M_n= 3700 g/mol, Đ= 1.42

PLL-3 *(N-Boc-1,6-hexanediamine initiated Poly(Cbz-L-lysine)) (73% yield);*

^{1}H-NMR (δ (ppm) 850 MHz, DMSO-d6): δ 8.49 – 7.69 (m, 1H, NH), 7.49 – 7.07 (m, 5H-Ar), 6.94 – 6.68 (m, 1H, NH), 5.12 – 4.88 (m, 2H, Cbz-CH_2), 4.48 – 3.72 (m, 1H, α-CH), 2.94 (s, 2H, ε-CH_2), 2.08 – 1.07 (m, 6H, α-γ-CH_2) ppm.

^{13}C NMR (214 MHz, DMSO) δ 156.09, 137.26, 128.50, 128.42, 127.90, 127.85, 65.33, 65.12, 39.99, 29.32, 28.31, 22.69 ppm.

GPC (DMF as eluent, against PS): M_n= 5400 g/mol, Đ= 1.32

PLL-4, PLL-5 and PLL-6 (*N-Boc-ethylenediamine initiated Poly(Cbz-L-lysine))(80%, 82% and 40% yield, respectively);*

^{1}H-NMR (δ (ppm) 700 MHz, DMSO-d6): δ 8.33 – 7.79 (m, 1H, NH), 7.48 – 7.07 (m, 5H-Ar), 6.88 – 6.63 (m, 1H, NH), 5.14 – 4.76 (m, 2H, Cbz-CH_2), 4.23 – 3.69 (m, 1H, α-CH), 2.93 (s, 2H, ε-CH_2), 2.08 – 0.92 (m, 6H, α-γ-CH_2) ppm.

GPC (DMF as eluent, against PS):
PLL-4: M_n= 10300 g/mol, Đ= 1.19
PLL-5: M_n= 12500 g/mol, Đ= 1.38
PLL-6: M_n= 6700 g/mol, Đ= 1.24

N-terminus dye functionalization of poly(Cbz-L-lysine)

(PLL-5 and PLL-6 terminal amine group modification with SO_3H-PDI-COOH)

SO_3H-PDI-COOH (**4.5**, 13.00 mg, 0.01 mmol, 2.50 eq) and HBTU (6.00 mg, $1.6*10^{-2}$ mmol, 4.00 eq) was dissolved in 2 mL of dry DMF and stirred for 30 minutes under inert atmosphere. NH_2-terminated polymer **PLL-5** (50.00 mg, $4*10^{-3}$ mmol, 1.00 eq) was dissolved in 2 mL of dry DMF and added to this carboxylic acid/HBTU solution. Reaction

mixture was stirred for additional 10 minutes and DIPEA (0.013 mL, $8*10^{-2}$ mmol, 20.00 eq) was added. Coupling reaction was proceeded at room temperature for 3 days. Polymer was precipitated by cold diethyl ether and purified by repeated washing with water to remove unreacted dye, and washed again with diethyl ether and dried under vacuum to yield reddish polymeric product (50 mg, 80% yield).

The same procedure and scale were applied to the modification of PLL-6 with SO_3H-PDI-COOH (45 mg, 71% yield).

^{1}H-NMR (δ (ppm) 700 MHz, DMSO-d6): δ 8.16 – 7.87 (m, 1H, NH), 7.58 – 7.47 (m, 6H, PDI), 7.27 – 6.96 (m, 5H, Ar), 6.73 – 6.65 (m, 6H, PDI), 4.98 – 4.77 (m, 2H, Cbz-CH_2), 3.85 – 3.61 (m, 1H, α-CH), 2.96 – 2.78 (m, 2H, ε-CH_2), 1.98 – 0.99 (m, 6H, α-γ-CH_2), 0.94 – 0.85 (s, 12H, PDI) ppm.

GPC (DMF as eluent, against PS): **PLL-6-PDI-SO_3H**: M_n=6200 g/mol, Đ= 1.38
PLL-5-PDI-SO_3H: M_n=17500 g/mol, Đ= 1.54

Synthesis of PDI-NH_2 initiated poly(Cbz-L-lysine)

(PLL-7, PLL-8 and PLL-9)

Three different chain length (DP=20, 40 and 60) poly(Cbz-L-lysine) was synthesized according to the procedure below. Synthetic details were presented in Table 5-9.

Cbz-Lysine NCA **(4.2)** was transferred from glovebox to schlenk line in schlenk flask and dry DMF was added under inert atmosphere as final concentration of monomer was adjusted to 0.5 M. To this a solution of desired amount of initiator, N-(2,6-diisopropylphenyl)-N'-(4-aminoethyl)-1,6,7,12-tetraphenoxyperylene-3,4:9,10 tetra carboxy diimide **(PDI-NH_2) (4.9)** in minimum amount of dry DMF was added. The reaction was left to stir in a cold salt/water bath of 0 ˚C equipped with cryostat for 4 days under argon atmosphere. The solution was precipitated in diethyl ether and polymer was filtered. Resulted red solid was dissolved in THF and intensively dialyzed against THF by using RC membrane (MWCO=1000 g/mol) for 3 days to completely remove the unreacted dye. Polymer was freeze dried and stored in the fridge.

Table 5-9. Synthetic details of PDI-NH_2 initiated Cbz-Lysine NCA polymerization

Pol.	DP (theo)	Monomer		PDI-NH_2		Yield %	GPC		DP (exp)
		m (g)	n (mmol)	m (g)	n (mmol)		M_n (g/mol)	Đ	
PLL-7	20	1	3.26	0.16	0.16	98	5100	1.31	15
PLL-8	40	1	3.26	0.08	0.082	91	8700	1.27	45
PLL-9	60	1	3.26	0.05	0.054	65	9600	1.27	60

^{1}H NMR (500 MHz, DMSO-d6): δ 8.25-7.97 (m, 1H, NH), 7.49 – 6.99 (m, 5H-Ar), 5.08 – 4.86 (m, 2H, Cbz-CH_2), 4.29 – 3.68 (m, 1H, α-CH), 3.03 – 2.89 (s, 2H, ε-CH_2), 2.05 – 1.11 (m, 6H, α-γ-CH_2), 0.99 (d, J = 6.7 Hz, 12H, PDI-isopropyl) ppm.

FTIR (ATR): 3290 (N-H str.), 3063; 3033 (ring C-H str.), 2935; 2864 (C-H str.), 1690 (amide C=O str. of Cbz), 1647 (amide C=O str. of backbone) and 1525 (amide N-H bend), 1343; 1234 (C-N str.), 734 (ring C-H bend), 694 (ring C=C bend) ppm.

GPC (DMF as eluent, against PS, UV detector at 520 nm): As given in Table 5-9.

Deprotection of Cbz groups (PLL-7dp, PLL-8dp and PLL-9dp)

*Cleavage of Cbz groups of three different chain length of PDI-NH_2 initiated Poly(Cbz-L-lysine) polymers **(PLL-7, PLL-8** and **PLL-9)** were carried out as described below (Table 5-10).*

Polymer was dissolved in 5 mL of TFA under inert atmosphere and desired amount of 33% wt. HBr in glacial CH_3COOH was added. Reaction mixture was stirred for 2 hours at room temperature and precipitated with diethyl ether. Solid was filtered, dissolved in water and again filtered if there is insoluble things and dialyzed against water for 3 days by using RC membrane (MWCO=1000 g/mol) to remove excess of acid and impurities.

Table 5-10. Synthetic details of deprotection of Cbz groups

Pol.	DP (theo)	m (mg)	HBr/CH_3COOH v (mL)	Yield %
PLL-7	20	154	0.25	89
PLL-8	40	112	0.50	91
PLL-9	60	220	0.75	75

^{1}H NMR (500 MHz, DMSO-d6): δ 8.05 (s, 1H, NH), 7.49 – 7.33 (m, 10), 7.32 – 7.25 (d, J = 8.0 Hz, 3H), 7.25 – 7.14 (d, J = 9.4 Hz, 4H), 7.09 – 7.00 (d, J = 7.8 Hz, 8H), 4.39 – 4.10 (s, 1H, α-CH), 2.86 – 2.68 (t, J = 7.3 Hz, 2H, ε-CH_2), 1.78 – 1.19 (m, 6H, α-γ-CH_2), 1.08 – 0.93 (t, J = 7.3 Hz, 12H, PDI-isopropyl) ppm.

FTIR (ATR): 3290 (N-H str.), 2935; 2864 (C-H str.), 1647 (amide C=O str. of backbone), 1525 (amide N-H bend), 1343; 1234 (C-N str.), 1177, 836, 802, 721 cm^{-1}.

UV-Vis (H_2O): λ max (ε) = 456 (6693), 546 (12960), 580 (16548) nm

Fluorescence (H_2O, excitation 580 nm): λ max = 636 nm

Synthesis of block copolymers

Two different block copolymer with three different chain lengths was synthesized as described below. Synthetic details were presented in Table 5-11.

PDI-Poly(Cbz-L-lysine)-*block*-poly(L-leucine) (BC11, BC12, BC13)

PDI-Poly(Cbz-L-lysine)-block-poly(L-leucine) block copolymers with three different chain length (BC11, BC12, BC13) was synthesized as described below. Synthetic details are presented in Table 5-11.

L-leucine NCA **(4.3)** was transferred from glovebox to schlenk line in schlenk flask and dry DMSO was added under inert atmosphere as final concentration of monomer was adjusted to 0.5 M. To this a solution of desired amount of initiator, PDI-*poly(Cbz-L-lysine) (PLL-X)* in minimum amount of dry DMSO was added. The reaction was left to stir at 35 ˚C

for 6 days under argon atmosphere. The solution was precipitated in diethyl ether and polymer was filtered. Resulted red solid was dissolved in THF and intensively dialyzed against THF by using RC membrane (MWCO=1000 g/mol) for 3 days. Polymer was freeze dried and stored in the fridge.

^{1}H NMR (700 MHz, DMSO-d6): δ 8.18-7.90 (m, 2H, 2NH), 7.25-7.03 (m, 5H-Ar), 4.93-480 (m, 2H, Cbz-CH_2), 4.18-4.14 (m, 1H, α-CH, Pleucine), 3.80 (m, 1H, α-CH, PLL), 2.92 – 2.89 (s, 2H, ε-CH_2), 1.94 – 1.23 (m, 6H, α-γ-CH_2), 0.99 (d, J = 6.7 Hz, 12H, PDI-isopropyl), 0.86-084 (m, 7H, Pleucine-isopropyl) ppm.

FT-IR (ATR): 3290 (N-H str.), 3063; 3033 (ring C-H str.), 2935; 2864 (C-H str.), 2957; 2933 (C-H str.), 1690 (amide C=O str. of Cbz), 1647 (amide C=O str. of backbone) and 1525 (amide N-H bend), 1343; 1234 (C-N str.), 734 (ring C-H bend), 694 (ring C=C bend) cm^{-1}.

PDI-Poly(Cbz-L-lysine)-*block*-poly(L-phenylalanine) (BC14, BC15, BC16)

PDI-Poly(Cbz-L-lysine)-block-poly(L-phenylalanine) copolymers with three different chain length (BC14, BC15, BC16) was synthesized as described for PDI-Poly(Cbz-L-lysine)-block-poly(L-leucine), except of using dry DMF as a solvent. Synthetic details are presented in Table 5-11.

^{1}H NMR (700 MHz, DMSO-d6): δ 8.30-7.90 (m, 2H, 2NH), 7.5-6.90 (m, 5H-Ar (Cbz), m-5H-Ar (Phenylalanine)), 5.1-4.8 (m, 2H, Cbz-CH_2), 4.6-4.4 (m, 1H, α-CH), 3.8-3.6 (m, 1H, α-CH, PLL), 3.5 (m, 2H), 3.2–2.9 (s, 2H, ε-CH_2), 2.0–1.20 (m, 6H, α-γ-CH_2), 0.99 (d, J = 6.7 Hz, 12H, PDI-isopropyl) ppm.

FT-IR (ATR): 3290 (N-H str.), 3063; 3033 (ring C-H str.), 2935; 2864 (C-H str.), 1690 (amide C=O str. of Cbz), 1647 (amide C=O str. of backbone) and 1525 (amide N-H bend), 1343; 1234 (C-N str.), 734 (ring C-H bend), 694 (ring C=C bend) cm^{-1}.

Table 5-11. Synthetic details of block copolymers by NCA polymerization

Polymer	$DP_{(theo)}$ PLL/PX	Monomer		PDI-PLL-NH_2		Yield (%)	Đ (GPC, 520 nm)	$M_{n\ (exp)}$ (g/mol)
		m (mg)	n (mmol)	m (mg)	n (mmol)			
BC11	20/40	200	1.27	196	0.032	76	1.22	7550
BC12	40/40	140	0.89	252	0.022	75	1.44	-
BC13	60/20	31	0.2	160	0.0096	68	1.39	18400
BC14	20/40	200	1.05	162	0.026	88	1.40	7850
BC15	40/40	200	1.05	300	0.026	78	1.35	14000
BC16	60/20	50	0.26	215	0.013	83	1.36	18500

Deprotection of Cbz groups

Cleavage of Cbz groups of all the block copolymers were carried out as described below. After deprotection following amphiphilic block copolymers are obtained:

PDI-Poly(L-lysine)-block-poly(L-leucine) (BC11dp, BC12dp and BC13dp)

PDI-Poly(L-lysine)-block-poly(L-phenylalanine) (BC14dp, BC15dp and BC16dp)

Polymer was dissolved in 5 mL of TFA under inert atmosphere and desired amount of 33% wt. HBr in glacial CH_3COOH was added. Reaction mixture was stirred for 2 hours at room temperature and precipitated with diethyl ether. Solid was filtered, dissolved in water and again filtered and dialyzed against water for 3 days by using RC membrane (MWCO=1000 g/mol) to remove excess of the acid and impurities.

PDI-Poly(L-lysine)-*block*-poly(L-leucine):

^{1}H NMR (700 MHz, DMSO-d6): δ 8.16 – 7.60 (m, NH), 7.54 – 6.84 (m, PDI Ar-H), 4.20 (s, 1H, α-CH), 4.01 (s, 1H, α-CH), 2.71 (d, J = 11.3 Hz, 2H, β-CH_2), 1.93 – 1.07 (m, 6H, α-γ-CH_2, 3H, Pleucine), 0.94 (d, J = 6.6 Hz, 12H, PDI-isopropyl), 0.87 – 0.68 (m, 6H, Pleucine) ppm.

^{1}H NMR (700 MHz, D2O): δ 7.64 – 7.44 (m, NH), 4.35 (s, 1H, α-CH), 3.03 (d, J = 8.0 Hz, 2H, β-CH_2), 1.91 – 1.35 (m, α-γ-CH_2), 1.28 – 0.72 (m) ppm.

FT-IR (ATR): 3290 (N-H str.), 2935; 2864 (C-H str.), 1647 (amide C=O str. of backbone), 1525 (amide N-H bend), 1343; 1234 (C-N str.), 1177, 836, 802, 721 cm^{-1}.

PDI-Poly(L-lysine)-*block*-poly(L-phenylalanine):

^{1}H NMR (700 MHz, DMSO-d6): 8.11-6.77 (m, 2H, NH; 25H, PDI; 5H, Phenylalanine)), 4.55-4.21 (s, 1H, α-CH), 4.19-3.72 (s, 1H, α-CH), 2.74 (m, 2H, β-CH_2), 2.64 – 2.47 (m, 2H, ε-CH_2), 1.65 – 0.95 (m, 6H, α-γ-CH_2), 0.90-0.76 (d, J = 6.7 Hz, 12H, PDI-isopropyl) ppm.

^{1}H NMR (700 MHz, D_2O): δ 7.94 (s, 2H, NH), 7.88 – 7.00 (m), 4.35 (s, 1H, α-CH), 3.17 – 2.87 (m, 2H, ε-CH_2), 1.77 (d, J = 62.2 Hz, 4H, α-γ-CH_2), 1.47 (d, J = 39.0 Hz, 2H, β-CH_2), 1.19 (t, J = 7.1 Hz) ppm.

FT-IR (ATR): 3290 (N-H str.), 3063; 3033 (ring C-H str.), 2935; 2864 (C-H str.), 1647 (amide C=O str. of backbone) and 1530-1525 (amide N-H bend), 1343; 1197 (C-N str.), 1163, 876, 694 (ring C=C bend) cm^{-1}.

Sample preparation of homopolymers for pH dependency studies

TRIS-HCl buffer solutions are prepared with pH values of 2,4,6,7,8,10 and 12. PLL-7dp, PLL-8dp and PLL-9dp solution with each buffer with a concentration of $3*10^{-5}$ M is prepared and filter through 0.45 μm syringe filter. Samples are exposed to measure UV-*vis*, FC, CD, TEM, SEM, CLSM and DLS.

Preparation of block copolymer micelles

Direct dissolution method: BC11dp and BC14dp block copolymers were directly dissolved in water with a concentration of 1 mg/mL. Samples are sonicated for 2 hours in ultrasonic bath and filtered through 0.8 μm syringe filter followed by stirring at RT for 1 week.

Thin film formation method: BC11dp and BC14dp block copolymers were dissolved in DMSO and solvent was removed under vacuum to form a thin film layer of the polymer on

the flask. Then polymers were hydrated with water (last concentration is adjusted to 1 mg/mL) and left to stir at RT for 1 week.

Visualization of the polymeric micelles

Block copolymer solutions (1 mg/mL) were directly applied for the TEM analysis *via* the uranyl acetate staining technique. Additionally, CLSM measurements were performed as described in the following:

Correlation study of TEM/CLSM of pure block copolymer micelles:

The study was performed for the correlation of pure block copolymer after uranyl acetate staining to verify the assignment of worm/micelle structure to fluorescence. Aqueous solution of uranyl acetate stained block copolymer was dropcasted on the trehalose film on the grids which were subsequently investigated by confocal microscopy (Figure 5.34). Leica TCS SP5 (Germany, Wetzlar), fluorescence was excited at 561nm and emission recorded with an APD in the wavelength range of 647nm - 703nm using a 20X dry objective (HC PL APO CS2 20x/0.75 DRY , Leica). After recording the fluorescence the sample was transfered to TEM imaging (FEI Tecnai F20, voltage: 200.000). Subsequently TEM images and fluorescent images were registered, allowing to identify the wormlike structures as fluorescent.

The live cell confocal images of block copolymers and correlation study with TEM and SEM:

Macrophage cell medium was incubated by copolymer solutions (1 mg/mL). Fluorescence was recorded on a Leica TCS SP5 (Germany, Wetzlar), excited at 561nm and emission recorded in the wavelength range of 601nm - 718nm using a 63X NA1.2 water immersion objective (Figure 5.35, a.,b).

After fixation, cells were stained with Osmium tetroxide (OsO_4) and uranyl acetate and embedded in EPON. Block was cut around 100nm thickness on a Leica Ultramicrotome Leica EM UC7:

- The cuts were transfered to TEM grids for recording the TEM images.

- For the correlation of light and electron microscopy EPON cuts were deposited on ITO glass and SEM investigation was conducted.

Cytotoxicity of the polymeric micelles

Cell viability of the block copolymer micelles were tested on A549 human lung adenocarcinoma cell line. A549 Cells (German Collection of Microorganisms and Cell Cultures, Braunschweig) were cultured in high glucose DMEM supplemented with 10% FCS, 10% Penicillin/Streptomycin, 1% MEM non essential amino acid at 37 °C/5% CO_2. Passages of cells were made near confluency in a T-75 Flask using standard trypsination protocol using Trypsin LE Express (ThermoFisher Scientific).

A549 cells (5000 cells/well) in a white 96-well (half-area) microplate and left to adhere overnight in an incubator at 37 °C/5% CO_2. The cells were treated with the prescribed amount of polymers (0.05 – 0.2 mg/mL in DMEM) and were incubated for 24 h at 37 °C/5% CO_2. (Polymers PLL-7dp, BC11dp, BC14dp, PLL, PEG/PLL (0.2, 0.1 and 0.05 mg/mL)). The cell viability was subsequently tested using CellTiter-Glo® Luminescence Cell Viability Assay (Promega) according to manufacturer's protocol. Cells without treatment are referenced as blank and the data is represented as % cell viability. All measurements were performed in triplicates.

CHAPTER 6

Synthesis and Characterization of Nanoplastics: Act as Stressors to the Innate Immune System of Fathead Minnow

6. Synthesis and Characterization of Nanoplastics: Act as Stressors to the Innate Immune System of Fathead Minnow

This project is a collaboration with Anne-Catherina Greven, Teresa Merk, Boris Jovanovic and Dusan Palic from the Chair for Fish Diseases and Fisheries Biology, Ludwig Maximilian University, Munich.

In this chapter, the synthesis and characterization of the plastic nanoparticles i.e. polystyrene and polycarbonate were performed and, *in vitro* study of the particles on the immune system of "Fathead minnow" (special fish type) was investigated by the collaboration partner.[340]

6.1. Introduction

Environmental pollution is one of the serious problems of our planet not only for human beings but also for living organisms in aqueous ecosystems. Plastic wastes are potential dangers year after year for the marine habitat due to the dramatic increase of the worldwide plastic production which reached 335 million metric tons in 2016 (Figure 6.1).[341] Additionally, lower recycling ratios of the plastics (26%) increase the risk of pollution. Eriksen et al.[187,188] reported that about 5.25 trillion particles are floating in the ocean which is around 268.940 million tons by weight.

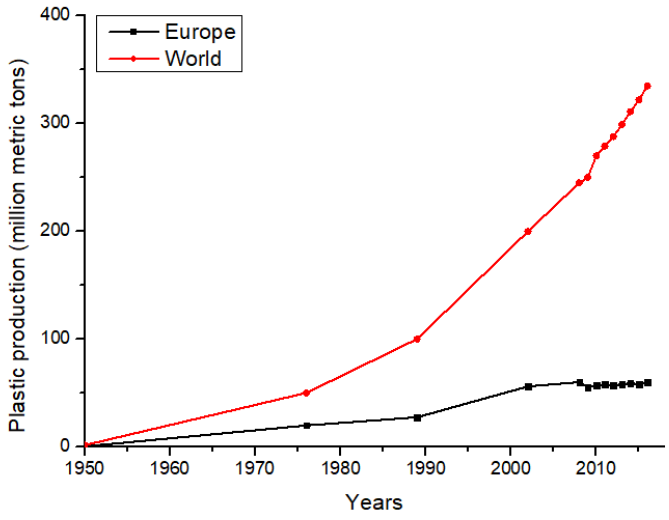

Figure 6.1. Increase on global plastic production from 1950 to 2016 (Statistic data source is https://www.statista.com/statistics/282732/global-production-of-plastics-since-1950/)[341]

Most of the plastic pollutants are carried to the oceans and seas *via* rivers and storm waters. Inadequate waste management, natural disasters, industrial pollutants, manufactural wastes, beach litter, untreated sewage and agricultural plastics are the main reasons for plastic pollution in aqueous ecosystems.[342,343] Plastic debris are generally non-biodegradable synthetic polymers which are toxic for living organisms. They are mainly prepared from petroleum-based materials and contain additives such as colorants, opacifiers, plasticizers, thermal and UV stabilizers, inorganic fillers, mating and luster agents that can have adverse effects on the habitat by leaking into the environment.[344,345]

It is well-known that fully degradation of the plastics in nature takes houndreds to thousands of years depending on the type of plastics, surrounding media, temperature, UV irradiation and fouling processes. By the influence of these factors eventually polymeric debris breaks down into smaller particles. The plastic particles can be classified in terms of their sizes as: megadebris>20 mm; 20 mm>macrodebris> 5 mm; microdebris<5 mm and, nanodebris<100 nm. Smaller particles, in particular nano-scale plastics interact easily with living tissues due to their proper size and surface characteristics, for example the interaction of polystyrene particles with immune systems was studied in the literature.[346,347] Polystyrene and polycarbonate are two major types of plastics causing the pollution all over the world.[189,190,348] Polystyrene is an aromatic polymer synthesized from styrene *via* radicalic polymerization routes. It is one of the most widely produced material in the world after polyolefins and polyvinyl chloride, used for packaging, containers, lids, bottles, trays, tumblers and disposable cutlery.[349–352] Polystyrene was produced industrially first in 1931 and later expanded polystyrene (EPS) was invented and patented as Styropor which is known for constructing and packaging fields.[353] The drawback of these polymers is their slow degradation in nature which is a big concern environmentally. Beside that, the leakage of the plastic additives to the marine ecosystem such as flame retardants i.e polybrominated diphenyl ethers (PBDE), hexabromocyclododecane (HBCD) that are potential bioaccumulates with toxic properties, is a high risk for living organisms.[354–356] Polycarbonate is a thermoplastic polymer produced by condensation polymerization of bisphenol A and phosgene.[357,358] Commercialized polymer has high impact strength with an easy processability in industry. Therefore it is used for the production of compact disks (CDs and DVDs), automotive parts and electrical components.[359,360] Additionally, it can be employed as a flame retardant

material in construction field. Besides these applications, injection molded poly(bisphenol A) is used in drinking bottles, glasses and food containers which is a big discussion in recent years because of the severe health effects of bisphenol a (BPA). The endocrine disrupting substance BPA can lead to cardiovascular disease, diabetes and disorders of sexual development. Therefore its utilization in this field has been decreased in recent years, for example, marketing of baby bottles containing BPA was prohibited in 2011 by the European Union.[361–363]

As environmental pollution is critical for the life of all living beings, it poses a great threat to the water ecosystem as well. In this section, polycarbonate and polystyrene, as the mostly disposed plastic wastes into nature, are selected as model compounds in order to investigate the adverse effects of plastic wastes on the immune system of marine species. Nonaqueous emulsion polymerization should be considered as a suitable technique for the generation of poly(bisphenol A carbonate) nanoparticles (Scheme 6.1). By conducting the polycondensation of bisphenol A with triphosgene in nonaqueous emulsion, a wide range of applicability of this platform should be demonstrated.

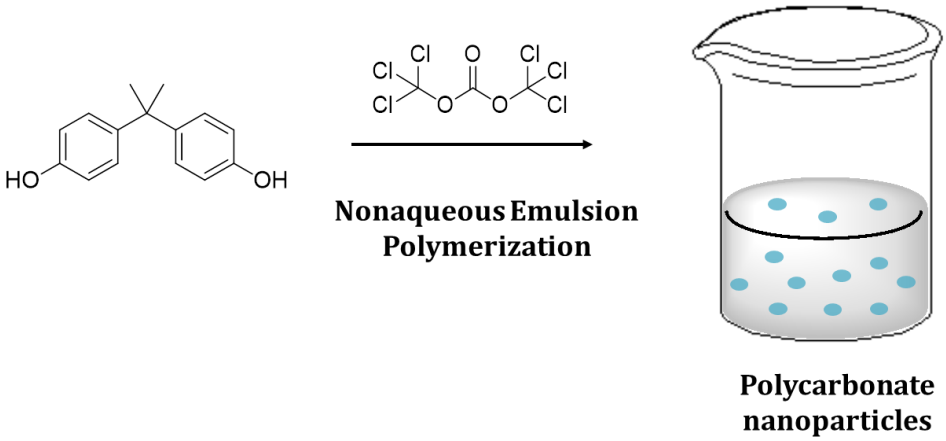

Scheme 6.1. Schematic illustration of poly(bisphenol A carbonate) nanoparticle synthesis

The straightforward emulsion polymerization should be considered for the preparation of spherical fluorescent nanoparticles by copolymerization of styrene and styryl boron-dipyrromethene (BODIPY) (Scheme 6.2). Fluorescently labelled particles offer the potential investigation of the response of the innate immune system of Fathead Minnow.

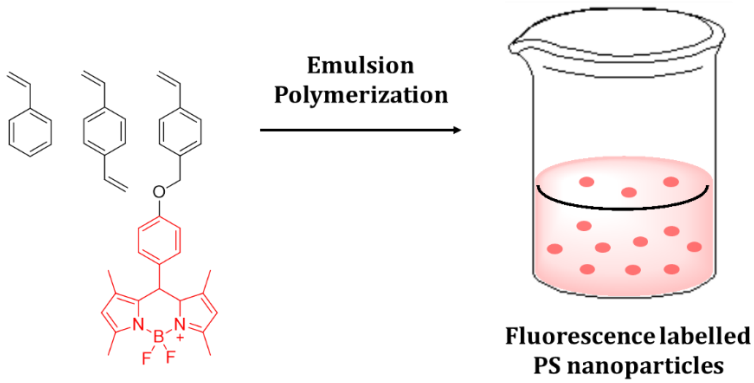

Scheme 6.2. Schematic illustration of PS nanoparticle synthesis

Fathead minnow (Pimephales promelas, Rafinesque 1820) is a North American omnivorous fish species that allows the study of the interaction of plastic particles and a freshwater fish species.[364,365] It should be considered to be used as a model animal to investigate the toxicological and immunological effect of both plastic nanoparticles *via* neutrophil-nanoplastic interactions.[340]

6.2. Results and Discussion

6.2.1. Synthesis of Poly(bisphenol A carbonate) Nanoparticles

Synthesis of poly(bisphenol A carbonate) is commonly proceeded in the literature by interfacial polymerization of BPA and phosgene in halogenated solvents in the presence of basic aqueous solutions as HCl scavanger.[359,360] Another route is the transesterification of BPA with diphenyl carbonate in bulk at high temperatures. Additionally, hydrolytic interfacial polycondensation of bisphenol-A bischloroformate is used for the synthesis of cyclic oligocarbonates. It should be noted that cyclic oligocarbonates are known as precursors for the high molecular weight polycarbonates by ROP above 250 °C.[366]

Polycondensation of bisphenol A (BPA) with phosgene derivatives in water-free organic systems was studied by Kricheldorf et al.[357,367] in dichloromethane and dioxane mixture and, linear and cyclic polymer formations were investigated. It was demonstrated by the same group that cyclization competes with the chain growth at any concentration and, any stage of the polycondensation.[358,366] For the preparation of polycarbonate nanoparticles, Kim et al.[368] developed the supercritical CO_2 method. In that study, high molecular weight polymeric nanoparticles (M_n=3.1*10^5 g/mol) were synthesized by transesterification between BPA and diphenyl carbonate in supercritical CO_2 using poly(propylene oxide)–poly(ethylene oxide)–poly(propylene oxide) triblock copolymer as an emulsifier, resulted in particles with a diameter of 30–140 nm.[368]

Herein, nonaqueous emulsion polymerization was employed for the generation of poly(bisphenol A) nanoparticles first the first time in the literature. Nonaqueous emulsion consists of two immiscible organic solvents which can be stabilized by block copolymer emulsifiers.[164,369] Previous research that has been done in our group revealed that DMF/n-hexane or acetonitrile/cyclohexane solvent combinations are well-stabilized by PI-*b*-PMMA or PEO-*b*-PI block copolymers. Obtained inert nano-reactors are a versatile tool for different polymerizations such as condensation or ring-opening.[161,164,369,370]

In this study, poly(bisphenol A carbonate) nanoparticles were prepared by nonaqueous emulsion polymerization using acetonitrile as dispersed phase and cyclohexane as continuous phase. Two different emulsifiers PI-*b*-PEO (molecular weight of 45700 g/mol,

polydispersity index is 1.06, molar block composition of 55% PI and 45% PEO (DP_{PI}=441, DP_{PEO}=357) and PI-*b*-PMMA (molecular weight of 65300 g/mol, polydispersity index is 1.09, molar block composition of 47% PI and 53% PMMA (DP_{PI}=311, DP_{PMMA}=351), respectively, were employed to optimize the synthesis and stabilization of the particles in the mentioned solvent system (Table 6-1). These high molecular weight block copolymers are necessary for the stabilization because of the low-interfacial-tensions present in an oil-in-oil emulsion. Due to the selective solubility of triphosgene and BPA in acetonitrile, the polymerization was proceeded to yield well-defined nanoparticles.

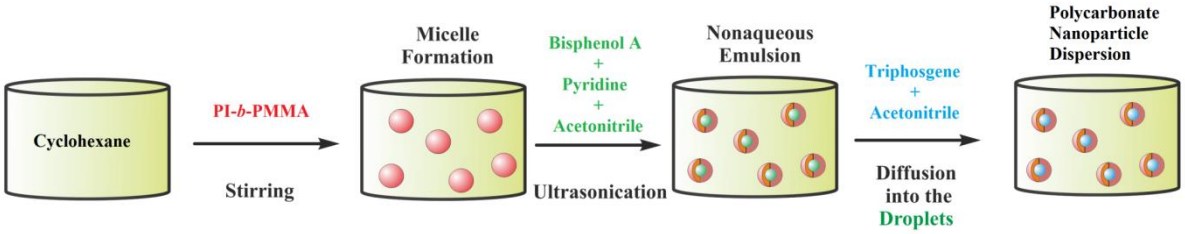

Figure 6.2. Nonaqueous emulsion polymerization of BPA and triphosgene

As presented in Figure 6.2, the block copolymer was dispersed in the nonpolar organic phase and BPA, dissolved in acetonitrile, was added to the dispersion followed by the addition of pyridine. Dropwise introduced triphosgene in acetonitrile started the polycondensation (Scheme 6.3). Reaction was proceeded in the droplets under the catalysis of pyridine at ambient temperature for 24 hours. Pyridine acts not only as a catalyst but also works as HCl acceptor during the polymerization.

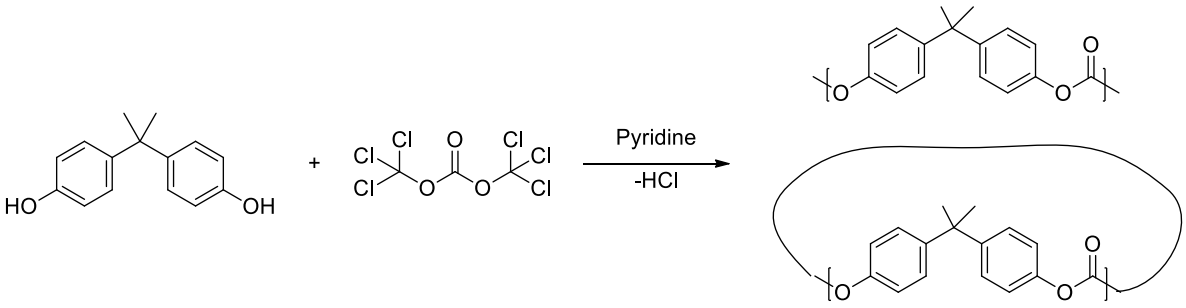

Scheme 6.3. Synthesis of poly(bisphenol A carbonate)

The morphology of the obtained polycarbonate nanoparticles was characterized by DLS and SEM measurement. To determine the number average molecular weights and

molecular weight distributions, the polymer was precipitated in methanol and dried to be analyzed by GPC.

Table 6-1. Polymerization data of poly(bisphenol A carbonate) nanoparticles

Pol.	Emulsifier	$n_{BPA}/n_{Triphosgene}$	M_n* (g/mol)	Đ*	R_h** (cyclohexane)	R_h** (HBSS)***	Zeta P. (mV)
PC1	PI-*b*-PMMA	2.7/1	4000	1.79	158 ± 41 nm	1710 ± 425 nm	2.0 ± 0.5
PC2	PEO-*b*-PI	2.7/1	4000	1.71	279 ± 29 nm	-	-

*M_n and Đ were determined via GPC versus PS standards, THF as eluent
**R_h-Hydrodynamic diameter was determined by DLS
***HBSS: Hank's Balanced Salt Solution

Nanoparticles prepared by PI-*b*-PMMA emulsifier (PC1)

Polymerization of BPA with triphosgene in nonaqueous emulsion stabilized by PI-*b*-PMMA resulted in a polymer (**PC1**) with a number average molecular weight of 4000 g/mol and a polydispersity index of 1.79. Obtained particles had a diameter of 158 nm in cyclohexane as DLS measurements revealed. Particle size was analyzed also in Hank's Balanced Salt Solution (HBSS) in order to mimic the physiological conditions. Strong aggregation was observed in this aqueous system as size was determined as 1710 nm. The morphology of the particles was investigated by SEM as presented in Figure 6.3. Particles are spherical but not very monomodally distributed as seen in the micrographs. The polycondensation reaction itself generally results in a polymer with high heterogeneity index. Additionally, polycondensation of BPA results in a mixture of linear and cyclic polycarbonates due to the nature of the polymerization (Scheme 6.3). Due to these factors that led to the increased polydispersity, particles were obtained with a broader size distribution. The drying effect while the sample preparation for SEM as well can affect the morphology of the particles.

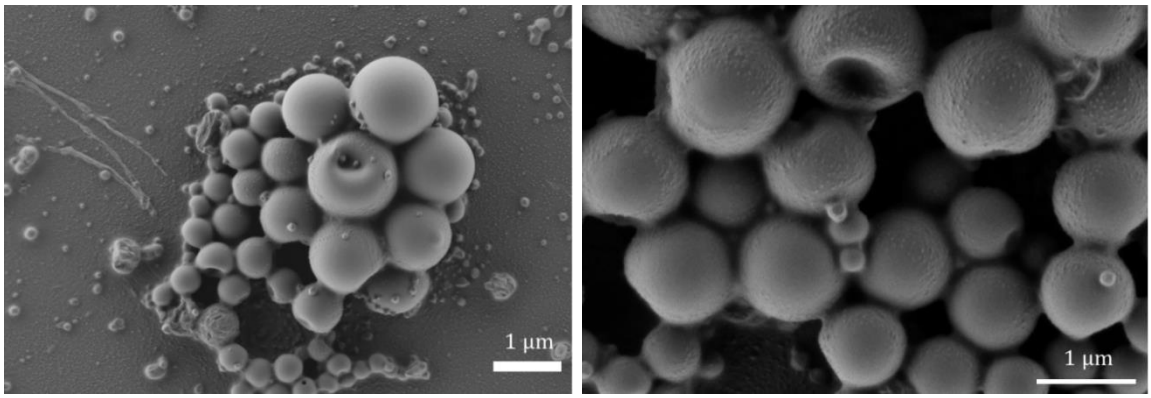

Figure 6.3. SEM micrographs of PC1 nanoparticles emulsified by PI-*b*-PMMA in cyclohexane

Nanoparticles prepared by PI-*b*-PEO emulsifier (PC2)

For the preparation of the particles PC2, all the conditions were identical with the previous polymerization except of using PI-*b*-PEO to stabilize the emulsion. Poly(bisphenol A carbonate) was obtained with a number average molecular weight 4000 g/mol with a polydispersity index 1.71. The hydrodynamic diameter of the particles in cyclohexane was determined as 279±29 nm in cyclohexane, rather larger than the PC1 nanoparticles stabilized with PI-*b*-PMMA. Heterogeneously distributed spherical particles with some larger aggregates were observed as presented in the SEM micrographs in Figure 6.4. Aforementioned mechanistic reasons might cause this polydispersity. Additionally, it should be noted that HCl release during the polymerization might destroy the particle morphology even though the usage of pyridine as HCl acceptor.

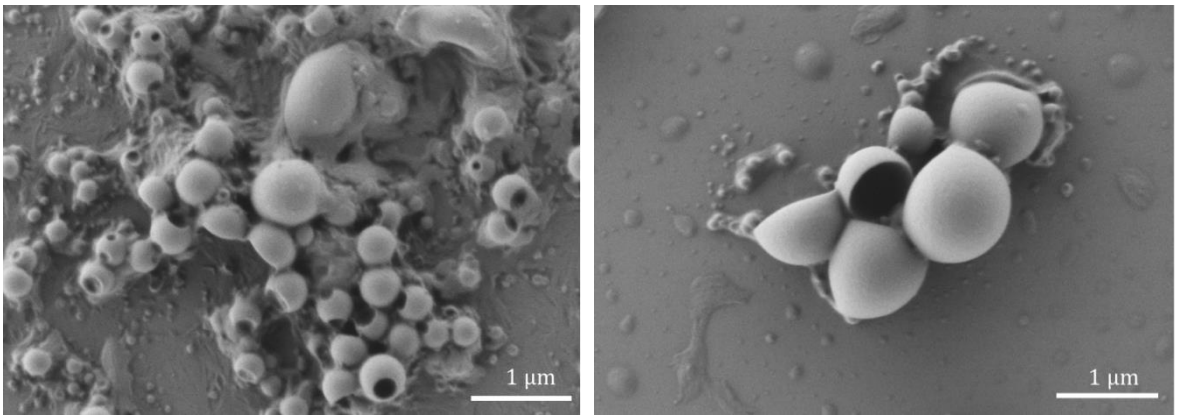

Figure 6.4. SEM micrographs of PC2 nanoparticles emulsified by PI-*b*-PEO in cyclohexane

6.2.2. Fluorescence Labeled Polystyrene Nanoparticles

Fluorescent polystyrene nanoparticles were synthesized by copolymerization of styrene, divinylbenzene and styryl boron-dipyrromethene (BODIPY) dye *via* emulsion polymerization as shown in Scheme 6.4.[371] Styryl boron-dipyrromethene was kindly prepared by Dajoune Joe as described in his dissertation.[371] Sodium dodecyl sulfate (SDS) was used to stabilize the emulsion and free radical polymerization was proceeded to yield the negatively charged polystyrene nanoparticles (Table 6-2). Covalent attachment of BODIPY to the polymer, does not affect its fluorescent properties, it shows maximum emission at 510 nm.[372]

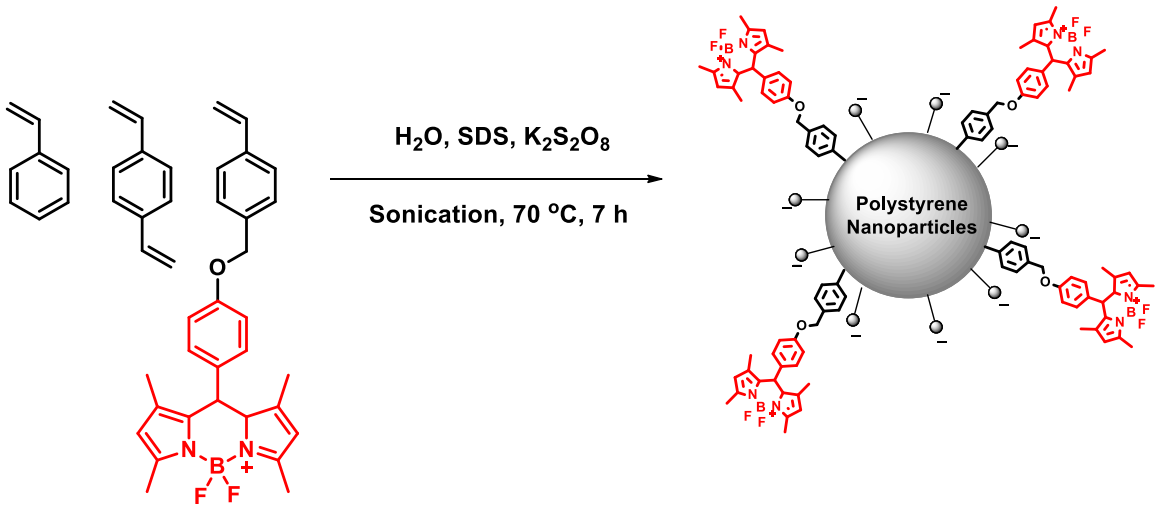

Scheme 6.4. Synthesis of fluorescent polystyrene nanospheres by emulsion polymerization

DLS measurements revealed that, the hydrodynamic diameter of the particles in water is around 41 nm. As SEM micrographs of the particles in water shown in Figure 6.5, well-defined, monomodally distributed spherical particles were obtained with a size 40 nm which is consistent with the DLS results. Particle size in HBSS was around 1000 nm due to the aggregation of the particles in physiological conditions.

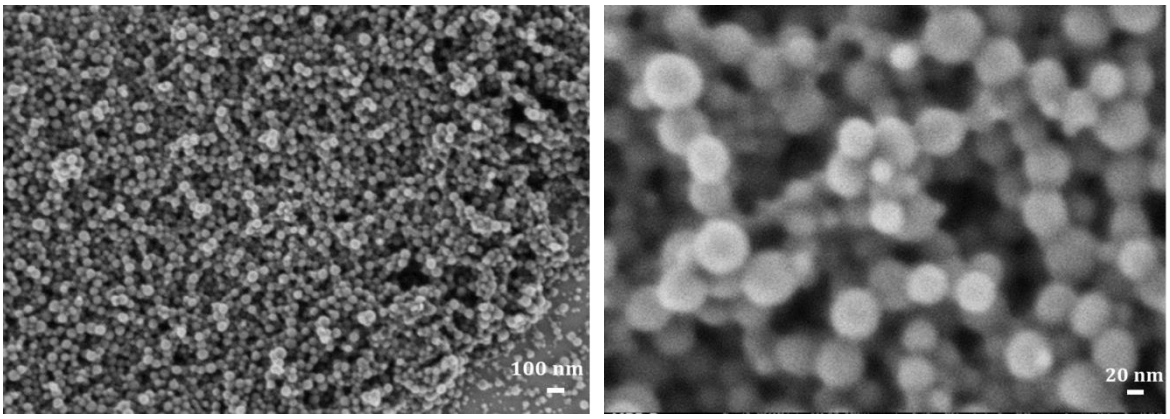

Figure 6.5. SEM micrographs of polystyrene nanoparticles emulsified by SDS in water

Table 6-2. Polymerization data of polystyrene nanoparticles

Pol.	Emulsifier	$n_{styrene}/n_{dvb}/n_{bodipy}$	R_h (water)	R_h (HBSS)	Zeta P. (mV)	Fluorophore
PS	SDS	152/18/1	41 ± 0.2 nm	1006 ± 380 nm	2.1 ± 0.4	BODIPY

Particles were intensively dialyzed against water to remove the surfactant SDS as much as possible to not cause any cytotoxicity on the fish medium during the *in vivo* tests.

6.2.3. Dynamic Light Scattering in Fathead Minnow Plasma

Understanding the aggregation behavior of the plastic nanoparticles in fish plasma is necessary before the final examination of the materials *in vitro*. Therefore, DLS measurements of polystyrene (PS) and poly(bisphenol A carbonate) (PC1) nanoparticles in Fathead minnow plasma was performed according to Rausch et al.[373] by Kristin Mohr in Landfester group. The autocorrelation function (ACF) of Fathead minnow plasma could be perfectly described by a sum of three exponentials (Equation 6.1), similar to human serum, giving an averaged hydrodynamic radius of R_h = 14 nm.[340]

$$g_{1,P}(t) = a_{1,P} \exp\left(-\frac{t}{\tau_{1,P}}\right) + a_{2,P} \exp\left(-\frac{t}{\tau_{2,P}}\right) + a_{3,P} \exp\left(-\frac{t}{\tau_{3,P}}\right) \qquad \textbf{(Equation 6.1)}$$

with the amplitudes a_i and the decay times $\tau_i = \frac{1}{q^2 D_i}$ while q is the absolute scattering vector ($q = \frac{4\pi n}{\lambda_0} \sin\left(\frac{\theta}{2}\right)$) and D_i the Brownian diffusion coefficient of component i. Data

from DLS, measured for particles and plasma separately, presented in Figure 6.6 and Table 6-3 (Particles were measured without filtration but Fathead minnow plasma was filtered through GS220nm filter). The ACFs for the polystyrene and polycarbonate particles alone were successfully fitted by a sum of two exponentials (Equation 6.2). Given a size of R_h=155 nm for the PS particle and a size of R_h=500 nm for the PC1 particle in phosphate-buffered saline solution (PBS).

$$g_{1,C}(t) = a_{1,C} \exp\left(-\frac{t}{\tau_{1,C}}\right) + a_{2,P} \exp\left(-\frac{t}{\tau_{2,C}}\right) \quad \textbf{(Equation 6.2)}$$

Table 6-3. Hydrodynamic radius of plasma, PC1 and PS nanoparticles

Polymers	R_h
PS	155 nm
PC1	515 nm (additional aggregates > 1µm not measurable with DLS)
Plasma	14 nm

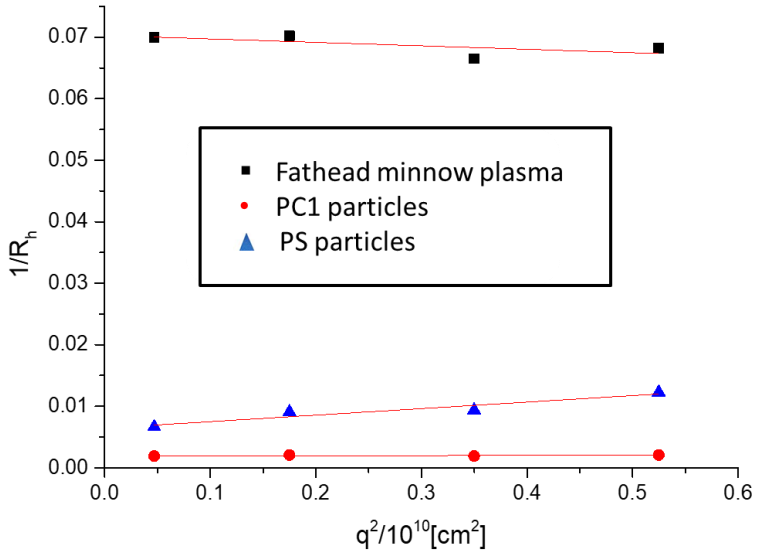

Figure 6.6. DLS measurements of the PC1 and PS-NPs in Fathead minnow plasma. Angular dependency of the reciprocal hydrodynamic radius of undiluted plasma, PC1 (concentration unknown due to precipitation), PS (0.1 mg/mL PBS)

Knowing the autocorrelation function (ACF) of Fathead minnow plasma and the respective particles, the correlation function of the plasma-particle mixtures could be analyzed. If no aggregation occurs, the resulting ACF of the plasma particle mixture correlates to the so-called force fit. In the force fit, the sum of the individual correlation functions with the known parameters of the two components (plasma/particle) is kept fixed and the intensity contributions for plasma f_P and particle f_C are the only fit parameters (Equation 6.3).

$$g_{1,m}(t) = f_P g_{1,P}(t) + f_C g_{1,C}(t) \qquad \textbf{(Equation 6.3)}$$

None of the investigated systems led to formation of aggregates with sizes larger than the largest size of the original components (particle/fathead minnow plasma). Figure 6.7. a and b show the results of the mixture of PS and PC with undiluted fathead minnow plasma, respectively.

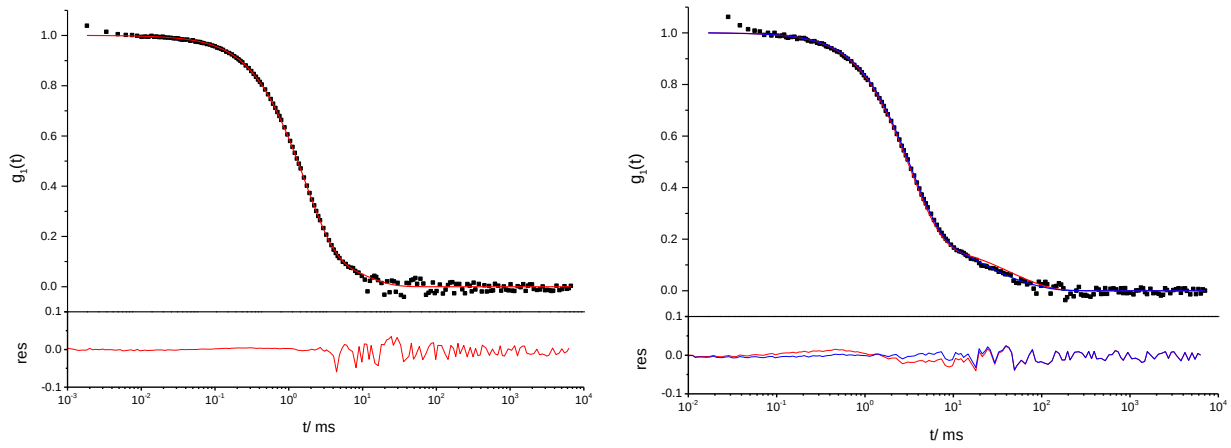

(a) **(b)**

Figure 6.7. (a) ACF of the PS nanoparticles in fathead minnow plasma. Red line, fit with eq. 6.3 and the resulting residue. Data points of the ACF. Scattering angle 60°, T = 310 K. (b) ACF of the PC1 nanoparticles in Fathead minnow plasma. Scattering angle 90° (30, 60° not representative due to macroscopic aggregation of the original particle sample), black boxes: data points of the mixture, red line fit with the force fit meaning: fixed parameters of the two components of the mixture (plasma and PC1) and below residue = data points – fit points. Blue line fit with additional aggregate function: R_h additional component 160 nm (smaller R_h main particle fraction)

6.2.4. Effect of Nanoplastics on Immune System of Fathead Minnow

After successful characterization of the particles in Fathead Minnow plasma, *in vitro* effects of the nanoplastics on the immune system of these fish species were investigated in this part of the study, by the collaboration with Greven et al.[340] from Ludwig Maximilian University. All details can be found in the published research by Greven and Karagöz et al.[340]

Immune system is mainly responsible to prevent the negative effects of the pathogens for the host by forming the immune responses. Macrophages and neutrophils are the main cell types for the phagocytosis in fish organism.[374] Neutrophils can encourage the defence via different functions such as phagocytosis, degranulation of primary granules, and formation of neutrophil extracellular traps (NETs).[375–377] The level of these responses is used to determine the reaction of the immune system.[377,378] The pathogens can be eradicated by the release of cytotoxic compounds from granules or by the formation of reactive oxygen species (ROS).[375–377] The formation of NETs is a mechanism to kill the pathogens extracellularly by releasing the antimicrobial protein DNAs.[379] Herein, the stress of the polystyrene and poly(bisphenol A) on neutrophil function of Fathead minnow was studied by measuring the oxidative burst (HDFFDA assay), degranulation (MPO assay), and release of NETs in vitro.[340]

In order to understand the actual function of the nanoparticles in biological medium, it is essential to enlightening the interaction of the nanoparticles with biological fluid. When nanoparticles get in contact with blood, biological molecules are immediately adsorbed on the surface of the nanoparticles. Proteins in the plasma covers the surface of the nanoparticles which called as protein corona.[380–382] The protein binding affinity to the surface of the nanoparticles depends on the size and surface characteristics of the particles which effects all the function and properties of the system. Another important criterion is the plasma exposure time of the particles. Due to the formation of corona, particle interaction with cells is modified, can shield recognition units, leading to the loss of targeting functionalities.[380–382] Protein corona determines the biological identity of the particles, thereby endocytosis and cytotoxicity. In the case of core crosslinked polymeric micelles with a hydrophobic core and hydrophilic shell, protein will first interact and entangle with hydrophilic shell and tries to diffuse into the hydrophobic core of the

particle. Because of the hydrophilic brushes, proteins will be kept away from the hydrophobic core if they are selected according to the "Whitesides rules". Thus, by this steric stabilization protein adsorption is prevented.[381] Additionally, core crosslinked micelles cannot dissociate to unimers and change the surface topology. However, noncrosslinked ones do that upon contact with the concentrated protein solution.[381] The interaction of various types of nanomaterials with plasma proteins will be different. If the nanoparticles stabilized by detergents with a low CMC, proteins can easily reach to the interface of the particles due to leaving of the surfactants from the hydrophobic patches, results in a protein corona formation.[383]

Protein adsorption onto negatively and positively charged polystyrene nanoparticles were determined by Landfester et al. as 350 to 1330 proteins per nanoparticle via ITC technique.[384] The different types of polystyrene nanoparticles were used which are identical in the average diameter and type of surfactant but have different functionality on the surface. The prominent factor for the interaction with cell membrane is surface charge. However, formed protein corona shows a small decrease on particle uptake.[384] Parak et al.[382] reported that positively charged nanoparticles have rapid interaction with living cells as they also have a higher toxicity. According to their study, cell uptake is affected by the size and surface charge of the particles and, by formation of the protein corona. Research results showed that positively charged particles were extensively interacted with the cell medium both in serum-free and serum-containing media. Nanoparticle internalization rate depends on the surface charge with or without the presence of protein corona.[382] The cell uptake properties of the plastic nanoparticles are also influenced by their surface characeristics. Positively charged particles can interact with cell medium more rapidly due to electrostatic interactions and hydrogen bonding.[385] As demonstrated in the literature, positively charged polystyrene particles covered with protein corona showed efficient cellular uptake than negatively charged ones.[380]

In our study, the size of the polystyrene nanoparticles in fish plasma may induce the corona formation and therefore leading to phagocytosis. Figure 6.7 shows the behavior of suspended polystyrene and poly(bisphenol A) particles in fish plasma. The size distribution of the particles did not limit the phagocytosis. Polystyrene and poly(bisphenol A) particles around of 1007 nm and 1710 nm in HBSS+, respectively, can be successfully phagocytized by neutrophiles, whereas neutrophils can phagocytize

aggregates up to 3mm.[386] The agglomeration behavior of polystyrene and polycarbonate nanoparticles in the fish plasma was also tested. Particles did not agglomerate and were able to be ingested by phagocytic cells. So, the uptaken particles could lead the response of immune system. In particular, polystyrene particles were observed to affect the membrane structure and decrease the molecular diffusion.[387] According to the literature, carboxyl polystyrene particles had high effect on oxidative burst and degranulation of primary granules in immune cells.[388] Polycarbonate particles were less induced to the immune system response in comparison to the polystyrene. The effect of nanoplastics on the function of human neutrophils by Fröhlich et al.[388] showed the similar results.

To investigate the immune system response of Fathead Minnow against nanoplastic particles, a neutrophile phagocytosis study by fathead minnow neutrophils was performed with fluorescent PS, visualized by Fluorescence Microscopy (Figure 6.8). After 1 hour of incubation, neutrophils phagocytized PS nanoparticle aggregates and cytoplasmic fluorescence was observed.[340]

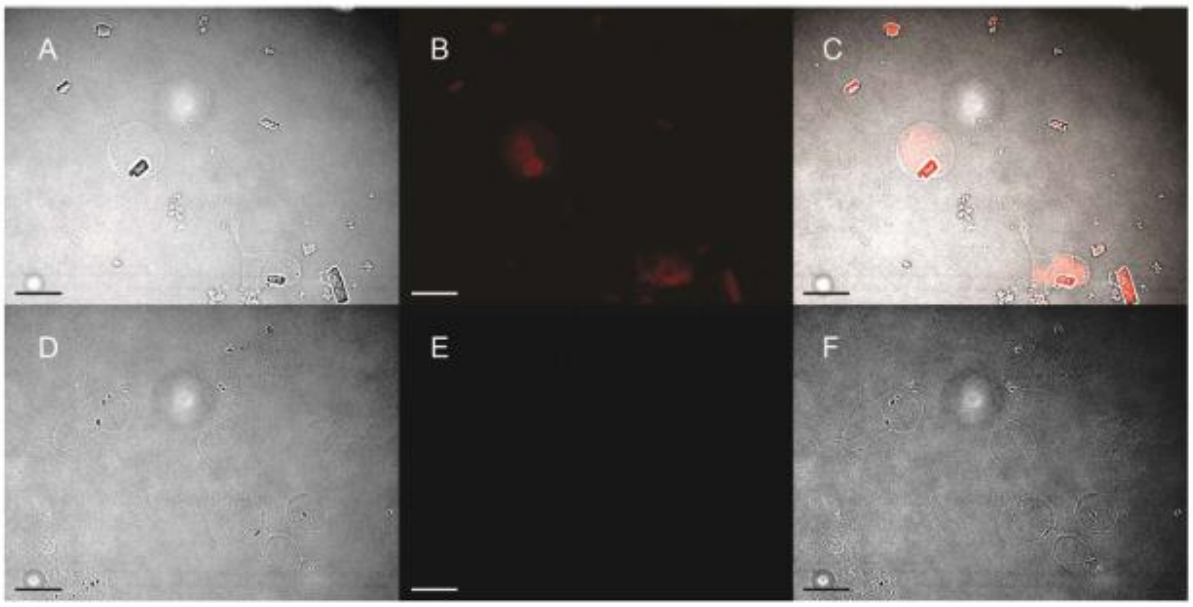

Figure 6.8. Neutrophil phagocytosis of polystyrene nanoparticles. (A–C) Neutrophils incubated with polystyrene nanoparticles. (A) Bright field microscopy of native cells and nanoparticles. (B) Fluorescent microscopy of native cells and nanoparticles, with Texas Red filter (emission 583, exposure time 178 ms). (C) Overlay of images A and B showing phagocytized nanoparticles and aggregates in the cytoplasm of neutrophils. (D–F) Control images, no polystyrene added, with identical microscope and imaging settings. Scale bar= 10 μm

As demonstrated in Figure 6.9, degranulation of primary granules and neutrophil extracellular trap release was increased by the interaction of PC and PS nanoparticles with neutrophils in comparison to the control experiment. Oxidative burst was the less affected function by PS, in contrast to PC nanoparticles. These results clearly shows the stress response of the innate immune system of the fish to polystyrene and polycarbonate nanoplastics.[340]

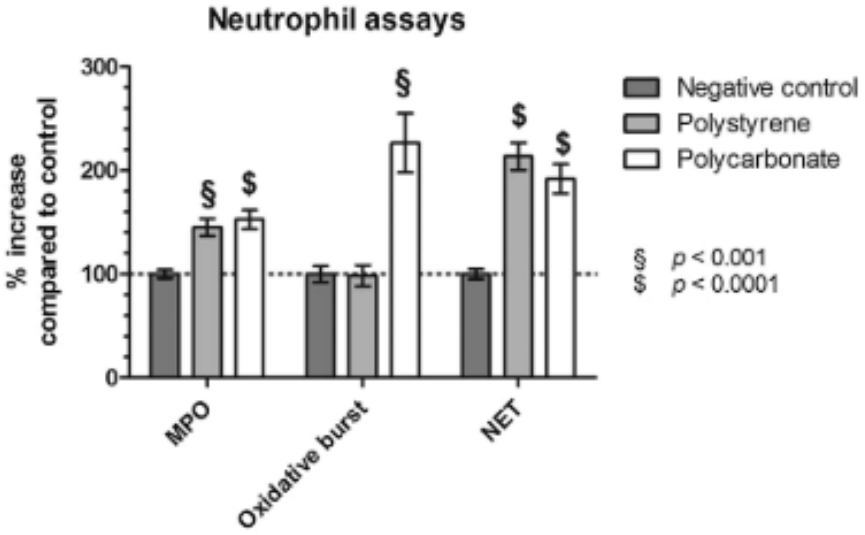

Figure 6.9. Neutrophil response of PS and PC nanoparticles in vitro. PS-NP (grey), PC-NP (white) indicate neutrophil function compared to nontreated control (HBSS+ with calcium, magnesium, no phenol red). MPO: degranulation of neutrophil primary granules measured as myeloperoxidase exocytosis compared to control. Oxidative burst: cumulative production of oxygen radicals compared to control. NET: neutrophil extracellular trap release from fathead minnow neutrophils compared to the negative control

6.3. Conclusion and Outlook

Water pollution due to the increasing amount of plastic litter wasted to the environment is getting a big concern in recent years. Small scale plastic particles can interact directly with the cells in living organisms due to their size and characteristic surface properties and cause toxicity on living organisms in aqueous ecosystems. In order to study the immune system response to plastic nanoparticles in marine species, polystyrene and polycarbonate nanoparticles were generated. Poly(bisphenol A carbonate) were synthesized by condensation polymerization of BPA and triphosgene in nonaqueous emulsion using acetonitrile/cyclohexane solvent couple which was stabilized by PI-*b*-PMMA and PI-*b*-PEO. Spherical particles around 158 nm were obtained as revealed by DLS and SEM measurements. Fluorescently labelled crosslinked polystyrene by styryl-boron-dipyrromethene (BODIPY) dye was prepared by free radical polymerization in water-based emulsion. Particles of around 41 nm were obtained with monomodal distribution as SEM micrographs demonstrated. Additionally, size determination of the PS and PC1 nanoparticles in Fathead minnow plasma was performed and resulted in sizes of around 155 nm and 515 nm, respectively. In the last part of the study, the effect of PS and PC nanoparticles on the innate immune system of Fathead Minnow was investigated via neutrophil function assays by collaboration partner. According to the study, PS and PC nanoparticles activated the neutrophil functions of fish, determined by observing the higher response of degranulation, oxidative burst activity, and neutrophil extracellular trap release. These results clearly show that these nanoparticles can potentially act as stressors for the immune system of this fish species.

The concept of the study can be enlarged by the synthesis of different plastic derivatives by the developed nonaqueous emulsion polymerization technique which is a convenient one pot system for the generation of hydrophobic nanoparticles. By encapsulation of hydrophilic fluorescent probes, cell uptake properties of the PC nanoparticles can also be investigated. The toxicity and immune system response of the plastic additives, studied by the encapsulation of them into mentioned plastic nanoparticles, might be an interesting future research direction. Additionally, in vivo feeding experiments would be the next step to study the effect of the nanoparticles.

6.4. Experimental Part

6.4.1. Materials and Methods

2,2-Bis(4-hydroxyphenyl)propane,4,4′-isopropylidenediphenol (BPA, Bisphenol A>99%), triphosgene, dry pyridine, styrene, divinyl benzene, sodium dodecyl sulfate, potassium persulfate, cyclohexane and acetonitrile were purchased from Sigma Aldrich. Styrene was purified by distillation before the polymerization. Solvents were purified by distillation before use. Styryl boron-dipyrromethene dye (BODIPY) was prepared kindly by Daejune Joe as described in his PhD thesis.[371]

Poly(isoprene-*block*-polymethylmethacrylate) (PI-*b*-PMMA, molecular weight: 65300 g/mol, polydispersity index: 1.09, molar block composition: 47% PI and 53% PMMA (DP_{PI}=311, DP_{PMMA}=351)) and **Poly(ethylene oxide-*block*-polyisoprene)** (PEO-*b*-PI, molecular weight: 45700 g/mol, polydispersity index: 1.06, molar block composition: 55% PI and 45% PEO (DP_{PI}=441, DP_{PEO}=357)) were kindly synthesized by Thomas Wagner and Jürgen Thiel in Butt group.

Characterization of the particles in Fathead minnow plasma was investigated via DLS measurements. Polystyrene (100 µg in 1 mL plasma) and poly(bisphenol A carbonate) particle dispersions (c=0.1 µg/mL) were prepared (exact concentration is not known due to the filtration of precipitation). Solutions were mixed with Fathead minnow plasma and filtered through Millex SV filters with a pore size of 5 mm (Merck Millipore) into dust-free quartz light scattering cuvettes (inner diameter 18 mm; Hellma), which were cleaned before with acetone in a Thurmont apparatus. Light scattering experiments were performed with an ALV-CGS 8 F SLS/ dynamic light scattering 5022F goniometer equipped with 8 simultaneously working ALV 7004 correlators and 8 QEAPD Avalanche photodiode detectors (ALV). A helium–neon laser (632.8 nm, 25mW output power) was utilized as the light source.

In vitro neutrophil assays were conducted as details were described by Greven and Karagöz et al.[340]

6.4.2. Synthesis

Synthesis of poly(bisphenol A carbonate) nanoparticles

PC1 (PI-*b*-PMMA as an emulsifier):

PI-*b*-PMMA (200.00 mg) were placed in a flask, dried under vacuum overnight and degassed with argon. Dry cyclohexane (8.30 mL) was added and stirred for 3 hours at room temperature followed by addition of bisphenol A (609.50 mg, 2.67 mmol in 1 mL of acetonitrile, 2.72 eq.). After addition of water-free pyridine (0.29 mL, 3.59 mmol, 3.66 eq.), dispersion was sonicated for 10 minutes. Triphosgene (291.50 mg, 0.98 mmol in 0.71 mL acetonitrile, 1.00 eq.) was dropwise added (5ml/h) to the emulsion and obtained emulsion was stirred at room temperature for 24 h under inert atmosphere. An aliquot was taken to analyze the particle size and morphology via DLS and SEM. The particles of the remaining emulsion were precipitated in methanol and separated by centrifugation to form of a white solid. Emulsifier was washed out by repeated centrifugation/redispersion in pure cyclohexane. Particles were precipitated by methanol and dried under vacuum for 24 h (**PC1**, 315 mg). Working suspension of poly(bisphenol A carbonate) nanoparticles for *in vitro* study was prepared by dispersing the solid particles in HBSS+.

^{1}H-NMR (δ (ppm) 700 MHz, 298 K, CD_2Cl_2): δ 7.30-7.29 (4 H, Ph), 7.19-7.17 (4 H, Ph), 1.71 (6H) ppm.

GPC (THF as eluent, against PS): M_n=4000 g/mol; Đ= 1.79

PC2 (PI-*b*-PEO as an emulsifier):

The same NAE procedure above was applied by using 200 mg PI-*b*-PEO as stabilizer instead of PI-*b*-PMMA (**PC2**, 260 mg).

^{1}H-NMR (δ (ppm) 700 MHz, 298 K, CD_2Cl_2): δ 7.30-7.29 (4 H, Ph), 7.19-7.17 (4 H, Ph), 1.71 (6H) ppm.

GPC (THF as eluent, against PS): M_n=4000 g/mol; Đ= 1.71

Synthesis of fluorescent polystyrene nanoparticles

Crosslinked polystyrene copolymer with fluorescent styryl-boron-dipyrromethene (BODIPY) dye was synthesized as described in the literature.[371] Sodium dodecyl sulfate (30 mg) was dissolved in 10.5 ml water. Distilled styrene (1.24 mL, 10.00 mmol, 8.20 eq.), divinylbenzene (0.16 g, 1.22 mmol, 1.00 eq.) and styryl boron-dipyrromethene (3.00 mg, 0.0657 mmol, 0.054 eq.) were added and stirred for 30 min. at 600 rpm. The dispersion was degassed with argon and heated at 70°C for one hour. $K_2S_2O_8$ (10.00 mg, 0.034 mmol, 0.034 eq.) was dissolved in 0.7 mL deionized water and added to the emulsion. After 6 h, emulsion was cooled down to room temperature and dialyzed for 3 days against water. (MWCO=25000 Da). Dialyzed emulsion was freeze dried for 24 h to obtain white-pinkish polystyrene nanoparticles as a fluffy solid (**PS**, 0.87 g). Working suspension of poly(styrene) nanoparticles for *in vitro* study was prepared by dispersing the solid particles in HBSS+.

CHAPTER 7

Summary and Outlook

7. Summary and Outlook

The main aim of this dissertation was the design and synthesis of functional polymeric nanocarriers for pharmaceutical applications such as drug delivery and bioimaging. Additionally, another aspect of this research was the investigation of the adverse effects of plastic nanoparticles on marine species. Figure 7.1 presents the overview of achieved nanoparticle systems in this dissertation.

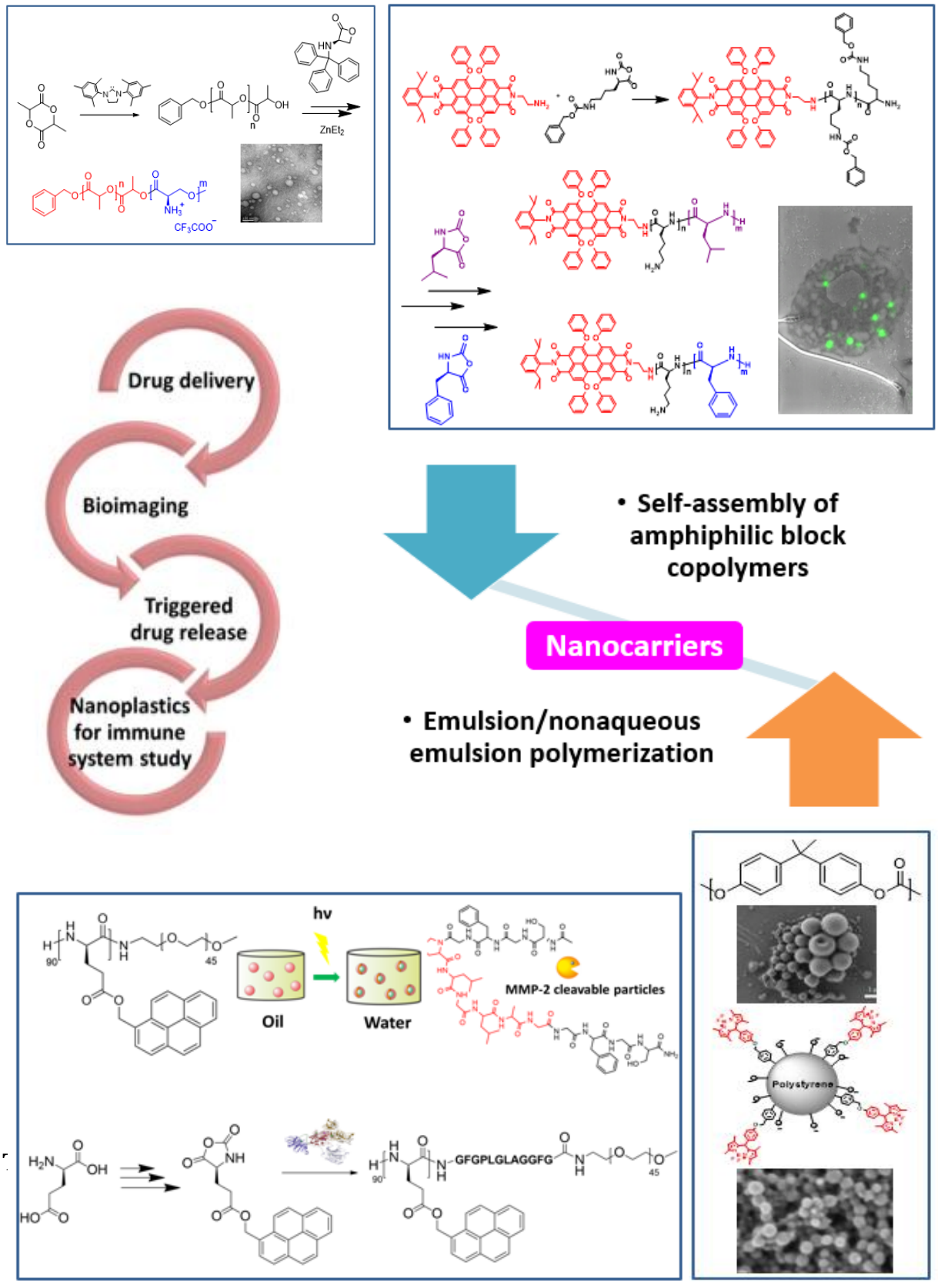

Figure 7.1. Overview of achieved nanocarriers

Biocompatibility and biodegradability are some of the most important issues for the materials used in the pharmaceutical field. These properties, however, have to be combined with a possibility to functionalized by enzymatically or hydrolytically degradable biopolymers such as poly(L-lactide)s, polypseudo(amino acid)s, poly(α-amino acid)s and peptides. Fulfilling certain requirements by such combinations, functional materials for cancer therapy, targeted drug delivery and bioimaging were developed. Nanocarriers were successfully fabricated from these materials either by self-assembly of pre-synthesized amphiphilic block copolymers (Chapter 3 and 5) or emulsion or nonaqueous emulsion polymerization (Chapter 4 and 6) and, their properties were studied.

In particular the development of a new PLLA-based polyester as a promising candidate for drug delivery applications is described (Chapter 3). Biocompatible particles must possess appropriate carrier size within 50 and 250 nm, stable encapsulation of the drug and a hydrophilic corona for sufficient stability in biological medium. Therefore, PLLA was modified by copolymerization with pseudo-poly(amino acid) derivatives, whereby combination of sequential polymerization techniques was presented. Hydroxyl-terminal PLLA with various chain lengths was synthesized by anionic ring-opening polymerization (ROP) of L-lactide catalyzed by SIMes, followed by sequential ROP of N-trityl serine lactone under the catalysis of organometallic $ZnEt_2$ in the presence of PLLA macro-initiators. Cleavage of the protecting groups led to the formation of amphiphilic and amino-functional poly(L-lactide)-*b*-poly(L-serine lactone) (PLLA-*b*-PLSL). Obtained AB type diblock copolymers were processed by dialysis method to prepare micellar solutions. Resulted particles were characterized by DLS and fluorescence spectroscopy in order to determine the CMC. Formation of hierarchically assembled spherical and long tube shape structures were investigated by TEM measurements. Biocompatibility was likely achieved as cell viability studies confirmed. Spherical and long tube shape micelles of PLLA-*b*-PLSL, with a diameter of around 100-200 nm, fulfill all necessary properties to consider the particles as-suitable drug delivery vehicles. The hydrophilic surface of the particles due to the amine groups is important for increasing the blood circulation time and cell uptake properties of the materials *in vivo*. In this context, PLLA-*b*-PLSL block copolymers have further advantages in terms of modification opportunities *via* reactive amine groups. This approach offers now the possibility for the modification of the biodegradable polymer with biologically active small molecules like vitamins, curcumin,

selegiline, carbohydrates, peptides or proteins, antibodies, aptamers, etc for targeted drug delivery applications.

In Chapter 4, polymerization of L-lactide *via* bifunctional peptides was achieved to yield polylactide-*b*-peptide-*b*-polylactide triblock copolymer nanoparticles in the presence of moisture sensitive SIMes catalyst in a single step. Nonaqueous emulsion polymerization was employed as one of the such techniques to generate the nanoparticles in one pot in the presence of moisture sensitive species. The peptide which is an MMP-2 enzyme-cleavable sequence was able to initiate the polymerization of L-Lactide by means of terminal hydroxyl groups. The enzyme MMP-2 is overexpressed in tumor tissue, where it can cleave the particles and release the encapsulated drug. Due to this special peptide sequence in the middle of the polymer chain, cargo release was studied by means of bioresponsivity of the system. During the nanoparticle fabrication, a photo-labile and biocompatible PEG-*b*-PGlu(Pyr) block copolymer was employed as an emulsifier and resulting particles were transferred into aqueous medium by UV-induced cleavage reaction. Both dye and drug loaded particles were also prepared with scrambled peptide sequence as control experiments. When incubated with MMP-2, particles based on the regular peptide sequence showed remarkable dye release. On the contrary, particles having a scrambled sequence that is not enzymatically recognized showed no cargo release. One step further, drug loaded ones were incubated in cancer cells, however, no cytotoxicity was observed.

In order to achieve successful drug release in cancer cells, enzyme cleavable emulsifier can be designed by incorporation of enzyme sensitive peptide sequence. By that strategy, nanoparticle surface will be in direct contact with the enzyme medium, which can increase the bioresponsivity of the system. Therefore, in the second part of this chapter, the successful synthesis of photocleavable monomer and its diblock and terblock copolymers was demonstrated. Previous synthesis of photocleavable emulsifiers was achieved by a post-polymerization modification approach, which was challenging due to the harsh reaction conditions during repeated protection/deprotection and purification steps. Therefore, this route cannot be applied in the presence of sensitive initiators. Herein, a photocleavable monomer, pyrene-Glu-NCA, was developed to use directly as a functional monomer for NCA polymerization. Copolymerization of the new functional monomer with a PEG-NH_2 macro-initiator was studied in order to optimize the polymerization conditions. Obtained block copolymer was able to stabilize the

nonaqueous emulsion, and resulted in the formation of spherical particles. In order to achieve enzyme degradable block copolymers, a new MMP-2 cleavable macro-initiator PEG-GFGPLGLAGGFG-NH_2 conjugate was synthesized and used for the polymerization of pyrene-Glu-NCA. Thus, enzyme and photo-cleavable bioresponsive smart block copolymers were developed successfully.

In the future, investigation of the self-assembly of this polymer is necessary to understand the stimuli responsive nature of the material. Nonaqueous emulsion polymerization can be used as a platform for the preparation of enzyme-degradable core-shell nanoparticles followed by UV irradiation to transfer the particles into aqueous phase. After the hydrophilization, the system is ready for the investigation of triggered release for cancer therapy. Polymers used as emulsifiers can be varied to nonionic or cationic polypeptides. Poly(L-lysine) or poly(L-serine) block copolymer derivatives can be used, which might increase the cell uptake properties in order to obtain a more efficient drug delivery system. Peptides used within the existing system can be varied to address different diseases. Moreover, covalently drug modified block copolymers can also be designed to lower multi-drug resistance. Apart from the organic particles, the application shall be extended to inorganic nanoparticles for example -SH based block copolymers can be used for the stabilization of gold nanoparticles, etc. To conclude, this approach allows making the tailor-made designs for various nanoparticle synthesis.

In Chapter 5, the production of covalently fluorescence-labeled, pH-sensitive polypeptide sensors and drug-nanocarriers was demonstrated for nanoparticle tracking and bioimaging studies. Within this project, C-terminal modification of homo- and block copolypeptides with a fluorescence label was described based on sequential ROP of amino acid NCAs. Thus, highly photo- and chemically stable amino functional N-(2,6-diisopropylphenyl)-N'-(4-aminoethyl)-1,6,7,12-tetraphenoxyperylene-3,4:9,10-tetracarboxydiimide (PDI-NH_2) was synthesized as a fluorescent initiator, which was successsfully utilized for the ROP of of L-lysine NCA. The cleavage of protecting groups led to the formation of water-soluble PDI-derivatives. The aggregation behavior of the amphiphile was characterized by DLS. The pH-induced folding behavior of the polypeptide was studied by means of optoelectronic properties, whereby correlation of UV-*vis*, Fluorescence and Circular Dichroism spectroscopy was studied. The successful cell visualization of the particles in biological medium by CLSM was achieved, whereas

the biocompatibility of the poly(L-lysine) was increased by incorporation of PDI, as cell experiments revealed. These fluorescent homopolymers show good water solubility, high fluorescence quantum yield and photostability and therefore might be of interest as pH sensor for monitoring pH fluctuations in living systems. Additionally, double end group-functionalized polypeptides can be used as linkers between different systems. The distance between separated moieties changes by pH stimuli. For example, FRET systems can be studied by that design, i.e one side PDI-modified polymer can be further modified by TDI at the N-terminus or inorganic nanoparticles (gold or iron etc.) can be incorporated in fluorescent systems. In the second part of this chapter, the synthesis of fluorescent block copolymer and their self-assembly were studied for the preparation of non-toxic nanocarriers with improved aggregation properties for drug delivery and bioimaging studies. The previously synthesized fluorescent PDI-poly(Cbz-L-lysine) homopolymers were used as macro-initiators for the polymerization of L-leucine and L-phenylalanine NCA, respectively. Further deprotection led to the formation of amphiphilic PDI-poly(L-lysine)-*b*-poly(L-leucine) and PDI-poly(L-lysine)-*b*-poly(L-phenylalanine) structures. Block copolymer micelles were prepared in water and resulting aggregates were characterized as fibrillated wormlike micelles in various lengths between 50-100 nm long by TEM measurements. In the final part of the study, biocompatibility of the wormlike fibrillated nanocontainers of both PDI-Poly(L-lysine)-*b*-poly(L-leucine) and PDI-Poly(L-lysine)-*b*-poly(L-phenylalanine) copolymers was demonstrated. In comparison to PDI-poly(L-lysine) homopolymer which only showed a biocompatibility of 20%, both block copolymers were more than 85% biocompatible. Finally, the potential of the fluorescent micelles for bioimaging applications was evaluated by CLSM. As a representative example, successful internalization of the fluorescent PDI-poly(L-lysine)-*b*-poly(L-phenylalanine) copolymer micelles into cell boundaries was detected by the correlation of SEM and TEM with CLSM, staining of the whole cells were observed.

In the future, a detailed investigation of the influence of the different block lengths and compositions of the block copolymers is suggested, as these have a major influence on self-organization. For this purpose, a library of diblock copolymers with varying block lengths and volume fractions should be prepared and the respective phase behavior could be studied. Further functionalization of the block copolymers *via* anchor amine groups of the poly(L-lysine) with biologically active molecules like vitamins, carbohydrates, peptides or proteins like CPPs or a special enzyme cleavable peptide sequences for

example MMP type etc. makes the materials potential for active targeted delivery and extend the application area for different diseases. On the ROP side, amino acids can be varied which allows the formation of micelles with different morphologies. This approach can also extend on graft copolymers by using the amine functionality on the side chain of the poly(L-Lysine). Furthermore, combination of PLLA and polypeptide block copolymers can lead to the formation of biocompatible nanocarriers to avoid folding and insolubility of the polypeptides.

In the last project, well-defined polycarbonate and polystyrene nanoparticles were prepared for the investigation of nanoplastics on Fathead Minnow immune system (Chapter 6). On one hand, poly(bisphenol A) particles were prepared by polymerization of bisphenol A and triphosgene *via* versatile nonaqueous emulsion platform. The polymerization was conducted by using different emulsifiers i.e PEG-*b*-PMMA and PEG-*b*-PI, respectively. Particle morphology was difficult to control due to the harsh reaction conditions, however, successful spherical nanoparticle formation was achieved. On the other hand, crosslinked polystyrene nanoparticles were generated by copolymerization with a Bodipy-modified styrene monomer *via* emulsion polymerization. Well-defined fluorescent polystyrene nanocarriers were obtained by the stabilization with SDS. These nanoplastics were subsequently applied for the investigation of immune system stress of fathead minnow in marine environment. Both PS and PC nanoparticles led to higher response of degranulation, oxidative burst activity, and neutrophil extracellular trap release, demonstrating the stress on the immune system of the fish species. In further research, bioimaging techniques can be used for the visualization of fluorescent polystyrene nanoparticles *in vivo*. Additionally, hydrophilic cargo molecules: dyes, drugs etc. can be encapsulated into polycarbonate nanoparticles via nonaqueous emulsion system in order to track the nanoparticles *in vivo*, to achieve a more specific investigation of health hazards of these pollutants on marine species.

CHAPTER 8

General Experimental Part

8. General Experimental Part

8.1. General Experimental Techniques

All work was done by the standard schlenk techniques or in the glovebox. 0 ˚C polymerizations for longer reaction times were performed with cryostat from Huber GmbH. Emulsion or homogenization was performed with a Brandelin Sonorex RK255H-W640 sonifier. Dialysis was performed using the membranes purchased from Spectrum Labs.

8.2. Instrumental Methods

8.2.1. Nuclear Magnetic Resonance Spectroscopy (NMR)

All the NMR spectra were recorded in the listed deuterated solvents using Bruker Avance III spectrometer operating at 300, 500 or 700 MHz. Block copolymer formation was investigated *via* diffusion ordered spectroscopy (DOSY). DOSY experiments were performed with a 5 mm BBI 1H/X z-gradient probe and a gradient strength of 5.516 [G/mm] on the 500 or 700 MHz spectrometer.

8.2.2. Gel Permeation Chromatography (GPC)

MZ gel columns SDplus 10e6, 10e4 and 500 were used for the GPC measurements. Determination of the relative molecular weights and the molecular weight distributions were carried out at a concentration of 1-2 mg/mL in THF or DMF as eluent (flow rate is 1 mL/min) *vs.* PEO or PS standards using refractive index and UV detectors from Waters, ERC, Rheodyne and Soma.

8.2.3. Infrared Spectroscopy (FT-IR)

Fourier Transform IR spectra were recorded on a Nicolet 730 spectrometer and a Spectrum BX from Perkin Elmer. Systems were equipped with a single-reflection ATR-IR probe head (ATR: Attenuated Total Reflection) from Thermo- Spectra-Tech. Samples

were applied to the crystal as a solid and measured using a He/Ne source with an emission wavelength of 633 nm as the laser.

8.2.4. Mass Spectrometry

FD mass spectra were measured with a VG Instruments ZAB 2-SE-FPD spectrometer. Matrix Assisted Laser Desorption/Ionization-Time of Flight (MALDI-TOF) MS was performed on a Bruker Reflex II TOF spectrometer with a 337 nm laser. 5 µL of the sample solution (c ≈ 1 mg/mL) and 15 µL of a saturated matrix solution (1,8-dihydroxy-10H-anthracene-9-one (dithranol) or tetracyanoquinodimethane (TCNQ)) was mixed and about 1 µL was applied to the sample carrier.

8.2.5. Thermal Analysis (TGA and DSC)

The thermal characterization of the polymers was performed by differential scanning calorimetry (DSC) and thermogravimetric analysis (TGA) on the devices DSC-822 and TGA-851 from Mettler Toledo. The measurements were carried out in each case under an N_2 atmosphere and, at a heating and cooling rate of 10 °C/min. Decomposition temperature (T_d) was determined from TGA curve from the inflection point of the mass loss, melting points (T_m) and glass transition temperatures (T_g) were determined by peak analysis of second heating curves of DSC.

8.2.6. Electron Microscopy (SEM and TEM)

Scanning electron microscopy (SEM) was performed with a Gemini 1530 microscope from Zeiss at an acceleration voltage of 100 kV. The samples were dropped from dilute dispersion on a Si-wafer. For transmission electron microscopy (TEM) images, a Tecnai F20 microscope from FEI was used with an acceleration voltage of 80-200 kV. Sample preparation was carried out by negative staining of the micelles with 5 wt % uranylacetate in trehalose and dropping the sample solution onto the carbon grid, followed by air-drying.

8.2.7. High Performance Liquid Chromatography (HPLC)

HPLC was performed by an Agilent Technologies Series 1200 instrument with a Rheodyne 7725i injection valve and Varian's ELSD Detector 385-LC.

8.2.8. Dynamic Light Scattering (DLS)

Dynamic light scattering (DLS) measurements were performed on a Malvern Zetasizer 3000 with a fixed scattering angle of 90° and on an ALV/LSE-5004-correlator using a He/Ne-laser operating at 632.8 nm.

8.2.9. UV-*vis* and Fluorescence Spectroscopy

UV-*vis* spectroscopy was performed on a Perkin- Elmer Lambda 100 spectrophotometer at room temperature in solution. Solution fluorescence spectra were recorded on a SPEX-Fluorolog II (212) spectrometer at room temperature.

8.2.10. Circular Dichroism Spectroscopy (CD)

Circular Dichroism spectroscopy (CD) was performed on JASCO J-1100 CD spectrometer at room temperature in water solution with various pH.

8.2.11. X-ray Diffraction (XRD)

XRD was employed to identify the liquid crystalline phases of the assemblies. Measurements were done in transmission geometry at a home build instrument using a rotating anode x-ray generator (Rigaku MicroMax 007), multilayer optics (Osmic Confocal Max-Flux, Cu Kα). Samples were contained in 1.5 mm glass capillaries and placed in a holder. A magnetic field was applied perpendicular to the x-ray beam to orient the sample in the discotic nematic phase. 2D diffraction pattern was recorded on an online image plate detector (Mar345) at a sample-detector distance of 35 cm. Diffraction patterns I vs. 2θ were obtained by radial averaging the 2D data.

8.2.12. Confocal Laser Scanning Microscopy (CLSM)

Confocal laser scanning fluorescence microscopy (CLSFM) was performed with Leica TCS SP5 (Germany, Wetzlar) using a 63X NA1.2 water immersion objective and with Leica TCS SP8 (Germany, Wetzlar) using a 20X dry objective (HC PL APO CS2 20x/0.75 DRY, Leica). LSCFM is a non-destructive method and can be simply employed by either staining an object with a dye or using a chemically modified dye to an object.

8.2.13. Fluorescence Correlation Spectroscopy (FCS)

Fluorescence Correlation Spectroscopy was performed with a commercial FCS setup (Carl Zeiss, Germany) consisting of the module ConfoCor 2 and an inverted microscope model Axiovert 200. The fluorophores were excited by the 580 nm line of an Argon laser and emission was collected.

References

9. References

1. Hubbell, J. A. Biomaterials in Tissue Engineering. *Bio/Technology* **13**, 565 (1995).
2. Langer, R. Biomaterials in Drug Delivery and Tissue Engineering: One Laboratory's Experience. *Acc. Chem. Res.* **33**, 94–101 (2000).
3. Nair, L. S. & Laurencin, C. T. Biodegradable polymers as biomaterials. *Prog. Polym. Sci.* **32**, 762–798 (2007).
4. Rodrigo-Navarro, A., Sankaran, S., Dalby, M. J., del Campo, A. & Salmeron-Sanchez, M. Engineered living biomaterials. *Nat. Rev. Mater.* **6**, 1175–1190 (2021).
5. Rao, D. A., Nguyen, D. X., Mishra, G. P., Doddapaneni, B. S. & Alani, A. W. G. Preparation and Characterization of Individual and Multi-drug Loaded Physically Entrapped Polymeric Micelles. *J. Vis. Exp.* **1800**, 1–5 (2015).
6. Deng, C. *et al.* A biodegradable triblock copolymer poly(ethylene glycol)-b-poly(l-lactide)-b-poly(l-lysine): Synthesis, self-assembly, and RGD peptide modification. *Polymer (Guildf).* **48**, 139–149 (2007).
7. Fuoco, T., Finne-Wistrand, A. & Pappalardo, D. A Route to Aliphatic Poly(ester)s with Thiol Pendant Groups: From Monomer Design to Editable Porous Scaffolds. *Biomacromolecules* **17**, 1383–1394 (2016).
8. Chanthaset, N. & Ajiro, H. Synthetic Biodegradable Polymers with Chain End Modification: Polylactide, Poly(butylene succinate), and Poly(hydroxyalkanoate). *Chem. Lett.* **50**, 767–777 (2020).
9. Jana, P., Shyam, M., Singh, S., Jayaprakash, V. & Dev, A. Biodegradable polymers in drug delivery and oral vaccination. *Eur. Polym. J.* **142**, 110155 (2021).
10. https://www.marketsandmarkets.com/Market-Reports/biomaterials-393.html. (2020).
11. Williams D. F. *The Williams Dictionary of Biomaterials*. (Liverpool University Press, 1999). doi:10.5949/UPO9781846314438.
12. Ratner, B. D., Hoffman, A. S., Schoen, F. J. & Lemons, J. E. *Biomaterials Science: An Introduction to Materials in Medicine*. *Elsevier Academic Press* (2004). doi:10.1017/CBO9781107415324.004.
13. Vert, M. Aliphatic Polyesters: Great Degradable Polymers That Cannot Do Everything. *Biomacromolecules* **6**, 538–546 (2005).

14. Tamada, J. A. & Langer, R. Erosion kinetics of hydrolytically degradable polymers. *Proc. Natl. Acad. Sci. U. S. A.* **90**, 552–556 (1993).
15. AU - McCall, R. L. & AU - Sirianni, R. W. PLGA Nanoparticles Formed by Single- or Double-emulsion with Vitamin E-TPGS. *JoVE* e51015 (2013) doi:doi:10.3791/51015.
16. Uhrich, K. E., Cannizzaro, S. M., Langer, R. S. & Shakesheff, K. M. Polymeric systems for controlled drug release. *Chem. Rev.* **99**, 3181–98 (1999).
17. Gunatillake, P. A., Adhikari, R. & Gadegaard, N. Biodegradable synthetic polymers for tissue engineering. *Eur. Cells Mater.* **5**, 1–16 (2003).
18. De Jong, W. H. & Borm, P. J. a. Drug delivery and nanoparticles:applications and hazards. *Int. J. Nanomedicine* **3**, 133–149 (2008).
19. Olson, E. S. *et al.* Activatable cell penetrating peptides linked to nanoparticles as dual probes for in vivo fluorescence and MR imaging of proteases. *Proc. Natl. Acad. Sci. U. S. A.* **107**, 4311–4316 (2010).
20. Matsumura, S., Aoki, I., Saga, T. & Shiba, K. A Tumor-Environment-Responsive Nanocarrier That Evolves Its Surface Properties upon Sensing Matrix Metalloproteinase-2 and Initiates Agglomeration to Enhance T2 Relaxivity for Magnetic Resonance Imaging. *Mol. Pharm.* **8**, 1970–1974 (2011).
21. Kareem, M. M. & Tanner, K. E. Methods of producing three dimensional electrospun scaffolds for bone tissue engineering: A review. *Proc. Inst. Mech. Eng. Part H J. Eng. Med.* 09544119211069463 (2022) doi:10.1177/09544119211069463.
22. Luo, Y., Zhang, T. & Lin, X. 3D printed hydrogel scaffolds with macro pores and interconnected microchannel networks for tissue engineering vascularization. *Chem. Eng. J.* **430**, 132926 (2022).
23. Kricheldorf, H. R. Syntheses and application of polylactides. *Chemosphere* **43**, 49–54 (2001).
24. Hurrell, S. & Cameron, R. E. Polyglycolide: Degradation and drug release. Part I: Changes in morphology during degradation. *J. Mater. Sci. Mater. Med.* **12**, 811–816 (2001).
25. Dechy-Cabaret, O., Martin-Vaca, B. & Bourissou, D. Controlled Ring-Opening Polymerization of Lactide and Glycolide. *Chem. Rev.* **104**, 6147–6176 (2004).
26. Dinarvand, R., Sepehri, N., Manoochehri, S., Rouhani, H. & Atyabi, F. Polylactide-co-

glycolide nanoparticles for controlled delivery of anticancer agents. *Int. J. Nanomedicine* **6**, 877–895 (2011).

27. Kamber, N. E., Jeong, W., Gonzalez, S., Hedrick, J. L. & Waymouth, R. M. N-Heterocyclic Carbenes for the Organocatalytic Ring-Opening Polymerization of ε-Caprolactone. *Macromolecules* **42**, 1634–1639 (2009).
28. Lu, J., Tappel, R. C. & Nomura, C. T. Mini-Review: Biosynthesis of Poly(hydroxyalkanoates). *Polym. Rev.* **49**, 226–248 (2009).
29. Ray, J. A., Doddi, N., Regula, D., Williams, J. A. & Melveger, A. Polydioxanone (PDS), a novel monofilament synthetic absorbable suture. *Surg. Gynecol. Obstet.* **153**, 497–507 (1981).
30. Pospiech, D. *et al.* Multiblock copolymers of L-lactide and trimethylene carbonate. *Biomacromolecules* **6**, 439–446 (2005).
31. Kwon, H. Y. & Langer, R. Pseudopoly (amino acids): A Study of the Synthesis and Characterization of Poly(trans-4-hydroxy-N-acyl-L-proline esters). *Macromolecules* **22**, 3250–3255 (1989).
32. Kohn, J. New Biomaterials: The Preparation of Polyesters Derived from Hydroxy Amino acids. in *Cosmetic and Pharmaceutical Applications of Polymers* 321–327 (1991).
33. Pulapura Satish & Kohn Joachim. Tyrosine-Derived Polycarbonates: Backbone-Modified "Pseudo"-Poly (Amino Acids) Designed for Biomedical Applications. *Biopolymers* **32**, 411–417 (1992).
34. Zhou, Q. & Kohn, J. Preparation of Poly(L-serine ester): A Structural Analogue of Conventional Poly(L-serine). *Macromolecules* **23**, 3399–3406 (1990).
35. Fiétier, I., Le Borgne, A. & Spassky, N. Synthesis of functional polyesters derived from serine. *Polym. Bull.* **24**, 349–353 (1990).
36. Vasiljevic, L. & Pavlović, S. Biodegradable Polymers Based on Proteins and Carbohydrates BT - Advances in Applications of Industrial Biomaterials. in (eds. Pellicer, E. et al.) 87–101 (Springer International Publishing, 2017). doi:10.1007/978-3-319-62767-0_5.
37. Cheng, J. & Deming, T. J. Synthesis of Polypeptides by Ring-Opening Polymerization of a-Amino Acid N-Carboxyanhydrides. *Top Curr Chem* (2011) doi:10.1007/128_2011_173.
38. Habraken, G. J. M., Peeters, M., Dietz, C. H. J. T., Koning, C. E. & Heise, A. How

controlled and versatile is N-carboxy anhydride (NCA) polymerization at 0 °C? Effect of temperature on homo-, block- and graft (co)polymerization. *Polym. Chem.* **1**, 514 (2010).

39. Dorresteijn, R., Billecke, N., Parekh, S. H., Klapper, M. & Müllen, K. Polarity reversal of nanoparticle surfaces by the use of light-sensitive polymeric emulsifiers. *J. Polym. Sci. Part A Polym. Chem.* **53**, 200–205 (2015).
40. Han, S. *et al.* Efficient delivery of antitumor drug to the nuclei of tumor cells by amphiphilic biodegradable poly(L -Aspartic Acid-co-Lactic Acid)/DPPE co-polymer nanoparticles. *Small* **8**, 1596–1606 (2012).
41. Lee, H., Park, J. B. & Chang, J. Y. Synthesis of poly(ethylene glycol)/polypeptide/poly(D,L-lactide) copolymers and their nanoparticles. *J. Polym. Sci. Part A Polym. Chem.* **49**, 2859–2865 (2011).
42. Smeets, N. M. B., Weide, P. L. J. Van Der, Meuldijk, J., Vekemans, J. a J. M. & Hulshof, L. a. A Scalable Synthesis of L -Leucine-N-carboxyanhydride Abstract : *Org. Process Res. Dev.* **9**, 757–763 (2005).
43. Choi, Y.-R. *et al.* Development of polymeric gene delivery carriers: PEGylated copolymers of L-lysine and L-phenylalanine. *J. Drug Target.* **15**, 391–398 (2007).
44. Rasal, R. M., Janorkar, A. V. & Hirt, D. E. Poly(lactic acid) modifications. *Prog. Polym. Sci.* **35**, 338–356 (2010).
45. Gupta, A. P. & Kumar, V. New emerging trends in synthetic biodegradable polymers - Polylactide: A critique. *Eur. Polym. J.* **43**, 4053–4074 (2007).
46. Mehta, R., Kumar, V., Bhunia, H. & Upadhyay, S. N. Synthesis of poly(lactic acid): A review. *J. Macromol. Sci. - Polym. Rev.* **45**, 325–349 (2005).
47. Balla, E. *et al.* Poly(lactic Acid): A Versatile Biobased Polymer for the Future with Multifunctional Properties—From Monomer Synthesis, Polymerization Techniques and Molecular Weight Increase to PLA Applications. *Polymers (Basel).* **13**, (2021).
48. H. Benninga. *A History of Lactic acid Making*. (Springer, 1990).
49. Carothers, W. H., Dorough, G. L. & Natta, F. J. van. Studies of Polymerization and Ring Formation. X. The Reversible Polymerization of Six-membered Cyclic Esters. *J. Am. Chem. Soc.* **54**, 761–772 (1932).
50. Garlotta, D. A Literature Review of Poly(Lactic Acid). *J. Polym. Environ.* **9**, 63–84 (2001).

51. Danhier, F. *et al.* PLGA-based nanoparticles: An overview of biomedical applications. *J. Control. Release* **161**, 505–522 (2012).
52. Liang, H.-F. *et al.* Paclitaxel-loaded poly(γ-glutamic acid)-poly(lactide) nanoparticles as a targeted drug delivery system against cultured HepG2 cells. *Bioconjug. Chem.* **17**, 291–9 (2006).
53. Vlachopoulos, A. *et al.* Poly(Lactic Acid)-Based Microparticles for Drug Delivery Applications: An Overview of Recent Advances. *Pharmaceutics* vol. 14 (2022).
54. Alam, F., Varadarajan, K. M. & Kumar, S. 3D printed polylactic acid nanocomposite scaffolds for tissue engineering applications. *Polym. Test.* **81**, 106203 (2020).
55. Chandy, T., Das, G. S., Wilson, R. F. & Rao, G. H. R. Development of polylactide microspheres for protein encapsulation and delivery. *J. Appl. Polym. Sci.* **86**, 1285–1295 (2002).
56. Roether, J. A. *et al.* Development and in vitro characterisation of novel bioresorbable and bioactive composite materials based on polylactide foams and Bioglass for tissue engineering applications. *Biomaterials* **23**, 3871–3878 (2002).
57. Masutani, K. & Kimura, Y. PLA Synthesis. From the Monomer to the Polymer. in *Poly(lactic acid) Science and Technology: Processing, Properties, Additives and Applications* 1–36 (2015). doi:10.1039/9781782624806-00001.
58. Moon, S.-I., Lee, C.-W., Taniguchi, I., Miyamoto, M. & Kimura, Y. Melt/solid polycondensation of l-lactic acid: an alternative route to poly(l-lactic acid) with high molecular weight. *Polymer (Guildf).* **42**, 5059–5062 (2001).
59. Zhong, W. *et al.* Study on biodegradable polymer materials based on poly(lactic acid). I. Chain extending of low molecular weight poly(lactic acid) with methylenediphenyl diisocyanate - ResearchGate. *J. Appl. Polym. Sci.* **74**, 2546–2551 (1999).
60. Södergård, A. & Stolt, M. Properties of lactic acid based polymers and their correlation with composition. *Prog. Polym. Sci.* **27**, 1123–1163 (2002).
61. Xiao, L., Wang, B., Yang, G., Gauthier, M. & Lin Xiao, Bo Wang, Guang Yang, M. G. Poly (Lactic Acid)-Based Biomaterials : Synthesis , Modification and Applications. in *Biomedical Science, Engineering and Technology* 249–283 (2012). doi:10.5772/23927.
62. Kricheldorf, H. R. Syntheses and application of polylactides. *Chemosphere* **43**, 49–54 (2001).

63. Kricheldorf, H. R. & Kreiser-Saunders, I. Polylactones, 19. Anionic polymerization of L-lactide in solution. *Die Makromol. Chemie* **191**, 1057–1066 (1990).
64. Penczek, S. & Slomkowski, S. Progress in Anionic Ring-Opening Polymerization. in *Recent Advances in Anionic Polymerization* (eds. Hogen-Esch, T. E. & Smid, J.) 275–295 (Springer Netherlands, 1987).
65. Bourissou, D., Martin-Vaca, B., Dumitrescu, A., Graullier, M. & Lacombe, F. Controlled Cationic Polymerization of Lactide. *Macromolecules* **38**, 9993–9998 (2005).
66. Mecerreyes, D., Jérôme, R. & Dubois, P. Novel Macromolecular Architectures Based on Aliphatic Polyesters: Relevance of the "Coordination-Insertion" Ring-Opening Polymerization BT - Macromolecular Architectures. in (eds. Hilborn, J. G. et al.) 1–59 (Springer Berlin Heidelberg, 1999). doi:10.1007/3-540-49196-1_1.
67. Gerhardt, W. W. *et al.* Functional lactide monomers: Methodology and polymerization. *Biomacromolecules* **7**, 1735–1742 (2006).
68. Kowalski, A., Duda, A. & Penczek, S. Polymerization of l,l-Lactide Initiated by Aluminum Isopropoxide Trimer or Tetramer. *Macromolecules* **31**, 2114–2122 (1998).
69. Deming, T. J. Preparation and development of block copolypeptide vesicles and hydrogels for biological and medical applications. *Wiley Interdiscip. Rev. Nanomedicine Nanobiotechnology* **6**, 283–297 (2014).
70. Deng, C. *et al.* Functional polypeptide and hybrid materials: Precision synthesis via α-amino acid N-carboxyanhydride polymerization and emerging biomedical applications. *Prog. Polym. Sci.* **39**, 330–364 (2014).
71. Huang, J. & Heise, A. Stimuli responsive synthetic polypeptides derived from N-carboxyanhydride (NCA) polymerisation. *Chem. Soc. Rev.* **42**, 7373–90 (2013).
72. Boddu, S. H. S. *et al.* Polyamide/Poly(Amino Acid) Polymers for Drug Delivery. *Journal of Functional Biomaterials* vol. 12 (2021).
73. Wang, T.-T., Xia, Y.-Y., Gao, J.-Q., Xu, D.-H. & Han, M. Recent Progress in the Design and Medical Application of In Situ Self-Assembled Polypeptide Materials. *Pharmaceutics* vol. 13 (2021).
74. Wu, L., Shimada, N., Kano, A. & Maruyama, A. Poly(l-lysine)-graft-dextran copolymer accelerates DNA hybridization by two orders. *Soft Matter* **4**, 744 (2008).

75. Hadjichristidis, N., Iatrou, H., Pitsikalis, M. & Sakellariou, G. Synthesis of well-defined polypeptide-based materials via the ring-opening polymerization of a-amino acid N-carboxyanhydrides. *Chem. Rev.* **109**, 5528–5578 (2009).
76. Oh, J. K. Polylactide (PLA)-based amphiphilic block copolymers: synthesis, self-assembly, and biomedical applications. *Soft Matter* **7**, 5096–5108 (2011).
77. Vlakh, E. G. *et al.* Self-assemble nanoparticles based on polypeptides containing C-terminal luminescent Pt-cysteine complex. *Sci. Rep.* **7**, 41991 (2017).
78. Duncan, R. Polymer conjugates as anticancer nanomedicines. *Nat. Rev. Cancer* **6**, 688–701 (2006).
79. Ulijn, R. V. Enzyme-responsive materials: a new class of smart biomaterials. *J. Mater. Chem.* **16**, 2217 (2006).
80. Dorresteijn, R. *et al.* Polylactide-block-polypeptide-block-polylactide copolymer nanoparticles with tunable cleavage and controlled drug release. *Adv. Funct. Mater.* **24**, 4026–4033 (2014).
81. *Biochemistry*. *Biochemical Education* vol. 23 (John Wiley & Sons, Ltd, 1995).
82. Huang, Y. *et al.* PH-triggered charge-reversal polypeptide nanoparticles for cisplatin delivery: Preparation and in vitro evaluation. *Biomacromolecules* **14**, 2023–2032 (2013).
83. Soppimath, K. S. *et al.* Multifunctional Core/Shell Nanoparticles Self-Assembled from pH-Induced Thermosensitive Polymers for Targeted Intracellular Anticancer Drug Delivery. *Adv. Funct. Mater.* **17**, 355–362 (2007).
84. Perin, F., Motta, A. & Maniglio, D. Amphiphilic copolymers in biomedical applications: Synthesis routes and property control. *Mater. Sci. Eng. C* **123**, 111952 (2021).
85. Klemm, P. *et al.* Self-assembled PEGylated amphiphilic polypeptides for gene transfection. *J. Mater. Chem. B* **9**, 8224–8236 (2021).
86. Merrifield, R. B. Solid Phase Peptide Synthesis. I. The Synthesis of a Tetrapeptide. *J. Am. Chem. Soc.* **85**, 2149–2154 (1963).
87. Sekiguchi, H. MECHANISM OF N-CARBOXY-α-AMINO ACID ANHYDRIDE (NCA) POLYMERIZATION. *Pure Appl. Chem.* **53**, 1689–1714 (1981).
88. Deming, T. J. Polypeptide and polypeptide hybrid copolymer synthesis via NCA polymerization. *Adv. Polym. Sci.* **202**, 1–18 (2006).
89. Kricheldorf, H. R. *α-Aminoacid-N-Carboxy-Anhydrides and Related Heterocycles:*

Syntheses, Properties, Peptide Synthesis, Polymerization. (Springer-Verlag Berlin Heidelberg, 1987). doi:10.1007/978-3-642-71586-0.

90. Gupta, S. S., Mishra, V., Mukherjee, M. Das, Saini, P. & Ranjan, K. R. Amino acid derived biopolymers: Recent advances and biomedical applications. *Int. J. Biol. Macromol.* **188**, 542–567 (2021).
91. Aliferis, T., Iatrou, H. & Hadjichristidis, N. Living polypeptides. *Biomacromolecules* **5**, 1653–1656 (2004).
92. Hadjichristidis, N., Iatrou, H., Pispas, S. & Pitsikalis, M. Anionic polymerization: high vacuum techniques. *J. Polym. Sci. Part A Polym. Chem.* **38**, 3211–3234 (2000).
93. Zhao, W., Gnanou, Y. & Hadjichristidis, N. From competition to cooperation: a highly efficient strategy towards well-defined (co)polypeptides. *Chem. Commun. (Camb).* **51**, 3663–3666 (2015).
94. Cao, H., Yao, J. & Shao, Z. Synthesis of poly (??-benzyl-L-glutamate) with well-defined terminal structures and its block polypeptides with alanine, leucine and phenylalanine. *Polym. Int.* **61**, 774–779 (2012).
95. He, X., Zhong, L., Wang, K., Luo, S. & Xie, M. Synthesis of Biodegradable and Biocompatible ABC Triblock Copolymers. *J. Appl. Polym. Sci.* **117**, 302–308 (2010).
96. Vayaboury, W., Giani, O., Cottet, H., Bonaric, S. & Schué, F. Mechanistic Study Of α-amino acid N-carboxyanhydride (NCA) polymerization by capillary electrophoresis. *Macromol. Chem. Phys.* **209**, 1628–1637 (2008).
97. Dimitrov, I. & Schlaad, H. Synthesis of nearly monodisperse polystyrene – polypeptide block copolymers via polymerisation of N -carboxyanhydrides. *Chem. Commun. (Camb).* 2944–2945 (2003).
98. Vayaboury, W., Giani, O., Cottet, H., Deratani, A. & Schué, F. Living Polymerization of α-Amino Acid N-Carboxyanhydrides (NCA) upon Decreasing the Reaction Temperature. *Macromol. Rapid Commun.* **25**, 1221–1224 (2004).
99. Tang, H. & Zhang, D. General route toward side-chain-functionalized alpha-helical polypeptides. *Biomacromolecules* **11**, 1585–1592 (2010).
100. Lu, H. & Cheng, J. Hexamethyldisilazane-mediated controlled polymerization of a-amino acid N-carboxyanhydrides. *J. Am. Chem. Soc.* **129**, 14114–14115 (2007).
101. Deming, T. J. Cobalt and iron initiators for the controlled polymerization of a-amino acid-N-carboxyanhydrides. *Macromolecules* **32**, 4500–4502 (1999).
102. Deming, T. J. Facile synthesis of block copolypeptides of defined architecture.

Nature **390**, 386–389 (1997).

103. Deming, T. J. Amino Acid Derived Nickelacycles: Intermediates in Nickel-Mediated Polypeptide Synthesis. *J. Am. Chem. Soc.* **120**, 4240–4241 (1998).
104. Curtin, S. A. & Deming, T. J. Initiators for End-Group Functionalized Polypeptides via Tandem Addition Reactions. *J. Am. Chem. Soc.* **121**, 7427–7428 (1999).
105. Langer, R. & Vacanti, J. P. Tissue engineering. *Science (80-.).* **260**, 920–926 (1993).
106. Kohn, J. & Langer, R. Polymerization reactions involving the side chains of alpha-L-amino acids. *J. Am. Chem. Soc.* **109**, 817–820 (1987).
107. Gelbin, M. E. & Kohn, J. Synthesis and Polymerization of N-Z-L-Serine-@-lactone and Serine Hydroxybenzotriazole Active Este. 3962–3965 (1992).
108. Karagöz, F. Synthesis and Characterization of Poly(d,l-lactic acid-co-serine-NH2) Copolymer. (Hacettepe University, 2014).
109. Balme, S., Rixte, J., Boustta, M., Vert, M. & Henn, F. Complex impedance spectroscopy to investigate degradable chondroitin-poly(amino-serinate) complexes. *Polym. Degrad. Stab.* **98**, 2161–2167 (2013).
110. Kohn, J. The Synthesis and Characzerization of Pseudopoly(aminoacids) New Polymers for Medical Applications. in 178–179 (1990).
111. Słomkowski, S. & Penczek, S. Influence of Dibenzo-18-crown-6 Ether on the Kinetics of Anionic Polymerization of β-Propiolactone. *Macromolecules* **9**, 367–369 (1976).
112. Wei, Y., Li, X. yuan, Jing, X. bin, Chen, X. si & Huang, Y. bin. Preparation of poly(serine ester)s by ring-opening polymerization of N-trityl serine lactone under catalysis of ZnEt2. *Chem. Res. Chinese Univ.* **29**, 177–182 (2013).
113. Wei, Y., Li, X., Jing, X., Chen, X. & Huang, Y. Synthesis and characterization of α-amino acid-containing polyester: Poly[(ε-caprolactone)-co-(serine lactone)]. *Polym. Int.* **62**, 454–462 (2013).
114. Gohy, J. F. Block Copolymer Micelles. *Adv. Polym. Sci.* **190**, 65–136 (2005).
115. Leibler, L. Theory of Microphase Separation in Block Copolymers. *Macromolecules* **13**, 1602–1617 (1980).
116. Riess, G. Micellization of block copolymers. *Prog. Polym. Sci.* **28**, 1107–1170 (2003).
117. Kataoka, K., Harada, A. & Nagasaki, Y. Block copolymer micelles for drug delivery: Design, characterization and biological significance. *Adv. Drug Deliv. Rev.* **47**, 113–

131 (2001).

118. Gaucher, G. *et al.* Block copolymer micelles: Preparation, characterization and application in drug delivery. *J. Control. Release* **109**, 169–188 (2005).
119. Börner, H. G. & Schlaad, H. Bioinspired functional block copolymers. *Soft Matter* **3**, 394 (2007).
120. Katayose, S. & Kataoka, K. Water-soluble polyion complex associates of DNA and poly(ethylene glycol)-poly(L-lysine) block copolymer. *Bioconjug. Chem.* **8**, 702–707 (1997).
121. Blanazs, A., Armes, S. P. & Ryan, A. J. Self-assembled block copolymer aggregates: From micelles to vesicles and their biological applications. *Macromol. Rapid Commun.* **30**, 267–277 (2009).
122. M., A. & S., F. Vesicles and Liposomes: A Self-Assembly Principle Beyond Lipids. *Adv. Mater.* **15**, 1323–1333 (2003).
123. Israelachvili, J. N., Mitchell, D. J. & Ninham, B. W. Theory of self-assembly of hydrocarbon amphiphiles into micelles and bilayers. *J. Chem. Soc. Faraday Trans. 2 Mol. Chem. Phys.* **72**, 1525–1568 (1976).
124. Discher, D. E. & Eisenberg, A. Polymer Vesicles. *Science (80-.).* **297**, 967 LP – 973 (2002).
125. Zhang, J., Li, X. & Li, X. Stimuli-triggered structural engineering of synthetic and biological polymeric assemblies. *Prog. Polym. Sci.* **37**, 1130–1176 (2012).
126. Coulembier, O., Mespouille, L., Hedrick, J. L., Waymouth, R. M. & Dubois, P. Metal-Free Catalyzed Ring-Opening Polymerization of Beta-Lactones : Synthesis of Amphiphilic Triblock Copolymers Based on Poly (dimethylmalic acid). *Macromolecules* **39**, 4001–4008 (2006).
127. Pitt, G. G., Gratzl, M. M., Kimmel, G. L., Surles, J. & Sohindler, A. Aliphatic polyesters II. The degradation of poly (DL-lactide), poly (ε-caprolactone), and their copolymers in vivo. *Biomaterials* **2**, 215–220 (1981).
128. Palmgren, R., Karlsson, S. & Albertsson, A.-C. Synthesis of degradable crosslinked polymers based on 1,5-dioxepan-2-one and crosslinker of bis-ϵ-caprolactone type. *J. Polym. Sci. Part A Polym. Chem.* **35**, 1635–1649 (1997).
129. Albertsson, A.-C. & Varma, I. K. Recent Developments in Ring Opening Polymerization of Lactones for Biomedical Applications. *Biomacromolecules* **4**, 1466–1486 (2003).

130. In't Veld, P. J. A. *et al.* Melt block copolymerization of ϵ-caprolactone and L-lactide. *J. Polym. Sci. Part A Polym. Chem.* **35**, 219–226 (1997).
131. Nguyen, T. B. T., Li, S. & Deratani, A. Reverse micelles prepared from amphiphilic polylactide-b-poly(ethylene glycol) block copolymers for controlled release of hydrophilic drugs. *Int. J. Pharm.* **495**, 154–161 (2015).
132. Dong, Y. & Feng, S.-S. Nanoparticles of poly(D,L-lactide)/methoxy poly(ethylene glycol)-poly(D,L-lactide) blends for controlled release of paclitaxel. *J. Biomed. Mater. Res. Part A* **78A**, 12–19 (2006).
133. Watanabe, J., Eriguchi, T. & Ishihara, K. Cell Adhesion and Morphology in Porous Scaffold Based on Enantiomeric Poly(lactic acid) Graft-type Phospholipid Polymers. *Biomacromolecules* **3**, 1375–1383 (2002).
134. Akimoto, J., Nakayama, M., Sakai, K. & Okano, T. Molecular design of outermost surface functionalized thermoresponsive polymeric micelles with biodegradable cores. *J. Polym. Sci. Part A Polym. Chem.* **46**, 7127–7137 (2008).
135. Ghassemi, A. H. *et al.* Preparation and characterization of protein loaded microspheres based on a hydroxylated aliphatic polyester, poly(lactic-co-hydroxymethyl glycolic acid). *J. Control. Release* **138**, 57–63 (2009).
136. Habraken, G. J. M., Heise, A. & Thornton, P. D. Block Copolypeptides Prepared by N - Carboxyanhydride Ring-Opening Polymerization. *Macromol. Rapid Commun.* **33**, 272–286 (2012).
137. Hidetoshi, A., Yuichi, O. & Tatsuro, O. The Formation of Biodegradable Polymeric Micelles from Newly Synthesized Poly(aspartic acid)-block-Polylactide AB-Type Diblock Copolymers. *Macromol. Rapid Commun.* **25**, 743–747 (2004).
138. Deng, C. *et al.* Synthesis and characterization of poly(ethylene glycol)-b-poly (L-lactide)-b-poly(L-glutamic acid) triblock copolymer. *Polymer (Guildf).* **46**, 653–659 (2005).
139. Deng, C. *et al.* Synthesis and Characterization of RGD Peptide Grafted Poly(ethylene glycol)-b-Poly(l-lactide)-b-Poly(l-glutamic acid) Triblock Copolymer. *Biomacromolecules* **7**, 590–596 (2006).
140. Sun, J. *et al.* Formation of Reversible Shell Cross-Linked Micelles from the Biodegradable Amphiphilic Diblock Copolymer Poly(l-cysteine)-block-Poly(l-lactide). *Langmuir* **24**, 10099–10106 (2008).
141. Yang, Y. *et al.* pH-dependent self-assembly of amphiphilic poly(l-glutamic acid)-

block-poly(lactic-co-glycolic acid) copolymers. *Polymer (Guildf).* **51**, 2676–2682 (2010).

142. Liang, H.-F. *et al.* Paclitaxel-Loaded Poly(γ-glutamic acid)-poly(lactide) Nanoparticles as a Targeted Drug Delivery System against Cultured HepG2 Cells. *Bioconjug. Chem.* **17**, 291–299 (2006).
143. Nicolas, J., Mura, S., Brambilla, D., Mackiewicz, N. & Couvreur, P. Design, functionalization strategies and biomedical applications of targeted biodegradable/biocompatible polymer-based nanocarriers for drug delivery. *Chem. Soc. Rev.* **42**, 1147–235 (2013).
144. Mai, Y. & Eisenberg, A. Self-assembly of block copolymers. *Chem. Soc. Rev.* **41**, 5969–5985 (2012).
145. Du, J. & Armes, S. P. Preparation of Primary Amine-Based Block Copolymer Vesicles by Direct Dissolution in Water and Subsequent Stabilization by Sol−Gel Chemistry. *Langmuir* **24**, 13710–13716 (2008).
146. Lee, E. S., Shin, J. H., Na, K. & Bae, Y. H. P oly (L -histidine)– PEG block copolymer micelles and pH-induced destabilization. *J. Control. Release* **90**, 363–374 (2003).
147. Lavasanifar, A., Samuel, J. & Kwon, G. S. Micelles self-assembled from poly(ethylene oxide)-block-poly(N-hexyl stearate l-aspartamide) by a solvent evaporation method: effect on the solubilization and haemolytic activity of amphotericin B. *J. Control. Release* **77**, 155–160 (2001).
148. Bilati, U., Allémann, E. & Doelker, E. Development of a nanoprecipitation method intended for the entrapment of hydrophilic drugs into nanoparticles. *Eur. J. Pharm. Sci.* **24**, 67–75 (2005).
149. Kita-Tokarczyk, K., Grumelard, J., Haefele, T. & Meier, W. Block copolymer vesicles - Using concepts from polymer chemistry to mimic biomembranes. *Polymer (Guildf).* **46**, 3540–3563 (2005).
150. Balasubramanian, V., Herranz, B., Vingadas Almeida, P., Hirvonen, J. & Santos, H. *Multifaceted Polymersome Platforms: Spanning from Self-assembly To Drug Delivery and Protocells*. *Progress in Polymer Science* vol. 60 (2016).
151. Shum, H. C., Kim, J.-W. & Weitz, D. A. Microfluidic Fabrication of Monodisperse Biocompatible and Biodegradable Polymersomes with Controlled Permeability. *J. Am. Chem. Soc.* **130**, 9543–9549 (2008).
152. Brooks, B. Suspension polymerization processes. *Chem. Eng. Technol.* **33**, 1737–

1744 (2010).

153. Antonietti, M. & Landfester, K. Polyreactions in miniemulsions. *Prog. Polym. Sci.* **27**, 689–757 (2002).
154. Crespy, D. & Landfester, K. Miniemulsion polymerization as a versatile tool for the synthesis of functionalized polymers. *Beilstein J. Org. Chem.* **6**, 1132–1148 (2010).
155. Dörfler, H.-D. *Grenzflächen und kolloid-disperse Systeme: Physik und Chemie*. (Springer-Verlag Berlin Heidelberg, 2002).
156. Schork, F. J. *et al.* Miniemulsion Polymerization. in (ed. Okubo, M.) 129–255 (Springer Berlin Heidelberg, 2005). doi:10.1007/b100115.
157. Harkins, W. D. A General Theory of the Mechanism of Emulsion Polymerization1. *J. Am. Chem. Soc.* **69**, 1428–1444 (1947).
158. Distler, D., Neto, W. S. & Machado, F. B. T.-R. M. in M. S. and M. E. Emulsion Polymerization. in *Encyclopedia of Materials: Science and Technology* 2769–2774 (Elsevier, 2001). doi:https://doi.org/10.1016/B978-0-12-803581-8.03746-2.
159. Landfester, K. Synthesis of Colloidal Particles in Miniemulsions. *Annu. Rev. Mater. Res.* **36**, 231–279 (2006).
160. Hoffmann, M. S., Haschick, R. & Klapper, M. Oil-in-Oil-Emulsions : Tailor-Made Amphipolar. (2011).
161. Müller, K., Klapper, M. & Müllen, K. Polyester nanoparticles by non-aqueous emulsion polycondensation. *J. Polym. Sci. Part A Polym. Chem.* **45**, 1101–1108 (2007).
162. Haschick, R., Mueller, K., Klapper, M. & Muellen, K. Nonaqueous emulsions as a tool for particles with unique core-shell topologies. *Macromolecules* **41**, 5077–5081 (2008).
163. Müller, K., Park, M. K., Klapper, M., Knoll, W. & Müllen, K. Synthesis and layer-by-layer deposition of spherical poly(3,4- ethylenedioxythiophene) nanoparticles - Toward fast switching times between reduced and oxidized states. *Macromol. Chem. Phys.* **208**, 1394–1401 (2007).
164. Klapper, M., Nenov, S., Haschick, R., Müller, K. & Müllen, K. Oil-in-Oil emulsions: A unique tool for the formation of polymer nanoparticles. *Acc. Chem. Res.* **41**, 1190–1201 (2008).
165. Periard, J. & Riess, G. Effet emulsifiant des copolymeres sequences et greffes polystyrene-polyisoprene Obtention d'emulsions huile dans huile. *Colloid Polym.*

Sci. **253**, 362–372 (1975).

166. J., P., A., B. & G., R. Emulsifying effect of block and graft copolymers — oil in oil emulsions. *J. Polym. Sci. Part B Polym. Lett.* **8**, 109–114 (1970).
167. Riess, G., Nervo, J. & Rogez, D. Emulsifying Properties of Block Copolymers. Oil-Water Emulsions and Microemulsions. *Am. Chem. Soc. Polym. Prepr. Div. Polym. Chem.* **18**, 329–334 (1977).
168. Cameron, N. R. & Sherrington, D. C. Non-aqueous high internal phase emulsions. Preparation and stability. *J. Chem. Soc. Faraday Trans.* **92**, 1543–1547 (1996).
169. N., B., F., T., M., W., K., L. & M., A. Miniemulsion polymerization: applications and new materials. *Macromol. Symp.* **151**, 549–555 (2000).
170. Riess, G. & Labbe, C. Block Copolymers in Emulsion and Dispersion Polymerization. *Macromol. Rapid Commun.* **25**, 401–435 (2004).
171. Nicolai, T., Colombani, O. & Chassenieux, C. Dynamic polymeric micelles versus frozen nanoparticles formed by block copolymers. *Soft Matter* **6**, 3111–3118 (2010).
172. Müller, K. Nicht-wässrige Emulsionspolymerisationen. (2008).
173. Müller, K., Klapper, M. & Müllen, K. Preparation of high molecular weight polyurethane particles by nonaqueous emulsion polyaddition. *Colloid Polym. Sci.* **285**, 1157–1161 (2007).
174. Khrenov, V., Schwager, F., Klapper, M., Koch, M. & M??llen, K. The formation of hydrophobic inorganic nanoparticles in the presence of amphiphilic copolymers. *Colloid Polym. Sci.* **284**, 927–934 (2006).
175. Dvorakova, G. *et al.* Molecularly Imprinted Nanospheres by Nonaqueous Emulsion Polymerization. *Macromol. Rapid Commun.* **31**, 2035–2040 (2010).
176. Müller, K., Klapper, M. & Müllen, K. Synthesis of conjugated polymer nanoparticles in non-aqueous emulsions. *Macromol. Rapid Commun.* **27**, 586–593 (2006).
177. Haschick, R., Klapper, M., Wagener, K. B. & Müllen, K. Nanoparticles by ROMP in nonaqueous emulsions. *Macromol. Chem. Phys.* **211**, 2547–2554 (2010).
178. Hansen, C. M. *Hansen Solubility Parameters*. (CRC Press, 1999).
179. Karagöz, F., Dorresteijn, R., Müllen, K. & Klapper, M. Biocompatible Nanoparticles for Selective Drug Release at Cancer Cells. in *Control of Amphiphile Self-Assembling at the Molecular Level: Supra-Molecular Assemblies with Tuned Properties* (2017).
180. Mohanraj, V. & Chen, Y. Nanoparticles – A Review. *Trop. J. Pharm. Res.* **5**, 561–573

(2006).

181. Lv, H., Zhang, S., Wang, B., Cui, S. & Yan, J. Toxicity of cationic lipids and cationic polymers in gene delivery. *J. Control. Release* **114**, 100–109 (2006).
182. Dorresteijn, R., Billecke, N., Parekh, S. H., Klapper, M. & Müllen, K. Polarity reversal of nanoparticle surfaces by the use of light-sensitive polymeric emulsifiers. *J. Polym. Sci. Part A Polym. Chem.* **53**, 200–205 (2015).
183. Luo, L., Tam, J., Maysinger, D. & Eisenberg, A. Cellular internalization of poly(ethylene oxide)-b-poly(epsilon-caprolactone) diblock copolymer micelles. *Bioconjug. Chem.* **13**, 1259–1265 (2002).
184. Brambilla, D. *et al.* Design of fluorescently tagged poly(alkyl cyanoacrylate) nanoparticles for human brain endothelial cell imaging. *Chem. Commun. (Camb).* **46**, 2602–4 (2010).
185. Chen, L., Li, C. & Müllen, K. Beyond perylene diimides: synthesis, assembly and function of higher rylene chromophores. *J. Mater. Chem. C* **2**, 1938–1956 (2014).
186. Monici, M. Cell and tissue autofluorescence research and diagnostic applications. in vol. 11 227–256 (Elsevier, 2005).
187. Eriksen, M. *et al.* Plastic Pollution in the World's Oceans: More than 5 Trillion Plastic Pieces Weighing over 250,000 Tons Afloat at Sea. *PLoS One* **9**, 1–15 (2014).
188. Eriksen, M. *et al.* Microplastic pollution in the surface waters of the Laurentian Great Lakes. *Mar. Pollut. Bull.* **77**, 177–182 (2013).
189. Rochman, C. M., Manzano, C., Hentschel, B. T., Simonich, S. L. M. & Hoh, E. Polystyrene Plastic: A Source and Sink for Polycyclic Aromatic Hydrocarbons in the Marine Environment. *Environ. Sci. Technol.* **47**, 13976–13984 (2013).
190. Sajiki, J. & Yonekubo, J. Leaching of bisphenol A (BPA) to seawater from polycarbonate plastic and its degradation by reactive oxygen species. *Chemosphere* **51**, 55–62 (2003).
191. Zhang, Q. *et al.* Bio-based polyesters: Recent progress and future prospects. *Prog. Polym. Sci.* **120**, 101430 (2021).
192. Gupta, P. K. *et al.* Recent trends in biodegradable polyester nanomaterials for cancer therapy. *Mater. Sci. Eng. C* **127**, 112198 (2021).
193. Dorresteijn, R. *et al.* Biocompatible polylactide-block-polypeptide-block-polylactide nanocarrier. *Biomacromolecules* **14**, 1572–1577 (2013).
194. Lu, C. *et al.* Micellization and gelation of aqueous solutions of star-shaped PEG-PCL

block copolymers consisting of branched 4-arm poly(ethylene glycol) and polycaprolactone blocks. *Eur. Polym. J.* **43**, 1857–1865 (2007).

195. Seyednejad, H., Ghassemi, A. H., Van Nostrum, C. F., Vermonden, T. & Hennink, W. E. Functional aliphatic polyesters for biomedical and pharmaceutical applications. *J. Control. Release* **152**, 168–176 (2011).
196. Williams, C. K. Synthesis of functionalized biodegradable polyesters. *Chem. Soc. Rev.* **36**, 1573–1580 (2007).
197. Riess, G. Micellization of block copolymers. *Prog. Polym. Sci.* **45**, 1107–1170 (2012).
198. Low, P. S., Henne, W. A. & Doorneweerd, D. D. Discovery and Development of Folic-Acid-Based Receptor Targeting for Imaging and Therapy of Cancer and Inflammatory Diseases. *Acc. Chem. Res.* **41**, 120–129 (2008).
199. Russell-Jones, G., McTavish, K., McEwan, J., Rice, J. & Nowotnik, D. Vitamin-mediated targeting as a potential mechanism to increase drug uptake by tumours. *J. Inorg. Biochem.* **98**, 1625–1633 (2004).
200. Ono, K., Hasegawa, K., Naiki, H. & Yamada, M. Curcumin has potent anti-amyloidogenic effects for Alzheimer's β-amyloid fibrils in vitro. *J. Neurosci. Res.* **75**, 742–750 (2004).
201. Sano, M. *et al.* A Controlled Trial of Selegiline, Alpha-Tocopherol, or Both as Treatment for Alzheimer's Disease. *N. Engl. J. Med.* **336**, 1216–1222 (1997).
202. Ehrhardt, C., Kneuer, C. & Bakowsky, U. Selectins—an emerging target for drug delivery. *Adv. Drug Deliv. Rev.* **56**, 527–549 (2004).
203. Cho, C. S. *et al.* Simple preparation of nanoparticles coated with carbohydrate-carrying polymers. *Biomaterials* **18**, 323–326 (1997).
204. Han, J.-H., Oh, Y.-K., Kim, D.-S. & Kim, C.-K. Enhanced hepatocyte uptake and liver targeting of methotrexate using galactosylated albumin as a carrier. *Int. J. Pharm.* **188**, 39–47 (1999).
205. Lindgren, M., Hällbrink, M., Prochiantz, a & Langel, U. Cell-penetrating peptides. *Trends Pharmacol. Sci.* **21**, 99–103 (2000).
206. Kulkarni, P. S. *et al.* MMP-9 responsive PEG cleavable nanovesicles for efficient delivery of chemotherapeutics to pancreatic cancer. *Mol. Pharm.* **11**, 2390–2399 (2014).
207. Li, J., Ge, Z. & Liu, S. PEG-sheddable polyplex micelles as smart gene carriers based

on MMP-cleavable peptide-linked block copolymers. *Chem. Commun.* **49**, 6974–6 (2013).

208. Torchilin, V. P., Lukyanov, A. N., Gao, Z. & Papahadjopoulos-Sternberg, B. Immunomicelles: Targeted pharmaceutical carriers for poorly soluble drugs. *Proc. Natl. Acad. Sci.* **100**, 6039 LP – 6044 (2003).
209. Farokhzad, O. C. *et al.* Nanoparticle-Aptamer Bioconjugates. *Cancer Res.* **64**, 7668 LP – 7672 (2004).
210. Lee, J. S. & Feijen, J. Polymersomes for drug delivery: Design, formation and characterization. *J. Control. Release* **161**, 473–483 (2012).
211. Planellas, M. & Puiggali, J. Synthesis and properties of poly(L-lactide)-b-poly (L-phenylalanine) hybrid copolymers. *Int. J. Mol. Sci.* **15**, 13247–13266 (2014).
212. Klinker, K. & Barz, M. Polypept(o)ides: Hybrid Systems Based on Polypeptides and Polypeptoids. *Macromol. Rapid Commun.* **36**, 1943–1957 (2015).
213. Birke, A. *et al.* Polypeptoid-block-polypeptide copolymers: Synthesis, characterization, and application of amphiphilic block copolypept(o)ides in drug formulations and miniemulsion techniques. *Biomacromolecules* **15**, 548–557 (2014).
214. Blauvelt, M. L. & Howell, A. R. Synthesis of epi-oxetin via a serine-derived 2-methyleneoxetane. *J. Org. Chem.* **73**, 517–521 (2008).
215. Dove, A. P. Organic catalysis for ring-opening polymerization. *ACS Macro Lett.* **1**, 1409–1412 (2012).
216. Kamber, N. E. *et al.* Organocatalytic Ring-Opening Polymerization. *Chem. Rev.* **107**, 5813–5840 (2007).
217. Nederberg, F., Connor, E. F., Möller, M., Glauser, T. & Hedrick, J. L. New Paradigms for Organic Catalysts: The First Organocatalytic Living Polymerization. *Angew. Chemie Int. Ed.* **40**, 2712–2715 (2001).
218. Lohmeijer, B. G. G. *et al.* Guanidine and Amidine Organocatalysts for Ring-Opening Polymerization of Cyclic Esters. *Macromolecules* **39**, 8574–8583 (2006).
219. Pratt, R. C., Lohmeijer, B. G. G., Long, D. A., Waymouth, R. M. & Hedrick, J. L. Triazabicyclodecene: A simple bifunctional organocatalyst for acyl transfer and ring-opening polymerization of cyclic esters. *J. Am. Chem. Soc.* **128**, 4556–4557 (2006).
220. Dove, A. P. *et al.* N-Heterocyclic carbenes: Effective organic catalysts for living

polymerization. *Polymer (Guildf).* **47**, 4018–4025 (2006).

221. Arduengo, A. J., Harlow, R. L. & Kline, M. A stable crystalline carbene. *J. Am. Chem. Soc.* **113**, 361–363 (1991).
222. Connor, E. F., Nyce, G. W., Myers, M., Möck, A. & Hedrick, J. L. First Example of N-Heterocyclic Carbenes as Catalysts for Living Polymerization: Organocatalytic Ring-Opening Polymerization of Cyclic Esters. *J. Am. Chem. Soc.* **124**, 914–915 (2002).
223. Enders, D., Niemeier, O. & Henseler, A. Organocatalysis by N-heterocyclic carbenes. *Chem. Rev.* **107**, 5606–5655 (2007).
224. Csihony, S. *et al.* Single-component catalyst/initiators for the organocatalytic ring-opening polymerization of lactide. *J. Am. Chem. Soc.* **127**, 9079–9084 (2005).
225. Coulembier, O. *et al.* Alcohol Adducts of N-Heterocyclic Carbenes: Latent Catalysts for the Thermally-Controlled Living Polymerization of Cyclic Esters. *Macromolecules* **39**, 5617–5628 (2006).
226. K, J., SH, H. & Y, I. Thermal characterization of polylactides. *Polymer (Guildf).* **29**, 2229–2234 (1988).
227. Deng, M. X. *et al.* Synthesis of four-armed poly(epsilon-caprolactone)-block-poly(ethylene oxide) by diethylzinc catalyst. *J. Polym. Sci., Part A Polym. Chem.* **42**, 950–959 (2004).
228. Lowe, J. R., Martello, M. T., Tolman, W. B. & Hillmyer, M. A. Functional biorenewable polyesters from carvone-derived lactones. *Polym. Chem.* **2**, 702–708 (2011).
229. Cohen, Y., Avram, L. & Frish, L. Diffusion NMR spectroscopy in supramolecular and combinatorial chemistry: An old parameter - New insights. *Angew. Chemie - Int. Ed.* **44**, 520–554 (2005).
230. Arimura, H., Ohya, Y. & Ouchi, T. Formation of core-shell type biodegradable polymeric micelles from amphiphilic poly(aspartic acid)-block-polylactide diblock copolymer. *Biomacromolecules* **6**, 720–725 (2005).
231. Domínguez, A., Fernández, A., González, N., Iglesias, E. & Montenegro, L. Determination of Critical Micelle Concentration of Some Surfactants by Three Techniques. *J. Chem. Educ.* **74**, 1227–1231 (1997).
232. Sun, T. *et al.* Engineered nanoparticles for drug delivery in cancer therapy. *Angew. Chemie - Int. Ed.* **53**, 12320–12364 (2014).

233. Matsumura, Y. & Maeda, H. A New Concept for Macromolecular Therapeutics in Cancer Chemotherapy: Mechanism of Tumoritropic Accumulation of Proteins and the Antitumor Agent Smancs. *Cancer Res.* **46**, 6387–6392 (1986).
234. Fang, J., Nakamura, H. & Maeda, H. The EPR effect: Unique features of tumor blood vessels for drug delivery, factors involved, and limitations and augmentation of the effect. *Adv. Drug Deliv. Rev.* **63**, 136–151 (2011).
235. Prabhu, R. H., Patravale, V. B. & Joshi, M. D. Polymeric nanoparticles for targeted treatment in oncology: Current insights. *Int. J. Nanomedicine* **10**, 1001–1018 (2015).
236. Xin, Y., Yin, M., Zhao, L., Meng, F. & Luo, L. Recent progress on nanoparticle-based drug delivery systems for cancer therapy. *Cancer Biol. Med.* **14**, 228 (2017).
237. Letchford, K. & Burt, H. A review of the formation and classification of amphiphilic block copolymer nanoparticulate structures: micelles, nanospheres, nanocapsules and polymersomes. *Eur. J. Pharm. Biopharm.* **65**, 259–269 (2007).
238. Mura, S., Nicolas, J. & Couvreur, P. Stimuli-responsive nanocarriers for drug delivery. *Nat. Mater.* **12**, 991–1003 (2013).
239. Cardoso, V. M. de O. *et al.* Chapter 4 - Stimuli-responsive polymeric nanoparticles as controlled drug delivery systems. in *Recent Advances in Tailor-Made Therapeutics* (eds. Gajbhiye, V., Gajbhiye, K. R. & Hong, S. B. T.-S.-R. N.) 87–117 (Academic Press, 2022). doi:https://doi.org/10.1016/B978-0-12-824456-2.00011-4.
240. Song, S. J. & Choi, J. S. Enzyme-Responsive Amphiphilic Peptide Nanoparticles for Biocompatible and Efficient Drug Delivery. *Pharmaceutics* vol. 14 (2022).
241. Harris, T. J. *et al.* Protease-triggered unveiling of bioactive nanoparticles. *Small* **4**, 1307–1312 (2008).
242. Zhong, Y. J., Shao, L. H. & Li, Y. Cathepsin B-cleavable doxorubicin prodrugs for targeted cancer therapy (Review). *Int. J. Oncol.* **42**, 373–383 (2013).
243. Egeblad, M. & Werb, Z. New functions for the matrix metalloproteinases in cancer progression. *Nat. Rev. Cancer* **2**, 161–174 (2002).
244. Brinckerhoff, C. E. & Matrisian, L. M. Matrix metalloproteinases: a tail of a frog that became a prince. *Nat. Rev. Mol. Cell Biol.* **3**, 207–214 (2002).
245. Cathcart, J., Pulkoski-Gross, A. & Cao, J. Targeting matrix metalloproteinases in cancer: Bringing new life to old ideas. *Genes Dis.* **2**, 26–34 (2015).

246. Kherif, S. *et al.* Expression of matrix metalloproteinases 2 and 9 in regenerating skeletal muscle: a study in experimentally injured and mdx muscles. *Dev. Biol.* **205**, 158–170 (1999).
247. Zhu, L., Kate, P. & Torchilin, V. P. Matrix metalloprotease 2-responsive multifunctional liposomal nanocarrier for enhanced tumor targeting. *ACS Nano* **6**, 3491–3498 (2012).
248. Dorresteijn, R. *et al.* Polylactide-block-polypeptide-block-polylactide copolymer nanoparticles with tunable cleavage and controlled drug release. *Adv. Funct. Mater.* **24**, 4026–4033 (2014).
249. Bawarski, W. E., Chidlowsky, E., Bharali, D. J. & Mousa, S. A. Emerging nanopharmaceuticals. *Nanomedicine Nanotechnology, Biol. Med.* **4**, 273–282 (2008).
250. Emerich, D. F. & Thanos, C. G. The pinpoint promise of nanoparticle-based drug delivery and molecular diagnosis. *Biomol. Eng.* **23**, 171–184 (2006).
251. Cho, K., Wang, X., Nie, S., Chen, Z. & Shin, D. M. Therapeutic nanoparticles for drug delivery in cancer. *Clin. Cancer Res.* **14**, 1310–1316 (2008).
252. de la Rica, R., Aili, D. & Stevens, M. M. Enzyme-responsive nanoparticles for drug release and diagnostics. *Adv. Drug Deliv. Rev.* **64**, 967–978 (2012).
253. McCawley, L. J. & Matrisian, L. M. Matrix metalloproteinases: Multifunctional contributors to tumor progression. *Mol. Med. Today* **6**, 149–156 (2000).
254. Rhodes, A. J. & Deming, T. J. Soluble, Clickable Polypeptides from Azide-Containing N-Carboxyanhydride Monomers. *ACS Macro Lett.* **2**, 351–354 (2013).
255. Engler, A. C., Bonner, D. K., Buss, H. G., Cheung, E. Y. & Hammond, P. T. The synthetic tuning of clickable pH responsive cationic polypeptides and block copolypeptides. *Soft Matter* **7**, 5627–5637 (2011).
256. Xiao, C. *et al.* Facile Synthesis of Glycopolypeptides by Combination of Ring-Opening Polymerization of an Alkyne-Substituted N-carboxyanhydride and Click "Glycosylation". *Macromol. Rapid Commun.* **31**, 991–997 (2010).
257. Zhang, Y., Lu, H., Lin, Y. & Cheng, J. Water-Soluble Polypeptides with Elongated, Charged Side Chains Adopt Ultrastable Helical Conformations. *Macromolecules* **44**, 6641–6644 (2011).
258. Yu, M., Nowak, A. P., Deming, T. J. & Pochan, D. J. Methylated mono- and diethyleneglycol functionalized polylysines: Nonionic, a-helical, water-soluble

polypeptides. *J. Am. Chem. Soc.* **121**, 12210–12211 (1999).

259. Hwang, J. & Deming, T. J. Methylated Mono- and Di(ethylene glycol)-Functionalized β-Sheet Forming Polypeptides. *Biomacromolecules* **2**, 17–21 (2001).
260. Kramer, J. R. & Deming, T. J. Glycopolypeptides with a Redox-Triggered Helix-to-Coil Transition. *J. Am. Chem. Soc.* **134**, 4112–4115 (2012).
261. Kramer, J. R. & Deming, T. J. Glycopolypeptides via Living Polymerization of Glycosylated- L-lysine N -Carboxyanhydrides. *J. Am. Chem. Soc.* **132**, 15068–15071 (2010).
262. Liu, G. & Dong, C. Photoresponsive Poly(S-(o-nitrobenzyl)-L-cysteine)-b-PEO from a L- Cysteine N-Carboxyanhydride Monomer: Synthesis, Self-Assembly, and Phototriggered Drug Release. *Biomacromolecules* **13**, 1573–1583 (2012).
263. Mabuchi, M. *et al.* Preparation and Characterization of the Langmuir−Blodgett Films Made of Hairy-Rod Polyglutamates Bearing Various Chromophores in the Side Chain. *Langmuir* **14**, 7260–7266 (1998).
264. Yan, L. *et al.* Photo-cross-linked mPEG-poly([gamma]-cinnamyl-l-glutamate) micelles as stable drug carriers. *Polym. Chem.* **3**, 1300–1307 (2012).
265. Heeswijk, W. A. R. Van, Eenink, M. J. D., Feijen, J. An Improved Method for the Preparation of Gamma Esters of Glutamic acid and beta esters of Aspartic acid. *Synthesis (Stuttg).* 744–747 (1982) doi:10.1017/CBO9781107415324.004.
266. Dong, J. *et al.* Multiple stimuli-responsive polymeric micelles for controlled release. *Soft Matter* **9**, 370–373 (2013).
267. Fuller, W. D., Verlander, M. S. & Goodman, M. A Procedure for the Facile Synthesis of Amino-Acid N-Carboxyanhydrides. *Biopolymers* **15**, 1869–1871 (1976).
268. Martin, M. E. & Rice, K. G. Peptide-guided gene delivery. *AAPS J.* **9**, E18–E29 (2007).
269. Patel, A., Patel, M., Yang, X. & Mitra, A. K. Recent advances in protein and Peptide drug delivery: a special emphasis on polymeric nanoparticles. *Protein Pept. Lett.* **21**, 1102–1120 (2014).
270. Lee, V. *Peptide and Protein Drug Delivery*. (CRC Press, 1990).
271. Liu, Y. & Yin, L. α-Amino acid N-carboxyanhydride (NCA)-derived synthetic polypeptides for nucleic acids delivery. *Adv. Drug Deliv. Rev.* **171**, 139–163 (2021).
272. Wang, X. *et al.* Polypeptide-based drug delivery systems for programmed release.

Biomaterials **275**, 120913 (2021).

273. Habibi, N., Kamaly, N., Memic, A. & Shafiee, H. Self-assembled peptide-based nanostructures: Smart nanomaterials toward targeted drug delivery. *Nano Today* **11**, 41–60 (2016).
274. Zhang, S. Fabrication of novel biomaterials through molecular self-assembly. *Nat. Biotechnol.* **21**, 1171–1178 (2003).
275. Kricheldorf, H. R. Polypeptides and 100 Years of Chemistry of α-Amino Acid N-Carboxyanhydrides. *Angew. Chemie Int. Ed.* **45**, 5752–5784 (2006).
276. M., H. G. J., E., K. C. & Andreas, H. Peptide block copolymers by N-carboxyanhydride ring-opening polymerization and atom transfer radical polymerization: The effect of amide macroinitiators. *J. Polym. Sci. Part A Polym. Chem.* **47**, 6883–6893 (2009).
277. Zhang, X., Li, J., Li, W. & Zhang, A. Synthesis and Characterization of Thermo- and pH-Responsive Double-Hydrophilic Diblock Copolypeptides. *Biomacromolecules* **8**, 3557–3567 (2007).
278. I., K. R. J. *et al.* Synthesis of poly(benzyl glutamate-b-styrene) rod-coil block copolymers by dual initiation in one pot. *J. Polym. Sci. Part A Polym. Chem.* **46**, 3068–3077 (2008).
279. Willy, A., Reda, A., Sébastien, L. & Daniel, T. Synthesis of Block Copolypeptides by Click Chemistry. *Macromol. Rapid Commun.* **29**, 1147–1155 (2008).
280. Lu, H. & Cheng, J. N-trimethylsilyl amines for controlled ring-opening polymerization of amino acid N-carboxyanhydrides and facile end group functionalization of polypeptides. *J. Am. Chem. Soc.* **130**, 12562–12563 (2008).
281. Hasannia, M. *et al.* Synthesis of block copolymers used in polymersome fabrication: Application in drug delivery. *J. Control. Release* **341**, 95–117 (2022).
282. Jain, S. & Bates, F. S. On the Origins of Morphological Complexity in Block Copolymer Surfactants. *Science (80-.).* **300**, 460 LP – 464 (2003).
283. Weiss, S. Fluorescence spectroscopy of single biomolecules. *Science (80-.).* **283**, 1676–1683 (1999).
284. Griffin, B. A., Adams, S. R. & Tsien, R. Y. Specific Covalent Labeling of Recombinant Protein Molecules Inside Live Cells. *Science (80-.).* **281**, 269 LP – 272 (1998).
285. Wolfbeis, O. S. An overview of nanoparticles commonly used in fluorescent bioimaging. *Chem. Soc. Rev.* **44**, 4743–4768 (2015).
286. Bou, S., Klymchenko, A. S. & Collot, M. Fluorescent labeling of biocompatible block

copolymers: synthetic strategies and applications in bioimaging. *Mater. Adv.* **2**, 3213–3233 (2021).

287. Lv, M., Jan Cornel, E., Fan, Z. & Du, J. Advances and Perspectives of Peptide and Polypeptide-Based Materials for Biomedical Imaging. *Adv. NanoBiomed Res.* **1**, 2000109 (2021).
288. Escobedo, J. O., Rusin, O., Lim, S. & Strongin, R. M. NIR dyes for bioimaging applications. *Curr. Opin. Chem. Biol.* **14**, 64–70 (2010).
289. Tsien, R. Y. The green fluorescent protein. *Annu. Rev. Biochem.* **67**, 509–44 (1998).
290. Moerner, W. E. Single-molecule optical spectroscopy of autofluorescent proteins. *J. Chem. Phys.* **117**, 10925–10937 (2002).
291. Chan, W. C. W. *et al.* Luminescent quantum dots for multiplexed biological detection and imaging. *Curr. Opin. Biotechnol.* **13**, 40–46 (2002).
292. Larson, D. R. *et al.* Water-Soluble Quantum Dots for Multiphoton Fluorescence Imaging in Vivo. *Science (80-.).* **300**, 1434 LP – 1436 (2003).
293. Zhang, J., Liu, K., Müllen, K. & Yin, M. Self-assemblies of amphiphilic homopolymers: synthesis, morphology studies and biomedical applications. *Chem. Commun. (Camb).* **51**, 11541–55 (2015).
294. Chatterjee, D. K., Fong, L. S. & Zhang, Y. Nanoparticles in photodynamic therapy: An emerging paradigm. *Adv. Drug Deliv. Rev.* **60**, 1627–1637 (2008).
295. Ze-Yong, L. *et al.* Porphyrin-functionalized amphiphilic diblock copolypeptides for photodynamic therapy. *J. Polym. Sci. Part A Polym. Chem.* **49**, 286–292 (2010).
296. Sun, P. *et al.* A perylene diimide zwitterionic polymer for photoacoustic imaging guided photothermal/photodynamic synergistic therapy with single near-infrared irradiation. *J. Mater. Chem. B* **6**, 3395–3403 (2018).
297. Sun, P. *et al. High Density Glycopolymers Functionalized Perylene Diimide Nanoparticles for Tumor-Targeted Photoacoustic Imaging and Enhanced Photothermal Therapy*. *Biomacromolecules* vol. 18 (2017).
298. H. Quante. No Title. (Johannes Gutenberg University (Mainz), 1995).
299. C. Kohl. No Title. (Johannes-Gutenberg University (Mainz), 2003).
300. Peneva, K. Design, Synthesis and Application of Ultrastable Rylene Dyes for Fluorescent Labeling of Biomolecules. (2008).
301. Klok, H. A., Hernández, J. R., Becker, S. & Müllen, K. Star-shaped fluorescent polypeptides. *J. Polym. Sci. Part A Polym. Chem.* **39**, 1572–1583 (2001).

302. Zhang, J. *et al.* pH-responsive self-assembly of fluorophore-ended homopolymers. *Chem. Commun.* **50**, 7511–7513 (2014).
303. Williams, A. J. & Gupta, V. K. Self-Assembly of a Rodlike Polypeptide on Solid Surfaces: Role of Solvent, Molecular Weight, and Time of Assembly. *J. Phys. Chem. B* **105**, 5223–5230 (2001).
304. Brzezinska, K. R., Curtin, S. A. & Deming, T. J. Polypeptide End-Capping Using Functionalized Isocyanates: Preparation of Pentablock Copolymers. *Macromolecules* **35**, 2970–2976 (2002).
305. Ren, T.-B., Xia, W.-J., Dong, H.-Q. & Li, Y.-Y. Sheddable micelles based on disulfide-linked hybrid PEG-polypeptide copolymer for intracellular drug delivery. *Polymer (Guildf).* **52**, 3580–3586 (2011).
306. Huang, Z. *et al.* Fabrication of amphiphilic fluorescent polylysine nanoparticles by atom transfer radical polymerization (ATRP) and their application in cell imaging. *RSC Adv.* **5**, 65884–65889 (2015).
307. Leuchs, H. Ueber die Glycin-carbonsäure. *Berichte der Dtsch. Chem. Gesellschaft* **39**, 857–861 (1906).
308. Coleman, D. & Farthing, A. C. 628. Synthetic polypeptides. Part II. Properties of oxazolid-2 : 5-diones and an initial study of the preparation of polypeptides there-from. *J. Chem. Soc.* 3218–3222 (1950) doi:10.1039/JR9500003218.
309. Farthing, A. C. & Reynolds, R. J. W. Anhydro-N-Carboxy-DL-β-Phenylalanine. *Nature* **165**, 647 (1950).
310. Poché, D. S., Moore, M. J. & Bowles, J. L. An Unconventional Method for Purifying the N-carboxyanhydride Derivatives of γ-alkyl-L-glutamates. *Synth. Commun.* **29**, 843–854 (1999).
311. Kramer, J. R. & Deming, T. J. General Method for Purification of r -Amino acid- N -carboxyanhydrides Using Flash Chromatography. *Bioconjug. Chem.* **11**, 3668–3672 (2010).
312. Fields, G. *Methods for Removing the Fmoc Group*. *Methods in molecular biology (Clifton, N.J.)* vol. 35 (1994).
313. Rodriguez-Hernandez, J. & Harm-Anton, K. Synthesis and Ring-Opening (Co) polymerization of L -Lysine N-Carboxyanhydrides Containing Labile Side-Chain Protective Groups. *J. Polym. Sci Part A Polym. Chem.* **41**, 1167–1187 (2003).
314. Niculescu-Duvaz, D., Getaz, J. & Springer, C. J. Long Functionalized Poly (ethylene

glycol) s of Defined Molecular Weight : Synthesis and Application in Solid-Phase Synthesis of Conjugates. *Bioconjug. Chem.* **19**, 973–981 (2008).

315. Carpino, L. A. An Efficient Peptide Coupling Additive'. *J.a.C.S* **115**, 4397–4398 (1993).
316. Li, C. Novel Functional Rylene Dyes for Dye-Sensitized Solar Cells. (2008).
317. Davidson, B. & Fasman, G. D. The conformational transitions of uncharged poly-L-lysine. Alpha helix-random coil-beta structure. *Biochemistry* **6**, 1616–1629 (1967).
318. Kessler, H. Conformation and Biological Activity of Cyclic Peptides. *Angew. Chemie Int. Ed. English* **21**, 512–523 (1982).
319. Scholtz, J. M. & Baldwin, R. L. The Mechanism of alpha-Helix Formation by Peptides. *Annu. Rev. Biophys. Biomol. Struct.* **21**, 95–118 (1992).
320. Sahl, M., Muth, S., Branscheid, R., Fischer, K. & Schmidt, M. Helix – Coil Transition in Cylindrical Brush Polymers with Poly-L-Lysine Side Chains. *Macromoleculars* **45**, 5167–5175 (2012).
321. Skinner, J. F., Calkins, H. H., Liles, W. C. J. & Kaplain, L. J. Spin-Label Studies of the pH-Induced Random Coil to a-Helix Conformational Transition in Poly (L-lysine). *Biopolymers* **21**, 833–847 (1982).
322. Royer, C. A. Probing Protein Folding and Conformational Transitions with Fluorescence. *Chem. Rev.* **106**, 1769–1784 (2006).
323. Lamba, J., Paul, S., Hasija, V., Aggarwal, R. & Chaudhuri, T. K. Monitoring protein folding and unfolding pathways through surface hydrophobicity changes using fluorescence and circular dichroism spectroscopy. *Biochem.* **74**, 393–398 (2009).
324. Ignatova, Z. & Gierasch, L. M. Monitoring protein stability and aggregation in vivo by real-time fluorescent labeling. *Proc. Natl. Acad. Sci.* **101**, 523–528 (2004).
325. Spano, F. C. The Spectral Signatures of Frenkel Polarons in H- and J-Aggregates. *Acc. Chem. Res.* **43**, 429–439 (2010).
326. Eisfeld, A. & Briggs, J. S. The J- and H-bands of organic dye aggregates. *Chem. Phys.* **324**, 376–384 (2006).
327. Stetefeld, J., McKenna, S. A. & Patel, T. R. Dynamic light scattering: a practical guide and applications in biomedical sciences. *Biophys. Rev.* **8**, 409–427 (2016).
328. Chiou, J. S. *et al.* The a-helix to b-sheet transition in poly(l-lysine): Effects of anesthetics and high pressure. *Biochim. Biophys. Acta (BBA)/Protein Struct. Mol.* **1119**, 211–217 (1992).

329. Bosterling, B. & Engel, J. Kinetic Study on the Helix-coil Transition of Fluorescent labelled Poly(L-lysine) by the temperature-Jump Technique. *Biophys. Chem.* **9**, 201–209 (1979).
330. Dos, A., Schimming, V. & Huot, M. C. Acid-Base Interactions and Secondary Structures of Poly-L-Lysine Probed by 15N and 13C Solid State NMR and Ab initio Model Calculations. *J. Phys. Chem. B* **112**, 15604–15615 (2008).
331. *Circular Dichroism and the Conformational Analysis of Biomolecules*. (Springer US, 1996). doi:10.1007/978-1-4757-2508-7.
332. Greenfield, N. Using circular dichroism spectra to estimate protein secondary structure. *Nat Protoc.* **1**, 2876–2890 (2007).
333. Trindle, C. The Circular Dichroism of P-Poly-L-lysine. *J. Am. Chem. Soc.* **91**, 220–222 (1969).
334. Greenfield, N. J. & Fasman, G. D. Computed circular dichroism spectra for the evaluation of protein conformation. *Biochemistry* **8**, 4108–4116 (1969).
335. Habraken, G. J. M., Wilsens, K. H. R. M., Koning, C. E. & Heise, A. Optimization of N-carboxyanhydride (NCA) polymerization by variation of reaction temperature and pressure. *Polym. Chem.* **2**, 1322 (2011).
336. Vayaboury, W., Giani, O., Cottet, H., Deratani, A. & Schué, F. Living polymerization of α-amino acid N-carboxyanhydrides (NCA) upon decreasing the reaction temperature. *Macromol. Rapid Commun.* **25**, 1221–1224 (2004).
337. Karayianni, M. & Pispas, S. Self-Assembly of Amphiphilic Block Copolymers in Selective Solvents. in *Fluorescence Studies of Polymer Containing Systems* (ed. Procházka, K.) vol. 16 27–63 (Springer International Publishing, 2016).
338. Do, T. D., Kincannon, W. M. & Bowers, M. T. Phenylalanine Oligomers and Fibrils: The Mechanism of Assembly and the Importance of Tetramers and Counterions. *J. Am. Chem. Soc.* **137**, 10080–10083 (2015).
339. Koo, A. N. *et al.* Disulfide-cross-linked PEG-poly(amino acid)s copolymer micelles for glutathione-mediated intracellular drug delivery. *Chem. Commun.* 6570–6572 (2008) doi:10.1039/B815918A.
340. Greven, A.-C. *et al.* Polycarbonate and polystyrene nanoplastic particles act as stressors to the innate immune system of fathead minnow (Pimephales promelas). *Environ. Toxicol. Chem.* **9999**, 1–8 (2016).
341. https://www.statista.com/statistics/282732/global-production-of-plastics-since-

1950/. (2018).

342. Ryan, P. G., Moore, C. J., Van Franeker, J. A. & Moloney, C. L. Monitoring the abundance of plastic debris in the marine environment. *Philos. Trans. R. Soc. B Biol. Sci.* **364**, 1999–2012 (2009).
343. Nunez, C. https://www.nationalgeographic.com/environment/freshwater/pollution/. (2010).
344. Hahladakis, J. N., Velis, C. A., Weber, R., Iacovidou, E. & Purnell, P. An overview of chemical additives present in plastics: Migration, release, fate and environmental impact during their use, disposal and recycling. *J. Hazard. Mater.* **344**, 179–199 (2018).
345. Lithner, D., Larsson, Å. & Dave, G. Environmental and health hazard ranking and assessment of plastic polymers based on chemical composition. *Sci. Total Environ.* **409**, 3309–3324 (2011).
346. Bhattacharya, P., Lin, S., Turner, J. P. & Ke, P. C. Physical adsorption of charged plastic nanoparticles affects algal photosynthesis. *J. Phys. Chem. C* **114**, 16556–16561 (2010).
347. Brown, D. M., Wilson, M. R., MacNee, W., Stone, V. & Donaldson, K. Size-Dependent Proinflammatory Effects of Ultrafine Polystyrene Particles: A Role for Surface Area and Oxidative Stress in the Enhanced Activity of Ultrafines. *Toxicol. Appl. Pharmacol.* **175**, 191–199 (2001).
348. Pawar, P. R., Shirgaonkar, S. S. & Patil, R. B. Plastic marine debris: Sources, distribution and impacts on coastal and ocean biodiversity. *PENCIL Publ. Biol. Sci.* **3**, 40–54 (2016).
349. Dyaba, A. K. F. K. F., Essawy, H. A. A., El-Mageed, A. I. A. A. & Taha, F. Preparation of polystyrene latex particles via emulsion polymerization using Hitenol BC-20 as a surfmer: Why the coating potential is different compared to the presence of emulsifying solid nanoparticles? (2013).
350. Brijmohan, S. B., Swier, S., Weiss, R. A. & Shaw, M. T. Synthesis and characterization of cross-linked sulfonated polystyrene nanoparticles. *Ind. Eng. Chem. Res.* **44**, 8039–8045 (2005).
351. Greszta, D. & Matyjaszewski, K. Mechanism of Controlled/“Living” Radical Polymerization of Styrene in the Presence of Nitroxyl Radicals. Kinetics and

Simulations. *Macromolecules* **29**, 7661–7670 (1996).

352. Lin, S.-Y., Chern, C.-S., Hsu, T.-J., Hsu, C.-T. & Capek, I. Emulsion polymerization of styrene: double emulsion effect. *Polymer (Guildf).* **42**, 1481–1491 (2001).
353. Dietzen, F.-J., Gerd, E., Bernhard, S., Martin, L. & Kirchheim, H. Method for Producing Expandable Polystyrene. (2010).
354. Rani, M. *et al.* Qualitative Analysis of Additives in Plastic Marine Debris and Its New Products. *Arch. Environ. Contam. Toxicol.* **69**, 352–366 (2015).
355. Koelmans, A. A., Besseling, E. & Foekema, E. M. Leaching of plastic additives to marine organisms. *Environ. Pollut.* **187**, 49–54 (2014).
356. Hermabessiere, L. *et al.* Occurrence and effects of plastic additives on marine environments and organisms: A review. *Chemosphere* **182**, 781–793 (2017).
357. Kricheldorf, H. R., Böhme, S. & Schwarz, G. Polycondensations of bisphenol-A with diphosgene or triphosgene in water-free organic solvents. *Macromol. Chem. Phys.* **206**, 432–438 (2005).
358. Kricheldorf, H. R., Böhme, S., Schwarz, G. & Schultz, C. L. Cyclic Polycarbonates by Poly Condensation of Bisphenol a with Triphosgene. *Macromolecules* **37**, 1742–1748 (2004).
359. Schnell, H. Polycarbonate, eine Gruppe neuartiger thermoplastischer Kunststoffe. Herstellung und Eigenschaften aromatischer Polyester der Kohlensäure. *Angew. Chemie* **68**, 633–640 (1956).
360. Le Grand, D. G. & Bendler, J. T. *Hanbook of Polycarbonate - Science and Technology*. (New York, 2000).
361. Aschberger, K. *et al. Bisphenol A and baby bottles: challenges and perspectives*. (2010).
362. Bertoli, S., Leone, A. & Battezzati, A. Human bisphenol a exposure and the "diabesity phenotype". *Dose-Response* **13**, (2015).
363. Phuong Truong, N. T. Bisphenol-A: Use in Europe and Alleged Health Impacts. (Metropolia University of Applied Sciences, 2018).
364. Ankley, G. T. & Villeneuve, D. L. The fathead minnow in aquatic toxicology: Past, present and future. *Aquat. Toxicol.* **78**, 91–102 (2006).
365. Mattsson, K. *et al.* Altered Behavior, Physiology, and Metabolism in Fish Exposed to Polystyrene Nanoparticles. *Environ. Sci. Technol.* **49**, 553–561 (2015).
366. Kricheldorf, H. R. Cyclic polymers: Synthetic strategies and physical properties. *J.*

Polym. Sci. Part A Polym. Chem. **48**, 251–284 (2010).

367. Kricheldorf, H. R., Böhme, S., Schwarz, G. & Schultz, C.-L. Syntheses of cyclic polycarbonates by the direct phosgenation of bisphenol M. *J. Polym. Sci. Part A Polym. Chem.* **43**, 1248–1254 (2005).
368. Lee, J.-Y., Song, C.-H., Kim, J.-I. & Kim, J.-H. Preparation of Aromatic Polycarbonate Nanoparticles using Supercritical Carbon Dioxide. *J. Nanoparticle Res.* **4**, 53–59 (2002).
369. Atanase, L. I. & Riess, G. Block copolymers as polymeric stabilizers in non-aqueous emulsion polymerization. *Polym. Int.* **60**, 1563–1573 (2011).
370. Dorresteijn, R., Haschick, R., Klapper, M. & Müllen, K. Poly(L -lactide) nanoparticles via ring-opening polymerization in non-aqueous emulsion. *Macromol. Chem. Phys.* **213**, 1996–2002 (2012).
371. Joe, D. Morphology control in metallocene-catalyzed polyolefin synthesis. (2013).
372. Grazon, C., Rieger, J., Charleux, B., Clavier, G. & Méallet-Renault, R. Ultrabright BODIPY-tagged polystyrene nanoparticles: Study of concentration effect on photophysical properties. *J. Phys. Chem. C* **118**, 13945–13952 (2014).
373. Rausch, K., Reuter, A., Fischer, K. & Schmidt, M. Evaluation of Nanoparticle Aggregation in Human Blood Serum. *Biomacromolecules* **11**, 2836–2839 (2010).
374. Secombes, C. J. & Fletcher, T. C. The role of phagocytes in the protective mechanisms of fish. *Annu. Rev. Fish Dis.* **2**, 53–71 (1992).
375. Lee, W. L., Harrison, R. E. & Grinstein, S. Phagocytosis by neutrophils. *Microbes Infect.* **5**, 1299–1306 (2003).
376. Papayannopoulos, V., Metzler, K. D., Hakkim, A. & Zychlinsky, A. Neutrophil elastase and myeloperoxidase regulate the formation of neutrophil extracellular traps. *J. Cell Biol.* **191**, 677–691 (2010).
377. Palić, D., Andreasen, C. B., Menzel, B. W. & Roth, J. A. A rapid, direct assay to measure degranulation of primary granules in neutrophils from kidney of fathead minnow (Pimephales promelas Rafinesque, 1820). *Fish Shellfish Immunol.* **19**, 217–227 (2005).
378. Jovanović, B. *et al.* Effects of nanosized titanium dioxide on innate immune system of fathead minnow (Pimephales promelas Rafinesque, 1820). *Ecotoxicol. Environ. Saf.* **74**, 675–683 (2011).
379. Fuchs, T. A. *et al.* Novel cell death program leads to neutrophil extracellular traps.

J. Cell Biol. **176**, 231–241 (2007).

380. Tenzer, S. *et al.* Rapid formation of plasma protein corona critically affects nanoparticle pathophysiology. *Nat. Nanotechnol.* **8**, 772–781 (2013).
381. Richtering, W., Alberg, I. & Zentel, R. Nanoparticles in the Biological Context: Surface Morphology and Protein Corona Formation. *Small* **16**, 1–8 (2020).
382. Hühn, D. *et al.* Polymer-coated nanoparticles interacting with proteins and cells: Focusing on the sign of the net charge. *ACS Nano* **7**, 3253–3263 (2013).
383. Zhdanov, V. P. Nanoparticles without and with protein corona: van der Waals and hydration interaction. *J. Biol. Phys.* **45**, 307–316 (2019).
384. Baier, G. *et al.* BSA Adsorption on Differently Charged Polystyrene Nanoparticles using Isothermal Titration Calorimetry and the Influence on Cellular Uptake. *Macromol. Biosci.* **11**, 628–638 (2011).
385. Bhattacharya, P., Lin, S., Turner, J. P. & Ke, P. C. Physical Adsorption of Charged Plastic Nanoparticles Affects Algal Photosynthesis. *J. Phys. Chem. C* **114**, 16556–16561 (2010).
386. Kumazawa, R. *et al.* Effects of Ti ions and particles on neutrophil function and morphology. *Biomaterials* **23**, 3757–3764 (2002).
387. Rossi, G., Barnoud, J. & Monticelli, L. Polystyrene Nanoparticles Perturb Lipid Membranes. *J. Phys. Chem. Lett.* **5**, 241–246 (2014).
388. Prietl, B. *et al.* Nano-sized and micro-sized polystyrene particles affect phagocyte function. *Cell Biol. Toxicol.* **30**, 1–16 (2014).

Appendix

10. Appendix

10.1. Appendix A: List of Figures

10.2. Appendix B: List of Schemes

10.3. Appendix C: List of Tables

10.4. Appendix D: Supporting Information

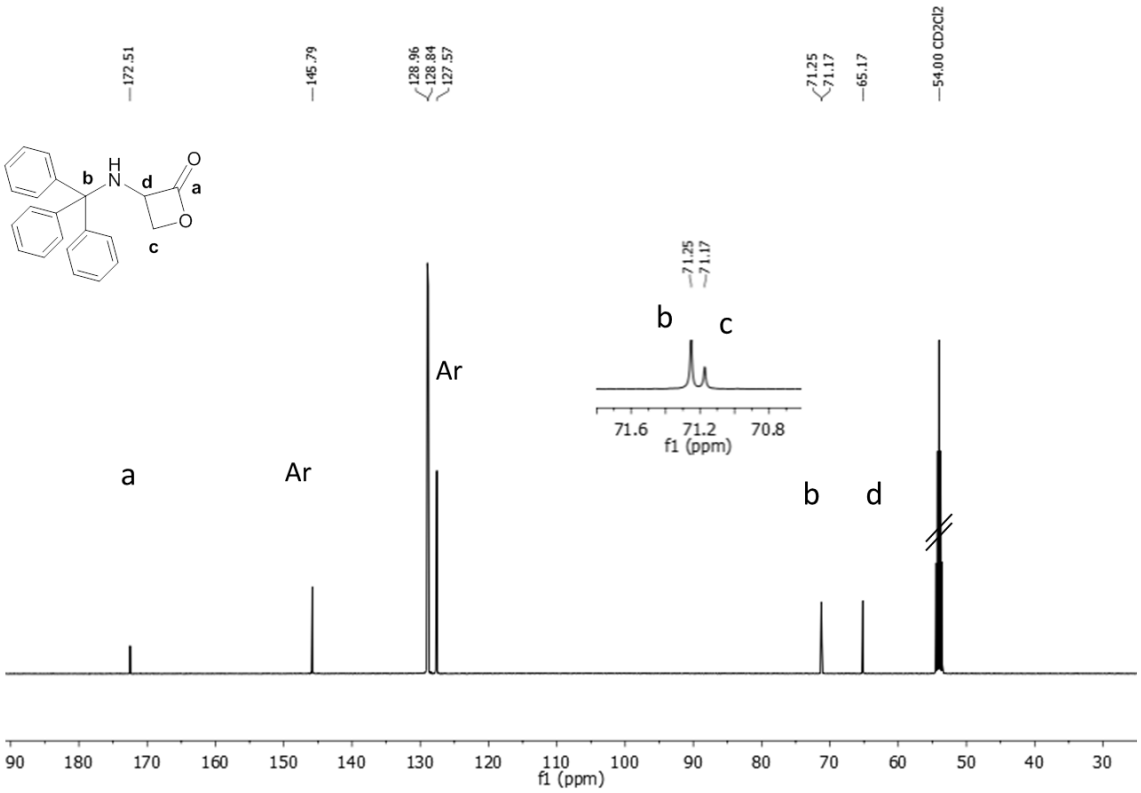

Figure 10.1. ^{13}C-NMR spectrum of NTSL monomer (CD_2Cl_2, 75 MHz, 298 K)

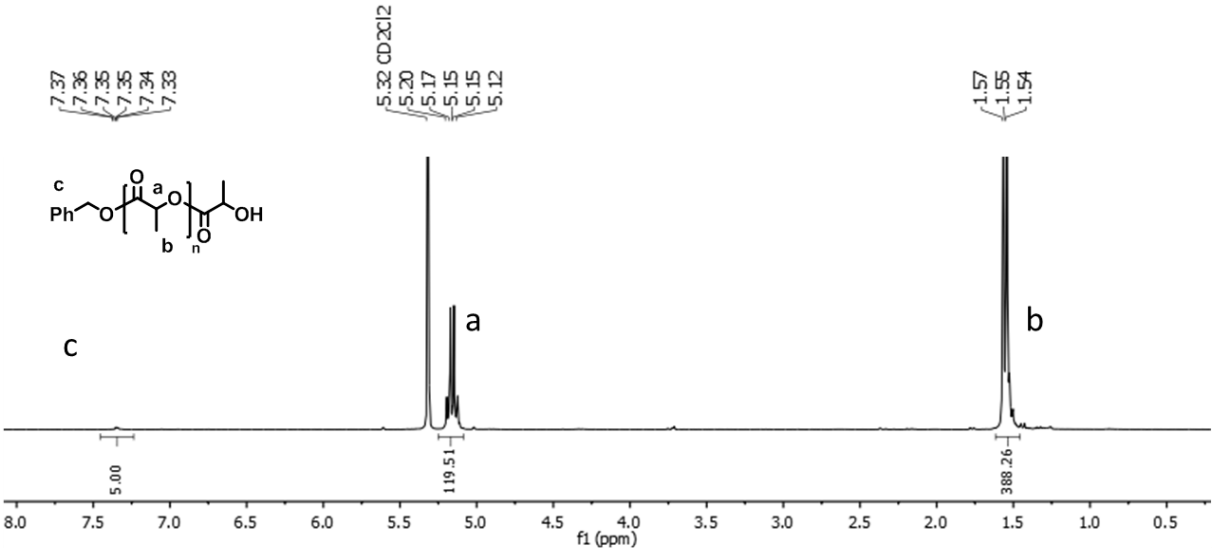

Figure 10.2. ^{1}H-NMR spectrum of benzyl alcohol initiated PLLA-4 (CD_2Cl_2, 500 MHz)

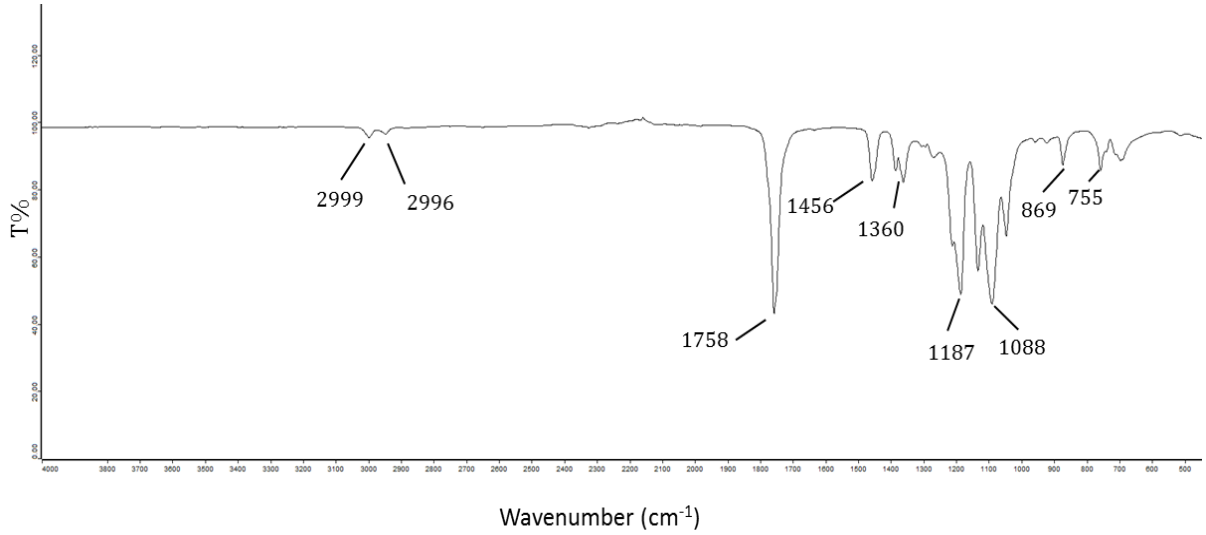

Figure 10.3. FT-IR spectrum of PLLA-4

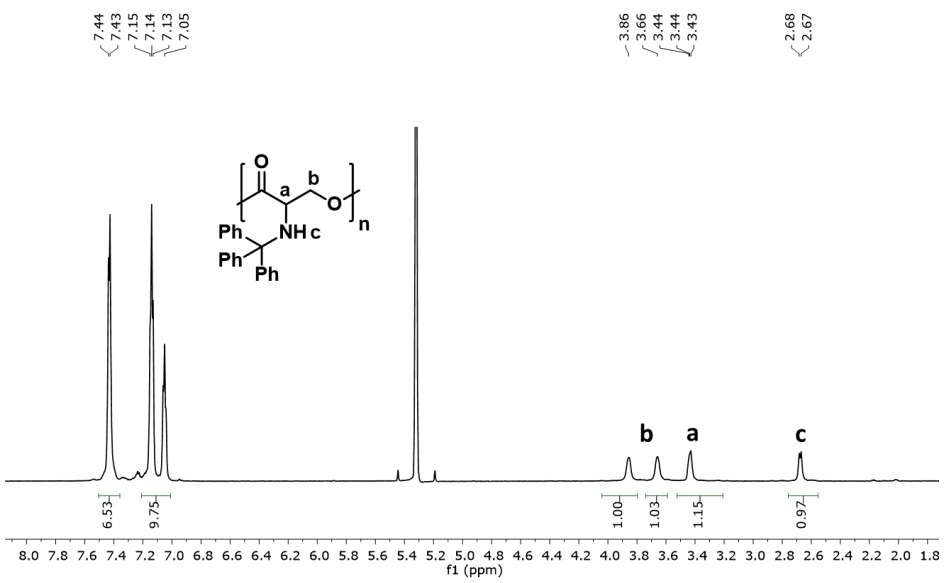

Figure 10.4. ^{1}H-NMR spectrum of PNTSL (CD_2Cl_2, 500 MHz)

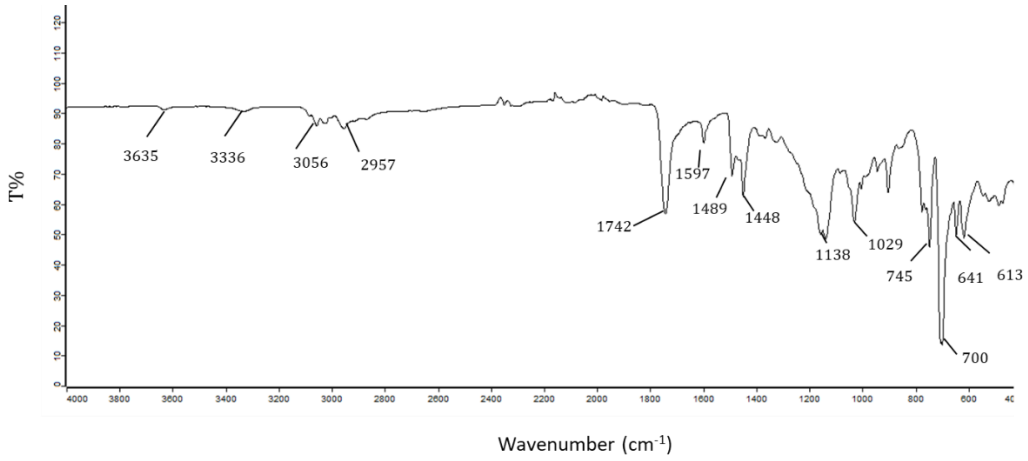

Figure 10.5. FT-IR spectrum of PNTSL

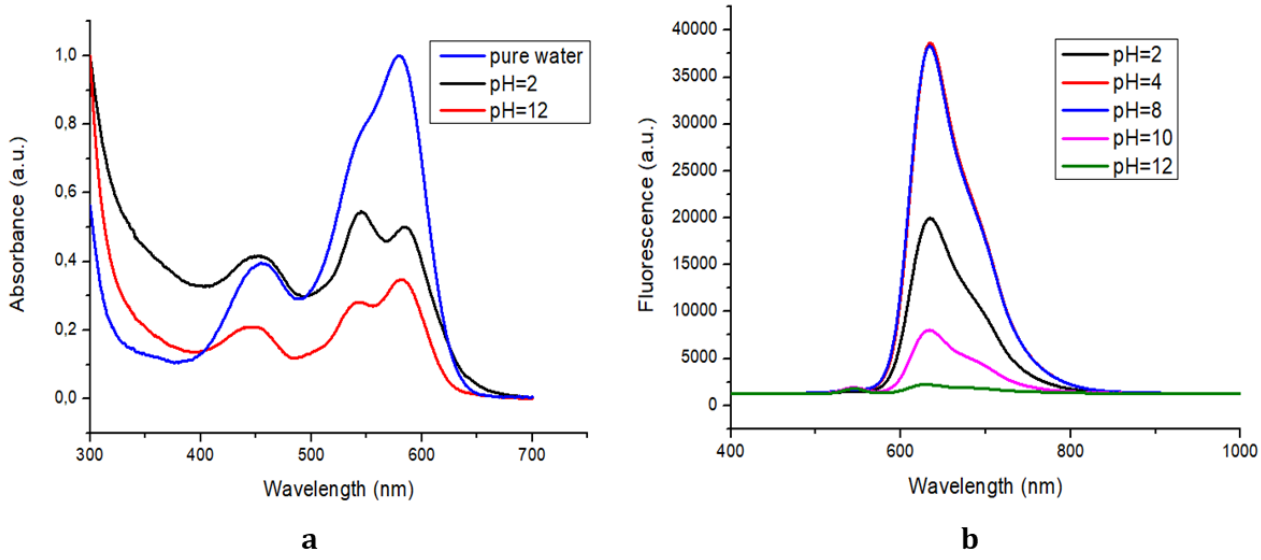

Figure 10.6. (a) UV-*vis* spectra of PLL-7dp in pure water and pH 2 and 12 adjusted by HCl-NaOH (b) Fluorescence spectra of PLL-7dp in water/HCl-NaOH ((λ_{ex}= 547 nm, λ_{em}= 636 nm)

Curriculum Vitae

PERSONAL DATA

Name: Filiz Karagöz
Birth date: 05.10.1989
Birth place: Ankara

EDUCATION

02/2014– 07/2018 PhD in Chemistry
Max Planck Institute for Polymer Research, Mainz, Germany

09/2011 –02/2014 Master in Chemistry
Hacettepe University, Department of Chemistry, Ankara, Turkey

07/2009 –09/2009 Internship
University of Aberdeen, Department of Chemistry, Aberdeen, Scotland

09/2011-Present Bachelor in Business Administration
Anadolu University, Eskisehir, Turkey

09/2006-07/2011 Bachelor in Chemistry
Ankara University, Department of Chemistry, Ankara, Turkey

Publications

- Greven, A. C., Merk, T., Karagöz, F., Mohr, K., Klapper, M., Jovanovic, B., Palic, D. "Polycarbonate and Polystyrene Nanoplastic Particles Act as Stressors to the Innate Immune System of Fathead Minnow (Pimephales promelas)" Environmental Toxicology and Chemistry, Vol. 9999, No. 9999, pp. 1-8, 2016.

- Karagoez F., Dorresteijn, R., Müllen K., Klapper, M., "Biocompatible Nanoparticles for a Selective Drug Release at Cancer Cells", Book Chapter for ACS Symposium Series "Control of Amphiphile Self-Assembling at the Molecular Level: Supra-Molecular Assemblies with Tuned, American Chemical Society: Washington, DC, 2017, 232-247.

Conferences

- ACS National Meeting, San Francisco/ USA - **04/2017**
  (Oral + Poster Presentation)
- 7. Nordrhein-Westfalens (NRW) Nano-Konferenz - **12/2016**
  (Poster Presentation)
- Makromolekular Kolloquium, Freiburg, Germany - **02/2015**
  (Oral + Poster Presentation)
- International Porous Powder Materials, Izmir, Turkey - **09/2013**
  (Poster Presentation)

Acknowledgments